



زانكۆی پۆلیتیه كنیکی هه ولیر
ERBIL POLYTECHNIC UNIVERSITY

MECHANICAL PROPERTIES OF HYBRID COMPOSITE USING HYBRID TOUGHENED MATRIX

A Dissertation

Submitted to the Council of the Erbil Technical Engineering College at Erbil Polytechnic University in Partial Fulfillment of the Requirements for the Degree of Doctor of Philosophy (PhD) of Science in Mechanical and Energy Engineering

By

Thaker Saleh Dawood

B.Sc. in Mechanical Engineering

M.Sc. in Applied Mechanics

Supervised by

Prof. Dr. Basim Mohammed Fadhil

Asst. Prof. Dr. Dlair Obaid Ramadan

Iraq - Kurdistan - Erbil

August 2024

DECLARATION

I declare that the PhD. dissertation entitled: “**MECHANICAL PROPERTIES OF HYBRID COMPOSITE USING HYBRID TOUGHENED MATRIX**” is my own original work, and hereby I certify that unless stated, all work contained within this dissertation is my own independent research and has not been submitted for the award of any other degree at any institution, except where due acknowledgment is made in the text.

Signature:



Student Name: Thaker Saleh Dawood

Date: August 2024

LINGUISTIC REVIEW

I confirm that I have reviewed the dissertation entitled “**MECHANICAL PROPERTIES OF HYBRID COMPOSITE USING HYBRID TOUGHENED MATRIX**” from the English linguistic point of view, and I can confirm that it is free of grammatical and spelling errors.

Signature: 

Name of Reviewer: Dr. Bashir E. Kareem

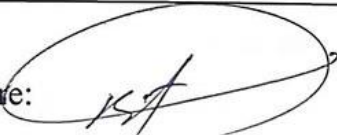
Date: 22 - 8 - 2024

Mail Address: bashir.kareem@epu.edu.iq

SUPERVISOR CERTIFICATE

This dissertation has been written under our supervision and has been submitted for the award of the degree of Doctor of Philosophy in Mechanical and Energy Engineering with our approval as supervisors.

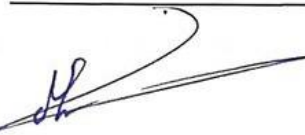
Signature:



Name: Prof. Dr. Basim M. Fadhil

Date 28/10/2024

Signature:



Name: Asst. Prof. Dr. Dlair O. Ramadan

Date 28/10/2024

I confirm that all requirements have been fulfilled.

Signature:



Name: Prof. Dr. Ahmed Mohammed Adham

Head of the Department of Mechanical and Energy Engineering Techniques

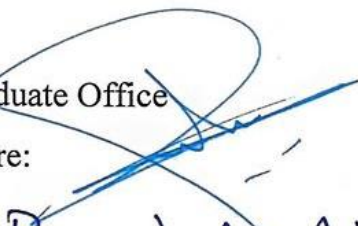
Date: 3/11/2024



I confirm that all requirements have been fulfilled.

Postgraduate Office

Signature:





Name: Byad A. Ahmed

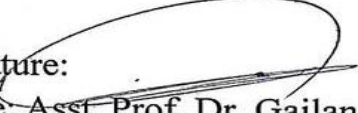
Date: 5-11-2024


EXAMINING COMMITTEE CERTIFICATION

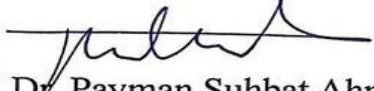
We certify that we have read this dissertation entitled “MECHANICAL PROPERTIES OF HYBRID COMPOSITE USING HYBRID TOUGHENED MATRIX” and as examining committee, examined the student (Thaker Saleh Dawood) in its content and what related to it. We approve that it meets the standards of a dissertation for the degree of Doctor of Philosophy in Mechanical and Energy Engineering.

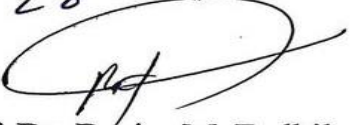
Signature: 
Name: Asst. Prof. Dr. Yassen M. Ahmed
Member 28/10/2024
Date:

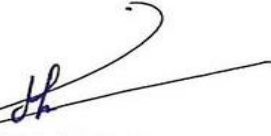
Signature: 
Name: Asst. Prof. Dr. Haval K. Asker
Member
Date: 28/10/2024

Signature: 
Name: Asst. Prof. Dr. Gailan I. Hassan
Member
Date: 28.10.2024

Signature: 
Name: Asst. Prof. Dr. Younis Kh. Khdir
Member
Date: 28/10/2024

Signature: 
Name: Prof. Dr. Payman Suhbat Ahmed
Chairman
Date: 28-10-2024

Signature: 
Name: Prof. Dr. Basim M. Fadhil
Supervisor
Date: 28/10/2024

Signature: 
Asst. Prof. Dr. Dlair O. Ramadan
Supervisor
Date: 28/10/2024

Signature: 
Name: Prof. Dr. Ayad Zaki Saber
Dean of Erbil Technical Engineering College
Date: 04-11-2024

DEDICATION

This dissertation is dedicated to my beloved family, who have been a constant source of support and encouragement during the challenges of my studies. I wholeheartedly thank my loving parents, who have always loved me unconditionally and whose good examples have taught me to work hard for the things I aspire to achieve.

My beloved siblings, stand by me and help me in all things, great and small.

I dedicate this work and give special thanks to all my friends who have supported me until my research was fully finished.

I am genuinely thankful to have you all in my life.

ACKNOWLEDGEMENTS

In the name of ALLAH, the most gracious, most merciful. All praise is due to ALLAH, the Lord of the Worlds.

Foremost, I am thankful to almighty ALLAH for giving me the strength, knowledge, ability, and opportunity to undertake and complete this research successfully.

I would like to express my deep and sincere gratitude to my research supervisors, Dr. Basim M. Fadhil and Dr. Dlair O. Ramadan, for their continuous support of this dissertation and for their patience, motivation, and immense knowledge. They consistently allowed this thesis to be my own work but steered me whenever they thought I needed it. I am really thankful for they help and support.

I would like to thank my wife for her support, prayers, benedictions and encouragement throughout my PhD study, during which time she always provided the inspiration and motivation that I needed. I would like to thank my son, daughters, brothers and sister for their continuous concern, support and advice.

My wholehearted thanks go to the late Asst. Prof. Dr. Laith M. Jassim in mechatronics department at the University of Mosul for his comments, support, and for sharing his knowledge.

Last but not least, I want to thank all of those people who, at one time or another, helped me begin this long journey. Unfortunately, their names are too numerous to mention, but many of them inspired me to continue learning and following the right path. Words cannot express how thankful I am to you for everything. So, thank you all.

ABSTRACT

This dissertation investigated the effect arrangement of layers in glass and carbon composites, focusing on the effects of longitudinal fiber orientation, thickness, and the addition of SiO₂ nanoparticles. Three batches of composite plates were produced. The first category comprised unidirectional glass fiber sheets arranged in a stacking sequence of 0° [G/G/G/G]_s with and without 2% silica dioxide nanoparticles and carbon fiber sheets arranged in a stacking sequence of 0° [C/C/C/C]_s with and without 2% silica dioxide nanoparticles. These sheets were specifically designed to assess the mechanical properties, namely the modulus of elasticity in the longitudinal and transverse directions E_1 and E_2 , shear modulus (G_{12}), and Poisson's ratio (ν_{12}) for glass/epoxy and carbon/epoxy composites.

The second group, characterized by quasi-isotropic-balanced distinct stacking sequences, comprised three primary unidirectional fiber orientations: 0°, 45°, and 90°. These sequences varied in thickness, consisting of eight layers (2 mm), ten layers (2.5 mm), and twelve layers (3 mm). Additionally, SiO₂ nanoparticles were utilized as a reinforcing agent within the epoxy matrix. The third group consisted of cross-layer configurations, with various stacking sequences examined. These sequences involved two primary unidirectional fiber orientations: 0° and 90°, and they exhibited different thicknesses. Specifically, the group included eight layers (2 mm), twelve layers (3 mm), sixteen layers (4 mm), and twenty layers (5 mm).

Furthermore, SiO₂ nanoparticles were employed as a reinforcing agent within the epoxy matrix. The vacuum-assisted resin infusion process was utilized to fabricate fourteen combinations of fiber-reinforced epoxy composites, including those with and without the addition of 2% silicon dioxide nanoparticle composites, designated as QS1, QS1N, QS2, QS2N, QS3, QS3N, CS1, CS1N, CS2, CS2N, CS3, CS3N, CS4, and CS4N. The quasi-static mechanical properties (tensile and three-point bending test) and dynamic (axial and flexural fatigue test)

behaviors of the material were examined through experimental analysis and validated using numerical simulations via the finite element method (ANSYS 2019/R3 Workbench).

The modulus of elasticity (E_1) and maximum stress for QS3 and QS3N increased by 20.97% and 18.65%, respectively. In comparison to CS1, which lacks SiO₂ nanoparticles, CS1N exhibited increases in E_1 and maximum stress of 2.5% and 12.7%, respectively. The incorporation of SiO₂ nanoparticles significantly enhanced the performance of glass/carbon hybrid composite materials. Axial fatigue tests demonstrated that the number of cycles of the hybrid composites (CS1 and CS1N), (CS2 and CS2N), and (CS3 and CS3N) increased by approximately 55%, 27%, and 58%, respectively, at a load level of 70%. In flexural fatigue testing, there was a stress increase of 17.4% between CS1 and CS₁N, and a similar increase of 13.11% between CS2 and CS2N. The sample pairs CS3 and CS3N showed a comparable percentage increase of 17.1%, while CS4 and CS4N exhibited an increase of 13.61%.

LIST OF CONTENTS

<i>Subject</i>	<i>Page No.</i>	
<i>DECLARATION</i>	<i>V</i>	
<i>DEDICATION</i>	<i>V</i>	
<i>ACKNOWLEDGEMENTS</i>	<i>VI</i>	
<i>ABSTRACT</i>	<i>VII</i>	
<i>LIST OF CONTENTS</i>	<i>IX</i>	
<i>LIST OF SYMBOLS</i>	<i>XIII</i>	
<i>LIST OF FIGURES</i>	<i>XV</i>	
<i>LIST OF TABLES</i>	<i>XX</i>	
<i>LIST OF NOMENCLATURE AND ACRONYMS</i>	<i>XXI</i>	
<i>CHAPTER ONE: INTRODUCTION</i>		
<i>1.1</i>	<i>Background</i>	<i>1</i>
<i>1.2</i>	<i>Glass/Carbon Hybrid Composite Materials</i>	<i>2</i>
<i>1.3</i>	<i>Silica Nanoparticles Reinforced Matrix</i>	<i>3</i>
<i>1.4</i>	<i>Glass and Carbon Hybrid Composite Materials with Nanoparticles</i>	<i>5</i>
<i>1.5</i>	<i>Problem Statement</i>	<i>6</i>
<i>1.6</i>	<i>Aim and Objectives</i>	<i>6</i>
<i>1.6.1</i>	<i>Aim</i>	<i>6</i>
<i>1.6.2</i>	<i>Objectives</i>	<i>7</i>
<i>1.7</i>	<i>Dissertation Layout</i>	<i>7</i>

CHAPTER TWO: LITERATURE REVIEW		
2.1	<i>Introduction to Composite Materials</i>	9
2.2	<i>Fiber-Reinforced Composite Materials</i>	10
2.2.1	<i>Fiber Glass Reinforced Composite Materials</i>	11
2.2.2	<i>Carbon Fiber Reinforced Composite Materials</i>	12
2.3	<i>Hybrid Composite Materials</i>	13
2.3.1	<i>Fiber-Hybrid Composites</i>	14
2.3.1.1	<i>Glass/Carbon Hybrid Composite Materials</i>	16
2.3.2	<i>Nanoparticles Hybrid Composite Materials</i>	23
2.4	<i>Fatigue of Composite Materials</i>	26
2.5	<i>Summary</i>	32
CHAPTER THREE: THEORETICAL WORK		
3.1	<i>Mechanics of Composite Materials</i>	34
3.1.1	<i>Micro-Mechanics of Lamina</i>	35
3.1.2	<i>Macro-Mechanics of Lamina</i>	39
3.1.3	<i>Macro-Mechanics of the Laminate</i>	41
3.1.3.1	<i>Laminate Under Tensile and Shear Load</i>	48
3.1.3.2	<i>Laminate under Bending Moment</i>	49
3.1.3.3	<i>Laminate under Fatigue Load</i>	52
3.2	<i>Failure Criteria</i>	53
3.2.1	<i>Failure Mechanism of Quasi-Static</i>	53
3.2.2	<i>Failure Mechanism of Fatigue</i>	56
3.3	<i>Fracture Mechanics</i>	58

3.3.1	<i>Linear Elastic Fracture Mechanics (LEFM)</i>	58
3.3.2	<i>Stress Intensity Factor (SIF)</i>	59
3.3.3	<i>Fatigue Crack Growth</i>	61
CHAPTER FOUR: EXPERIMENTAL AND NUMERICAL WORK		
4.1	<i>Materials</i>	63
4.2	<i>Manufacturing Methods</i>	64
4.2.1	<i>Vacuum Infusion</i>	64
4.2.2	<i>Adding Silica Dioxide Nanoparticles to Epoxy Resin</i>	68
4.3	<i>Preparation Test Specimens</i>	71
4.3.1	<i>Manufacturing of Glass/Epoxy and Carbon/ Epoxy Laminates</i>	71
4.3.2	<i>Manufacturing of Quasi-Isotropic Ply Laminates</i>	75
4.3.3	<i>Manufacturing of Cross-Ply Laminates</i>	77
4.4	<i>Mechanical Tests</i>	79
4.4.1	<i>Tensile and Three-Point Bending Tests</i>	79
4.4.2	<i>Axial Fatigue Test</i>	82
4.4.3	<i>Flexural Fatigue Test</i>	83
4.4.3.1	<i>Manufacturing Test Rig</i>	83
4.4.3.2	<i>Validation and Testing</i>	85
4.5	<i>Numerical Modeling</i>	88
4.5.1	<i>Materials Designer</i>	89
4.5.2	<i>Tensile Test Modeling</i>	90
4.5.3	<i>Three Point Bending Test Modeling</i>	91
4.5.4	<i>Fatigue Test Modeling</i>	92

4.6	<i>Scanning Electron Microscopy (SEM)</i>	94
CHAPTER FIVE: RESULTS AND DISCUSSION		
5.1	<i>Engineering Constants of Laminates</i>	95
5.2	<i>Tensile Test</i>	97
5.2.1	<i>Tensile Test of Quasi-Isotropic Laminate</i>	97
5.2.2	<i>Tensile Test of Cross-Ply Laminate</i>	103
5.3	<i>Three Points Bending Test</i>	109
5.3.1	<i>Three Point Bending Test of Quasi-Isotropic Laminate</i>	109
5.3.2	<i>Three Points Bending Test of Cross-Ply Laminate</i>	116
5.4	<i>Fatigue Test</i>	124
5.4.1	<i>Axial Fatigue Test for Cross-Ply Laminate</i>	124
5.4.2	<i>Flexural Fatigue</i>	131
5.4.2.1	<i>Flexural fatigue Quasi Isotropic-Ply Laminate</i>	132
5.4.2.2	<i>Flexural fatigue Cross-Ply Laminate</i>	138
5.5	<i>Failure analysis</i>	147
CHAPTER SIX: CONCLUSIONS AND RECOMMENDATIONS		
6.1	<i>Conclusion</i>	150
6.2	<i>Recommendation for Future work</i>	152
	<i>References</i>	R-1

LIST OF SYMBOLS

<i>Symbol</i>	<i>Meaning</i>	<i>Units</i>
$\begin{Bmatrix} \varepsilon_x \\ \varepsilon_y \\ \varepsilon_{xy} \end{Bmatrix}$	<i>Laminate Strains</i>	<i>mm/mm</i>
$\begin{Bmatrix} \varepsilon_x^0 \\ \varepsilon_y^0 \\ \gamma_{xy}^0 \end{Bmatrix}$	<i>Midplane Strains</i>	<i>mm/mm</i>
$\begin{Bmatrix} K_x \\ K_y \\ K_{xy} \end{Bmatrix}$	<i>Flexural Strains</i>	<i>mm/mm</i>
$[\bar{Q}]$	<i>Transformed Reduced Stiffness Matrix</i>	<i>MPa</i>
A_{ij}, B_{ij}, D_{ij}	<i>Extensional, Extensional- Bending Coupling and Bending Stiffness Matrices</i>	<i>Pa.m, Pa.m², Pa.m³</i>
E_x	<i>Effective longitudinal Young Modulus</i>	<i>MPa</i>
ν_{xy}	<i>Major Effective Poisson's Ratio</i>	
E_y	<i>Effective Transverse Young Modulus</i>	<i>MPa</i>
G_{xy}	<i>Effective Shear Modulus</i>	<i>MPa</i>
E_x^f	<i>Effective Flexural Longitudinal Modulus</i>	<i>MPa</i>
E_y^f	<i>Effective Flexural Transverse Modulus</i>	<i>MPa</i>
ν_{xy}^f	<i>Major Effective Flexural Poisson's Ratio</i>	
G_{xy}^f	<i>Effective Flexural Shear Modulus</i>	<i>MPa</i>
h	<i>total laminate thickness</i>	<i>Mm</i>
$w_0(x, y)$	<i>Plate Lateral Deflection</i>	<i>Mm</i>
$q(x, y)$	<i>Lateral load</i>	<i>N</i>
a, b	<i>plate length and width</i>	<i>Mm</i>
d_{mn}	<i>Bending Stiffness Coefficient</i>	<i>Pa/m</i>
W_{mn}	<i>Deflection Coefficient</i>	<i>M</i>
Q_{mn}	<i>Load Coefficient</i>	<i>N</i>
E_l	<i>Longitudinal Elastic Modulus</i>	<i>MPa</i>

E_2	<i>Transverse Modulus</i>	<i>MPa</i>
G_{12}	<i>In-Plane Shear Modulus</i>	<i>MPa</i>
ν_{12}	<i>Poisson's Ratio</i>	
σ_1	<i>Uniform Stress</i>	<i>MPa</i>
L	<i>Initial Length of the Volume</i>	<i>mm</i>
ΔL	<i>Elongation Generated by the Stressed Applied</i>	<i>mm</i>

LIST OF FIGURES

Figure No.	Subject	Page No.
2-1	Tensile characteristics for different stacking of hybrid composite.	21
2-2	A schematic illustration of two-ply drops together shows potential fractures, tunneling cracks, and delamination cracks.	28
2-3	Illustration of single-fiber push-out test's layout.	32
3-1	Typical laminate made of three laminae.	35
3-2	Representative volume of a single lamina: matrix (blue line) and fibers (orange lines). Principal direction 1 parallel to the fiber.	36
3-3	Exemplary components loaded in a direction where ΔL is the elongation caused by the stress applied, and L is the volume's original length.	37
3-4	Exemplary component loaded in direction 2.	38
3-5	Stress distribution on the element volume.	39
3-6	N-layered laminate is shown geometrically.	46
3-7	Forces and moments generated by a laminate.	46
3-8	Typical S-N Curve.	52
3-9	An illustration of deterioration inside the lamina.	55
3-10	Development of damage in composite laminate.	57
3-11	Main modes of crack opening.	59
3-12	Schematic sigmoidal behavior of fatigue crack growth rate versus ΔK .	62
4-1	(a) Unidirectional glass fiber, (b) Unidirectional carbon fiber	64
4-2	Epoxy resin and hardener	65
4-3	materials required to manufacture of the hybrid composite material	66
4-4	(a) Laminate before vacuum, (b) pressure gauge	67
4-5	Vacuum bag and curing technique.	68
4-6	(a) SiO_2 weight measurement (b) mixing SiO_2 nanoparticles manually	69
4-7	Ultrasonic mixer	69
4-8	Vacuum chamber (b) Removing bubbles	70
4-9	Resin injected in to fiber's layers	70
4-10	(a) Unidirectional Glass/epoxy laminate (b) Unidirectional Carbon/epoxy laminate	72

4-11	(a) Stacking setup; (b) Strain gauge for calculating E_1 and E_2	73
4-12	Specimens of glass/epoxy for tensile test (a) without SiO_2 nanoparticles, (b) with SiO_2 nanoparticles	74
4-13	Specimens of carbon/epoxy for tensile test (a) without SiO_2 nanoparticles, (b) with SiO_2 nanoparticles	74
4-14	Unidirectional glass/carbon quasi-isotropic laminate	75
4-15	Tensile and axial fatigue specimens (a) specimen dimensions, (b) specimen's photograph	76
4-16	Bending and flexural fatigue specimens (a) specimen dimensions, (b) specimen's photograph	77
4-17	Unidirectional Glass/carbon cross-ply laminate	79
4-18	Tensile Test Using SHIMADZU Universal Testing Machine with a Force Capability of 100 kN	81
4-19	Three-Point Bending Test Using SHIMADZU Universal Testing Machine with a Force Capability of 100 kN	81
4-20	Shimadzu brand Servo-Hydraulic Fatigue Tester	83
4-21	Schematic diagram of flexural fatigue test machine	85
4-22	HSM20 alternating bending fatigue machine	86
4-23	Comparison between results of HSM20 and the test rig.	86
4-24	(a) Fatigue test rig (b) Fatigue test Specimens	88
4-25	Representative volume element (RVE)	89
4-26	Steps for modelling for the laminates in the ANSYS 2019/R3 Workbench (a) tensile and three-point bending, (b) Axial and flexural fatigue test.	90
4-27	Geometric model of the tensile test specimen.	91
4-28	FE model of tensile test specimen with boundary conditions.	91
4-29	Geometric model of the three-point bending test specimen.	92
4-30	FE model of three-points bending test specimen with boundary conditions.	92
4-31	Geometry of the model used for (a) Axial fatigue analysis (b) Flexural fatigue analysis.	93
4-32	(a) Axial fatigue model with boundary condition (b) Flexural fatigue model with boundary conditio.	94
4-33	Scanning Electron Microscopy (SEM).	94
5-1	Influence of adding SiO_2 nanoparticles on the mechanical characteristics.	96

5-2	Tensile stress-strain plot of glass/carbon hybrid composites(a) 8-layer, (b) 10-layer, (c) 12-layer.	98
5-3	Tensile specimens after failure: (a) QS1 (without SiO ₂ nanoparticles), (b) QS1N (with SiO ₂ Nanoparticles).	99
5-4	Influence of adding SiO ₂ nanoparticles on modulus of elasticity and tensile stress of glass/carbon hybrid composite laminate.	100
5-5	Figure 5-5 Effect of stacking sequences on glass/carbon hybrid composite (a) without adding SiO ₂ nanoparticles (b) with adding SiO ₂ nanoparticles.	101
5-6	Ultimate tensile strength distribution through Quasi-isotropic hybrid laminates.	102
5-7	Experimental and numerical ultimate tensile strength of quasi-isotropic laminates.	103
5-8	Tensile stress-strain plot of glass/carbon hybrid composites (a) 8-layer, (b) 12-layer (c) 16-layer, (d) 20-layer.	104
5-9	Influence of adding SiO ₂ nanoparticles on modulus of elasticity and tensile stress of glass/carbon hybrid composite laminate.	106
5-10	Effect of stacking sequences on glass/carbon hybrid composite (a) without adding SiO ₂ nanoparticles (b) with adding SiO ₂ nanoparticles.	107
5-11	Ultimate tensile strength distribution through cross-ply laminates of FRPC plies.	108
5-12	Experimental and numerical ultimate tensile strength of cross-ply laminates.	109
5-13	Flexural stress-strain plot of Quasi isotropic-ply glass/carbon hybrid composites (a) 8-layer, (b) 12-layer (c) 16-layer.	110
5-14	Increment of adding SiO ₂ nanoparticles of Quasi-ply glass/carbon hybrid composite laminate	112
5-15	Three points bending failure specimens: (a) QS1 (without SiO ₂ Nanoparticles), (b) QS1N (with SiO ₂ Nanoparticles).	113
5-16	Effect of stacking sequences on Quasi-ply glass/carbon hybrid composite (a) without adding SiO ₂ nanoparticles (b) with adding SiO ₂ nanoparticles.	114
5-17	Ultimate Flexural strength distribution three points bending through quasi-isotropic laminates of FRPC plies.	115

5-18	Experimental and numerical ultimate three-points bending strength of quasi-isotropic laminates.	116
5-19	Bending stress-strain plot of glass/carbon hybrid composites (a) 8-layers, (b) 12-layers (c) 16-layers, (d) 20-layers	117
5-20	Effect of adding SiO ₂ on Bending Stress of cross-ply glass/carbon hybrid composites.	118
5-21	Increment of adding SiO ₂ nanoparticles of cross-ply glass/carbon hybrid composite laminates.	120
5-22	Three points bending failure specimens (a) without SiO ₂ nanoparticles, (b) with SiO ₂ nanoparticles.	120
5-23	Effect of stacking sequences on three points bending test of cross-ply glass/carbon hybrid composite (a) without adding SiO ₂ nanoparticles (b) with adding SiO ₂ nanoparticles.	122
5-24	Ultimate flexural strength distribution through cross-ply laminates of FRPC plies.	123
5-25	Experimental and Numerical (ANSYS) ultimate flexural strength comparison of cross-ply laminates	124
5-26	S-N curves for hybrid composite (a) CS1 and CS1N (b) CS2 and CS2N (c) CS3 and CS3N.	126
5-27	General increment percentage in axial fatigue limit of cross ply laminate.	128
5-28	S-N curves for hybrid composite (a)without adding SiO ₂ nanoparticles, (b) with adding SiO ₂ nanoparticles.	129
5-29	Fatigue life and safety factor analysis of cross ply for both neat epoxy laminates and epoxy laminates containing SiO ₂ nanoparticles.	130
5-30	S-N curves for Quasi Isotropic - ply hybrid composite laminates (a) QS1 and QS1N (b) QS2 and QS2N (c) QS3 and QS3N.	133
5-31	General increment percentage in fatigue life for Quasi Isotropic-ply hybrid composite laminates.	134
5-32	General increment percentage in stress for increasing number of layers (a) without SiO ₂ nanoparticles (b) with SiO ₂ nanoparticles.	135
5-33	Figure 5-33 S-N curves for quasi-isotropic hybrid composite (a)without adding SiO ₂ nano- particles, (b) with adding SiO ₂ nano-particles.	136
5-34	Fatigue life and safety factor analysis of quasi-isotropic ply for both QS and QSN.	137

5-35	S-N curves for cross-ply hybrid composite (a) CS1 and CS1N (b) CS2 and CS2N (c) CS3 and CS3N (d) CS4 and CS4N.	139
5-36	Increment percentage in endurance limit (a) CS1 and CS1N (b) CS2 and CS2N (c) CS3 and CS3N (d) CS4 and CS4N.	140
5-37	General increment percentage in fatigue life (a) CS1 and CS1N (b) CS2 and CS2N (c) CS3 and CS3N (d) CS4 and CS4N.	141
5-38	General increment percentage in increasing number of layers (a) without SiO ₂ nanoparticles (b) with SiO ₂ nanoparticles.	142
5-39	S-N curves for hybrid composite (a) without adding SiO ₂ nanoparticles, (b) with adding SiO ₂ nanoparticles.	143
5-40	Fatigue life analysis neat epoxy of eight ply (CS1).	144
5-41	Fatigue life and safety factor analysis of cross ply for both neat epoxy laminates and epoxy laminates containing SiO ₂ nanoparticles.	146
5-42	Scanning electronic microscopy fractography unidirectional composite without SiO ₂ Nano particles subjected to fatigue (a) Delamination, (b) Fiber pull-out, (c) Debonding and matrix fragmentation, (d) Fiber imprint.	148
5-43	Scanning electronic microscopy fractography unidirectional composite with SiO ₂ Nano particles subjected to fatigue (a) Delamination and Fiber Bundle, (b) Crack propagation, (c) Fiber pull-out, (d) Fiber breakage.	149

LIST OF TABLES

Table		Page No.
4-1	<i>L285 resin and H285 hardener properties.</i>	63
4-2	<i>Glass and carbon fiber mechanical properties.</i>	71
4-3	<i>Stacking Sequence of Quasi-Isotropic Laminates.</i>	75
4-4	<i>Stacking Sequence of Cross-Ply Laminates.</i>	78
5-1	<i>Glass and Carbon Fiber Mechanical Properties</i>	95
5-2	<i>Mechanical Properties of Hybrid Laminates at Tensile Test for Quasi Isotropic Laminates.</i>	99
5-3	<i>Mechanical Properties of Glass / Carbon Hybrid Composite at Tensile Test for Cross Ply Laminates</i>	105
5-4	<i>Experimental and theoretical results of the three points bending test for quasi-isotropic laminates.</i>	111
5-5	<i>Mechanical Properties of Hybrid Cross-Ply Laminates at the Three Points Bending Test.</i>	119
5-6	<i>Summarizes the numerical and experimental findings for cross ply laminates.</i>	131
5-7	<i>Summary of the numerical and experimental results of quasi-isotropic laminates.</i>	138
5-8	<i>Summary of the numerical and experimental results of of cross-ply laminates</i>	146

LIST OF NOMENCLATURE AND ACRONYMS

<i>Abbreviation</i>	<i>Meaning</i>
FRPC	Fiber Reinforced Polymer Composite
GFRP	Glass Fiber Reinforced Polymer
CFRP	Carbon Fiber Reinforced Polymer
G	Glass Fiber
C	Carbon Fiber
K	Kevlar Fiber
ARAL	Aramid Fiber Composite/Aluminum base FML
GLARE	glass Fiber Composite/Aluminum base FML
CARAL	Carbon Fiber Composite/Aluminum base FML
SiO ₂	Silica Oxide Nano Powder
FRM	Fiber Reinforced Matrix
VARTM	Vacuum-Assisted Resin Transfer Molding
ACP(Pre)	ANSYS Composite Pre-Post
MGS L285	Laminating epoxy resin
H285	Hardener
UDMM	Ultrasonic Dual Mixing Method
VARIM	Vacuum-Assisted Resin Infusion Molding
FEM	Finite Element Method
SEM	Scanning Electron Microscopy
LEFM	Linear Elastic fracture Mechanics
SIF	Stress Intensity Factor
NDT	Non-Destructive Testing
CDS	Characteristic Damage State
CLT	Classical Lamination Theory

FAA	Federal Aviation Administration
AFM	Atomic Force Microscopy
APTMS	Amino propyl trimethoxy
L.A.L	Laminate Analysis Layer
HGM	Hollow Glass Microspheres
PC	polycarbonate
FDG	fatigue delamination growth
UTS	ultimate tensile strength
SENB	Single-Edge Notched Beam
NFRP	Natural Fiber Reinforced Polymer
GO	graphene oxide
CNTs	carbon nanotubes
ILSS	inter-laminar shear strength
FDG	Fatigue Delamination Growth
ENF	End-Notched-Flexure
LCM	Liquid Composite Moulding
RVE	Representative Volume Element

CHAPTER ONE

INTRODUCTION

1.1 Background

Composite materials, known for their superior high strength-to-weight ratios and versatile applications, have emerged as a cornerstone in the modern engineering landscape. In recent years, hybrid composites – which consist of two or more distinct reinforcing materials within a common matrix – have gained increased attention due to their enhanced mechanical properties, such as improved strength, stiffness, and fracture toughness (Safri *et al.*, 2018; Chandel, Sharma and Bansal, 2021). These attributes make hybrid composites promising candidates for applications in aerospace, automotive, marine, and civil engineering sectors, among others (Mouritz, 2012).

Despite their many advantages, hybrid composites are not exempt from the phenomenon of fatigue, which is an important consideration in the design and performance of engineering structures subjected to cyclic loading. Fatigue crack growth is a critical aspect of material degradation and can lead to catastrophic failure in structures if not adequately understood and managed. It is therefore essential to investigate the fatigue crack growth characteristics of hybrid composites and develop models that can accurately predict and assess their behavior under various loading and environmental conditions (Schijve, 2009).

Numerous studies have investigated the fatigue behavior of glass and carbon fiber composites individually. However, the fatigue crack growth characteristics of glass/carbon fiber hybrid composites remain less explored, despite their potential for improved performance. The interaction between the different fibers, matrix materials, and the interface between them adds to the complexity of the fatigue crack growth process in hybrid composites. Existing studies on fatigue

crack growth in composite materials have primarily focused on traditional, single-fiber composites, while research on hybrid composites remains limited (Harris, 2004; Talreja, 2008). Moreover, the complex interactions between different constituents in hybrid composites introduce new challenges in understanding and predicting fatigue crack growth behavior. This necessitates the development of comprehensive analytical and experimental frameworks to explore the underlying mechanisms governing fatigue crack growth (Kaminski et al., 2015).

The fatigue behavior of composite materials is an essential factor influencing their long-term performance, particularly in applications where cyclic loading is prevalent (Ritchie, 2011). Fatigue crack growth, which refers to the propagation of existing cracks under cyclic loading, is a critical aspect of fatigue behavior that can ultimately lead to structural failure (Suresh, 2013). The study of fatigue crack growth in hybrid composites is essential for understanding the mechanisms governing their fatigue performance, as well as for developing accurate models and prediction tools (Reddy, 2004; Wisnom, 2009).

1.2 Glass /Carbon Hybrid Composite Materials

Among composites, carbon fiber-reinforced polymers, denoted by CFRP, and glass fiber-reinforced polymers, denoted by GFRP, are two widely used materials, each possessing its own distinct advantages (Vasiliev and Morozov, 2013). However, to optimize the benefits of both materials, researchers have developed glass/carbon hybrid composite materials, which combine the strengths of GFRP and CFRP while mitigating their respective weaknesses. Glass/carbon hybrid composites consist of a polymer matrix reinforced with both glass and carbon fibers. This dual reinforcement approach results in a synergistic effect, yielding a material with improved mechanical properties and performance characteristics.

The hybrid composites' manufacturing processes are similar to those of traditional composites, such as hand lay-up, vacuum-assisted resin transfer

molding (VARTM), and prepreg autoclave processing. The use of hybrid composites has been growing in various applications, including aerospace, automotive, marine, and civil engineering sectors (Tavares, 2015). The hybridization of glass and carbon fibers provides a cost-effective alternative to expensive CFRP while maintaining superior mechanical properties, such as tensile strength, stiffness, and fatigue resistance, compared to GFRP alone (Jangam, Reddy and Raja, 2018). In conclusion, glass/carbon hybrid composite materials present a promising solution to the ever-growing demand for advanced materials with tailored properties. Their unique combination of attributes, coupled with the potential for cost reduction and application-specific customization, paves the way for a new era in material engineering.

1.3 Silica Nanoparticles Reinforced Matrix

Silica nanoparticles, also known as silicon dioxide (SiO_2) nanoparticles, have garnered considerable attention in recent years due to their unique properties, such as high mechanical strength, low thermal expansion, and exceptional chemical stability (Brinker and Scherer, 2013). The incorporation of these nanoparticles into various matrix materials, such as polymers, metals, and ceramics, has emerged as an innovative approach for the development of advanced nanocomposites with enhanced mechanical, thermal, and electrical properties (Mittal et al., 2015; Lvov et al., 2016).

This field of research has attracted numerous researchers worldwide, as it holds promising potential for a wide range of applications, including automotive, aerospace, electronics, and biomedical industries (Balandin, 2011; Kumar et al., 2017). The reinforcement of matrix materials with silica nanoparticles can significantly improve their overall performance by tailoring the interfacial interactions between the nanoparticles and the matrix, which ultimately results in improved stress transfer and dispersion (Fu et al., 2008).

A plethora of studies have been conducted to systematically investigate the influence of silica nanoparticle reinforcement on various matrix materials. Furthermore, considerable efforts have been dedicated to understanding the role of surface functionalization and the size of silica nanoparticles in the reinforcement of matrix materials. Surface functionalization has been shown to improve the compatibility and dispersion of nanoparticles within the matrix, leading to better overall performance. On the other hand, silica (SiO₂) nanoparticle (SNP) is one of the most important nanofillers and found at the forefront in the field of polymer composite materials due to its abundance and high-performance features. (Karnati, Agbo and Zhang, 2020).

The distribution of silica nanoparticles within the epoxy matrix plays a crucial role in enhancing the properties of fiber-reinforced epoxy composite known as silica nanoparticle-reinforced fiber reinforcement. However, this high-performance fabrication process enhanced by silica nanoparticles faces significant challenges in achieving efficient dispersion of nanoparticles within the epoxy matrix. The main challenge in this context is achieving a consistent dispersion of individual silica nanoparticles in the epoxy matrix. This is because the interaction force between multiple nanoparticles is greater than that with the epoxy matrix at high loading (Wetzel, Hauptert and Zhang, 2003; Cho, Joshi and Sun, 2006).

Producing an optimized polymer nanocomposite using evenly distributed silica nanoparticles appears challenging due to the preference of nanoparticles for forming aggregates. Therefore, polymeric nanocomposites may exhibit worse mechanical performance than conventional molecular/polymer composite systems unless the problem of dispersion of nanoparticles in the polymer matrix is effectively addressed. Nanoparticles can be mixed with the polymer matrix using SONICS device that uses ultrasonic nanoparticle dispersion method (Patel and Purohit, 2018).

1.4 Glass and Carbon Hybrid Composite Materials with Nanoparticles

Glass hybrid composite materials with nanoparticles are a type of composite material that combines the properties of glass fibers with the unique properties of nanoparticles. The resulting material has improved mechanical properties, such as strength and toughness, as well as enhanced optical and electrical properties (Sathishkumar, Satheeshkumar and Naveen, 2014; Hussain, 2020)

Glass hybrid composite materials with nanoparticles have been the subject of extensive research in recent years. Nanoparticles, which are particles with dimensions less than 100 nm, have unique properties such as high surface area-to-volume ratio, quantum size effect, and surface energy, which can be utilized to enhance the properties of composite materials (Ma et al., 2013; Karnati, Agbo and Zhang, 2020).

Various types of nanoparticles, such as carbon nanotubes, graphene, metal oxides, and clay nanoparticles, have been used to enhance the properties of glass hybrid composite materials. These materials are a combination of carbon fibers and other reinforcing materials, that are integrated into a matrix material, such as epoxy resin or thermoplastic. Research in this area has shown that the properties of these materials can be tailored by varying the type, size, and concentration of the nanoparticles used, as well as the processing conditions during manufacturing. Furthermore, carbon hybrid composite materials with nanoparticles have been explored for various applications, including aerospace, automotive, energy, and biomedical fields (Zakaria et al., 2019).

The addition of nanoparticles to the carbon fiber-reinforced polymer (CFRP) matrix can improve the mechanical, thermal, and electrical properties of the resulting composite material. For example, graphene oxide (GO) nanoparticles can improve the mechanical strength and stiffness of CFRP materials, while

carbon nanotubes (CNTs) can enhance the electrical conductivity and thermal stability (Kinloch et al., 2018; Li et al., 2019).

1.5 Problem Statement

Glass/carbon hybrid composites are gaining attention due to their strength, stiffness, and lightweight properties. However, they face challenges in mechanical performance, fatigue resistance, and matrix toughness. The inherent differences between glass and carbon fibers make it difficult to optimize performance. Additionally, they are susceptible to fatigue failure under cyclic loading conditions, which reduces their lifespan. We need a toughened matrix to enhance energy absorption, resist crack growth, and boost durability and impact resistance. Addressing these issues will advance their application in high-performance, lightweight materials.

1.6 Aim and Objectives

1.6.1 Aims

In this study, glass-carbon hybrid composite laminates were manufactured with and without adding SiO₂ nanoparticles. The aims of this work consist of the following:

1. Manufacturing of laminate thickness and stacking sequence such as isotropic quasi-ply and cross-ply specific on the mechanical characteristics, such as tensile, bending, axial fatigue, and bending fatigue behaviors. The investigations were carried out experimentally, numerically using ANSYS simulation tool, and theoretically.
2. Investigating the effects of adding silicon dioxide (SiO₂) nanoparticles to the resin matrix on the mechanical properties of the laminates listed above.

1.6.2 Objectives

The research work has the following specific objectives:

1. Establish numerical models using ANSYS to predict tensile, bending, and fatigue behavior of hybrid composites.
2. Manufacture hybrid composite specimens with varying stacking sequences and thicknesses, while ensuring a consistent fiber volume percentage, through the process of design and fabrication. The fabrication process was conducted both with and without the addition of SiO₂.
3. Conducting tensile, three points bending, and fatigue test for the hybrid composite specimens with and without SiO₂ nanoparticles.
4. Figure out the failure mechanism of the specimens by using SEM.
5. Determining the properties of hybrid composite, such as modulus of elasticity in tension and three-point bending tests, of laminates.
6. Comparing the experimental, numerical, and analytical results reveals significant correlations, providing valuable insights for refining predictive methodologies.

1.7 Dissertation Layout

The chapters of this dissertation are organized under the following headings: Introduction, Literature Review, Theoretical Work, Experimental Work, Results and Discussions, and finally Conclusions and Recommendations for future work.

An outline of each chapter is provided below:

- Chapter One: Introduction. This chapter contains an introduction, which includes an overview of hybrid composite materials in general, reinforcement types, problem statements, and the aim and objectives of the study.

- Chapter Two: Literature Review. This chapter reviews the literature on various composite materials, manufacturing techniques, and mechanical properties.
- Chapter Three: Theoretical Work. This chapter examines hybrid composite materials, mechanical properties, quasi-static properties, and fatigue resistance. Lamina micromechanics and laminate macro-mechanics are used to start. Next, the chapter discusses how composite materials react to fatigue, focusing on event failure mechanisms.
- Chapter Four: Experimental and Numerical Work. This chapter describes the material selection, experimental setup, manufacturing of the laminates, apparatus selection for testing, and design and fabrication of the bending fatigue apparatus used in this study.
- Chapter Five: Results and Discussions. The findings of the experimental and numerical analyses are listed and discussed.
- Chapter Six: Conclusions and Recommendations. The significant findings of this work are presented in this chapter, along with some recommendations for future studies.

CHAPTER TWO

LITERATURE REVIEW

This chapter provides a comprehensive review of the previous research related to the mechanical properties of fiber-reinforced composites and nanoparticles such as silicon dioxide polymer composites. In addition, adequate review has also been done on the factors influencing fatigue crack growth and failure.

2.1 Introduction to Composite Materials

Composite materials, also known as composites, are specially designed materials that are created by combining two or more constituent materials with distinct physical or chemical properties. Joining these elements results in a composite that possesses distinct features not found in the individual components. Composite materials possess a significant benefit in their capacity to merge the positive attributes and reduce the negative aspects of their individual components, resulting in a material that exhibits exceptional performance in particular uses. Composites are generally categorized based on their matrix material, which serves to bond the reinforcements together (Pellicer, 2021).

Common matrix types encompass polymers, metals, and ceramics. The addition of reinforcement, typically in the form of fibers, particles, or flakes, enhances the strength and rigidity of the composite material. For instance, glass fibers embedded within a polymer matrix compose fiberglass, a commonly used composite material. Carbon fiber composites, renowned for their exceptional strength-to-weight ratio, consist of carbon fibers embedded within a polymer matrix. Several industries widely use composite materials due to their distinctive characteristics, which include a high strength-to-weight ratio, resistance to corrosion, and flexibility in design (Pettarin, 2016).

Composites play a critical role in the aerospace industry by effectively decreasing aircraft weight, resulting in enhanced fuel efficiency and overall performance. The automobile industry uses composites to achieve lightweighting in order to optimize vehicle economy and minimize emissions. Moreover, composites are of utmost importance in the fields of building, sports equipment, and renewable energy, specifically in the manufacturing of wind turbine blades. Advancements in material science and engineering are driving ongoing progress in the creation and use of composite materials. Scientists are continuously investigating novel combinations of materials and production methods to improve the efficiency and eco-friendliness of composites, therefore facilitating their incorporation into a broader range of uses (Ngo, 2020; Agrawal *et al.*, 2022).

2.2 Fiber-Reinforced Composite Materials

The reinforcing matrix is the main parameter for classifying composite materials into metal matrix composites (MMC), ceramic matrix composites (CMC), and polymer matrix composites (PMC) (Lu, Weng and Cao, 2006). Because polymer matrix composites may be easily customized to meet the user's specific needs, they are the most preferred material for engineering and structural applications (Beg, 2007). The composites may be categorized as polymer or natural fiber based on the matrix. Short or continuous fibers are encased in an organic polymer matrix to form polymer matrix composites. PMCs, or polymer matrix composites, possess numerous advantages compared to conventional composites. They are characterized by their lightweight, high strength, and high stiffness, among other desirable properties. However, the utilization of PMCs has become limited due to the adverse ecological impacts they have on the environment (Rajak *et al.*, 2019).

2.2.1 Fiber Glass Reinforced Composite Materials

Morampudi *et al.* (2021) conducted a study on glass fiber-reinforced polymer (GFRP) composites. These composites were manufactured using several types of glass matrix materials and various manufacturing techniques. Glass fibers have excellent characteristics such as high strength, flexibility, stiffness, and durability. The characteristics of GFRP composites improved as the amount of glass fiber components increased.

El-Assal and Khashaba (2007) studied the fatigue behavior of GFRP composites subjected to simultaneous torsional and bending loads stepwise at room temperature. Various theories of failure were used to create the failure model of the GFRP composite via a series of rigorous torsional fatigue experiments. The obtained stress-strain curves were analyzed and contrasted with the findings from both tension and fatigue tests. The results indicate that unidirectional glass fiber-reinforced polyester composites have lower torsional fatigue strength than the experimental findings of pure bending fatigue strength. The quantity of stress cycles likewise increases with the augmentation of fiber volume fraction. The failure curves derived from the experimental data exhibit strong concordance with the predictions made at various processes.

EL-Wazery *et al.* (2017) conducted a study on the significance of glass fiber-reinforced polyester composites in various applications due to their superior specific strength, stiffness, and modulus. This study involved the development of a reinforced polymer composite using E-glass fibers arranged in a random orientation. The composite was created using the hand lay-up approach with different weight percentages of fibers (15%, 30%, 45%, and 60%). An investigation was conducted to examine the impact of the percentage of glass fiber on mechanical parameters, including tensile strength, bending strength, and impact strength. The hardness of composites was assessed using a Brinell

hardness tester. As the glass fiber contents increased, the results showed a significant improvement in the mechanical characteristics of the composite.

2.2.2 Carbon Fiber Reinforced Composite Materials

High stiffness, high tensile strength, low weight, strong chemical resistance, high-temperature tolerance, and minimal thermal expansion are some of the characteristics of carbon fibers. Because pitch-based carbon fibers have a highly graphitized structure and a high modulus, they are used commercially in the racing, civil engineering, and aerospace sectors by making laminated samples with a cross-ply arrangement. But it is somewhat pricey compared to other fibers, like glass fiber (Park, 2018).

Alen and Sanu (2014) stated that carbon fiber reinforced epoxy and carbon fiber reinforced polymer (CFRP) are very robust and lightweight polymer composites with carbon fibers. CFRP is composed of carbon fiber and epoxy, and these two components determine the material qualities. The strengthening will enhance the strength and stiffness of the CFRP. Contrary to isotropic materials like steel, CFRP exhibits directional strength properties. The properties of CFRP depend on the configuration and proportion of carbon fiber. CFRP, or carbon fiber reinforced polymer, has become a viable alternative to traditional materials like steel and iron in various applications. This is due to its advantageous features, including an ease of producing complex shapes, excellent fatigue resistance, high tensile and compressive strength, and low coefficient of thermal expansion.

Rahmani *et al.* (2015) looked into the elastic properties of T700 CFRP, which is used in the aerospace industry. They discovered that the fiber orientations played an influential role in the laminated composites' strength. In a different study, Bitkina, Lee, and Darlington (2016) conducted experiments to determine how the disorientation angle affected the deformation of carbon composite plates. Various industries, such as aviation, wind energy, and aerospace, employ eight-

layer carbon composite structures, making these findings applicable in an industrial setting. Researchers have discovered that raising the disorientation angle enhances the deformation of the composite structures, as it alters the symmetry of the composite layered structure.

Robertson *et al.* (2018) examined thermosetting epoxy matrices in most carbon fiber reinforced polymers (CFRPs), particularly in aerospace applications requiring a high ratio of strength and stiffness to weight. Over the years, advancements have been made in aerospace epoxy thermosetting matrices to enhance the binding strength between carbon fibers and the matrix and improve the mechanical characteristics. In recent years, there has been a significant reduction in the time it takes for thermosetting resins to cure. This decrease has been particularly notable for specific chemical compositions, with curing times dropping from several hours to less than a minute.

2.3 Hybrid Composite Materials

Fiber-reinforced polymer laminated composites (FRPC) are progressively substituting traditional metals in structural uses such as aerospace, vehicles, and turbine blades. These properties are a result of their high specific strength (ratio of strength to density), high specific stiffness (ratio of modulus to density), lightweight composition, and enhanced resistance to corrosion, wear, and fatigue (Ab Ghani, Ngatiman, *et al.*, 2021). The two most common types of fibers utilized in manufacturing are glass and carbon. While carbon fiber possesses impressive strength and modulus, its limited strain-to-failure ratio renders it unsuitable for standalone usage in structural components. To overcome the limitations of carbon fiber, structural components incorporate an alternative material, glass fiber, as an additive. Glass fiber possesses a lower strength and modulus compared to carbon fiber, but it exhibits a higher strain-to-failure ratio (Jiang *et al.*, 2022). Establishing an ideal bond between the fiber and matrix is crucial for efficient

transmission of loads from the matrix to the fiber. Adding nanoparticles or microparticles as reinforcement to the matrix makes the hybrid laminated epoxy composite better at supporting weight.

Nanofillers commonly use concentrations ranging from 0% to 2% to prevent particle aggregation in the matrix, which can deteriorate mechanical characteristics (Matykiewicz, 2020).

2.3.1 Fiber-Hybrid Composites

Research on hybrid composites, which employ two or more reinforcements to strengthen a matrix material, is currently at a significant level. The main goal of hybrid composites is to address the limitations of single-reinforcement composites by including an additional type of reinforcement. In addition to the qualities, there are instances where the cost of reinforcing is prohibitively high, making composite production impractical for common applications. Consider carbon fibers as an example, which are renowned for their exceptional strength and rigidity but exhibit limited resistance to impacts and come with a significant price tag. Glass fibers, with their exceptional resistance to strain-induced failure and affordable cost, resolved this issue. Researchers have tested hybrid composites for a variety of applications, including wind turbine blades, automotive drive shafts, and fuselage structures (Badie, Mahdi and Hamouda, 2011; Naito and Oguma, 2017).

In their study, Ghafaar *et al.* (2006) found that full-carbon composites exhibit the highest bending stress and stiffness, while full-glass fiber laminates have the lowest values. The difference in bending strength between the two materials is around four times greater, as documented in another study (Madhavi *et al.*, 2021). Consequently, the inclusion of carbon fibers on the sides of glass fiber composites that experience tension will result in an increase in flexural strength. Conversely, on the side that experiences compression, the strength will decrease (Sudarisman,

de San Miguel and Davies, 2009; Madhavi *et al.*, 2021). Dong and Davies, (2012) found that the greatest flexural strength is obtained when the glass fibers make up approximately 12.5% of the material and are all positioned on the compressive side. (Oskouei and Taleie, 2010) found that the flexural strength of hybrid carbon/glass composites is 40% and 9% higher than that of all-carbon and all-glass composites, respectively. However, the tensile and compression strength of Kevlar fibers significantly differ, influencing the flexural characteristics of composites reinforced with these fibers. For example, the strain on the compression side is greater than the strain on the tension side. This causes the neutral axis to shift towards the side experiencing tension as the compressive yield area expands. These materials can undergo nonlinear plastic deformation due to structural flaws in the fiber chain under axial compression or bending.

Ortega *et al.* (2017) conducted an experiment to evaluate the translaminar fracture of nine inter-ply hybrid laminates. Weaved carbon fabric, glass fabric, and unidirectional carbon tape combine to create laminates. Tensile and compressive tests were conducted on the translaminar fracture characteristics of all specimens. The positioning of material plies along the thickness does not affect the compact tension and compression. Blending woven glass and carbon plies and inserting carbon fibers in the laminate's outer plies increases compact compression. Blocking multiple loading-direction unidirectional plies promotes compact-tension specimen energy dissipation. Ply blocking enhances matrix fractures and delamination, releasing energy and decreasing crack tip stress intensity. The mixing hypothesis was evaluated to estimate inter ply hybrid laminate toughness using single-material ply data. The mixing hypothesis comes close to describing hybrid laminates' toughness, but it ignores how material orientation and stacking sequence affect translaminar fracture propagation.

2.3.1.1 Glass/Carbon Hybrid Composite Materials

Zhang *et al.* (2012) conducted research on five different kinds of composite laminates, namely [C]₈, [C2G2]_s, [CG3]_s, [CGCG]_s, and [G]₈ composites. These composites were subjected to static loading in tension, compression, and three-point bending. A glass-carbon (50:50) fiber reinforcement was used in order to significantly increase the tensile, compressive, and flexural strength of the plain glass fiber composite. This reinforcement was implemented either by positioning the carbon layers on the outside of the composite or by positioning various kinds of fibers in alternating positions. Using the same hybrid composition, the stacking sequence did not have any discernible effect on the tensile characteristics; nevertheless, it had a considerable impact on the flexural and compressive properties.

A unique kind of hybrid composite was produced by Nagaraja *et al.* (2019) reinforcing carbon and E-glass into an epoxy matrix with seven plies. These novel mixed composite materials are made using the resin infusion technique, which maintains the 0°/90° orientation of each layer of fibers. The impact of varying the stacking order of the glass and carbon layers on different mechanical characteristics has been investigated. The fiber-to-matrix ratio is kept constant at 60:40. Where they ascended and conducted a comparison between two distinct stacking sequences. The findings of comparing the laminates with and without carbon fiber on the extreme surfaces showed that the laminate with carbon fiber on the outer surfaces produced superior flexural characteristics. Additionally, the effects of the orientation of each layer and the location of the fiber reinforcement on the mechanical behavior of the materials were investigated based on an investigation of glassy carbon composites. Comparing the mechanical characteristics of stacking sequences with the results of the conducted experiments.

The effects of stacking order on the strength of hybrid composites made of materials with varying stiffness and stability were studied by Zhang *et al.* (2012) where glass and carbon-woven fabrics were combined in different ratios inside an epoxy matrix to create hybrid composite laminates. Various static tests, such as tension, compression, and three-point bending, were performed on composite laminates with different carbon-to-glass ratios. According to the findings, hybrid composite laminates with 50% carbon fiber reinforcement provide the most excellent flexural qualities when the carbon layers are on the outside, and the maximum compressive strength is achieved with an alternating carbon/glass lay-up. The stacking order does not affect the tensile strength. Additionally, analytical solutions are created and shown to have a strong connection with the experimental data, enabling the hybrid composite stacking sequence to be optimized for optimal strength.

Researchers (Zhang *et al.*, 2012; Mandal, *et al.*, 2018; Mohanty, *et al.*, 2018; Nayak, *et al.*, 2018; Jesthi and Nayak, 2019; Kamal, Hassan and Khdir, 2024) examined the effect of hybrid ratio and stacking sequence of woven carbon and glass on the stiffness and strength of inter-ply hybrid (FRP). Researchers assessed the mechanical properties of the glass-carbon (G:C) hybrid when the ratio of glass to carbon was 1:1. This evaluation involved placing carbon layers either alternating different types of layer or on the surface (Zhang *et al.*, 2012). In the studies by (Mandal, *et al.*, 2018; Mohanty, *et al.*, 2018; Nayak, *et al.*, 2018; Jesthi and Nayak, 2019), in total, ten layers of glass and carbon (laminated composites) were manufactured. The [G/C/G/G/C]s exhibit greater flexural and tensile strengths compared to the [C/G/G/C/G]s. On the other hand, [C/G/G/C/G]s demonstrate a greater flexural and tensile modulus, with a 20 percent and 36.2 percent increase, respectively, in comparison to [G/C/G/G/C]s (Nayak, *et al.*, 2018). The tensile strength, flexural extension, and stresses of [G3C2]s were 11.5 percent, 23 percent, and 39 percent more than [C2G3]s, respectively. However,

the modulus and flexural strength of [C2G3]s were 23 percent and 64 percent more than [G3C2]s (Mohanty, *et al.*, 2018). Compared to [CG3C]s, the tensile strength and flexural strength of [G2C2G]s were 10.5% and 2.5% higher, respectively. Additionally, the flexural extension and tensile strain of [G2C2G]s were 17.5 percent and 35.8 percent more, respectively, than those of [CG3C]s (Mandal *et al.*, 2018).

Abed, Faris and Naemah (2023) looked at how fiber orientations affected the mechanical characteristics of composite materials used in airplanes. They employed graphite powder, carbon fiber Sikawrap-301 C, e-glass fiber EWR450, and aluminum alloy sheet 2024-T3 for manufacture, taking into account two alternative fiber-to-matrix ratios. The hand lay-up method was used to make samples of carbon fiber, glass fiber, and glass carbon fiber, which were then put through tensile and flexural tests using standard testing equipment. The results of the tensile tests showed that, although a 45° orientation of the fiber produced the maximum stress resistance for single-layer samples, the strength of double-layer carbon fiber-reinforced polymer (CFRP) composites declined with increasing fiber orientation. Flexural testing revealed that, compared to glass carbon fiber and glass fiber orientations, the 45° carbon fiber orientation displayed greater strength. Overall, the mechanical characteristics and adhesion were enhanced by fiber orientation, and carbon fiber-reinforced aluminum laminates were lighter than aviation wing alloy 2024-T3 as a result.

The mechanical and dynamic characteristics of these items (C1, C1WN, C2, C2WN, Q1, Q1WN, Q2, and Q2WN) are examined and confirmed using experimental and numerical methods, including the utilization of the finite element method (ANSYS workbench). The researchers have found that the items C1, C1WN, C2, C2WN, Q1, Q1WN, Q2, and Q2WN demonstrate exceptional mechanical and dynamic characteristics. The stacking sequence GGCCCCGG has

superior tensile capabilities, whereas GCCGGCCG demonstrates superior flexural qualities (Kamal, Hassan and Khdir, 2024).

GuruRaja and Rao (2013) investigated samples made using epoxy resin as an adhesive and oriented towards various carbon/glass hybrid layer orientations. For the research, they considered three directions: $0^\circ/90^\circ$, $45^\circ/45^\circ$, and $30^\circ/60^\circ$. The hybrid composites' mechanical characteristics, including their tensile strength, tensile modulus, and maximum load, were ascertained per ASTM guidelines. The hybrid samples were produced using the vacuum packing technique. When compared to other directions, it was found that the angle layer direction at $0^\circ/90^\circ$ had a much higher tensile property. The interfacial characteristics of carbon-woven glass hybrid composites were assessed qualitatively using scanning electron micrographs of shattered surfaces. The findings indicate that increasing laminate thickness enhances tensile strength, with a 1 mm increase requiring 40–50% more load for fracture, particularly in the 30° orientation. Elongation and Young's modulus also increase with thickness in tensile tests. Conversely, flexural stress and Young's modulus increase as thickness decreases. More load is needed to fracture laminates at 90° orientation, while the highest elongation occurs at 45° and minimal elongation at 30° .

Motoc, Bou and Gimeno (2015) conducted a study to examine the influence of mechanical properties on differentiating between materials that are stiff and strong, considering both static and dynamic loading as well as uniaxial and multi-axial loading. How the hybrid composites deform when exposed to static loading differs from that of traditional composites is an intriguing question that academics and industry practitioners frequently pose. Due to its tensile modulus of elasticity and more likely failure to strain ratio compared to carbon fiber, glass fiber enhances the hybrid composites. It is crucial to consider the tensile parameters, such as the tensile modulus and tensile strength in both the longitudinal and transverse directions and the failure strain, while aiming to achieve cost savings.

Sivakandhan and Prabhu (2015) attempted to construct drive shafts out of composite materials such as E-glass, carbon fiber, and hybrid composite layers of E-glass, carbon, and S-glass with varying fiber orientations. Tensile, bending, and torsion tests were used to investigate the strength of the fabricated composite drive shafts. They discovered that the hybrid composite shaft had extremely high strength qualities and the requisite bending stiffness compared to previous composite beams.

Kumar, Krishna and Rajanna (2014) presented research investigating carbon fiber and glass fiber composites' tensile, and flexural characteristics. Hand layup method is used to create samples in compliance with ASTM standards for varied thicknesses of 2 mm and 3 mm and fiber orientations of 30 degrees, 45 degrees, and 60 degrees. The characteristics of composite materials are studied by fitting various materials together to acquire the required qualities by increasing the thickness and orientation of the fibers. The tensile strength of the hybrid composite was measured at different thicknesses and compared to the findings of finite element analysis. The test-ready specimens were exposed to tensile and bending stresses on the universal testing machine (UTM). They discovered that the tensile and flexural strength of laminated polymer composites is mainly determined by fiber orientation and thickness.

Irina *et al.* (2015) looked into three different hybrid configurations of carbon fiber and E-glass fiber and tested them in the lab: [CWW]₆, [BC]₆, and [CBBC]₃. C, W, and B represent carbon fiber, E glass stitch biaxial (± 45), and E glass plain woven, respectively. The [CWCW]₆ configurations, where better characteristics obtained with C and W manufactured from woven carbon and glass fiber, in a tensile test. It was shown that the [CWW]₆ configuration of carbon and woven glass fibers could sustain stress in the direction of 0° textiles. Figure 2-1 displays the tensile characteristics of the composites that were assessed. It illustrates how biaxial layup may reduce tensile modulus and tensile strength due to failure in the

in-plane shear direction. The pattern of the weave is robust at points of tension and in other directions where the stresses disentangle them. Stronger yarn may be produced because there are more secondary bonding pressures between the fibers when they are packed closely together. This pertains to the study's quasi-isotropic layup, which has an orientation similar to the pattern's weave.

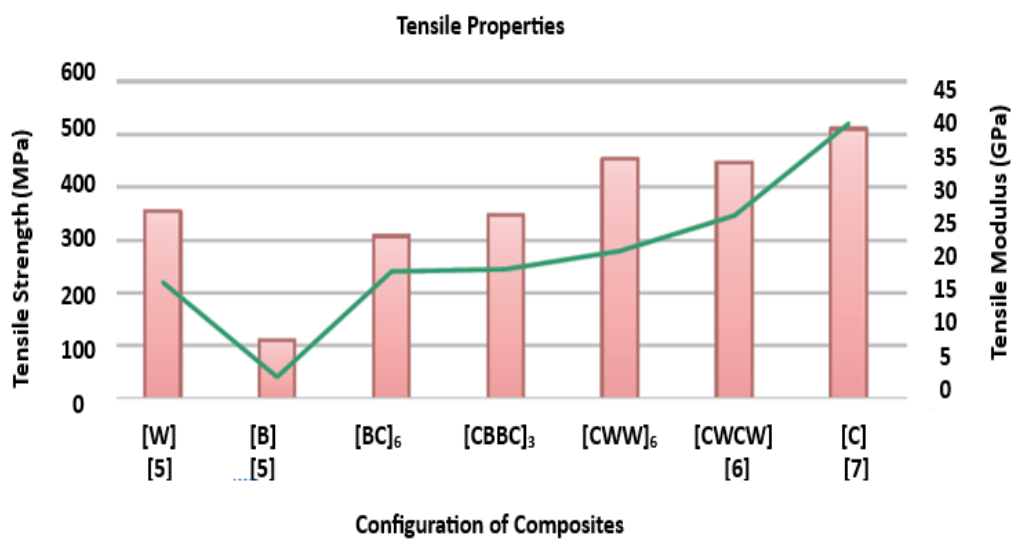


Figure 2-1 Tensile characteristics for different stacking of hybrid composite (Irina et al. 2015)

Jagannatha and Harish (2015) manufactured hybrid composite materials by combining several fiber types implanted in the same resin matrix. The mechanical properties of an epoxy hybrid composite reinforced with glass and carbon fibers were also investigated. The hybrid composite materials were created using the vacuum packing technique. Furthermore, the mechanical parameters of the hybrid composites, such as hardness, tensile strength, tensile modulus, flexibility, and maximum load, were determined using ASTM standards. The mechanical properties of the matrix were enhanced by increasing the fiber-reinforcing content.

Dixit and Padhee (2019) conducted a study on composite specimens made from five distinct types of fibers, which included natural fibers (banana, cactus, and

jute) and synthetic fibers (glass and carbon). Various configurations were selected using permutation and combination methods. After designing the model, multiple finite element method (FEM) analyses were performed with 'ANSYS' Mechanical APDL, applying a point load to the samples. The results indicated that synthetic fibers, specifically carbon and glass, show potential as viable alternatives for designing composites with high strength and deformation resistance. Conversely, natural fiber composites are recommended for applications requiring intermediate strength and environmental sustainability.

Ghani *et al.* (2021) investigated the hybrid composite deformed under flexural, shear, and tensile stresses in a study. They also focused on the most recent advances in vehicle mechanics, which provide the fundamental basics to understand the behavior and deformation of hybrid composites under different various loading circumstances. In their work, they also studied the mechanical behavior of hybrid composites under static loading (tension, shear, and flexure). Understanding the principle regulating the mechanism of sheet composites exposed to a load, this applies to Carbon/Glass fiber reinforcement polymer hybrid composites, is critical. Fibers with high modulus of elasticity provide load-bearing and stiffness capacities to the composite, while fibers with low modulus provide more durable and cost-efficient. They discovered the hybrid composite characterization in their study. Tensile stress, shear loading, and bending of the hybrid composite are all predicted to cause complex deformation. The link between the various compositions of the hybrid composite was investigated in terms of tensile characteristics, shear property characterization, and bending deformation. Carbon-fiberglass-reinforced hybrid composites are an alternative to standard metal materials and have potential uses in aviation component manufacture in contemporary aircraft.

2.3.2 Nanoparticles Hybrid Composite Materials

Nanocomposites (NCs) are a hybrid material that combines the finest qualities of nano-fillers and polymers. Polymers are materials that are easily made, have a low weight, and are ductile. Nano-fillers, on the other hand, demonstrate better physical, chemical, and even electrochemical properties (Lu, Weng and Cao, 2006). In addition to this, they exhibit strong thermal and mechanical durability, as well as stiffness (Kango *et al.*, 2013). In the process of reducing the size of the nanofiller materials to less than 100 nanometers, they exhibited remarkable characteristics that were distinct from their microstate (Mallakpour and Mani, 2014). Nanoparticles (NPs) change the way molecules interact at the phase interfaces of the materials that are made when they are added to the polymer matrix (Camargo, Satyanarayana and Wypych, 2009). This is because nanoparticles have a high surface-to-volume ratio, which can be measured in terms of their specific surface area. Furthermore, the synergy between two different components bestows exceptional qualities on the NCs, and these features may be used in a wide variety of advanced domains, such as the automotive and aerospace industries, packaging materials, coatings, building supplies, sports commodities, and so on (Kango *et al.*, 2013). Up to this point, a variety of attempts have been made to optimize the attributes of NCs in order to adapt them for the many applications that have been developed.

According to the research by Ajaj *et al.* (2013), they looked into how epoxy/SiO₂ nanocomposites wear down over time with different amounts of SiO₂ nanoparticles (1%, 3%, 5%, 7%, and 10%). They used atomic force microscopy (AFM) and scanning probe microscopes to measure the particle size of the SiO₂ nanoscale particles. The composites with a volume proportion of SiO₂ nanoparticles that were determined to have the lowest roughness were the ones that they discovered to have the lowest roughness. Epoxy/SiO₂ nanocomposites were made stronger with six layers of chopped mat E-glass fiber. The fatigue

behavior of these composites was also described. The rotational bending technique was used to conduct the fatigue test, and the kind of loading used was a sinusoidal wave with a stress ratio of ($R = -1$). The loading frequency used was 5 Hz, and it is claimed that this combination resulted in a temperature increase that was insignificant during the time of the test. Following the analysis of S-N curves, the values of fatigue strength, fatigue life, and fatigue limit of the composites that were tested are presented. The findings indicate that the incorporation of SiO₂ nanoparticles leads to an increase in fatigue values; however, the most significant improvement was seen in the epoxy/SiO₂ nanocomposite that was reinforced with six layers of chopped mat E-glass fiber layers.

Ngah and Taylor (2018) describe the first practical application of hybrid toughening to improve the quasi-static interlaminar fracture energy, G_{IC} , and the fatigue threshold strain-energy release rate, G_{th} . Using carboxyl-terminated butadiene acrylonitrile (CTBN), a chemical that can make rubber particles as small as a few microns and silica nanoparticles as large as 20 nm, strengthened amine-cured epoxy glass-fiber composites well. It was determined that the processes responsible for toughening include the cavitation of rubber particles and the debonding of silica nanoparticles, by followed the formation of a plastic void structure. In addition to the nanoparticles, the CTBN contributes significantly to the enhancement of G_{IC} . Both particles, when combined as a hybrid, have a synergistic impact on the fatigue resistance of the overall material. This highlights the efficacy of hybrid toughening, which makes it possible to develop composites optimized by combining microparticles and nanoparticles, respectively.

The role of surface-functionalized crystalline nanosilica addition to epoxy resin was explored by (Dani and Venkateshwaran, 2021). Their research focused on the effects of this addition on fatigue, fracture toughness, and drop load impact damage behavior with different stacking sequences of E-glass fiber. Identifying

the significance of surface-functionalized crystalline nanosilica particles in E-glass fiber-reinforced epoxy composites was the primary purpose of this experiment that is now being carried out. For reinforcements, crystalline nanosilica with a 20nm particle size and E-glass fiber with a 600 grams per square meter (GSM) were used. The 3-Amino propyl trimethoxy (APTMS) method was used to add functional groups to the surface of both the particles and the fiber. Different fiber stacking sequences were used in the preparation of the hybrid composites, which were made using the hand layup method. According to the findings of the mechanical tests, the L.A.L has stacking sequence ($0^{\circ}/90^{\circ}/45^{\circ}/0^{\circ}/90^{\circ}$) fiber pattern that included 1.0 volume percent of nanosilica proved to have the maximum tensile and flexural strength. Upon analysis of the fatigue findings, it was discovered that the incorporation of 0.5 volume percent of crystalline nanosilica into the glass-epoxy composite symmetry (ES_1) resulted in the greatest fatigue life cycle of 38544 in 50% of tensile stress. Similar to the previous point, the results of the fracture toughness test showed that the composite designation glass-epoxy composite symmetry (ES_2) had the greatest fracture toughness, which was measured at 31.5 MPa. Very high drop-load impact resistance is provided by the composite material, which has a surface-functionalized crystalline nano-silica fiber pattern and comprises 1.0 volume percent of surface-functionalized nano-silica. It is thus possible that these composites might be better suited and substituted for applications involving high-strength structural applications, automobiles, airplanes, and sports-related applications.

According to Blackman *et al.* (2007), the incorporation of nano-silica particles into an epoxy polymer resulted in a significant enhancement of the epoxy polymer's cyclic-fatigue behavior. This development was accompanied by an increase in the initial toughness of the epoxy polymer, as measured by fracture toughness, K_{Ic} . Because of this, the considerable increases in the values of the

range of applied stress-intensity factor at threshold, ΔK_{th} , that were obtained from cyclic-fatigue tests for nanosilica-modified materials are highly remarkable. Another reason why these increases are very noteworthy is that they come with significant improvements in initial toughness.

Zheng, Ning and Zheng (2005) looked at the inclusion of SiO₂ nanoparticles, which were manufactured in order to explore the impact that they had on the mechanical characteristics. The positron annihilation spectroscopy technique was used in order to determine the size and concentration of the free volume. According to the findings of the experiments, the uniform dispersion of nanoparticles is a significant factor that contributes to the enhancement of the overall performance of nanocomposites. At three weight percent of nanoparticles, an increase of 115%, 13%, and 60% in tensile strength, tensile modulus, and impact strength, respectively, was accomplished without any adverse effects. According to the research that looked at how SiO₂ nanoparticles affect the properties of glass-fiber composites, the SiO₂ nanoparticles can generally make the properties of the composites better, especially the bend strength, which goes up by 69.4%. The presence of nanoparticles is responsible for the increased bonding forces that occur between glass fibers and matrices. This is the reason for the observed phenomenon.

2.4 Fatigue of Composite Materials

The majority of applications employing hybrid composites function under fatigue loading conditions and are exposed to an extensive number of fatigue cycles throughout their operational lifespan. In fact, existing literature substantiates that fatigue or fatigue-associated mechanisms are the predominant failure modes in conventional engineering components (Hofer, Stander and Bennett, 1978; Booker, Raines, and Swift, 2001).

Ribeiro, Sena, and Vassilopoulos (2021) investigated the fatigue performance of these materials under cyclic loading conditions. They found that hybrid

glass/carbon composites exhibited superior fatigue resistance compared to carbon/carbon composites. The enhanced performance was attributed to the synergistic effects between the glass and carbon fibers, which led to an efficient load-sharing mechanism between them. The study also demonstrated the influence of various factors, such as fiber orientation, stacking sequence, and load ratio, on the fatigue life of hybrid composites. The authors highlighted the importance of understanding these factors to optimize the design and application of hybrid composite materials in different industries.

Vassilopoulos (2020) provided a comprehensive overview of the development and evolution of fatigue studies in fiber-reinforced polymer (FRP) composite laminates. The author traced the historical advancements in understanding the fatigue behavior of these materials and highlighted significant milestones in both experimental and theoretical research. Furthermore, Vassilopoulos emphasized the growing importance of FRP composites in various industries due to their superior mechanical properties, such as high strength-to-weight ratio, corrosion resistance, and design flexibility. The author also identified knowledge gaps and areas that warrant further investigation, such as multiscale modelling, damage mechanisms, and real-time monitoring techniques, to enhance the understanding and prediction of fatigue behavior in FRP composite laminates.

According to Goutianos and Sorensen (2021) fatigue damage in composite structures like wind turbine rotor blades is studied using a representative element test specimen with ply drops. Examining the rate at which delamination cracks from thin to thick sections is the aim. With the exception of one, which doubled its development rate in thicker portions, the majority of delamination fractures started as tunneling cracks and ceased expanding after a few cycles. Results from the finite element method support experimental findings. The primary emphasis of the research is on Crack, 1's crack development rate and how it varies as it passes through various thicknesses. Although tunneling fractures are difficult to

stop, neither the integrity nor stiffness of the structure are significantly impacted. Concerning only Crack 1, which is located between Ply Drop 1 and the Composite Beam, although interlaminar characteristics may be changed to limit development, thicker areas will still experience faster growth, as shown in Figure 2-2. Therefore, while predicting fracture growth cycles, geometry effects should be taken into account. Preventing delamination from reaching the next ply drop might be a design criterion. Further research into the effects of friction and fiber bridging on crack propagation rates is advised.

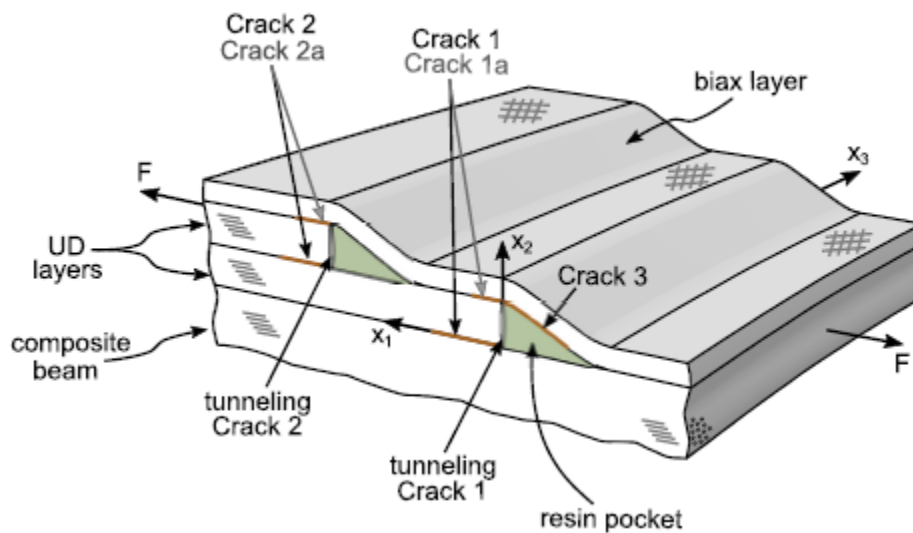


Figure 2-2 A schematic illustration of two-ply drops together shows potential fractures, tunneling cracks, and delamination cracks (Goutianos and Sørensen, 2021)

Song and Lim (2007) explored the fiber orientation of polymer composites, which are frequently used in the aerospace and automotive sectors, utilizing microtoming techniques, and their fatigue behavior under mechanical stress. Tensile tests and scanning electron microscopy (SEM) were used to examine the mechanical characteristics of polycarbonate (PC) composite parent and weld sections. In low-cyclic-loading testing, tensile and hardness parameters were found to be fiber orientation dependent, and fatigue crack development behavior differed between parent and weld sections depending on fiber orientation.

Conclusions indicated that mold location impacted microstructure and fiber orientation, with weld lines considerably lowering injection-molded component strength owing to fiber orientation rather than bonding condition. During tensile stress, fiber debonding from the PC matrix occurred, and fracture lengths were consistent across measuring methodologies. The rate of fatigue crack development seemed to be influenced by fiber orientation, with fracture initiation occurring at the fiber-matrix interface and developing under repeated fatigue stress.

Using an end-notch flexure test (ENF), Bieniaś and Dadej (2020) looked into the rate of fatigue delamination growth (FDG) in composite laminates made of aluminum and carbon/glass fibers. The findings indicated that the epoxy matrix controls the fatigue delamination threshold at metal-composite interfaces, while the cohesiveness between the fibers and the matrix determines the FDG rate. Compared to carbon fiber-reinforced laminates, glass fiber-reinforced laminates had superior delamination growth resistance, with adhesive joint Al/GFRP exhibiting higher fatigue delamination growth resistance owing to a higher static critical strain energy release rate. Both laminates' fatigue delamination growth rates tended to converge on a single threshold value, and abnormalities in the stress state during the end notch flexure (ENF) tests had an impact on the fatigue delamination growth (FDG) rates. The report suggests examining test findings for maximum delamination lengths of half the supporting fixture's span and taking friction between newly formed surfaces into consideration.

Arora *et al.* (2023) investigated the fatigue behavior of glass-filled epoxy composites exposed to cyclic loading with glass fiber volume fractions of 0%, 5%, 10%, and 15% embedded in the epoxy matrix. Mechanical characteristics are evaluated using monotonic tensile loading and tension-tension cyclic fatigue loading, and in-situ low cycle fatigue testing is used to investigate the damage processes that lead to fracture initiation and propagation. Fracture initiation

behavior and longevity are influenced by many fracture initiation locations, including the epoxy-fiber interface, matrix, and fiber. Fractography indicates that the volume fractions of glass fibers have a major influence on fracture coalescence, propagation, and failure, with 10% volume fraction specimens displaying the longest fatigue life under cyclic loading. The goal of the research is to characterize the behavior of particulate polymer composites under cyclic loading using low cycle fatigue experiments on epoxy resin reinforced with various volume fractions of glass fibers. In-situ studies of fatigue crack starting sites and fractures allow for a comprehensive connection between fractographic investigation and crack propagation. The maximum ultimate tensile strength (UTS) and failure strain for pristine epoxy specimens, higher UTS and elastic modulus with increasing glass fiber volume fraction, and varying crack initiation and fatigue life dependent on glass fiber content are among the key results. Factors such as matrix-fiber interface, fiber orientation, and glass fiber volume fraction all impact fracture initiation and propagation behavior, with 10% V_f specimens having the longest fatigue life due to delayed crack propagation.

Accurately Kennedy, Brádaigh and Leen (2013) produced a multiaxial fatigue damage model for fiber-reinforced polymer composites that takes into account fatigue-induced fiber strength and modulus deterioration, irreversible cyclic strain effects, and inter-fiber fatigue. The static failure component of inter-fiber fatigue is based on a fatigue-modified version of the Puck multiaxial failure criteria. The model is constructed in a user material finite element subroutine and calibrated against unidirectional glass fiber epoxy fatigue test data. A set of uniaxial fatigue tests on quasi-isotropic glass fiber epoxy laminates confirms the approach across a wide range of stress levels. The model improves on an existing quasi-static technique for predicting damage caused by the initial fatigue cycle on glass fiber-reinforced polymer laminates, as well as continuous matrix-dominated modulus damage throughout fatigue cycling. It takes into consideration fiber direction

damage, as well as creep strain caused by tensile stress. Predictions are produced at the ply level, allowing for the modelling of any laminate arrangement and its fatigue cycle behavior. The model predicts stiffness loss in the first few fatigue cycles of quasi-isotropic laminates, as well as total laminate stiffness decreases before eventual breakage. However, at high stress levels, it overpredicts deterioration. When compared to experimentally determined fatigue life, the model predicts fatigue life.

Yan Ma *et al.* (2017) used the same carbon fibers but two distinct matrices, thermoplastic polyamide 6 and thermosetting epoxy, to create two different forms of unidirectional carbon fiber reinforced plastic. The research assessed the mechanical characteristics and failure behaviors of both kinds of laminates using many on-axis tensile tests, taking into account fiber dispersion, impregnation conditions, and interfacial shear strength. As a consequence of the epoxy resin's capacity to wet fibers in their pre-polymer state, the findings demonstrated that fibers in epoxy laminates had a more uniform distribution than those in polyamide 6 laminates. Polyamide 6 laminates showed greater interfacial shear strength than epoxy laminates when fiber impregnation was effective. However, polyamide 6 laminates performed poorly without the proper impregnation. Both kinds of laminates' tensile strengths were within the Weibull distribution, with the epoxy laminate having a larger Weibull modulus. Epoxy laminates did not exhibit an evident crack or fiber breaking until ultimate failure, but the fracture process of polyamide 6 laminates displayed matrix cracking and fiber breakage prior to ultimate failure as shown in Figure 2-3.

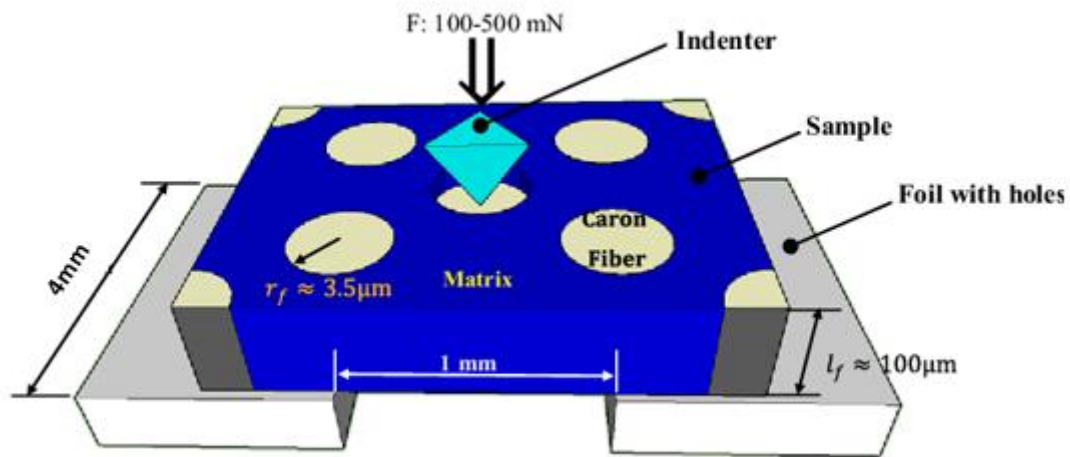


Figure 2-3 Illustration of single-fiber push-out test's layout (Ma et al., 2017)

Composites are becoming more common, although they are more costly and harder to comprehend and anticipate than traditional metals. However, the benefits of composite materials are critical to the demands of the industry. For example, in military equipment such as airplanes and ships, the lighter weight of composite materials allows for longer missions before refueling, while the use of composite materials significantly reduces the chance of enemy detection (Haller, 2020).

2.5 Summary

After reviewing numerous studies on hybrid composite materials involving glass fiber and carbon fiber and investigating the impact of silicon dioxide nanoparticles on quasi-static and dynamic mechanical properties, this dissertation presents a novel approach. It focuses on the fabrication of hybrid composite material plates composed of unidirectional glass fibers, unidirectional carbon fibers, and resin reinforced with silicon dioxide nanoparticles, arranged in various stacking sequences and thicknesses. The research includes an extensive series of mechanical property tests, such as tensile and flexural tests, as well as axial and flexural fatigue tests. Additionally, it seeks to establish a relationship between fatigue in fibers, matrix, and composites, aiming to develop a reliable model that

can predict composite failure and estimate the lifespan before catastrophic collapse. The research gap lies in the limited knowledge of how silicon dioxide nanoparticles and stacking sequences of unidirectional glass and carbon fibers affect the mechanical properties of hybrid composites. While previous studies have examined these aspects individually, there is a lack of comprehensive work on their combined impact, particularly on fatigue behavior and interactions within the fibers, matrix, and composite. Additionally, the need for a predictive model to forecast failure and estimate the lifespan of these materials remains unaddressed.

CHAPTER THREE

THEORETICAL WORK

This chapter looks further into the mechanical properties of composite materials and their quasi-static and fatigue resistances. It begins with conventional composite mechanics ideas, such as lamina micromechanics and laminate macro-mechanics. The chapter then delves into the concept of how composite materials respond to fatigue, with a particular emphasis on the mechanisms that lead to failure during events. This section also provides a short overview of methods for detecting and assessing degradation in composite materials.

3.1 Mechanics of Composite Materials

This part of chapter's major goal is to provide an overview of the mechanical characteristics inherent in laminated composite materials. The three unique theories were: micromechanics of the lamina, macro-mechanics of the lamina, and macro-mechanics of the laminate, each of which investigates a different aspect of composite mechanics. The prediction of a lamina's mechanical characteristics based on the characteristics and types (volume fraction) of its components is known as lamina micromechanics, which are the matrix and fibers that make up the layer. In contrast, macro-mechanics of the lamina analyzes the overall mechanical response of a single lamina under certain stresses without digging into the relationships between its constituent components. The theory of micromechanics of the lamina is very important for describing the laminate's macro-mechanics, which looks at how the overall structure responds to a laminated material made by joining many laminae with different fiber orientations. As shown in Figure 3-1, a lamina, a thin layer with a thickness of roughly 0.01 inch (0.25 millimeters) in a composite material, serves as the foundation for forming a laminate. Individual laminae are the basic building blocks of a laminate. It is

critical to underline that comprehending the laminate analysis requires understanding the mechanical analysis of a lamina. A lamina differs from an isotropic, homogenous material in that its stiffness changes depending on whether the location is inside the fiber, the matrix, or the fiber-matrix contact. When doing a macroscopic mechanical evaluation of a lamina, it is viewed as homogenous, with average attributes taken into consideration (Kaw, 2005).

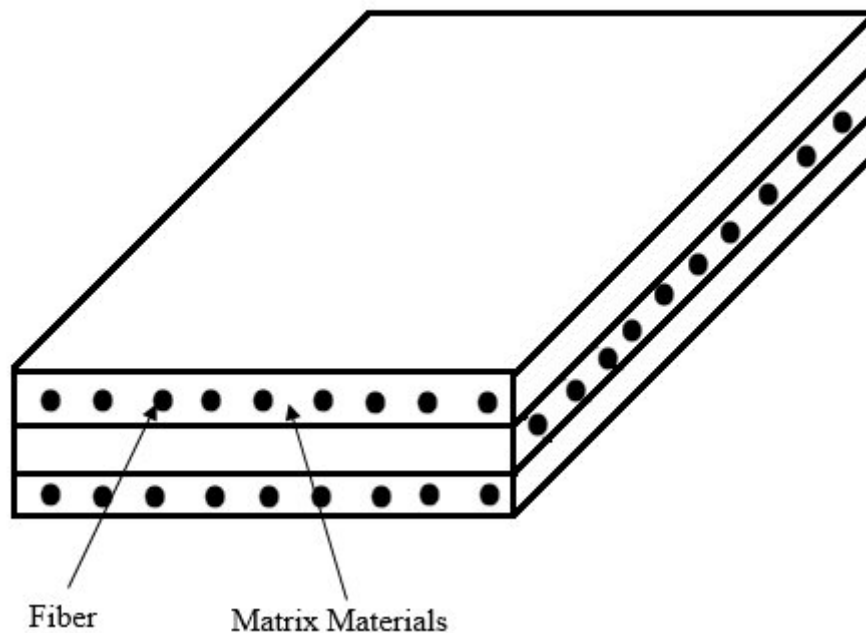


Figure 3-1 Typical laminate made of three laminae (Haider and Majumdar, 2016)

3.1.1 Micro-Mechanics of Lamina

This area of composite mechanics focuses on the examination of layers of composite materials as separate structural components, with reinforcement and matrix components treated separately. Notably, these two parts have significant differences in intrinsic characteristics, including density, Poisson's coefficient, and Young's modulus. It is critical to understand the interaction between the material qualities of these components and the eventual properties of the lamina.

This insight is crucial throughout the structural design and material selection stages. Micromechanics is primarily concerned with calculating the elastic moduli of the lamina from the matrix and fiber Young's moduli. However, owing to its sensitivity to the impacts of age, production techniques, and environmental variables, the prediction of lamina strength gets comparably less attention. As a result, the predictability of forecasted strength values may be jeopardized.

Micromechanics characterizes lamina further under different assumptions. The lamina is initially assumed to be stress-free, macroscopically homogeneous, and linearly elastic. The matrix and fibers are also idealized as being homogeneous, isotropic, linearly elastic, precisely aligned, effectively bonded, and equally spaced. This assumption allows the smallest area to be identified as representative volume where stresses may be regarded as macroscopically constant. As a result, the study may be expanded to include the whole volume and used in typical volume situations. It's important to note that laminated composites are typically described using three main directions: first direction (1) corresponds to the longitudinal axis of the fibers, whereas second direction (2) is perpendicular to first direction (1) and is within the same plane. Third direction (3), as seen in Figure 3-2, is aligned with the thickness of the laminate (Kaw, 2005).

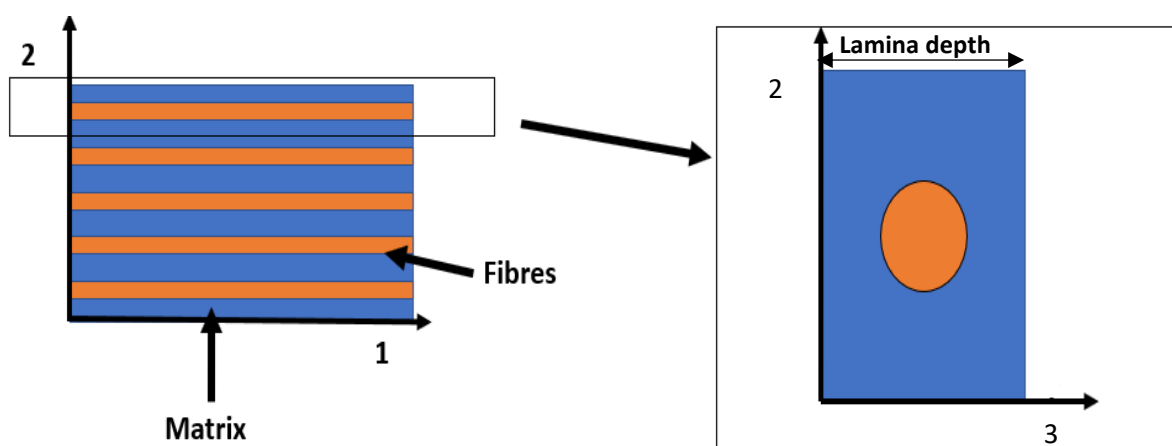


Figure 3-2 Representative volume of a single lamina: matrix (blue line) and fibers (orange lines). Principal direction 1 parallel to the fiber. (Rizzo, 2020)

With the use of this volume element, the E_1 may be calculated. In this calculation, the law of mixing is used, especially when the lamina is under a uniform stress, σ_1 , along the fiber direction (which is usually called primary direction 1), as seen in Figure 3-3.

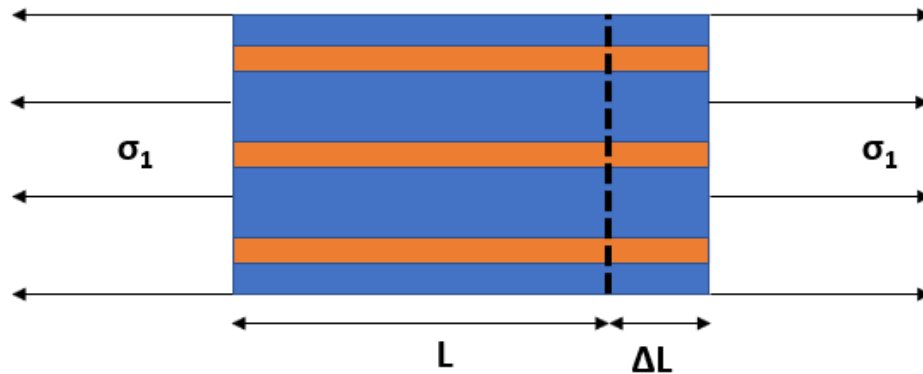


Figure 3-3 Exemplary components loaded in a direction where ΔL is the elongation caused by the stress applied, and L is the volume's original length. (Rizzo, 2020)

Because perfect bonding was assumed between the matrix and fibers, the strain (ϵ_1) on the fiber is the same as on the matrix. The longitudinal modulus (E_{11}) of the materials can be calculated by using Equation 3.1 below, as the materials are linearly elastic.

$$E_{11} = E_f V_f + E_m V_m \quad (3.1)$$

where E represents the modulus of elasticity, V represents the volume fraction, and the subscripts f and m stand for the fiber and matrix, respectively.

The highest proportion of fibers typically found in a lamina is around 0.65. When determining E_{22} (lamina's transverse modulus) (direction 2), as shown in Figure 3-4, it is not possible to assume that the strain (ϵ_2) remains the same in all of the fibers and the matrix. When a stress (σ_2) is applied to the element (Rizzo, 2020).

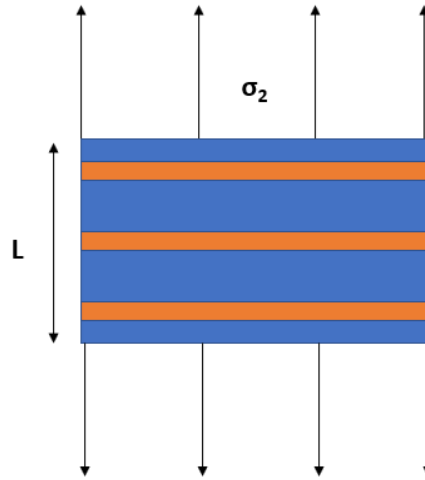


Figure 3-4 Exemplary component loaded in direction 2. (Rizzo, 2020)

But because the stress that is applied to the fibers and the matrix is the same, the transverse modulus may be calculated using the following equation:

$$E_{22} = \frac{E_f E_m}{V_m E_f + E_m V_f} \quad (3.2)$$

Under the same underlying assumptions, other equations exist to represent additional quantities, such as Poisson's ratio (ν_{12}) and shear modulus (G_{12}).

The following is how these equations are expressed:

$$G_{12} = \frac{G_f G_m}{V_m G_f + G_m V_f} \quad (3.3)$$

$$\nu_{12} = \nu_f V_f + \nu_m V_m \quad (3.4)$$

where G is shear modulus, V represents the volume fraction, and ν is the Poisson's ratio. The subscripts f and m stand for the fiber and matrix, respectively.

It is noteworthy that various studies have alternate formulations of these equations. Because of this diversity, the mechanical characteristics of different kinds of materials, such as discontinuous fiber-reinforced laminates (He, Hoa and

Ganesan, 2000; Chen *et al.*, 2021) and angle-ply laminates (O'Regan, Akay and Meenan, 1999), may be predicted using micromechanics.

3.1.2 Macro-Mechanics of Lamina

Understanding the response of a macroscopic layer to applied stresses without taking into account the interactions between its microscopic elements is the main goal of this branch of composite mechanics. The layer's entirely linear, elastic nature is the primary restriction in this area. The generalized Hooke's law can be used to study a tiny volume of material (Jones, 1999). The following is how this law describes the connection between stresses and strains to characterize the mechanical behavior of a material in three dimensions in the Cartesian coordinate system:

$$\sigma_i = C_{ij}\varepsilon_j \quad i, j = 1, 2, \dots, 6 \quad (3.5)$$

The stress component in this equation is denoted by σ_i , the strain component is represented by ε_i , and the stiffness matrix is indicated by C_{ij} .

Figure 3-5 shows how these components are distributed inside the volume element.

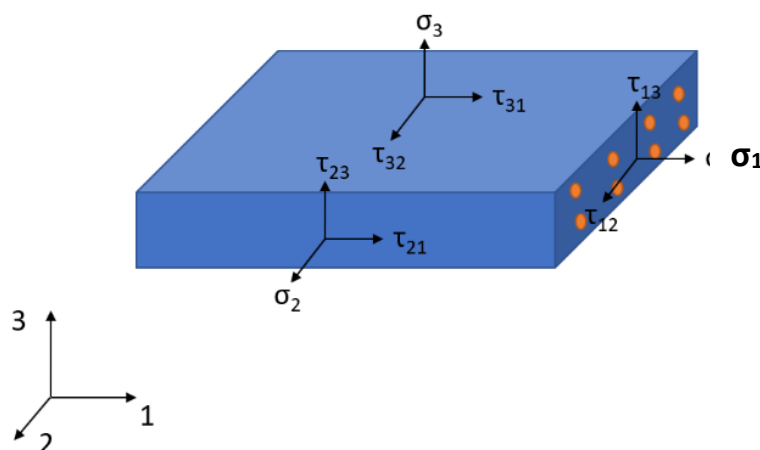


Figure 3-5 Stress distribution on the element volume (Rizzo, 2020).

The matrix representation may also be used to illustrate this equation:

$$\begin{bmatrix} \sigma_1 \\ \sigma_2 \\ \sigma_3 \\ \tau_{23} \\ \tau_{31} \\ \tau_{12} \end{bmatrix} = \begin{bmatrix} C_{11} & C_{12} & C_{13} & C_{14} & C_{15} & C_{16} \\ C_{21} & C_{22} & C_{23} & C_{24} & C_{25} & C_{26} \\ C_{31} & C_{32} & C_{33} & C_{34} & C_{35} & C_{36} \\ C_{41} & C_{42} & C_{43} & C_{44} & C_{45} & C_{46} \\ C_{51} & C_{52} & C_{53} & C_{54} & C_{55} & C_{56} \\ C_{61} & C_{62} & C_{63} & C_{64} & C_{65} & C_{66} \end{bmatrix} \begin{bmatrix} \varepsilon_1 \\ \varepsilon_2 \\ \varepsilon_3 \\ \gamma_{23} \\ \gamma_{31} \\ \gamma_{12} \end{bmatrix} \quad (3.6)$$

The engineering shear strain γ is conventionally calculated using the equation $\gamma=2\varepsilon$, where ε denotes the engineering strain. Anisotropic materials often employ this terminology, necessitating the specification of 36 constants to completely describe their mechanical behavior. However, as a result of symmetry of the stiffness matrix, only 21 unique constants are required. Incorporating material with orthotropic symmetry planes reduces the required constants where only nine independent constants are required. Three principal directions are existed in orthotropic materials. There is no correlation between normal stresses and shear strains. The matrix representation of an orthotropic lamina can be represented as follow (Kaw, 2005):

$$\begin{bmatrix} \sigma_1 \\ \sigma_2 \\ \sigma_3 \\ \tau_{23} \\ \tau_{31} \\ \tau_{12} \end{bmatrix} = \begin{bmatrix} C_{11} & C_{12} & C_{13} & 0 & 0 & 0 \\ C_{21} & C_{22} & C_{23} & 0 & 0 & 0 \\ C_{31} & C_{32} & C_{33} & 0 & 0 & 0 \\ 0 & 0 & 0 & C_{44} & 0 & 0 \\ 0 & 0 & 0 & 0 & C_{55} & 0 \\ 0 & 0 & 0 & 0 & 0 & C_{66} \end{bmatrix} \begin{bmatrix} \varepsilon_1 \\ \varepsilon_2 \\ \varepsilon_3 \\ \gamma_{23} \\ \gamma_{31} \\ \gamma_{12} \end{bmatrix} \quad (3.7)$$

Usually, micromechanical formulas or experimental tests are used to determine the constants. The relative engineering characteristics may be used in place of the stiffness constants, yielding the following mathematical expression:

$$\begin{bmatrix} \sigma_1 \\ \sigma_2 \\ \sigma_3 \\ \tau_{23} \\ \tau_{31} \\ \tau_{12} \end{bmatrix} = \begin{bmatrix} E_{11} & C_{12} & C_{13} & 0 & 0 & 0 \\ C_{21} & E_{22} & C_{23} & 0 & 0 & 0 \\ C_{31} & C_{32} & E_{33} & 0 & 0 & 0 \\ 0 & 0 & 0 & G_{23} & 0 & 0 \\ 0 & 0 & 0 & 0 & G_{31} & 0 \\ 0 & 0 & 0 & 0 & 0 & G_{12} \end{bmatrix} \begin{bmatrix} \varepsilon_1 \\ \varepsilon_2 \\ \varepsilon_3 \\ \gamma_{23} \\ \gamma_{31} \\ \gamma_{12} \end{bmatrix} \quad (3.8)$$

3.1.3 Macro-Mechanics of the Laminate

This section describes the macroscopic mechanical behavior of several laminae that are bond together and behave as a whole. This hypothesis excludes interactions between individual components. The primary reason for stacking laminae in a stacking sequence or lamination sequence is the extremely tiny thickness of a lamina and the need to expand it in order to enhance overall strength and stiffness. This structure is one of a kind because the orientation of the individual laminae can change as they are stacked. This lets different types of laminates with different overall mechanical properties form. This theory's primary goal is to understand the mechanical response in case of the lamination sequence is defined which is considered one of the primary goals of this theory. The classical lamination theory (CLT) describes the essential assumptions required to analyze this aspect of composite mechanics. The CLT displays plane stress behavior on the laminae bonded within the laminate. An orthotropic lamina expresses the stress-strain relationship as follows (Jones, 1999):

$$\begin{bmatrix} \sigma_1 \\ \sigma_2 \\ \tau_{12} \end{bmatrix} = \begin{bmatrix} Q_{11} & Q_{12} & 0 \\ Q_{12} & Q_{22} & 0 \\ 0 & 0 & Q_{66} \end{bmatrix} \begin{bmatrix} \varepsilon_1 \\ \varepsilon_2 \\ \gamma_{12} \end{bmatrix} \quad (3.9)$$

where: Q_{ij} the terms are defined by the use of engineering constant formulae and pertain to the decreased stiffness coefficients for the 1-2 plane stress situation:

$$\begin{aligned} Q_{11} &= \frac{E_{11}}{1-\nu_{12}\nu_{21}} \\ Q_{22} &= \frac{E_{22}}{1-\nu_{12}\nu_{21}} \\ Q_{12} &= \frac{\nu_{21}E_{11}}{1-\nu_{12}\nu_{21}} \\ \nu_{21} &= \frac{\nu_{12}E_{22}}{E_{11}} \\ Q_{66} &= G_{12} \end{aligned} \quad (3.10)$$

It is possible to generalize this equation since it is necessary to maintain this connection even in cases where the reinforcement is directed differently from the applied stress. The following equation may be used to transfer stresses from a local 1-2 reference system to a global x-y reference system for any arbitrary alignment of the fibers and applied stresses, along with the use of a polar transformation matrix:

$$\begin{bmatrix} \sigma_x \\ \sigma_y \\ \tau_{xy} \end{bmatrix} = \begin{bmatrix} \cos^2\theta & \sin^2\theta & -2\cos\theta\sin\theta \\ \sin^2\theta & \cos^2\theta & 2\cos\theta\sin\theta \\ \cos\theta\sin\theta & -\cos\theta\sin\theta & \cos^2\theta - \sin^2\theta \end{bmatrix} \begin{bmatrix} \sigma_1 \\ \sigma_2 \\ \tau_{12} \end{bmatrix} \quad (3.11)$$

$$\begin{bmatrix} \sigma_x \\ \sigma_y \\ \tau_{xy} \end{bmatrix} = [T]^{-1} \begin{bmatrix} \sigma_1 \\ \sigma_2 \\ \tau_{12} \end{bmatrix}$$

where [T] is called the transformation matrix and is defined as

$$[T] = \begin{bmatrix} \cos^2\theta & \sin^2\theta & 2\cos\theta\sin\theta \\ \sin^2\theta & \cos^2\theta & -2\cos\theta\sin\theta \\ -\cos\theta\sin\theta & \cos\theta\sin\theta & \cos^2\theta - \sin^2\theta \end{bmatrix}$$

$$[T]^{-1} = \begin{bmatrix} \cos^2\theta & \sin^2\theta & -2\cos\theta\sin\theta \\ \sin^2\theta & \cos^2\theta & 2\cos\theta\sin\theta \\ \cos\theta\sin\theta & -\cos\theta\sin\theta & \cos^2\theta - \sin^2\theta \end{bmatrix}$$

With equations (3.9) and (3.11), the following may be written:

$$\begin{bmatrix} \sigma_x \\ \sigma_y \\ \tau_{xy} \end{bmatrix} = [T]^{-1}[Q] \begin{bmatrix} \varepsilon_1 \\ \varepsilon_2 \\ \gamma_{12} \end{bmatrix} \quad (3.12)$$

$$\begin{bmatrix} \varepsilon_1 \\ \varepsilon_2 \\ \frac{\gamma_{12}}{2} \end{bmatrix} = [T] \begin{bmatrix} \varepsilon_x \\ \varepsilon_y \\ \frac{\gamma_{xy}}{2} \end{bmatrix} \quad (3.13)$$

which can be rewritten as

$$\begin{bmatrix} \varepsilon_1 \\ \varepsilon_2 \\ \gamma_{xy} \end{bmatrix} = [R][T][R]^{-1} \begin{bmatrix} \varepsilon_x \\ \varepsilon_y \\ \gamma_{xy} \end{bmatrix} \quad (3.14)$$

where $[R]$ is the Reuter matrix and is defined as (Kaw, 2005):

$$[R] = \begin{bmatrix} 1 & 0 & 0 \\ 0 & 1 & 0 \\ 0 & 0 & 2 \end{bmatrix} \quad (3.15)$$

Then, substituting Equation (3.14) in Equation (3.12) gives

$$\begin{bmatrix} \sigma_x \\ \sigma_y \\ \tau_{xy} \end{bmatrix} = [T]^{-1}[Q][R][T][R]^{-1} \begin{bmatrix} \varepsilon_1 \\ \varepsilon_2 \\ \gamma_{12} \end{bmatrix} \quad (3.16)$$

$$\begin{bmatrix} \sigma_x \\ \sigma_y \\ \tau_{xy} \end{bmatrix} = \begin{bmatrix} \overline{Q}_{11} & \overline{Q}_{12} & \overline{Q}_{16} \\ \overline{Q}_{12} & \overline{Q}_{22} & \overline{Q}_{26} \\ \overline{Q}_{16} & \overline{Q}_{26} & \overline{Q}_{66} \end{bmatrix} \begin{bmatrix} \varepsilon_1 \\ \varepsilon_2 \\ \gamma_{12} \end{bmatrix} \quad (3.17)$$

$$[\sigma] = [\overline{Q}][\varepsilon]$$

$$[\overline{Q}] = [T]^{-1}[Q][T] \quad (3.18)$$

Any arbitrary layer inside a multi-layer laminate may have its behavior described using this stress-strain relationship. For a laminate of k layers, this assertion can restate as follows:

$$[\sigma]_k = [\overline{Q}]_k[\varepsilon]_k \quad (3.19)$$

where \overline{Q}_{ij} are called the elements of the transformed reduced stiffness matrix $[\overline{Q}]$ and are given by

$$\begin{aligned}
\bar{Q}_{11} &= Q_{11}\cos^4\theta + Q_{22}\sin^4\theta + 2(Q_{12} + 2Q_{66})\sin^2\theta\cos^2\theta \\
\bar{Q}_{12} &= (Q_{11} + Q_{22} - 4Q_{66})\sin^2\theta\cos^2\theta + Q_{12}(\cos^4\theta + \sin^2\theta) \\
\bar{Q}_{22} &= Q_{11}\sin^4\theta + Q_{22}\cos^4\theta + 2(Q_{12} + 2Q_{66})\sin^2\theta\cos^2\theta \\
\bar{Q}_{16} &= (Q_{11} - Q_{12} - 2Q_{66})\cos^3\theta\sin\theta - (Q_{22} - Q_{12} - 2Q_{66})\sin^3\theta\cos\theta \quad (3.20) \\
\bar{Q}_{26} &= (Q_{11} - Q_{12} - 2Q_{66})\cos\theta\sin^3\theta - (Q_{22} - Q_{12} - 2Q_{66})\cos^3\theta\sin\theta \\
\bar{Q}_{66} &= (Q_{11} + Q_{22} - 2Q_{12} - 2Q_{66})\sin^2\theta\cos^2\theta + Q_{66}(\sin^4\theta + \cos^2\theta)
\end{aligned}$$

The $[Q]$ matrix has six elements. However, examining equation (3.20) reveals that these six parameters are fundamentally reliant on four stiffness factors: Q_{11} , Q_{12} , Q_{22} , and Q_{66} , in addition to the lamina's orientation angle, θ .

Inverting equation (3.17) gives

$$\begin{bmatrix} \varepsilon_x \\ \varepsilon_y \\ \gamma_{xy} \end{bmatrix} = \begin{bmatrix} \bar{S}_{11} & \bar{S}_{12} & \bar{S}_{16} \\ \bar{S}_{12} & \bar{S}_{22} & \bar{S}_{26} \\ \bar{S}_{16} & \bar{S}_{26} & \bar{S}_{66} \end{bmatrix} \begin{bmatrix} \sigma_x \\ \sigma_y \\ \tau_{xy} \end{bmatrix} \quad (3.21)$$

Where S_{ij} are the elements of the transformed reduced compliance matrix and are given by

$$\begin{aligned}
\bar{S}_{11} &= S_{11}\cos^4\theta + S_{22}\sin^4\theta + 2(S_{12} + S_{66})\sin^2\theta\cos^2\theta \\
\bar{S}_{12} &= (S_{11} + S_{22} - S_{66})\sin^2\theta\cos^2\theta + S_{12}(\cos^4\theta + \sin^2\theta) \\
\bar{S}_{22} &= S_{11}\sin^4\theta + S_{22}\cos^4\theta + (2S_{12} + S_{66})\sin^2\theta\cos^2\theta \\
\bar{S}_{16} &= (2S_{11} - 2S_{12} - S_{66})\cos^3\theta\sin\theta - (2S_{22} - 2S_{12} - S_{66})\sin^3\theta\cos\theta \quad (3.22) \\
\bar{S}_{26} &= (2S_{11} - 2S_{12} - S_{66})\cos\theta\sin^3\theta - (2S_{22} - 2S_{12} - S_{66})\cos^3\theta\sin\theta \\
\bar{S}_{66} &= 2(2S_{11} + 2S_{22} - 4S_{12} - S_{66})\sin^2\theta\cos^2\theta + S_{66}(\sin^4\theta + \cos^2\theta)
\end{aligned}$$

For an angle lamina, from Equation (3.17) and Equation (3.21), coupling takes place between the normal and shearing terms of strains and stresses. If only normal stresses are applied to an angle lamina, the shear strains are nonzero; if only shearing stresses are applied to an angle lamina, the normal strains are nonzero. Therefore, Equation (3.17) and Equation (3.21) are stress–strain equations for what is called a generally orthotropic lamina (Kaw, 2005).

The resulting moments and forces were computed using equation (3.19) through an integration method and the stress distribution. Before describing the process for obtaining these findings, it is important to establish some assumptions. These assumptions include the following: laminae with tiny thicknesses are taken into account, shearing deformation under load is not present, and there is complete bonding between laminae. With these assumptions, the equations that regard the laminate as a collection of k layers can be used to calculate the resulting forces and moments acting on the laminate.

$$\begin{bmatrix} N_x \\ N_y \\ N_{xy} \end{bmatrix} = \int_{-\frac{t}{2}}^{\frac{t}{2}} \begin{bmatrix} \sigma_x \\ \sigma_y \\ \tau_{xy} \end{bmatrix} dz = \sum_{k=1}^N \int_{z_{k-1}}^{z_k} \begin{bmatrix} \sigma_x \\ \sigma_y \\ \tau_{xy} \end{bmatrix}_k dz \quad (3.23)$$

$$\begin{bmatrix} M_x \\ M_y \\ M_{xy} \end{bmatrix} = \int_{-\frac{t}{2}}^{\frac{t}{2}} \begin{bmatrix} \sigma_x \\ \sigma_y \\ \tau_{xy} \end{bmatrix} z dz = \sum_{k=1}^N \int_{z_{k-1}}^{z_k} \begin{bmatrix} \sigma_x \\ \sigma_y \\ \tau_{xy} \end{bmatrix}_k z dz \quad (3.24)$$

Here, N_x , N_y , and N_{xy} stand for the laminate section's forces per unit width, while M_x , M_y , and M_{xy} stand for the moments per unit width. The quantity t indicates the laminate's thickness. Furthermore, as shown in Figure 3-6, z_k and z_{k-1} represent the separations between the top and lower ply surfaces and a reference system that is positioned on the laminate's center plane. It is important to remember that the z -axis is thought to have a downward (positive direction). Figure 3-7 reports the depiction of moments and forces.

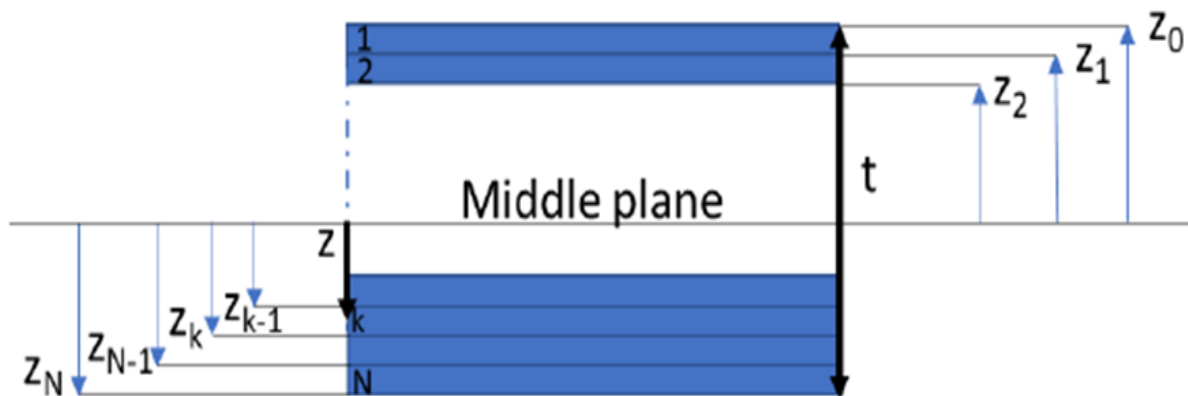


Figure 3-6 N -layered laminate is shown geometrically. (Rizzo, 2020)

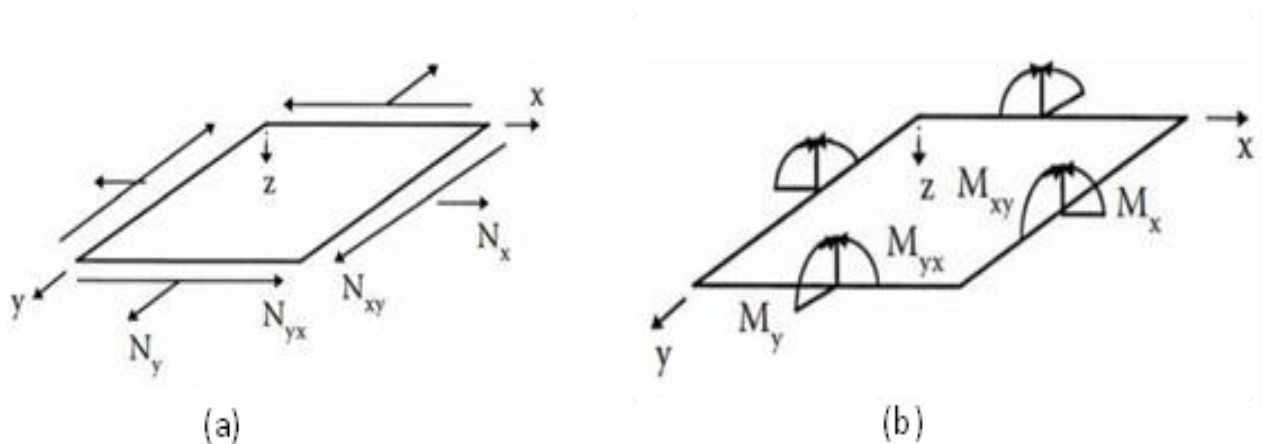


Figure 3-7 Forces and moments generated by a laminate (Kaw, 2005).

By inserting equation (3.10) into equation (3.19) and including equations (3.23) and (3.24), a link between the resultant moments and forces and the decreased coefficients of stiffness may be created. It is important to note that the decreased stiffness matrix is treated as a constant throughout the lamina, enabling it to be factored out of the integral (Kaw, 2005). Furthermore, the strain components may be separated into two distinct elements: the longitudinal strain, designated as ε^0 , which signifies the strain encountered by the central plane, and the curvature strain, referred to as κ , which describes the deflection that occurs during bending while considering the kinematics of plate deformation (Rizzo, 2020).

$$\begin{bmatrix} N_x \\ N_y \\ N_{xy} \end{bmatrix} = \sum_{k=1}^N \begin{bmatrix} \overline{Q_{11}} & \overline{Q_{12}} & \overline{Q_{16}} \\ \overline{Q_{12}} & \overline{Q_{22}} & \overline{Q_{26}} \\ \overline{Q_{16}} & \overline{Q_{26}} & \overline{Q_{66}} \end{bmatrix} \int_{z_{k-1}}^{z_k} \begin{bmatrix} \varepsilon_x \\ \varepsilon_y \\ \gamma_{xy} \end{bmatrix}_k dz \quad (3.25)$$

$$\begin{bmatrix} M_x \\ M_y \\ M_{xy} \end{bmatrix} = \sum_{k=1}^N \begin{bmatrix} \overline{Q_{11}} & \overline{Q_{12}} & \overline{Q_{16}} \\ \overline{Q_{12}} & \overline{Q_{22}} & \overline{Q_{26}} \\ \overline{Q_{16}} & \overline{Q_{26}} & \overline{Q_{66}} \end{bmatrix} \int_{z_{k-1}}^{z_k} \begin{bmatrix} \varepsilon_x \\ \varepsilon_y \\ \gamma_{xy} \end{bmatrix}_k z dz \quad (3.26)$$

$$\begin{bmatrix} \varepsilon_x \\ \varepsilon_y \\ \gamma_{xy} \end{bmatrix} = \begin{bmatrix} \varepsilon_x^0 \\ \varepsilon_y^0 \\ \gamma_{xy}^0 \end{bmatrix} + z \begin{bmatrix} \kappa_x \\ \kappa_y \\ \kappa_{xy} \end{bmatrix} \quad (3.27)$$

Substituting Equation (3.27) in Equations (3.25) and (3.26), as a function of the applied strains, the resulting forces and moments may be calculated.

$$\begin{bmatrix} N_x \\ N_y \\ N_{xy} \end{bmatrix} = \sum_{k=1}^N \begin{bmatrix} \overline{Q_{11}} & \overline{Q_{12}} & \overline{Q_{16}} \\ \overline{Q_{12}} & \overline{Q_{22}} & \overline{Q_{26}} \\ \overline{Q_{16}} & \overline{Q_{26}} & \overline{Q_{66}} \end{bmatrix} \int_{z_{k-1}}^{z_k} \begin{bmatrix} \varepsilon_x^0 \\ \varepsilon_y^0 \\ \gamma_{xy}^0 \end{bmatrix} + z \begin{bmatrix} \kappa_x \\ \kappa_y \\ \kappa_{xy} \end{bmatrix} dz \quad (3.28)$$

$$\begin{bmatrix} M_x \\ M_y \\ M_{xy} \end{bmatrix} = \sum_{k=1}^N \begin{bmatrix} \overline{Q_{11}} & \overline{Q_{12}} & \overline{Q_{16}} \\ \overline{Q_{12}} & \overline{Q_{22}} & \overline{Q_{26}} \\ \overline{Q_{16}} & \overline{Q_{26}} & \overline{Q_{66}} \end{bmatrix} \int_{z_{k-1}}^{z_k} \begin{bmatrix} \varepsilon_x^0 \\ \varepsilon_y^0 \\ \gamma_{xy}^0 \end{bmatrix} + z \begin{bmatrix} \kappa_x \\ \kappa_y \\ \kappa_{xy} \end{bmatrix} z dz \quad (3.29)$$

The strain terms exhibit independence from the variable "z", therefore, enabling their extraction outside the summing operator. Through the process of rearranging the equations and doing the integrations, as described in the methodology indicated in reference, the ultimate equations employed to characterize the resultant forces and moments that occur can be derived (*Rizzo, 2020*).

$$\begin{bmatrix} N_x \\ N_y \\ N_{xy} \end{bmatrix} = \begin{bmatrix} A_{11} & A_{12} & A_{16} \\ A_{12} & A_{22} & A_{26} \\ A_{16} & A_{26} & A_{66} \end{bmatrix} \begin{bmatrix} \varepsilon_x^0 \\ \varepsilon_y^0 \\ \gamma_{xy}^0 \end{bmatrix} + \begin{bmatrix} B_{11} & B_{12} & B_{16} \\ B_{12} & B_{22} & B_{26} \\ B_{16} & B_{26} & B_{66} \end{bmatrix} \begin{bmatrix} \kappa_x \\ \kappa_y \\ \kappa_{xy} \end{bmatrix} \quad (3.30)$$

$$\begin{bmatrix} M_x \\ M_y \\ M_{xy} \end{bmatrix} = \begin{bmatrix} B_{11} & B_{12} & B_{16} \\ B_{12} & B_{22} & B_{26} \\ B_{16} & B_{26} & B_{66} \end{bmatrix} \begin{bmatrix} \varepsilon_x^0 \\ \varepsilon_y^0 \\ \gamma_{xy}^0 \end{bmatrix} + \begin{bmatrix} D_{11} & D_{12} & D_{16} \\ D_{12} & D_{22} & D_{26} \\ D_{16} & D_{26} & D_{66} \end{bmatrix} \begin{bmatrix} \kappa_x \\ \kappa_y \\ \kappa_{xy} \end{bmatrix} \quad (3.31)$$

where

$$A_{ij} = \sum_{k=1}^N (\overline{Q}_{ij})_k (z_k - z_{k-1}) \quad (3.32)$$

$$B_{ij} = \frac{1}{2} \sum_{k=1}^N (\overline{Q}_{ij})_k (z_k^2 - z_{k-1}^2) \quad (3.33)$$

$$D_{ij} = \frac{1}{3} \sum_{k=1}^N (\overline{Q}_{ij})_k (z_k^3 - z_{k-1}^3) \quad (3.34)$$

Where, A_{ij} , B_{ij} , D_{ij} are extensional, extensional- bending coupling, and bending stiffness matrices, respectively (Kaw, 2005).

3.1.3.1 Laminate Under Tensile and Shear Load

For symmetric laminated fiber composite $[B] = 0$, then equation (3.30) can be reduced into the following equation (Kaw, 2005).

$$\begin{bmatrix} \varepsilon_x^0 \\ \varepsilon_y^0 \\ \gamma_{xy}^0 \end{bmatrix} = \begin{bmatrix} A_{11}^* & A_{12}^* & A_{16}^* \\ A_{12}^* & A_{22}^* & A_{26}^* \\ A_{16}^* & A_{26}^* & A_{66}^* \end{bmatrix} \begin{bmatrix} N_x \\ N_y \\ N_{xy} \end{bmatrix} \quad (3.35)$$

For laminate subjected only to normal load N_x then the effective longitudinal Young modulus E_x is

$$E_x = \frac{1}{hA_{11}^*} \quad (3.36)$$

The major effective Poisson's ratio is

$$\nu_{xy} = -\frac{A_{12}^*}{A_{11}^*} \quad (3.37)$$

For laminate subjected only to normal load N_y then the effective transverse Young modulus E_y is (Kaw, 2005)

$$E_y = \frac{1}{hA_{22}^*} \quad (3.38)$$

The minor effective Poisson's ratio is

$$\nu_{yx} = -\frac{A_{12}^*}{A_{22}^*} \quad (3.39)$$

For laminate subjected only to shear load N_{xy} then the effective shear modulus G_{xy} is (Kaw, 2005)

$$G_{xy} = \frac{1}{hA_{66}^*} \quad (3.40)$$

where

h = total laminate thickness.

3.1.3.2 Laminate under Bending Moment

Regarding the bending moment for the symmetric laminate, Equation (3.31) can be reduced into the following equation, where the matrix $[B] = 0$.

$$\begin{bmatrix} K_x \\ K_y \\ K_{xy} \end{bmatrix} = \begin{bmatrix} D_{11}^* & D_{12}^* & D_{16}^* \\ D_{12}^* & D_{22}^* & D_{26}^* \\ D_{16}^* & D_{26}^* & D_{66}^* \end{bmatrix} \begin{bmatrix} M_x \\ M_y \\ M_{xy} \end{bmatrix} \quad (3.41)$$

For laminate subjected only to bending moment M_x , then the effective flexural longitudinal modulus E_x^f is

$$E_x^f = \frac{12}{h^3 D_{11}^*} \quad (3.42)$$

The effective flexural transverse modulus E_y^f is

$$E_y^f = \frac{12}{h^3 D_{22}^*} \quad (3.43)$$

The effective flexural shear modulus G_{xy}^f is

$$G_{xy}^f = \frac{12}{h^3 D_{66}^*} \quad (3.44)$$

The major effective flexural Poisson's ratio is

$$\nu_{xy}^f = -\frac{D_{12}^*}{D_{11}^*} \quad (3.45)$$

The minor effective flexural Poisson's ratio is

$$\nu_{yx}^f = -\frac{D_{12}^*}{D_{22}^*} \quad (3.46)$$

where h is the total laminate thickness.

Studying these equations allows for the distinction of unique features that illuminate various aspects of the laminate's microscopic activity. The extensional stiffness matrix, or A_{ij} establishes the link between longitudinal strain and normal forces. The off-diagonal components ($i \neq j$) in this matrix are related to in-plane shear, while the diagonal elements ($i = j$) are connected to normal extension (Kaw, 2005).

On the other hand, D_{ij} indicates the laminate's bending stiffness matrix, which links the curvature strain components to moments. The diagonal terms in this matrix represent pure bending, whereas the off-diagonal components represent twisting.

In contrast, B_{ij} is what gives composite materials their unique mechanical response. It acts as a coupling matrix and makes the stretching and bending processes interact with each other. To put it another way, A normal force on the material would always result in bending and twisting in addition to the longitudinal strain that the center plane would experience.

It is difficult to use composite materials in structural applications because of these characteristics. Adhering to strict design requirements is crucial to limiting the interaction between bending and extensional components. One strategy is to use a symmetrical lamination sequence, which removes all of the B_{ij} terms (which cause this coupling) from the matrix. To make this happen, pairs of laminae of the same material, thickness, and orientation are symmetrically introduced at equal distances from the center plane. Their exact opposite contributions to the B matrix cancel each other out as a result. However, the link between the twisting and bending actions remains. Laminates may be balanced in design to handle this. In addition to having symmetric properties, balanced laminates a unique subset of symmetric laminates also include pairs of plies oriented at opposing angles. To follow the concept of a symmetric laminate, two laminae added at $(+45^\circ)$ must be balanced by two additional plies introduced at (-45°) . Because they may remove interactions between shear-extension, bending-extension, and bending-twisting components, balanced laminates are thus often used. But it's important to remember that this theory may change when hybrid fibrous reinforcement is utilized or when more layers of reinforcement are added.

3.1.3.3 Laminate under Fatigue Load

Fatigue occurs when subjected to repetitive stresses that are normally less than the yield stress. Cyclic stress causes microcracks to propagate and increase with each cycle, finally leading to failure. As a result, it is critical to be able to forecast a material's service life and how many cycles it can withstand before failing. An S-N (stress-No. of cycles) curve depicts the connection between cyclic stress amplitude and the number of cycles before failure. The S-N curves are highly useful in assessing a material's service life since they represent the number of cycles until failure under any given load. Curves may potentially represent a material's endurance limit or an endless life. The S-N curves are generated from fatigue testing of materials at various stress amplitudes, counting the cycles to failure, and are used in structural design to help predict service life. Figure 3-8 shows a typical S-N curve (Haller, 2020).

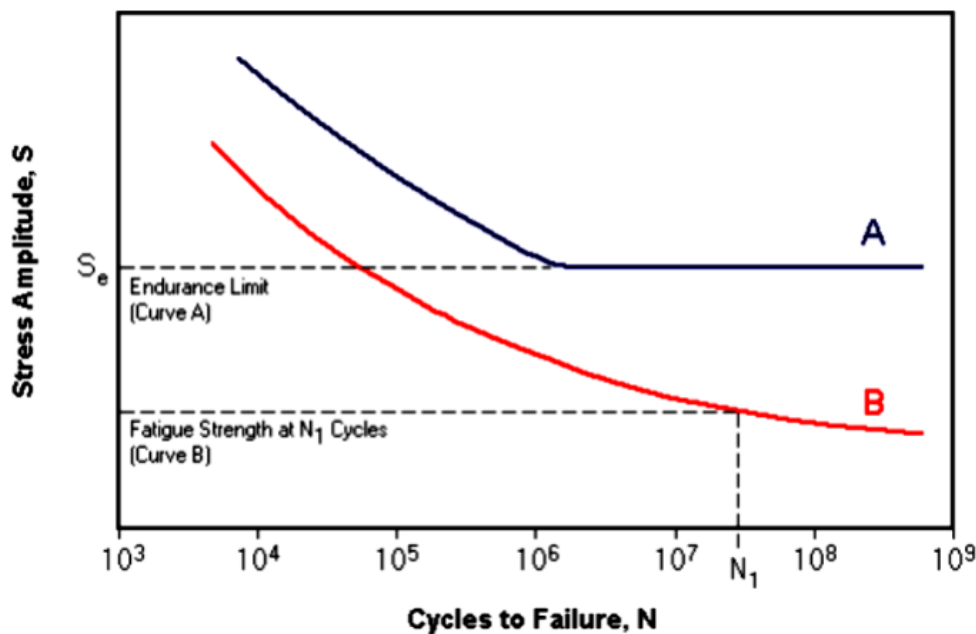


Figure 3-8 Typical S-N Curve (Haller, 2020).

The point, in the figure mentioned above, where the curve flattens out for material (A) represents the point at which, with any stress at or below the stress at the endurance limit (S_e), the material will have an unlimited life and will not fail due to fatigue.

The damage and failure of common metals are reasonably well known; fatigue fractures and propagation are considerably simpler to anticipate than composite materials due to metals' isotropic composition (Giurgiutiu, 2016). Composite materials fail differently under tension than in compression, and their deterioration might be difficult to detect (See Material **B** in the Figure 3-8).

3.2 Failure Criteria

When a material is exposed to particular stress and strain conditions, defective zones develop inside it. Understanding these factors and establishing criteria for forecasting whether the structure can withstand the imposed load without failure is critical. These criteria are designed with the notion of a homogeneous orthotropic solid ply in mind.

3.2.1 Failure Mechanism of Quasi-Static

The laminate's strength under tension along the fiber direction (X_T) and compression along the same direction (X_C), as well as the strengths associated with transverse shear (S_{12} and S_{13}), are prerequisites for Hashin's fiber failure criteria. Zhang and Abrate have shown that this criterion is stated in the Equation (3.47). (Zhang *et al.*, 2002; Abrate, 2011).

$$\left(\frac{\sigma_{11}}{X_T}\right)^2 + \left(\frac{\sigma_{12}}{S_{12}}\right)^2 + \left(\frac{\sigma_{13}}{S_{13}}\right)^2 = 1 \quad \text{if } \sigma_{11} > 0 \quad (3.47)$$

$$|\sigma_{11}| = X_c \quad \text{if } \sigma_{11} < 0 \quad (3.48)$$

In this instance, σ_{12} and σ_{13} represent the shear stresses acting on the laminate, whereas σ_{11} represents the normal stress along the fiber direction. These formulas provide a way to look at the distribution of stress in the material and see whether the circumstances are right for fiber breakdown. Similar to this, Kim and Chung, (2007) used criterion of Hashin of predicting failure of matrix under compression

and tension, which is dependent on a mix of shear stresses (σ_{12} and σ_{13}) and transverse normal stresses (σ_{22} and σ_{33}).

$$\left(\frac{\sigma_{22} + \sigma_{33}}{Y_T}\right)^2 + \frac{\sigma_{23}^2 - \sigma_{22}\sigma_{33}}{S_{23}^2} + \left(\frac{\sigma_{12}}{S_{12}}\right)^2 + \left(\frac{\sigma_{13}}{S_{13}}\right)^2 = 1 \quad (3.49)$$

$$\text{if } (\sigma_{22} + \sigma_{33}) > 0$$

$$\left(\frac{\sigma_{22} + \sigma_{33}}{2\sigma_{12}}\right)^2 + \frac{\sigma_{22} + \sigma_{33}}{Y_c} \left[\left(\frac{Y_c}{2S_T}\right)^2 - 1 \right] + \frac{\sigma_{23}^2 - \sigma_{22}\sigma_{33}}{S_{23}^2} \quad (3.50)$$

$$+ \left(\frac{\sigma_{12}}{S_{12}}\right)^2 + \left(\frac{\sigma_{13}}{S_{13}}\right)^2 \geq 1 \quad \text{if } (\sigma_{22} + \sigma_{33}) < 0$$

In this context, Y_T and Y_C stand for transverse strengths under compression and tension, respectively. S_{23} shows the shear strength in relation to the stress acting on the plane with normal orientation along the fiber direction. S_T , on the other hand, stands for the tension shear strength (Kaw, 2005).

In addition to Hashin's criteria, there is another criterion that takes into account the effects of stresses acting in all directions inside the laminate called the criterion of three-dimensional Tsai-Hill, which is a complete criterion of failure.

$$\left(\frac{\sigma_{11}}{X}\right)^2 + \left(\frac{\sigma_{22}}{Y}\right)^2 + \left(\frac{\sigma_{33}}{Z}\right)^2 + \left(\frac{\sigma_{23}}{S_{23}}\right)^2 + \left(\frac{\sigma_{13}}{S_{13}}\right)^2 + \left(\frac{\sigma_{12}}{S_{12}}\right)^2 - \sigma_{11}\sigma_{22}\left(\frac{1}{X^2} + \frac{1}{Y^2} - \frac{1}{Z^2}\right) - \sigma_{11}\sigma_{33}\left(\frac{1}{X^2} + \frac{1}{Z^2} - \frac{1}{Y^2}\right) - \sigma_{22}\sigma_{33}\left(\frac{1}{Y^2} + \frac{1}{Z^2} - \frac{1}{X^2}\right) = 1 \quad (3.51)$$

The strengths along the fiber direction, transverse direction, and through-thickness direction are represented, respectively, by X , Y , and Z in the given equation. It's crucial to remember that equal tension and compression strengths are expected. To have a deeper comprehension of the many kinds of damage (see Figure 3-9).

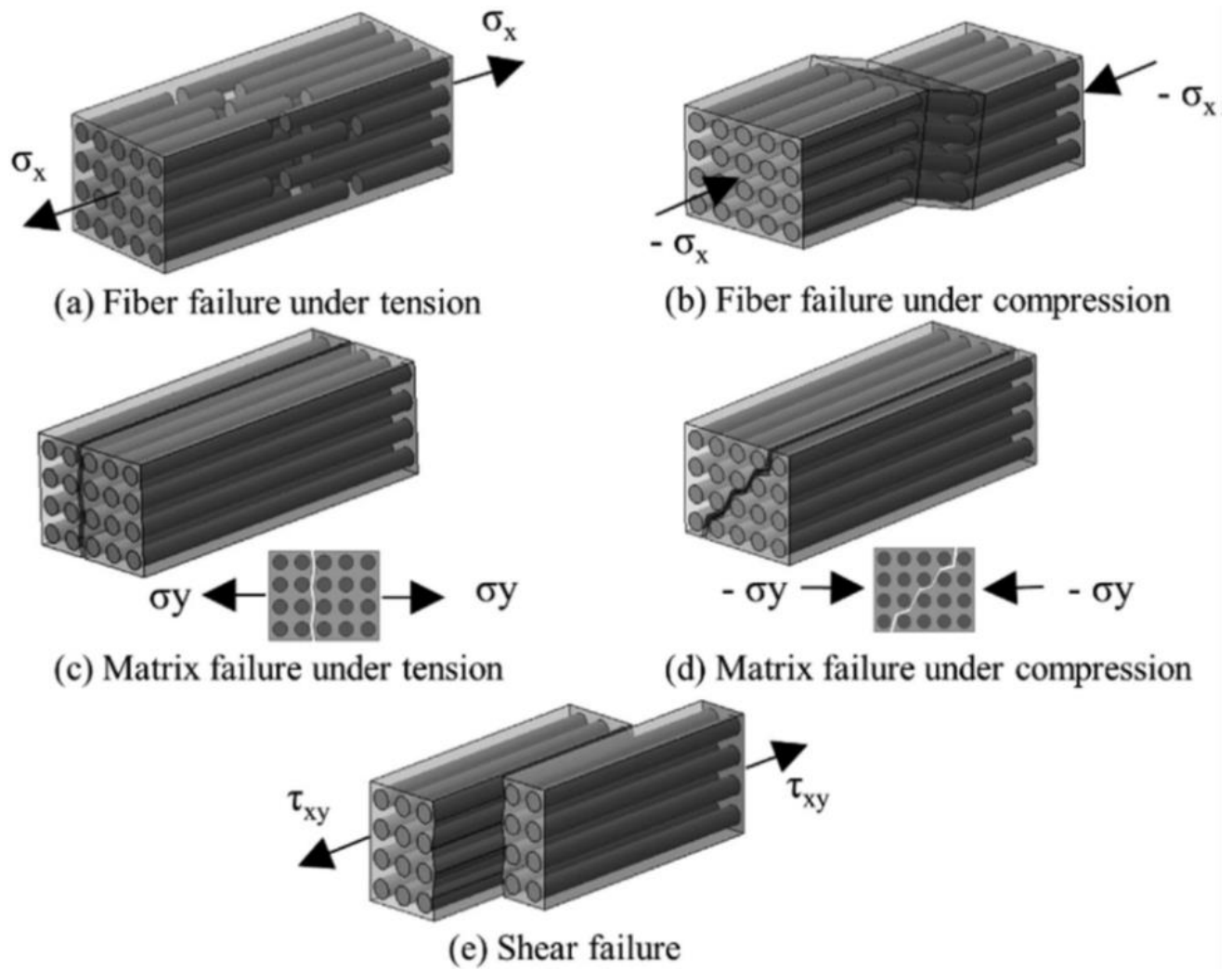


Figure 3-9 An illustration of deterioration inside the lamina (Shah et al., 2019).

In order to forecast the stress levels under which delamination occurs, Liu and Wang (2007) created criteria for compression, whereas Yeh and Kim, (1994) produced interlaminar failure criteria for tension. Based on stress conditions, these criteria are used to identify when layer separation, or delamination, begins.

$$\left(\frac{\sigma_{33}}{Z_T}\right)^2 + \left(\frac{\sigma_{13}}{S_{13}}\right)^2 + \left(\frac{\sigma_{23}}{S_{23}}\right)^2 \geq 1 \quad \text{if } \sigma_{33} > 0 \quad (3.52)$$

$$\left(\frac{\sigma_{13}}{S_{13}}\right)^2 + \left(\frac{\sigma_{23}}{S_{23}}\right)^2 \geq 1 \quad \text{if } \sigma_{33} < 0 \quad (3.53)$$

Where Z_T stands for relative strength in these equations, and σ_{33} for the stress in the thickness direction. With the use of these formulas, it is possible to determine whether there is a delaminated area in the laminate by determining if the local stress distribution satisfies the predetermined standards.

3.2.2 Failure Mechanism of Fatigue

The study of dispersed damages' beginning and progression when a material is exposed to external fatigue loading is known as the fatigue damage mechanism. Damage in the FRP composites is the collective term for any permanent alterations, including fiber breakage, matrix fractures, and fiber bridging cracks. Various fiber orientations in each layer of the FRP materials experience various stresses depending on the applied loading. At the fiber-matrix contacts, these stresses are passed between the fibers via the matrix. It's the stress-transferring abilities of the fiber, matrix, and fiber-matrix interfaces that cause the composites to fail and crack at the micro-level. As a result, the combined effects of anisotropy and inhomogeneity frequently result in complicated fracture initiation and development processes. The term "damage mechanism" refers to the documented literature on several processes of fracture formation. Figure 3-10 depicts a general damage path for the FRP composites in five distinguishable phases (Luthada, 2016; Ribeiro, Sena-Cruz and Vassilopoulos, 2021). The recognized phases are:

1. Matrix cracking: Matrix cracking is the first step in the onset of microcracks under fatigue stress. The hardness and ductility of the matrix influence the growth and density of these cracks. Primary cracks are matrix fractures that propagate either perpendicularly or along the fiber direction in their respective laminar planes.
2. Crack coupling and interfacial debonding: The main cracks stop growing at the characteristic damage state (CDS), which shows the highest level of saturation for the main matrix fractures. In-plane transverse fractures, which start with subsequent loading cycles and develop perpendicular to

the crack tip, are the most likely cause of interfacial debonding. These cracks are referred to as secondary cracks.

3. Delamination: In the interlaminar layers, the secondary fractures start off tiny and isolated. A portion of these interlaminar fractures combine to form zones look like strips, which causes extensive debonding (also known as delamination) between the layers.
4. Fiber breaking: The material's fiber reinforcements serve as a barrier to stop the stabilized initial fractures. Near the main fracture tip, there is a significant risk of further crack propagation, which results in fiber cutting and lowers the strength of the composite material.
5. Fracture: Because different localized damages often cause sudden failure, the ultimate failure of the FRP composites is very unpredictable.

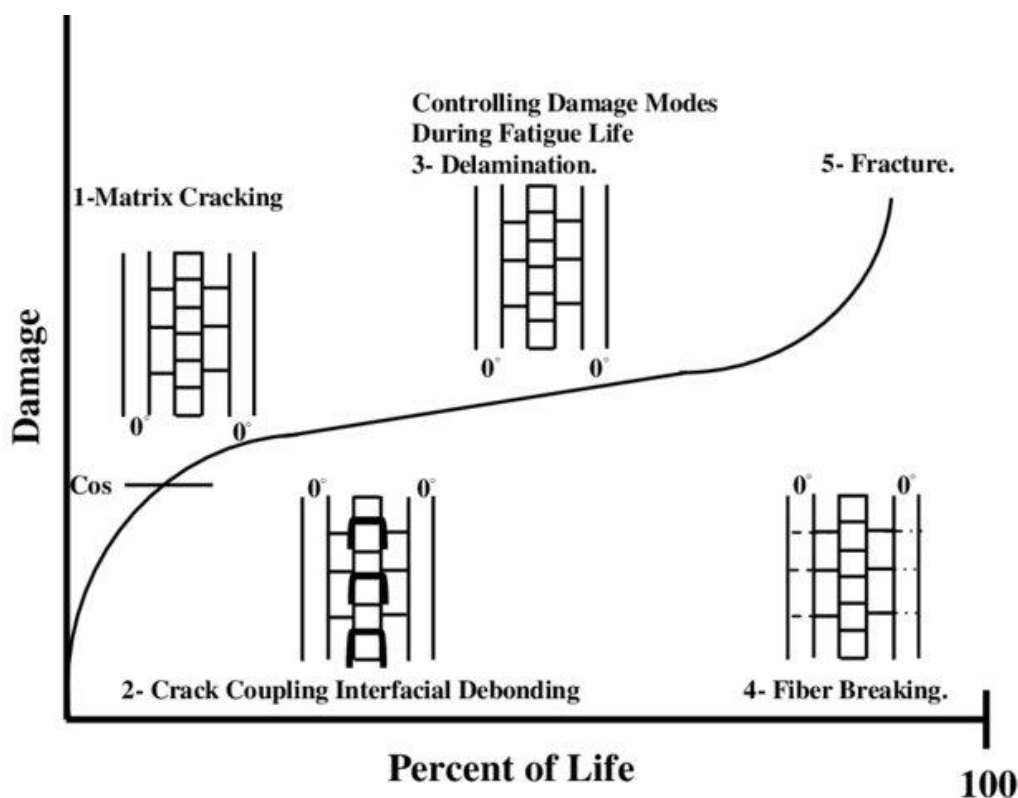


Figure 3-10 Development of damage in composite laminate (Ribeiro, Sena-Cruz and Vassilopoulos, 2021)

3.3 Fracture Mechanics

Although the S-N curve has been extensively used in many sectors throughout the design stage, fracture mechanics is acknowledged as a more effective technique for fatigue analysis. This is mainly due to the fact that fracture mechanics' strength overcomes the S-N curves' main drawbacks, especially when it comes to forecasting and simulating the structural integrity of fractured components. Fracture mechanics has advanced quickly over the last sixty years and is now regarded as a crucial component of safety assessments (Meyers and Chawla, 2009).

Fracture mechanics takes into account three important factors that are essential to assessing structural integrity: crack size, fracture toughness, and design stress. These variables differ from traditional techniques, which focus largely on design stress and material yield stress. In the following sections, the linear elastic fracture mechanics (LEFM), the stress intensity factor (SIF) and crack growth will be discussed in details.

3.3.1 Linear Elastic Fracture Mechanics (LEFM)

When a crack or other imperfection appears, Linear Elastic Fracture Mechanics (LEFM) offers a flexible method for determining the strength of the structure or component. According to the LEFM, the stress fields around the fracture tip govern a crack's behavior. The load applied, the shape of the crack, and the characteristics of the material all affect the stress distribution close to a crack tip (Erdogan, 2000). It may be used to fatigue crack development at any stage of the process, from initial fault or crack identification through the ultimate breakage. As a result, the LEFM, as its name implies, is a technique for evaluating the spread of cracks in materials that is based on the fundamental idea that material conditions typically exhibit linear elasticity throughout the fatigue process. In more conventional design techniques, the expected design stress and the yield

stress of the material are typically the main factors in assessing the material's structural integrity (William F. Hosford, 2011).

In contrast to yield strength, which replaces fracture toughness as the pertinent material attribute, the three main components of the LEFM technique are design stress, crack size, and fracture toughness. Three modes are distinguished among the fracture surface displacement modes in the LEFM, which indicate the possible directions in which a crack may spread. All three forms of crack opening are shown in Figure 3-11. When fatigue-related failures occur, Mode I, sometimes referred to, as the opening mode, is the most prevalent and commonly seen mode. Mode II deals with in-plane shearing or sliding, while Mode III denotes tearing or anti-plane shearing. Since cracks usually develop perpendicular to the direction of maximal primary stress, Mode I predominates in crack extension (Farahmand, 2001).

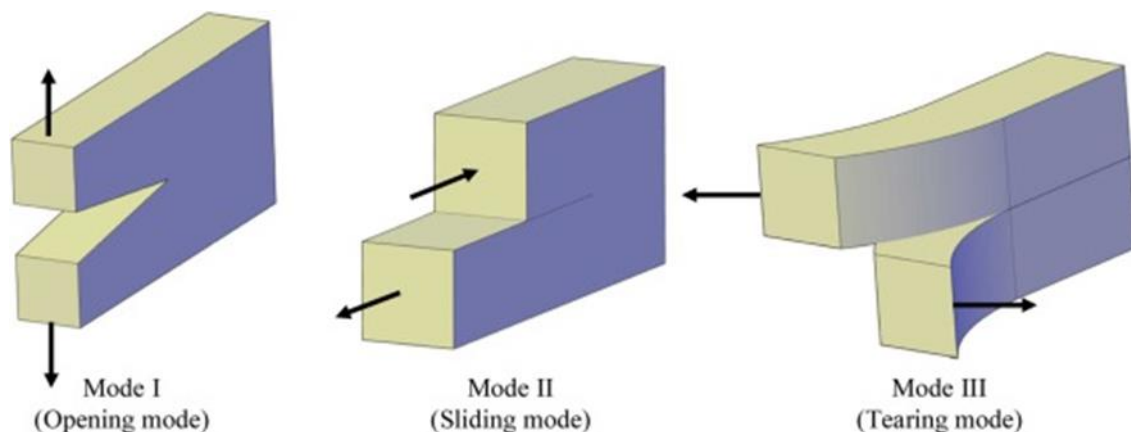


Figure 3-11 Main modes of crack opening (Schlüter, Kuhn and Müller, 2014)

3.3.2 Stress Intensity Factor (SIF)

Since it is believed that the stress field close to the crack tip determines the behavior of the crack, understanding the stress and strain distribution around a crack tip is essential to understanding fracture mechanics. The stresses at the fracture tip of linear elastic materials are exactly proportional to the externally applied load, and the crack length parameter (a) is the only dimension that all cracked geometries have in common. This connection may be described between

the overall circumstances and the stress intensity factor (SIF), represented by the letter "K" (Erdogan, 2000):

$$K = f(\sigma, \sqrt{a}) \quad (3.54)$$

In order for this stress field connection to exist, plastic deformation must either not exist at the fracture tip or, if it does, it must only exist in a tiny area relative to the crack's overall dimensions and the body that contains it. The basic format for expressing the range of stress intensity factor (SIF) in engineering settings is as follows:

$$\Delta K = Y \Delta \sigma \sqrt{\pi a} \quad (3.55)$$

where

ΔK = the range of the stress intensity factor for the matching applied stress range.

Y = correction factor for geometry.

$\Delta \sigma$ = range of nominal applied stress.

a = crack length.

Equation 3.54 shows that the stress intensity factor (SIF) range depends on a number of factors, such as the size of the crack, the shape of the fracture, and the amount of external load. The geometry correction factor, often represented as "Y," is a non-dimensional SIF or normalized SIF that depends on the geometries of the component and fracture, as well as the loading circumstances. In Equation (3.55), both the SIF and the applied stress are shown as ranges. This is necessary to explain how fatigue-induced fracture propagation happens when loads are applied and removed over and over again. Empirical evidence has shown the major impact of the SIF on the formation of fatigue cracks (Nestor, 2017). Furthermore, it has been observed that when the stress intensity range (ΔK) is held constant, the rate of fatigue fracture growth in a homogeneous material stays consistent.

3.3.3 Fatigue Crack Growth

Linear Elastic Fracture Mechanics (LEFM) is a way to help us understand how structures break when they are statically loaded and how fatigue cracks spread. The process of crack formation, which results from cyclic loading, has been studied thanks to the derivation of the stress intensity factor (SIF). Plotting fracture depth (a) against fatigue cycles (N) is a common way to visualize a structure's fatigue crack propagation life. Not to be mistaken with its equivalent in the S-N curve, where (N) indicates the number of cycles until failure, is the usage of (N) in the LEFM. Crack growth rate (da/dN) vs. ΔK (ΔK indicates the range of the SIF) may be shown by adding the stress intensity factor to the fatigue crack growth data. The Paris Law Equation (3.56) may be used to represent the fatigue fracture propagation rate for the majority of composite materials.

$$\frac{da}{dN} = C(\Delta K)^m \quad (3.56)$$

Equation (3.56) may then be integrated to get the number of cycles needed for a crack to propagate from its starting length, (a_i) to its ending length, (a_f).

$$N = \int_{a_i}^{a_f} \frac{da}{C(\Delta K)^m} \quad (3.57)$$

By substituting Equation (3.55) in Equation (3.57) get.

$$N = \int_{a_i}^{a_f} \frac{da}{C(Y\Delta\sigma\sqrt{\pi a})^m} \quad (3.58)$$

Where C and m stand for the empirical material coefficients, or Paris Law coefficients. Figure 3-12 below provides a schematic representation of a typical crack propagation log-log plot of da/dN vs. ΔK (under constant amplitude loading).

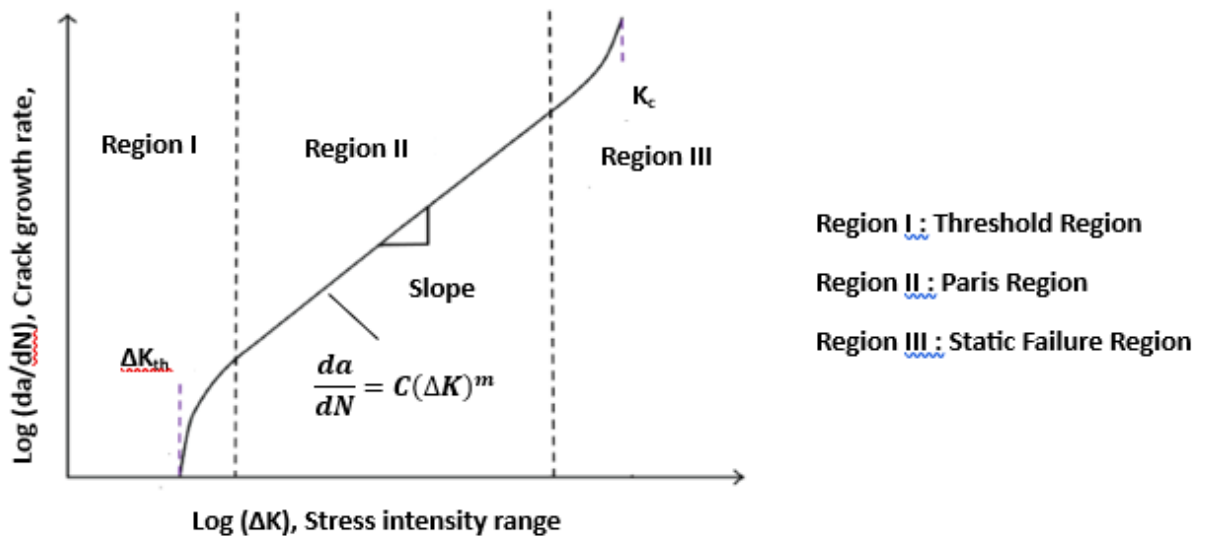


Figure 3-12 Schematic sigmoidal behavior of fatigue crack growth rate versus ΔK (Alexandre Trudel, Mario Turgeon, 2017)

It is essential to acknowledge that the use of linear elastic fracture mechanics (LEFM) in defect evaluation has some practical constraints, particularly in the context of analyzing the evolution of short fatigue cracks. This constraint results from the comparatively broad, in elastic plastic zone around the fracture tip, which is the main factor influencing the development of small fatigue cracks. The stress field ahead of the crack tip is dramatically changed by the preponderance of plasticity at the crack tip, such that the stress intensity factor is no longer the only factor governing the stress field in the uncracked body. But the approximation correlations in the LEFM technique provide a strong tool for describing fatigue development behavior, especially when the fracture size is much bigger than the plastic zone at the crack tip (Alexandre Trudel, Mario Turgeon, 2017).

CHAPTER FOUR

EXPERIMENTAL AND NUMERICAL WORK

This chapter covers the preparation and manufacturing of specimens, including the vacuum infusion technique, and the static and dynamic tests that need to be conducted, including tensile and flexural tests, in addition to the axial and bending fatigue tests. Scanning electron microscopy (SEM) has been used.

4.1 Materials

The matrix used in this work was composed of MGS L285 laminating epoxy resin and its corresponding hardener 285, with a resin-to-hardener mixing ratio of 100:40. The fiber reinforcement utilized consisted of a unidirectional carbon fabric with a weight of 300 g/cm² and a tow equivalent to 12K, as well as a unidirectional E-glass fabric with a weight of 330 g/cm². The carbon fabric had a stitch pattern of UD 0–90-stitch, with a weight of 0° = 283 gr, 90° = 37 gr, and stitch fiber = 10 gr. A filler reinforcement employed in this study was a spherical nano powder/nanoparticle SiO₂ (silicon dioxide), with a size of 15–35 nm, a purity of 99.5+%, and being amorphous. Table 4-1 displays the technical characteristics of resin and hardener.

Table 4-1 L285 resin and H285 hardener properties (nickel, 2016)

	Density (g/cm³)	Viscosity (mPa.s)	Epoxy equivalent, (g/equivalent)	Amine value, (mg KOH/g)	Refractory index
Nominal L285 Resin	1.18-1.23	600-900	155-170	-----	1.525-1.530
Nominal H 285 Hardener	0.94-0.97	50-100	-----	480-550	1.5020- 1.5500

4.2 Manufacturing Methods

Various manufacturing techniques, including pultrusion, resin transfer moulding, vacuum infusion, hand layout, injection moulding, and filament forming, can produce advanced hybrid composite materials. The choice was made to attempt to create the hybrid composite using one of the previously enumerated techniques. The available equipment limited the type of vacuum infusion that could be used.

4.2.1 Vacuum Infusion

Vacuum infusion is a manufacturing method that involves combining fibers, such as glass or carbon, with a resin matrix under vacuum pressure. This process results in creating a composite material that is both strong and lightweight. This approach extensively manufactures diverse components for sectors such as aerospace, automotive, marine, and sports equipment.

The type of fibers, namely unidirectional glass and unidirectional carbon fibers, was chosen based on the required properties of the composite, as shown in Figure 4-1. Carbon fiber is known for its high strength and rigidity, while glass fiber provides good impact resistance and is more cost-effective. The resin (epoxy and hardener) was also chosen, as shown in Figure 4-2, to build the requirements of the plate for mechanical and fatigue properties tests.

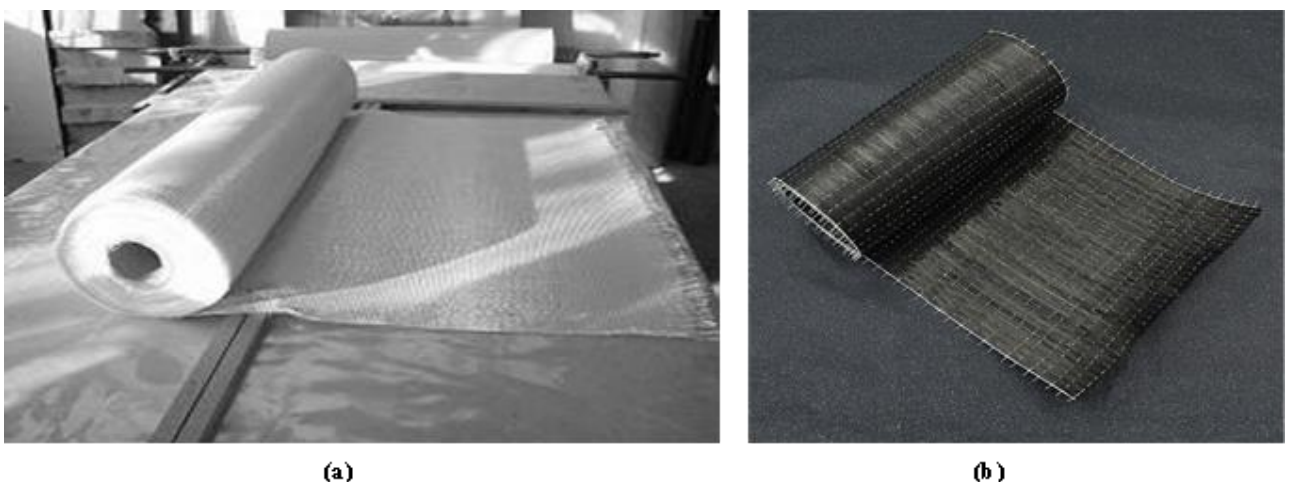


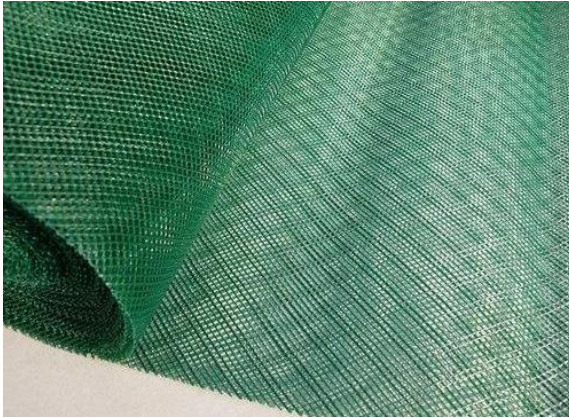
Figure 4-1 (a) Unidirectional glass fiber, (b) Unidirectional carbon fiber



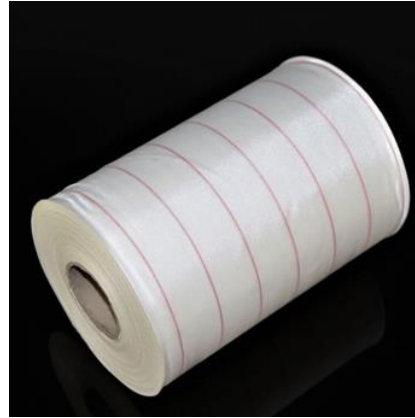
Figure 4-2 Epoxy resin and hardener

The first step in vacuum packaging is to prepare the mould, where an aluminum flat plate of dimension 1m x 2m was used as a mould for making the composite panel.

The aluminum flat plate must be clean and polished to facilitate the moulding process. After that, the fibers (glass and carbon) are prepared and cut according to the required dimensions (50 cm x 50 cm), as well as the preparation of other materials required to complete the manufacture of the hybrid composite material (release film, infusion mesh, peel ply, vacuum bag, spiral hose, sealer tape), as shown in Figure 4-3.



Infusion Mesh



peel ply



release film



sealer tape



vacuum bag



spiral hose

Figure 4-3 materials required to manufacture of the hybrid composite material

After fulfilling and preparing all necessary requirements, the process of manufacturing laminate commences. This involves placing the release film on a flat sheet of paper. Next, the sealing tape is placed (this adhesive is double-sided) and glued to the edge of the film release very tightly. After that, the layers of glass and carbon are arranged in the required directions and angles. The peel ply, as a fabric, is placed to ensure that the composite material does not stick to the infusion

mesh placed directly on the peel ply. A spiral infusion hose is installed on both sides of the sheet, and then the vacuum bag, made of thermal nylon, is placed properly and secured by sealing tape fixed to a flat sheet. Then, after installing the inlet and outlet tubes and connecting them with a spiral hose for leakage, the bag is completely emptied of air until the pressure gauge reaches -760 mm Hg (-1.01324 bar), as shown in Figure 4-4.

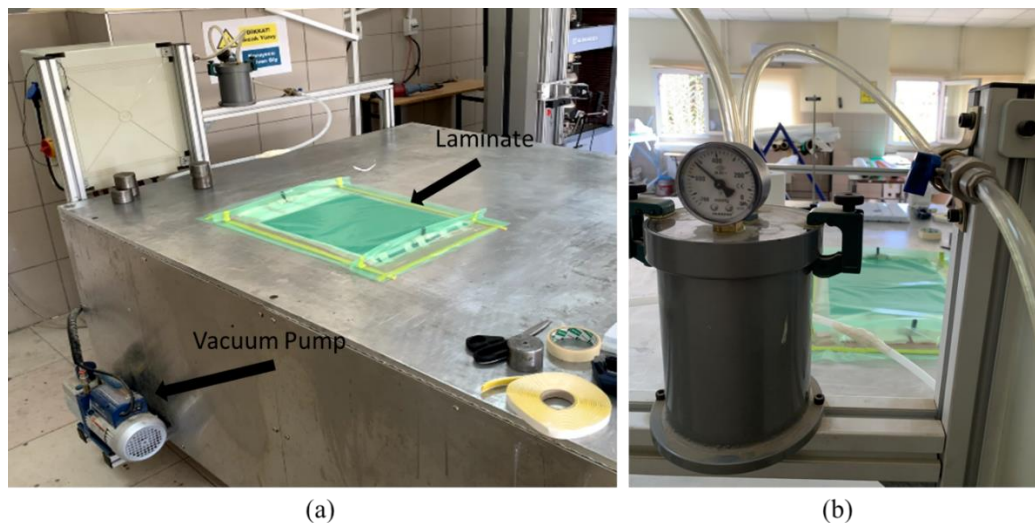


Figure 4-4 (a) Laminate before vacuum, (b) pressure gauge

The inlet and outlet tubes were securely sealed and left for 30 minutes to ensure no leakage occurred in the bag prior to the introduction of the epoxy. After arranging the layers of glass fibers and carbon fibers according to the specified orientations and fulfilling other manufacturing requirements, the interior and exterior of the bag were sealed following the removal of air. The temperature of the flat plate was then raised to 80 °C to initiate the curing process. The resin was prepared by mixing with the hardener at a ratio of 40 g of hardener per 100 g of resin, in accordance with the manufacturer's specifications.

Using a vacuum pump, the system is emptied of air, which allows the resin to penetrate deeply and completely into the fibers, thus ensuring that there are no voids inside the laminate. As a result, a high adhesion force between the fibers and the resin was obtained (Figure 4-5). Next, the inlet and outlet tubes were

closed tightly, and the laminate was left for 15 hours to cure. After completing the curing process, the plate is extracted from the system and is ready to be cut for testing specimens.

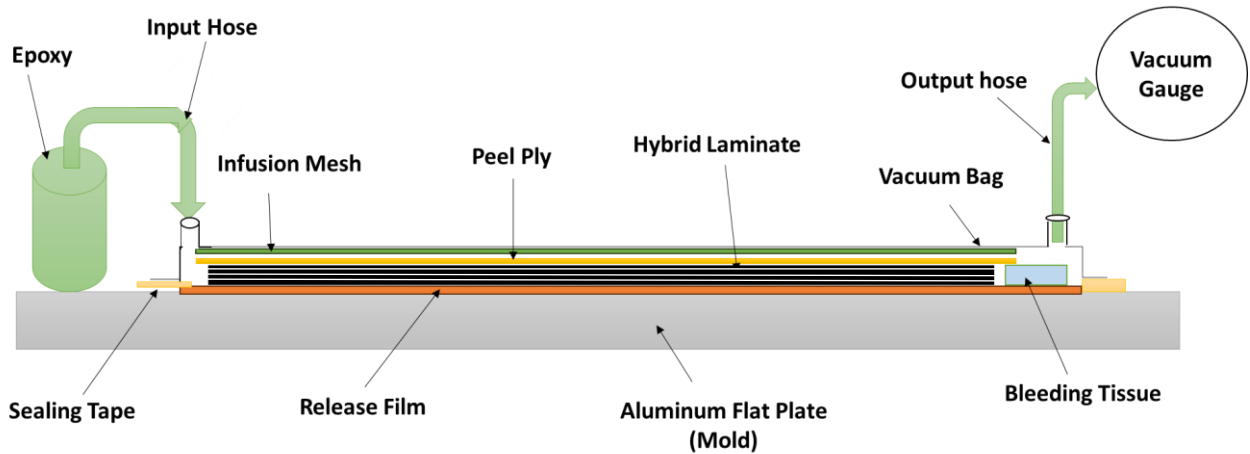


Figure 4-5 Vacuum bag and curing technique.

4.2.2 Adding Silica Dioxide Nanoparticles to Epoxy Resin

Nanosilica powder (SiO_2) was added to MGS L285 epoxy base resin at a weight fraction of 2%, subsequently, the mixture was manually blended (Figure 4-6).

In order to uniformly distribute the silica nanoparticles within the resin, ultrasonic mixer device to uniformly distribute the silica nanoparticles within the resin. This device relies on the so-called magnetic fish, which significantly contributes to this distribution through magnetic pulses, causing the magnetic fish to rotate in the mixture at a rate of 350 revolutions per minute. This procedure is a periodic or alternating action, with two seconds on and three seconds off. The entire mixing process takes place within two hours. Therefore, to prevent the resin from deteriorating during the ultrasonic dual mixing process, an ice bath was installed around the mixture container, as shown in Figure 4-7.



(a)



(b)

Figure 4-6 (a) SiO₂ weight measurement (b) mixing SiO₂ nanoparticles manually



Figure 4-7 Ultrasonic mixer

A vacuum degassing process was conducted for about 15 minutes to ensure that all bubbles were out, after the ultrasonic dual mixing in order to remove air bubbles that were formed during the mixing process as shown in Figure 4-8.

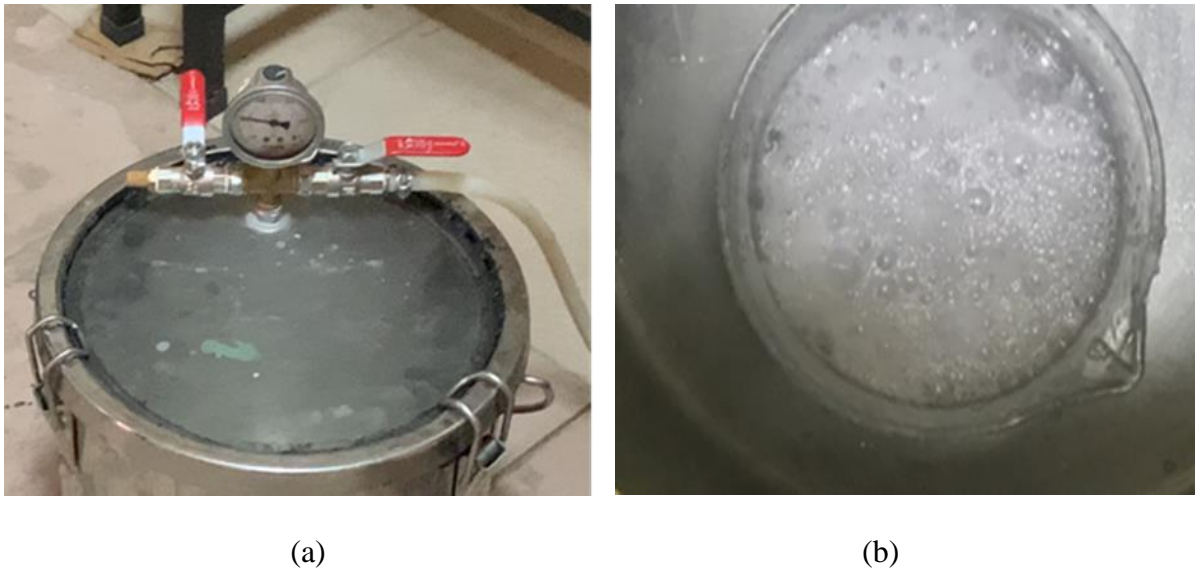


Figure 4-8 (a) Vacuum chamber (b) Removing bubbles

Ultimately, the mixture that had been stripped of gas was combined with a hardener. Subsequently, the mixture was pulled into a laminated fiber composite via applying a vacuum pressure system, known as vacuum-assisted resin infusion (vacuum infusion); as shown in Figure 4-9.

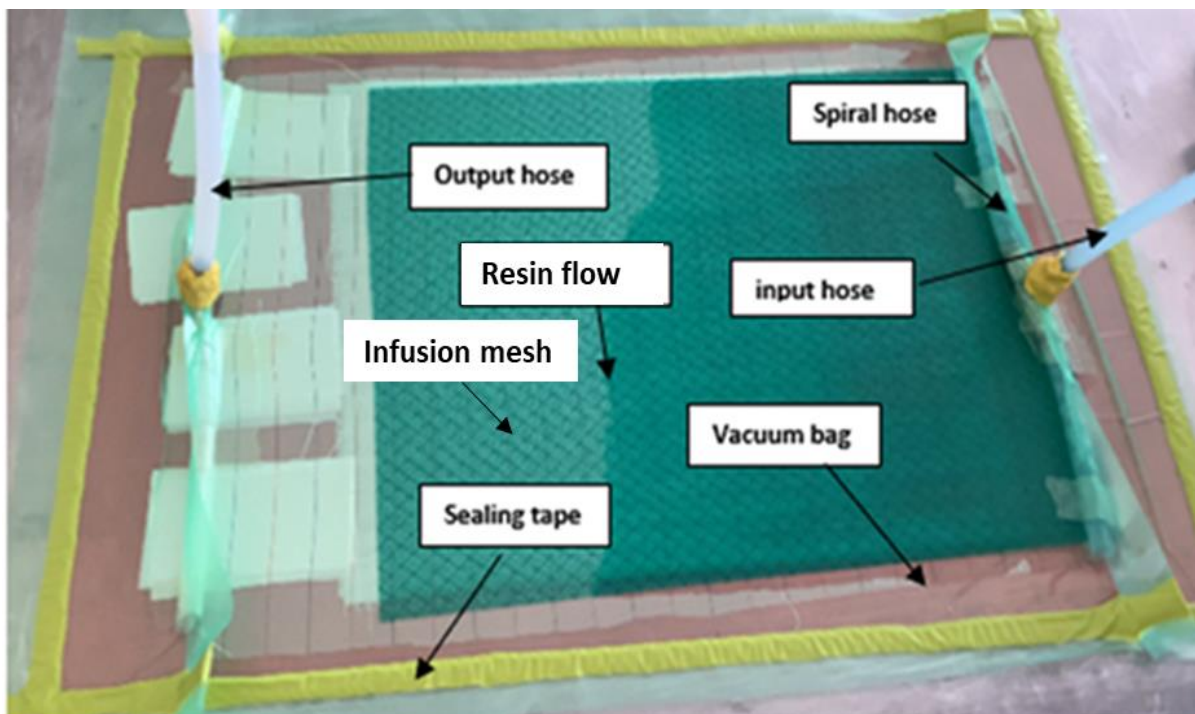


Figure 4-9 Resin injected into fiber's layers

4.3 Preparation Test Specimens

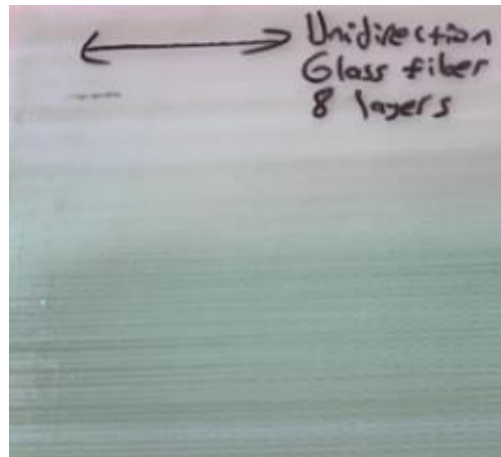
Three different groups of hybrid composite laminates were manufactured. Each group contains two sets, one without SiO₂ nanoparticles and the other with SiO₂ nanoparticles at a weight ratio of 2%. All composite laminates were manufactured using vacuum bag technology.

4.3.1 Manufacturing of Glass/Epoxy and Carbon/Epoxy Laminates

The glass and carbon consist of two laminates created utilizing a 55% fiber volume fraction of unidirectional glass fibers/epoxy, as shown in Table 4-2. Each laminate has eight layers with a 0-degree orientation angle. One laminate includes SiO₂ nanoparticles, while the other does not. Furthermore, two laminates were built using unidirectional carbon fibers/epoxy with a fiber volume fraction of 50% and eight layers at an angle of 0-degree. One carbon fiber laminate, like the glass fiber laminates, includes SiO₂ nanoparticles, whereas the other does not, as shown in Figure 4-10.

Table 4-2 Glass and carbon fiber mechanical properties

	Samples	Composite type	Stacking Sequences	No. of Layers	Thick. mm	Density g/cm ³	Weight g
First group	G	[G] ₈	[0°] ₈	8	2	1.6576	1195.2
	GN	[G] ₈	[[0°] ₈	8	2	1.8413	1205.8
	C	[G] ₈	[0°] ₈	8	2	1.4838	880
	CN	[G] ₈	[0°] ₈	8	2	1.5056	888.8



(a)



(b)

Figure 4-10 (a) Unidirectional Glass fiber/epoxy laminate (b) Unidirectional Carbon fiber/epoxy laminate

These laminates were fabricated particularly, to study the mechanical properties, such as longitudinal modulus (E_1), transverse modulus (E_2), in-plane shear modulus (G_{12}), and Poisson's ratio (ν_{12}). Figure 4-11 depicts the experimental setup and laminate configurations.

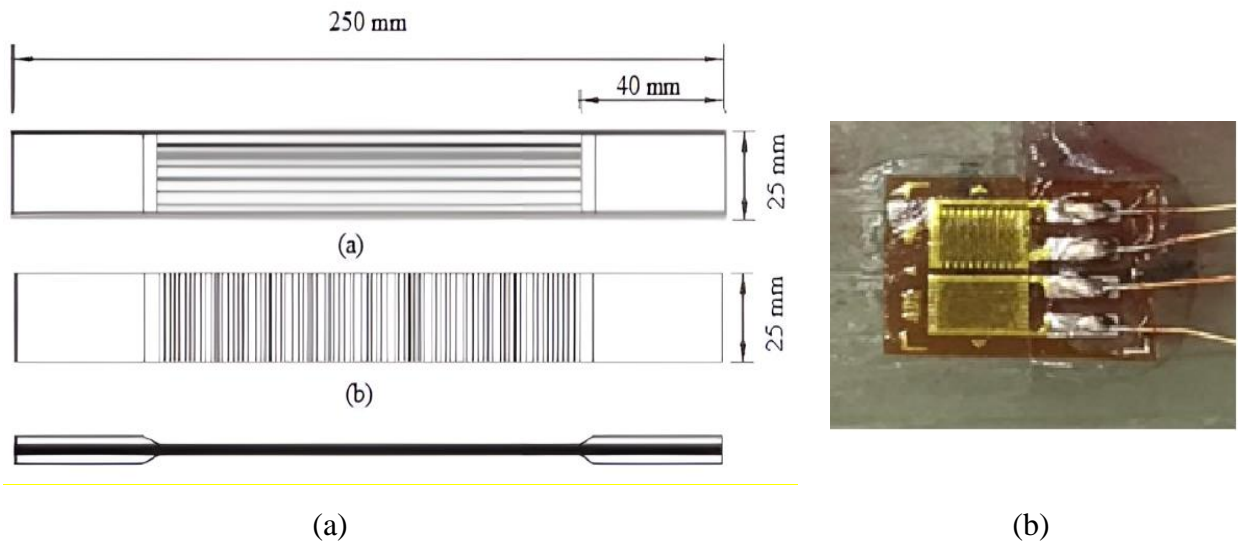


Figure 4-11 (a) Stacking setup ASTM D3039- 2020 standard; (b) Strain gauge for calculating E_1 and E_2

Five specimens for mechanical testing were produced from each composite laminates. The tensile specimens were manufactured according to the ASTM D3039-2020 standards (ASTM International, 2020a). The dimensions of these specimens were 250 mm long and 25 mm wide, for glass/epoxy and carbon/epoxy specimens, as shown in Figure 4-12 and Figure 4-13, respectively. To prevent the tensile specimens from slipping off the machine's jaw, thickeners made of glass/epoxy material were used to grip the ends of the specimens.

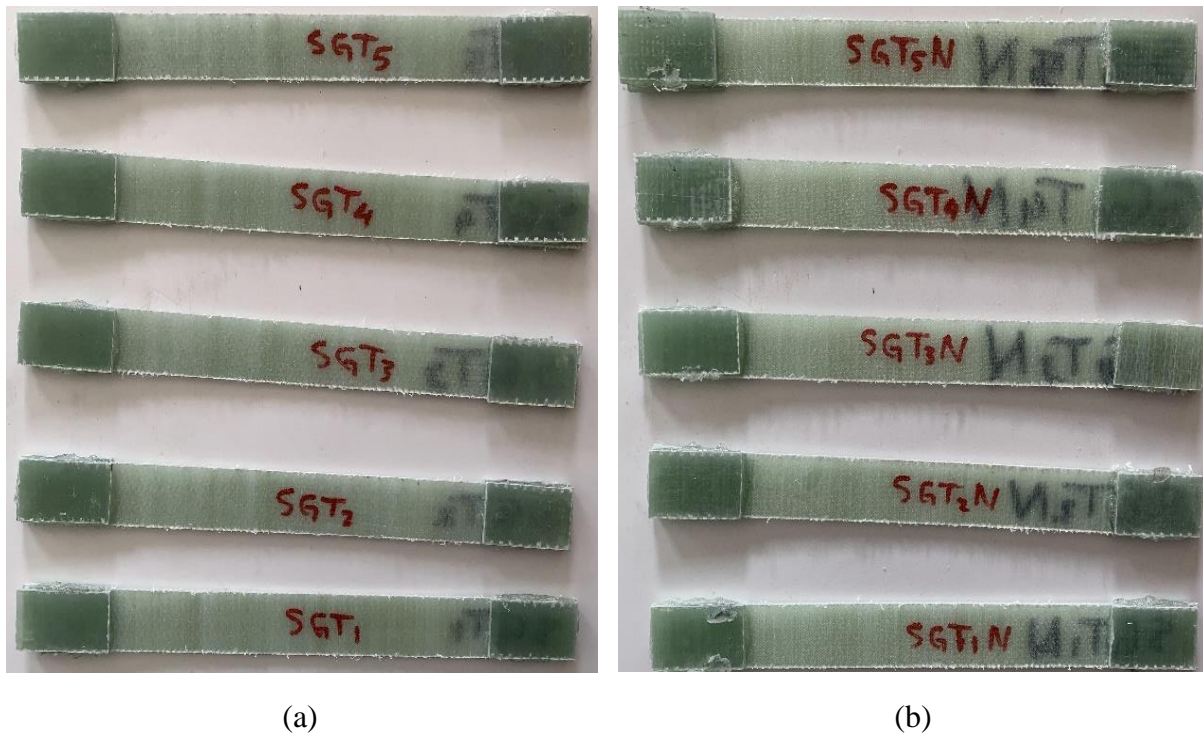


Figure 4-12 Specimens of glass/epoxy for tensile test (a) without SiO_2 nanoparticles, (b) with SiO_2 nanoparticles

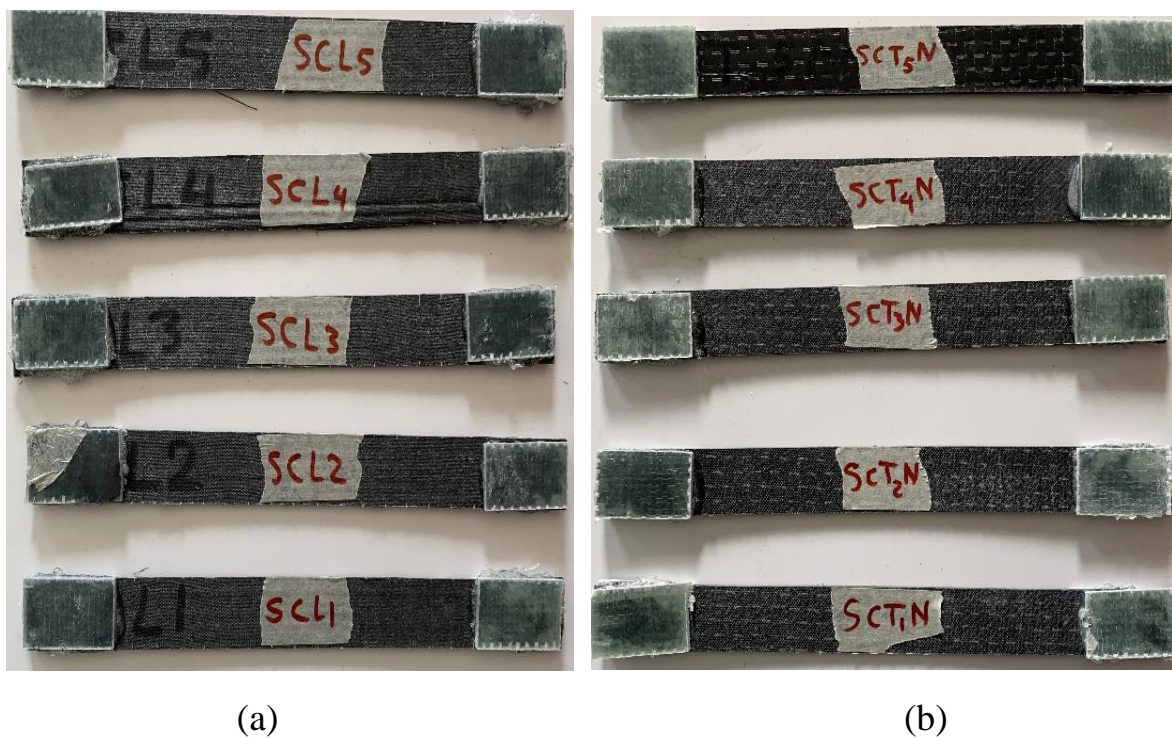


Figure 4-13 Specimens of carbon/epoxy for tensile test (a) without SiO_2 nanoparticles, (b) with SiO_2 nanoparticles

4.3.2 Manufacturing of Quasi-Isotropic Ply Laminates

The of quasi-isotropic ply Laminates, as shown in Table 4-3, is known as a quasi-isotropic laminate that consists hybrid composite plates with 2% wt. of SiO₂ nanoparticles and without SiO₂ nanoparticles. The hybrid laminates contain of resins, glass fibers, and carbon fibers, with varying layers (8, 10, and 12 layers) and a fiber volume fraction of 53.33%, as shown in Figure 4-14.

Table 4-3 Stacking Sequence of Quasi-Isotropic Laminates

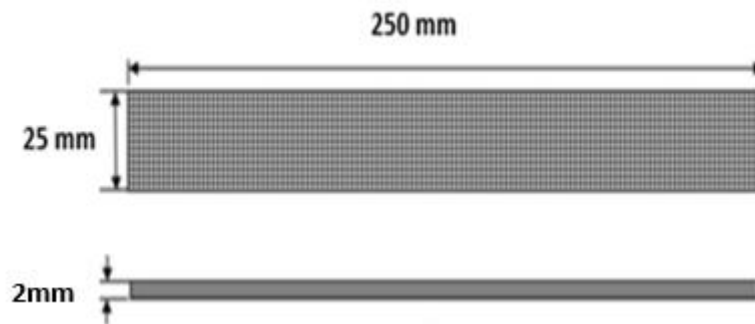
	Samp.	Composite type	Stacking Sequences	No. of Layers	Thick. mm	Density g/cm ³	Weight g
Second group	QS1	[G/C/G/C] _s	[0°/45°/90°/0°] _s	8	2.4	1.621	1037.6
	QS2	[G/C/G/C/G] _s	[0°/45°/90°/0°/45°] _s	10	2.65	1.662	1297
	QS3	[G/C/G/C/G/C] _s	[0°/45°/90°/0°/45°/90°] _s	12	2.84	1.672	1556.4
	QS1N	[G/C/G/C] _s	[0°/45°/90°/0°] _s	8	2.42	1.657	1037.6
	QS2N	[G/C/G/C/G] _s	[0°/45°/90°/0°/45°] _s	10	2.66	1.690	1297
	QS3N	[G/C/G/C/G/C] _s	[0°/45°/90°/0°/45°/90°] _s	12	2.87	1.689	1556.4

*QS: Quasi-isotropic plates without SiO₂ Nano particles, QSN: Quasi-isotropic plates with SiO₂ Nano particles, G: Glass fibers, C: Carbon fibers.



Figure 4-14 Unidirectional glass/carbon quasi-isotropic laminate

Five specimens for mechanical testing were produced from each composite laminates. The tensile and axial fatigue specimens were manufactured according to the ASTM D3039 standards (ASTM International, 2020a). While the three points bending and flexural fatigue specimens were fabricated according to ASTM D790 (ASTM International, 2020b). The dimensions of the tensile and axial fatigue specimens were 250 mm long and 25 mm wide, as shown in Figure 4-15. While the bending and flexural fatigue specimen dimensions were 100 mm long and 10 mm wide, as shown in Figure 4-16. As mentioned, thickeners made of glass/epoxy material were used, to prevent the specimens from slipping off the machine's jaw, to grip the ends of both the tensile and axial fatigue specimens.



(a)



(b)

Figure 4-15 Tensile and axial fatigue specimen (a) specimen dimensions Stacking setup ASTM D3039- 2020 standard, (b) specimen's photograph

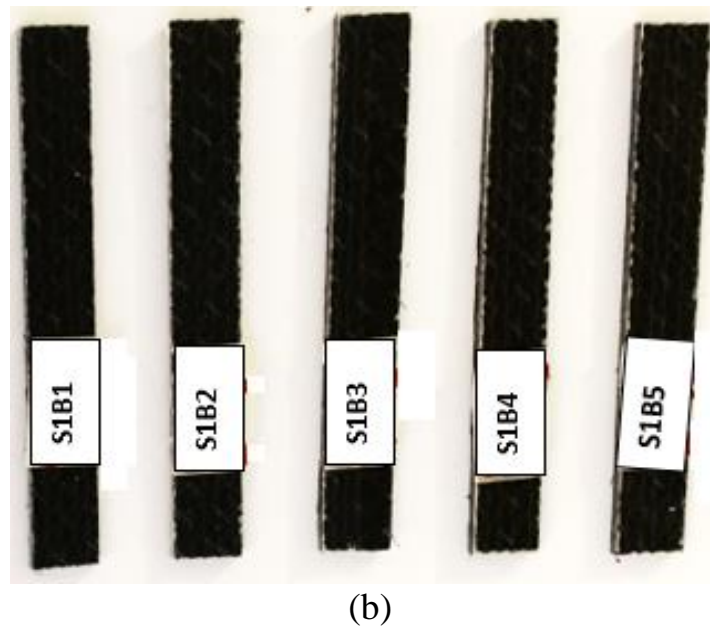
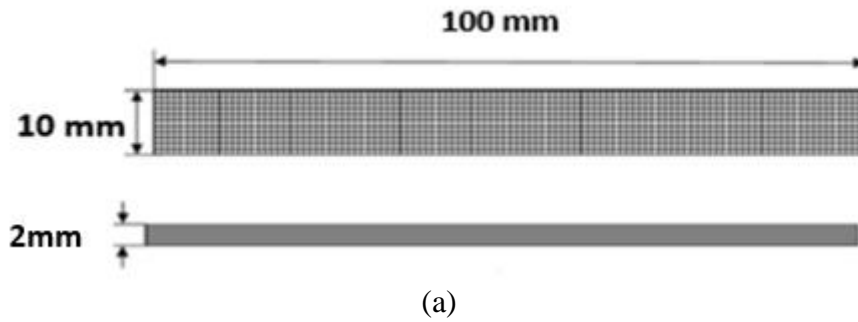


*Figure 4-16 Bending and flexural fatigue specimen (a) specimen dimensions
Stacking setup ASTM D790- 2020 standard, (b) specimen's photograph*

4.3.3 Manufacturing of Cross-Ply Laminates

The third group, as indicated in Table 4-4, is referred to as a cross-ply laminate, which comprises hybrid composite plates containing 2% weight of SiO_2 nanoparticles and plates without SiO_2 nanoparticles. The hybrid laminates consist resins, glass fibers, and carbon fibers. The laminates were composed of different numbers of layers (8, 12, 16, and 20 layers) and have a fiber volume fraction of 53.33%, as depicted in Figure 4-17.

Table 4-4 Stacking Sequence of Cross- Ply Laminates

Samp.	Composite type	Stacking Sequences	No. of	Thick. mm	Density g/cm ³	Weight g
CS1	[G/C/G/C] _s	[0°/90°/90°/0°]s	8	2.02	1.621	1037.6
CS2	[G/C/G/C/G/C] _s	[0°/0°/90°/90°/0°/0°]s	12	3	1.662	1297
CS3	[G/C/G/C/G/C/G/C] _s	[0°/90°/90°/0°/0°/90°/90°/0°]s	16	4	1.672	1556.4
CS4	[G/C/G/C/G/C/G/C/G/C] _s	[0°/0°/90°/90°/0°/0°/90°/90°/0°/0°]s	20	4.67	1.713	1815.8
CS1N	[G/C/G/C] _s	[0°/90°/90°/0°]s	8	2	1.657	1037.6
CS2N	[G/C/G/C/G/C] _s	[0°/0°/90°/90°/0°/0°]s	12	3	1.69	1297
CS3N	[G/C/G/C/G/C/G/C] _s	[0°/90°/90°/0°/0°/90°/90°/0°]s	16	4	1.699	1556.4
CS4N	[G/C/G/C/G/C/G/C/G/C] _s	[0°/0°/90°/90°/0°/0°/90°/90°/0°/0°]s	20	4.69	1.723	1815.8
Third Group						

*CS: cross-ply plates without SiO₂ Nano particles, QSN: cross-ply plates with SiO₂ Nano particles, G: Glass fibers, C: Carbon fibers.



Figure 4-17 Unidirectional Glass/carbon cross-ply laminate

The DIAMANT RUBI cutter machine was utilized to cut the specimens, as was previously described. As mentioned in Section 4.3.2, specimens for each test were manufactured tensile, axial fatigue, three-point bending, and flexural fatigue. As previously indicated, thickeners composed of glass/epoxy material were utilized to grasp the ends of the tensile and axial fatigue specimens and keep them from slipping off the machine's jaw.

4.4 Mechanical Tests

4.4.1 Tensile and Three-Point Bending Tests

The tensile tests were carried out in accordance with the standard test procedure outlined by ASTM D3039. Five specimens were manufactured for each composite laminate groups. The experiments were carried out using a Shimadzu universal testing machine (AGS-X Plus) (shown in Figure 4-18) at a cross-head speed of

2 *mm/min*, and a strain rate of 0.01 s⁻¹ with a load cell of 100 *kN*. Five readings were taken for each composite laminates to determine an average tensile strength.

In compliance with the specifications outlined in ASTM D 790. Shimadzu machine (shown in Figure 4-19) was employed to carry out bending tests at a cross-head velocity of 1 *mm/min* and with a load cell rating of 100 *kN*. Five specimens were manufactured for each composite laminate group. Five readings were taken for each group of composite laminate to determine an average bending strength. The experimental procedure included placing a typical rectangular flexural sample between two roller supports with a diameter of 30 *mm* and a span length of 60 *mm*. The nose load point diameter was 10 *mm*, located at the midpoint of the sample. The following equations were used to assess the experimental flexural strength, strain, and flexural modulus of elasticity.

$$\sigma_f = \frac{3PL}{2bd^2} \quad (4.1)$$

$$\varepsilon_f = \frac{6 D d}{L^2} \quad (4.2)$$

Where σ_f is the flexural strength in *MPa*, ε_f is the flexural strain in *mm/mm*, *P* is the load in *N*, *d* is the thickness of the specimen in *mm*, *b* is the width of the specimen in *mm* and *D* is the central deflection of the beam in *mm*. (Kaw, 2005).

The specimen was held in place by a beam that allowed it to move freely for the whole of the test, and the load was brought to the center of the specimen. All tests were conducted at room temperature.

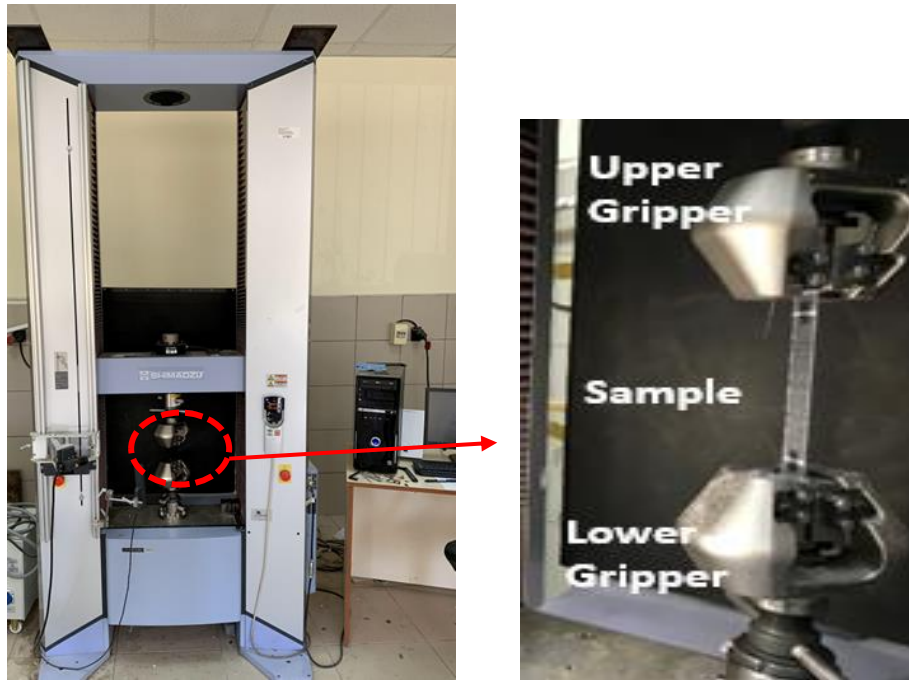


Figure 4-18 Tensile Test Using SHIMADZU Universal Testing Machine with a Force Capability of 100 kN

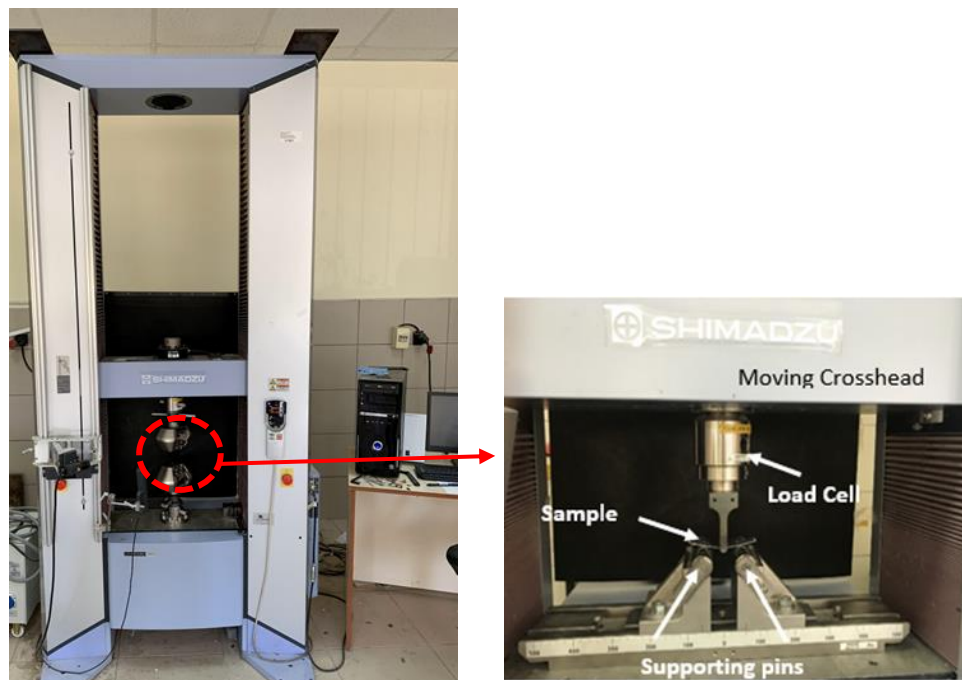


Figure 4-19 Three-Point Bending Test Using SHIMADZU Universal Testing Machine with a Force Capability of 100 kN

4.4.2 Axial Fatigue Test

One of the most frequent failure types in materials is fatigue, with cyclic stress being the most prevalent contributing element. As a result, determining the fatigue life of the suggested composite is critical, particularly when considering lightweight industrial applications such as glass/carbon hybrid composite materials. The unidirectional glass/carbon hybrid composite materials that are stacked in a certain order and put through axial fatigue testing make up the structure. The ASTM D3039 standard was followed while cutting the specimens for the axial fatigue testing. As shown in Figure 4-20, fatigue tests were conducted using a 100 *kN* load cell device at room temperature and 50% humidity using the Shimadzu brand Servo-Hydraulic fatigue tester machine. Fatigue tests were conducted using the ($R = 0.1$) stress ratio, 8 *Hz* frequency, and sine wave load to ascertain the samples' fatigue limits (Favela-Gallegos and Soutis, 2012; Shah and Tarfaoui, 2014). The produced unidirectional hybrid composites had an average thickness of 2, 3, 4, and 5 mm. To avoid early failures at the tensile jaws, 40 x 25 x 2 mm glass fiber composite tabs were affixed to the ends of the unidirectional hybrid composites.

The fatigue behaviors of the glass/carbon hybrid composite laminates were investigated under different load levels of 40%, 50%, 60%, and 70%. At least three specimens for each parameter of neat epoxy hybrid composites and SiO₂ nanoparticle reinforced hybrid composites were subjected to fatigue tests and the cycle numbers of hybrid composites were obtained from these samples.



Figure 4-20 Shimadzu brand Servo-Hydraulic Fatigue Tester

4.4.3 Flexural Fatigue Test

Due to the unavailability of a flexural fatigue test machine, a flexural fatigue testing apparatus was designed and manufactured in this study. The following section describes the manufacturing procedure for the flexural fatigue test rig.

4.4.3.1 Manufacturing Test Rig

Figure 4-21 presents a schematic diagram for the test rig that was used in this study. The manufacturing process included precision manufacturing, welding, and assembly of components to meet design specifications. Careful attention was paid to ensuring the structural integrity of the device and its operational reliability under cyclic loading conditions. The main components used in manufacturing the test rig are:

- 1- Steel structure:** A steel structure was used to install the main components on it. The frame is strong enough to withstand high cyclic loading and ensure stability during testing.

- 2- **Three-phase electric motor:** The main function of the electric motor in a fatigue tester is to apply cyclic loads to the test specimen. This involves converting electrical energy into mechanical motion, which is used to repeatedly stress the material or component under test.
- 3- **Holding fixtures:** The holding fixture firmly grips the test specimen in place, ensuring it does not move or slip during the test. And it ensures proper alignment of the test specimen with respect to the loading mechanism, which helps distribute the applied load uniformly across the test specimen.
- 4- **Dial gauge:** A dial gauge was utilized to measure the deflection of the specimens.
- 5- **Connecting rod:** Its function to convert the rotational motion to reciprocating motion.
- 6- **Magnetic sensors:** Two magnetic sensors were used; one of them is to compute the number of cycles, while the other is to turn off the motor.
- 7- **An electronic control box:** This box has the following functions:
 - a. Controlling the frequency and calculating the number of cycles until failure.
 - b. Sensing the number of cycles and self-extinguishing when the specimen is fractured (failure).
 - c. Using an information cable to connect this system to the laptop for control and recording purposes.

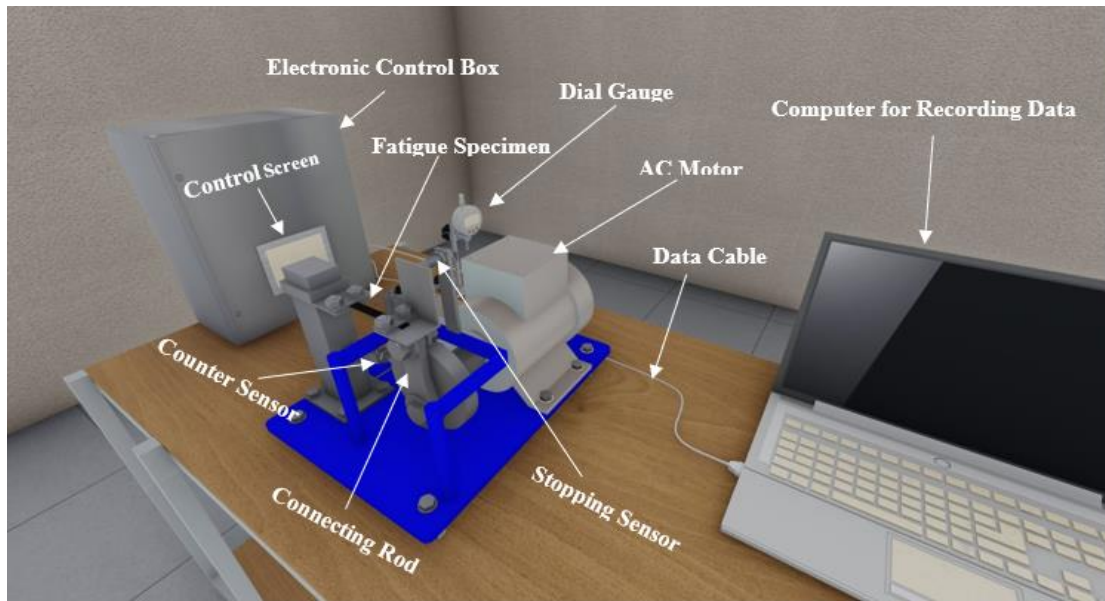


Figure 4-21 Schematic diagram of flexural fatigue test machine

4.4.3.2 Validation and Testing

To validate the flexural fatigue results, a standard bending fatigue apparatus was used from the University of Mosul/ Mechatronics Engineering Department. The standard apparatus (Type HSM20), as shown in Figure 4-22. Validation between two fatigue testers involves a comparative analysis to ensure both systems yield consistent and accurate results under similar testing conditions. This process includes selecting a standardized test specimen and conducting fatigue tests on both machines while maintaining identical parameters such as load amplitude, frequency, and environmental conditions. Figure 4-23 shows the validation results between the test rig, use in this study, and the standard flexural fatigue machine. It can be seen from the figure that there is a good correlation between the results. Therefore, the test rig was employed in this work.



Figure 4-22 HSM20 alternating bending fatigue machine

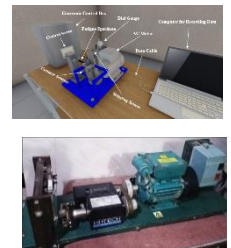
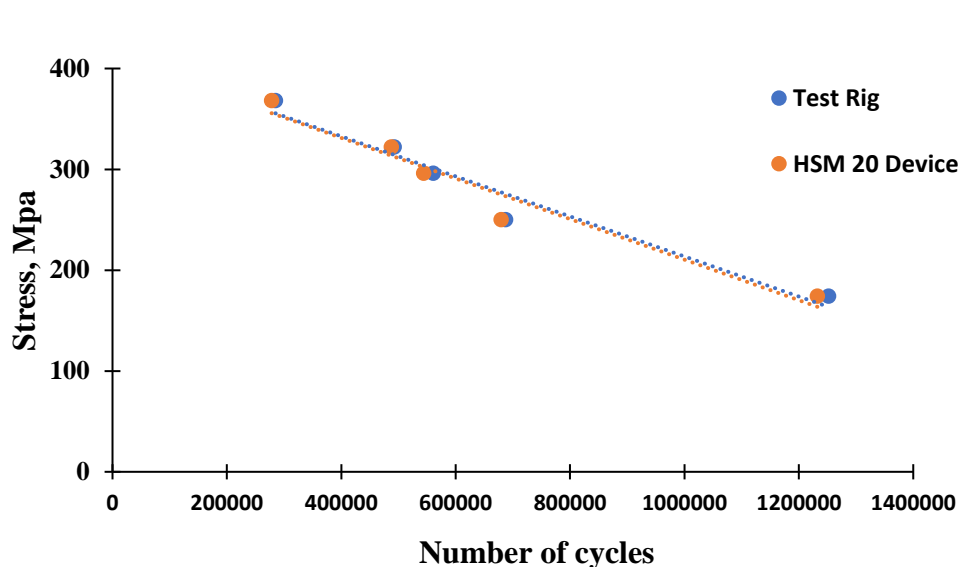


Figure 4-23 Comparison between results of HSM20 and the test rig

The test rig depicted in Figure 4-24-a was used to apply fully reversed bending stress. In order to ensure appropriate fixation of the specimens, grips were provided. The free end of the specimen is subjected to a fluctuating load by using a reciprocating arm. This arm is turned by a crank and connecting rod. The test was conducted by applying loads equivalent to (40, 50, 60, 70, and 80%) of the bending maximum stress. The bending fatigue test was conducted in accordance with the following steps: Equation (4.1) was first used to compute the applied

stress, and Equation (4.2) was then used to determine the force. The displacement δ that was subjected to the free end of the specimen to produce the necessary stress was finally determined using Equation (4.3). A dial gauge was used to measure the displacement at the free end, and with the connecting rod adjusted, the required displacement will be applied during the fatigue tests.

$$(\sigma_b)_{Applied} = (\sigma_b)_{max.} \times A \quad (4.1)$$

where

$(\sigma_b)_{Applied}$: The applied stress

$(\sigma_b)_{max.}$: Maximum bending stress

A: stress level factor which equal to (40,50,60,70, and 80%)

$$(\sigma_b)_{Applied} = \frac{Fl}{z} = \frac{6fl}{bt^2} \quad (4.2)$$

$$\delta = \frac{4fl^3}{Ebt^3} \quad (4.3)$$

Where δ is the displacement. The number of cycles is recorded by the revolution counter fitted to the motor. Cut-out switches automatically stop the machine when the specimen breaks. A cyclic stress ratio (R) = -1 (fully reversed) conditions, while maintaining a frequency of 10 Hz was used in all the bending fatigue tests. The dimensions of the test specimens (length = 100 mm, width = 10 mm, thickness = 2 mm) are presented in Figure 4-24-b.

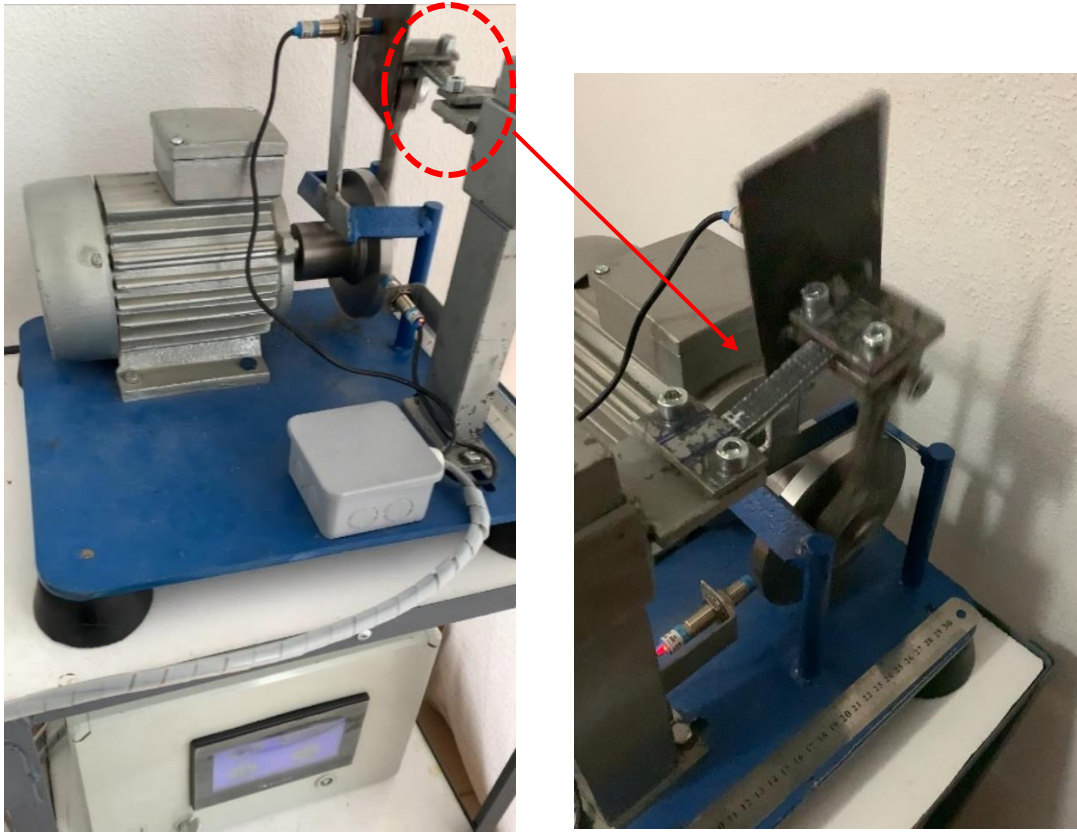


Figure 4-24 (a) Fatigue test rig (b) Fatigue test Specimens

4.5 Numerical Modeling

All the experimental data, including tensile, three-point bending, axial fatigue, and flexural fatigue, were analyzed and compared with numerical results using ANSYS ACP 2019/R3 workbench software. The numerical modeling process utilized in this study was consistent with the methodology used to investigate the behavior of neat epoxy composite materials and hybrid composite materials containing silica nanoparticles. Utilizing the ANSYS software with the ACP module (Karnati, Agbo and Zhang, 2020), the FE models were created. This software program provides sophisticated simulation and analysis capabilities for structural systems.

4.5.1 Materials Designer

For accurate simulations, Ansys Material Designer, within Ansys Workbench, enables the creation of homogeneous models for complex materials using prebuilt or customizable geometries, including lattices and composites. Through the finite element method, it meshes a representative volume element (RVE) as shown in Figure 4-25, applies loads, and determines effective properties based on the response. This section is used to predict the material properties for both axial fatigue simulation and bending fatigue simulation.

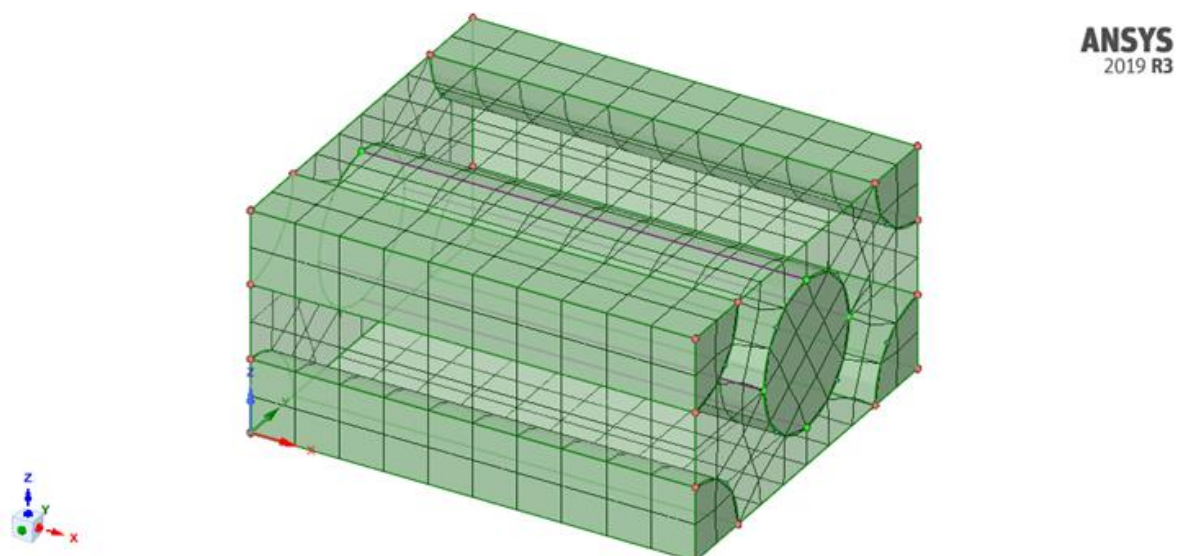
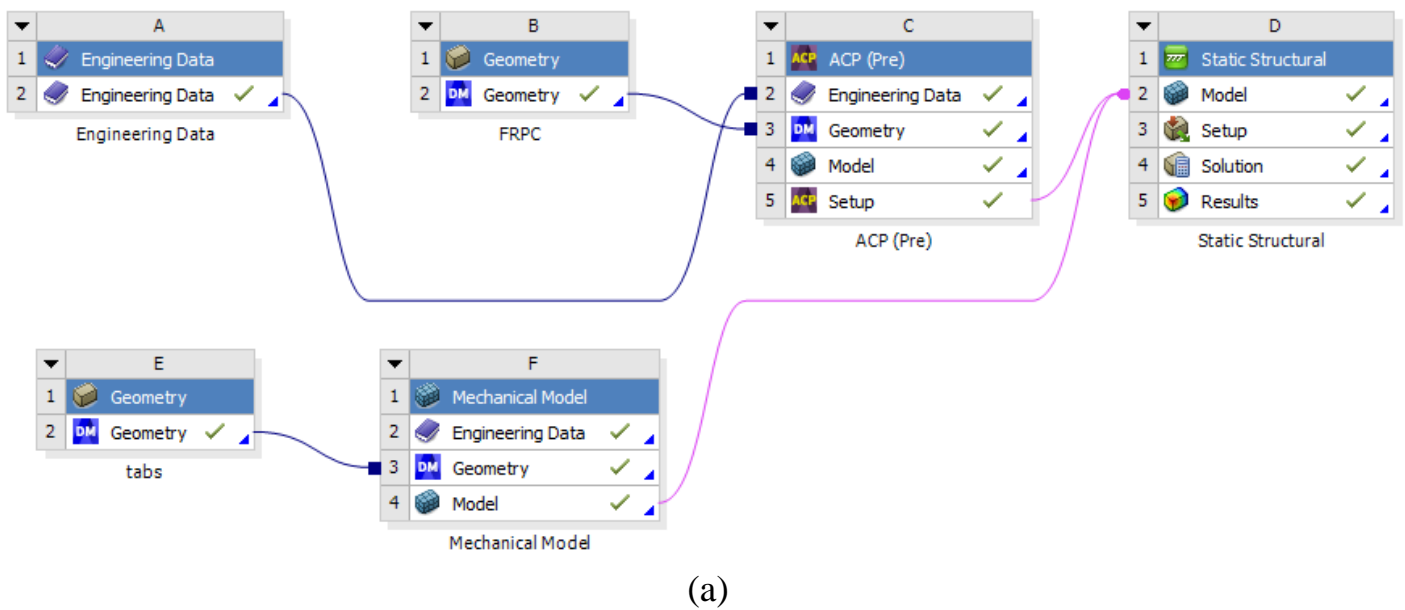
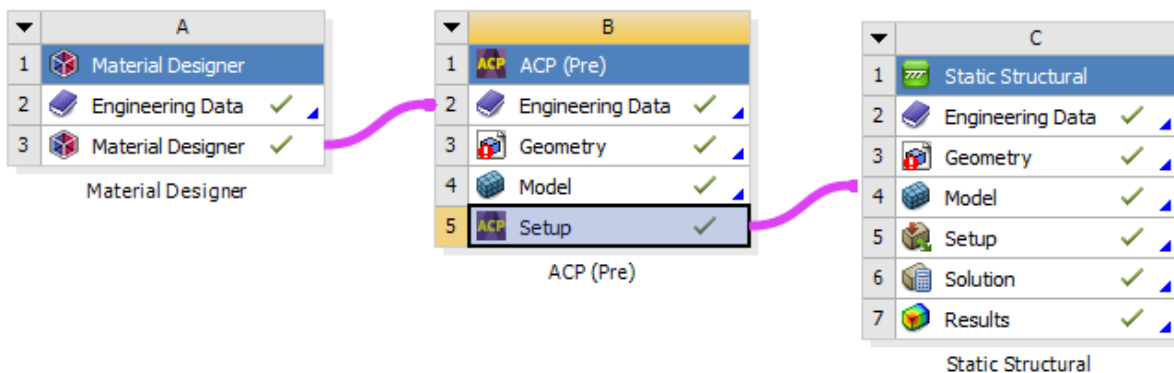


Figure 4-25 Representative volume element (RVE)

Figure 4-26 illustrates how to verify the experimental ultimate tensile strength, bending strength, axial fatigue, and flexural fatigue using an ANSYS workbench simulation.



(a)



(b)

Figure 4-26 Steps for modelling for the laminates in the ANSYS 2019/R3 Workbench (a) tensile and three-point bending, (b) Axial and flexural fatigue test.

4.5.2 Tensile Test Modeling

A 3D finite element model of a hybrid composite specimen under static load was modeled with 22964 nodes and 5525 elements, and stress analysis was conducted. The test specimen is rectangular, measuring 250 mm in length, 25 mm in width, 2 mm in thickness, and 40 mm from each end for grasping, as shown in Figure 4-27. To reproduce the all-tensile test, the same boundary and loading conditions are used as in the original experiment.

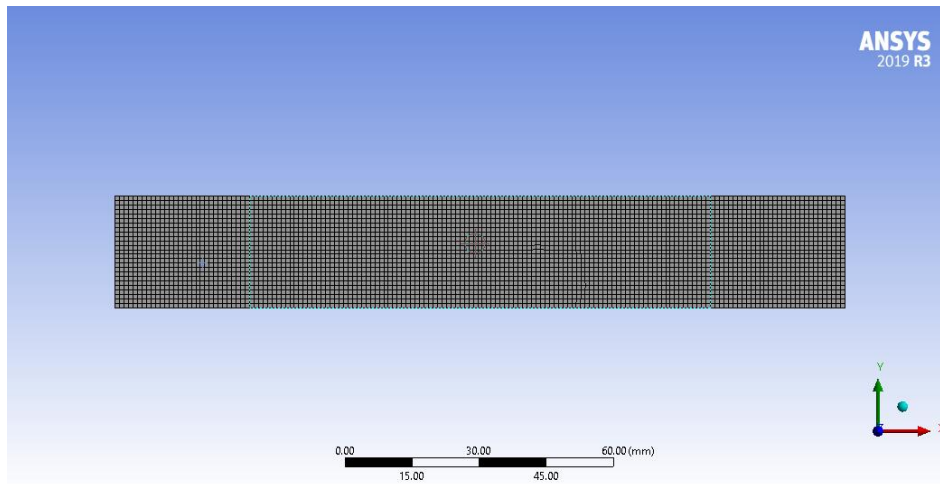


Figure 4-27 Geometric model of the tensile test specimen.

The tensile boundary conditions were utilized for the finite element models. As shown in Figure 4-28, one end of the specimen allows displacement only along the neutral axis (X-axis), while the other end remains fixed in all directions. We constructed this model on ANSYS ACP, utilizing the SOLID186 element type, a three-dimensional, 20-node solid element. SHELL181 is utilized for structural analysis and has four nodes, each with six degrees of freedom. CONTA174 represents the sliding contact between three-dimensional target surfaces. TARGE170 denotes the various three-dimensional target surfaces linked to corresponding contact elements (CONTA174).

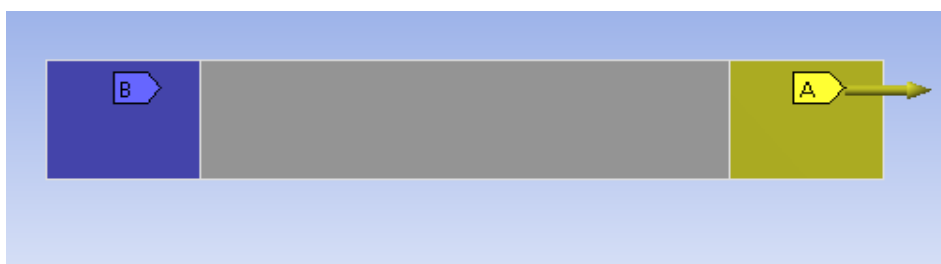


Figure 4-28 FE model of tensile test specimen with boundary conditions

4.5.3 Three Point Bending Test Modeling

A 3D finite element model has been built for the three-point bending test with 2309 nodes and 1198 elements, as shown in Figure 4-29. The three-point had adopted as boundary conditions for the FE models. The displacement allowed

only in the direction of the (Z-axis). The free ends of the model were simply supported, as shown in Figure 4-30. This model was built by using ANSYS ACP, element type SOLID186 which is a 3-D, 20-node solid element. SHELL181 which is used to analyze structures and has four nodes with six degrees of freedom. CONTA174 represent the contact of sliding between 3-D target surfaces. TARGE170 represents the different 3-D target surfaces to associated contact elements (CONTA174)

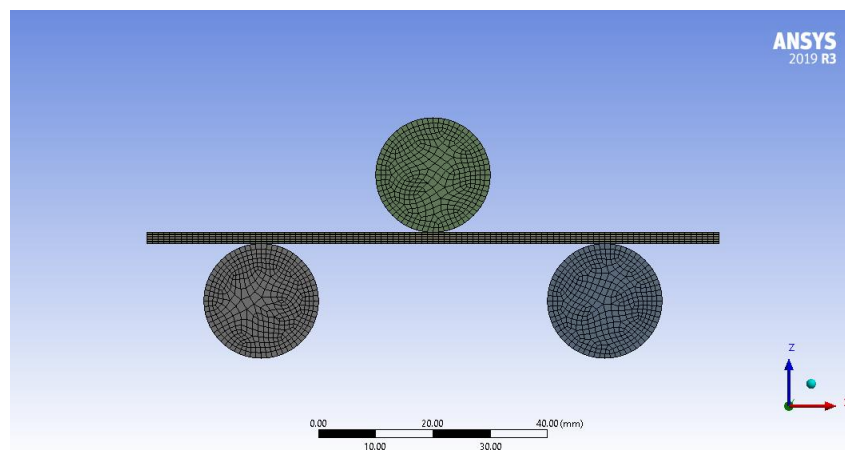


Figure 4-29 Geometric model of the three-point bending test specimen.

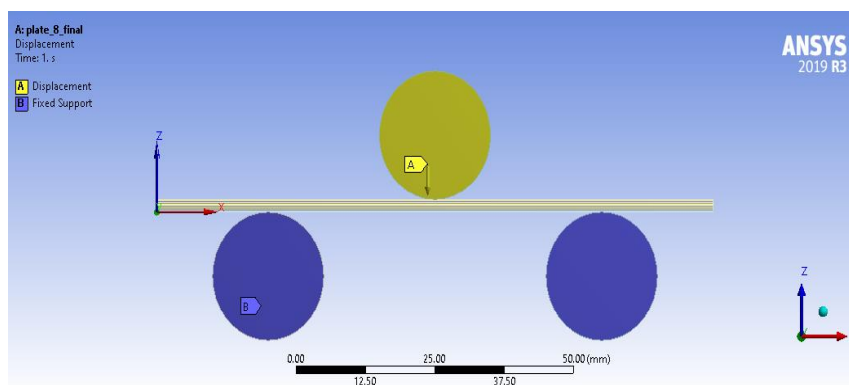
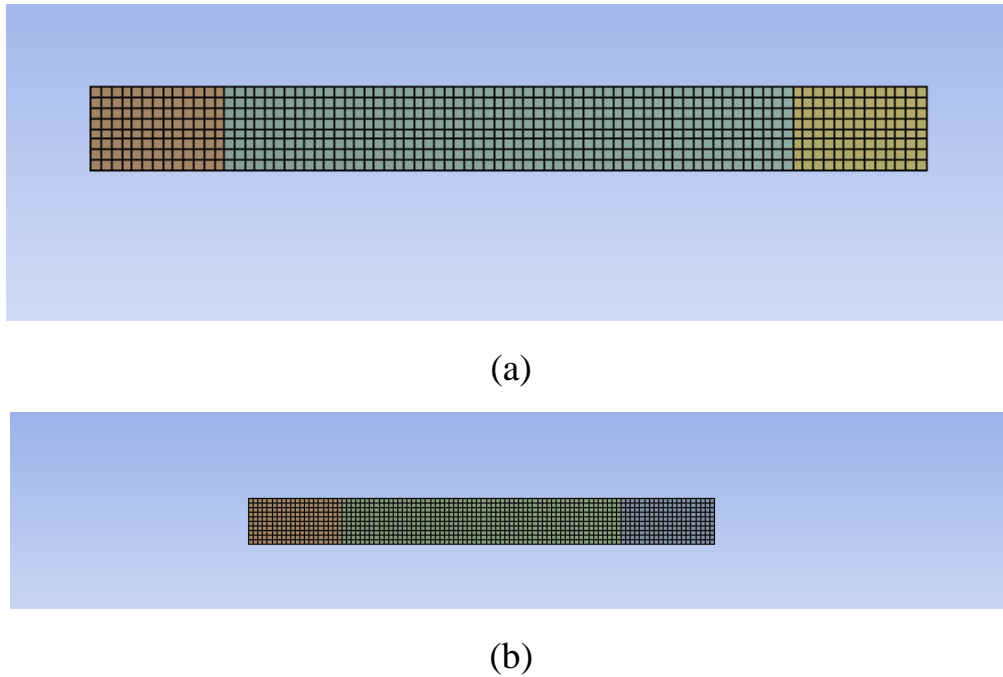


Figure 4-30 FE model of three-points bending test specimen with boundary conditions

4.5.4 Fatigue Test Modeling

Two different models were built for the axial and flexural fatigue tests. ANSYS APDL 2019/R3 was used to build these models in three dimensions (3D) The models were meshed using the automated size control (automatic mesh), as shown

in Figure 4-31. The axial fatigue test model consisted of 22964 nodes and 5525 elements, whereas for the flexural fatigue test model, the number of nodes and elements was 3674 and 884, respectively.



*Figure 4-31 Geometry of the model used for (a) Axial fatigue analysis
(b) Flexural fatigue analysis.*

The axial fatigue boundary conditions were employed for the finite element models. Figure 4-32-a demonstrates that the specimen allows displacement only along the neutral axis (X-axis), while the opposite end faces constraints in all directions. This model was developed in ANSYS ACP using the SOLID186 element type, a three-dimensional, 20-node solid element. SHELL181 is employed for structural analysis and has four nodes, each with six degrees of freedom. CONTA174 denotes the sliding interaction between three-dimensional target surfaces. TARGE170 represents the diverse three-dimensional target surfaces associated with the relevant contact components (CONTA174). The flexural fatigue test follows the same boundary conditions as the axial fatigue, with the exception of the moving part moving perpendicular to the sample (Z-axis), as illustrated in Figure 4-32-b.

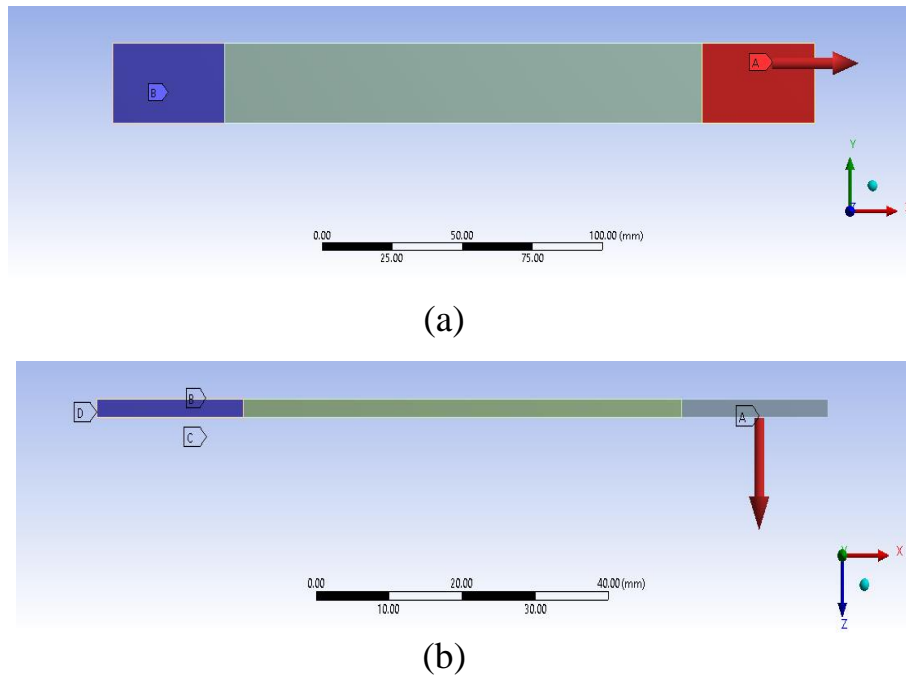


Figure 4-32 (a) Axial fatigue model with boundary condition (b) Flexural fatigue model with boundary condition.

4.6 Scanning Electron Microscopy (SEM)

Unidirectional hybrid composites comprising glass/carbon fibers and nano-silica particles were examined using Scanning Electron Microscopy (SEM) (ZEISS (1000X) field-emission SEM). Figure 4-33 presents the SEM that used in this study.



Figure 4-33 Scanning Electron Microscopy (SEM).

CHAPTER FIVE

RESULTS AND DISCUSSION

This chapter presents the experimental findings of the quasi-static for tensile and three-point bending tests as well as the axial and flexural fatigue tests that have been carried out in order to investigate the effect of laminate thickness, stacking sequence, and the addition of silicon dioxide (SiO₂) nanoparticles. This chapter also introduces a comparison between the experimental results and the numerical results obtained by using the ANSYS tool.

5.1 Engineering Constants of Laminates

As mentioned in Chapter 4, three different groups of hybrid composite laminates were produced. Table 5-1 presents the findings of the initial group's investigation, which concerned measuring the engineering constants, namely E_1 , E_2 , G_{12} , ν_{12} , and density.

Table 5-1 Glass and Carbon Fiber Mechanical Properties

Sample	Material	E_1 GPa	E_2 GPa	G_{12} GPa	ν_{12}	Density g/cm ³
G[0°] ₈	Pure Glass /Epoxy	31.80	10.95	4.27	0.21	1.6576
GN[0°] ₈	Glass /Epoxy with SiO ₂ nanoparticles	33.36	13.41	4.48	0.26	1.8413
C [0°] ₈	Pure Carbon / Epoxy	99.44	6.27	4.03	0.24	1.4838
CN [0°] ₈	Carbon /Epoxy with SiO ₂ nanoparticles	101.60	6.41	4.12	0.30	1.5056

It can be seen clearly from the above table that the engineering constants of both the epoxy/glass and epoxy/carbon fiber composites increased when silica nanoparticles were added. The data also indicate that ν_{12} was the parameter most affected by adding SiO₂, followed by E_2 , density, and G_{12} , while E_1 was the parameter

least affected by adding the nanoparticles due to the fact that the tensile force and the fiber direction are in the same direction, as shown in Figure 5-1.

The above results show that the effect of adding SiO₂ nanoparticles on the engineering constants of the epoxy/carbon fiber composite is much lower than that of the epoxy/glass composite except for ν_{12} . That is because glass fiber provides good strength and toughness, but it is generally less strong and stiff compared to carbon fibers. It is also more fragile. While carbon fiber is known for its exceptional strength-to-weight ratio and high stiffness, it also has excellent tensile strength and is stronger and more rigid than glass fiber. In terms of density, glass fibers are denser compared to carbon fibers, which means that they contribute more to the total weight of the composite material. These results are in agreement with those obtained by (Karnati, Agbo and Zhang, 2020; Kamal, Hassanand, and Khdir, 2024).

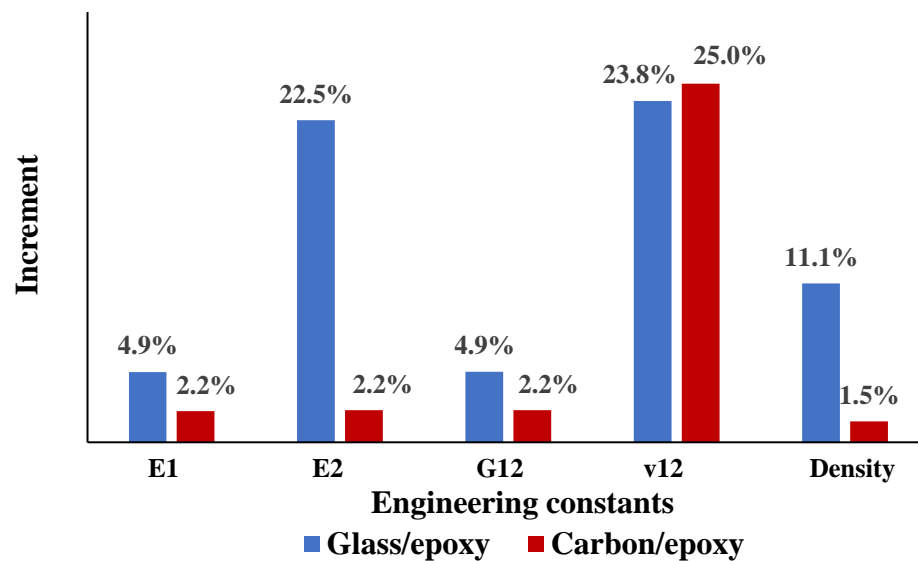


Figure 5-1 Influence of adding SiO₂ nanoparticles on the mechanical characteristics.

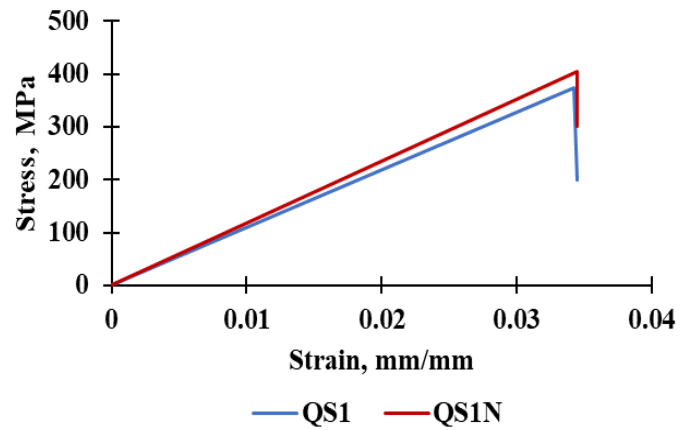
5.2 Tensile Test

The results of the second (quasi-isotropic laminate) and third group (cross-ply laminate) of glass/carbon hybrid composite laminates, which were manufactured to figure out the effect of SiO₂ nanoparticles, stacking sequence, and laminate thickness on the tensile properties, are presented in the following sections.

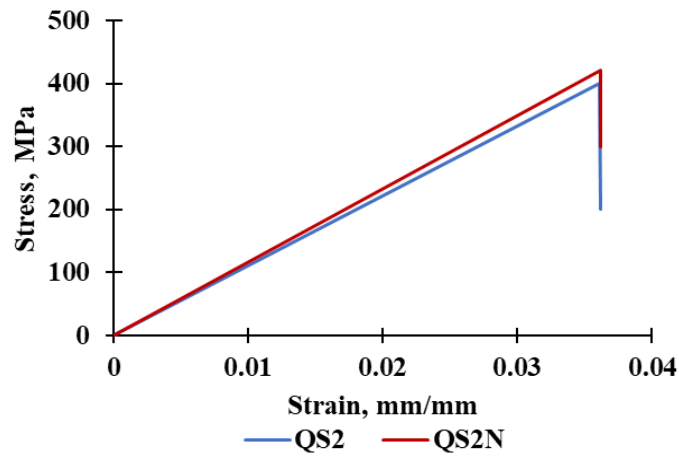
5.2.1 Tensile Test of Quasi-Isotropic Laminate

The quasi-isotropic laminate tensile results are presented in Figure 5-2. The results indicate that the incorporation of SiO₂ nanoparticles had a greater impact on the laminates at the 12 layers in comparison to the other layers. This result is attributed to SiO₂'s impact on improving the epoxy's characteristics. According to Rabbi *et al.*, (2023), nanoparticles prevent stress concentration and subsequent fracture initiation by filling in any manufacturing voids in composites. On the other hand, these nanoparticles can act as inclusions to prevent cracks from growing (Sasaki *et al.*, 2023). These results strongly correlate with the outcomes and conclusions of Megahed, Megahed and Agwa, (2019).

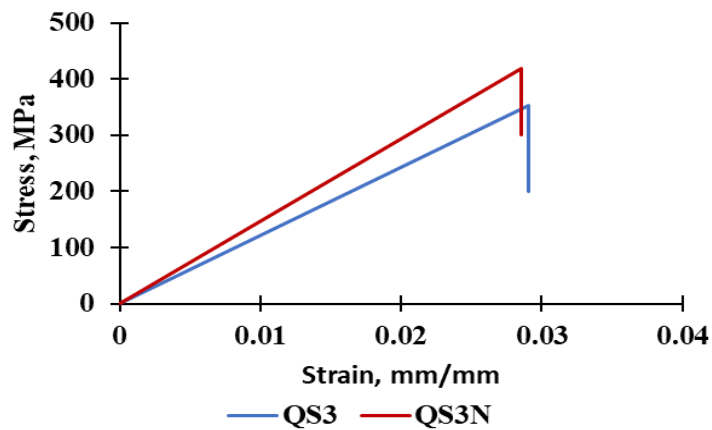
Table 5-2 compares the values of the tensile test features with and without SiO₂ nanoparticles, including modulus of elasticity, maximum load, and maximum tensile stress. The table clearly shows that mechanical properties of glass/carbon hybrid composites with nanoparticles are much better than those of composites without nanoparticles. From a tensile strength behavior perspective, this is in line with what Karnati, Agbo and Zhang (2020) found.



(a)



(b)



(c)

Figure 5-2 Tensile stress-strain plot of glass/carbon hybrid composites (a) 8-layer, (b) 10-layer, (c) 12-layer.

Table 5-2 Mechanical Properties of Hybrid Laminates at Tensile Test for Quasi Isotropic Laminates

Samples	No. of layers	Modulus of elasticity E_1 (GPa)	Maximum tensile load, (kN)	Maximum tensile stress, (MPa)
QS1	8	10.93	22.44268	374.05
QS1N	8	11.75	24.30492	405.08
QS2	10	11.07	26.49791	399.97
QS2N	10	11.67	27.95325	421.94
QS3	12	12.11	25.09006	352.14
QS3N	12	14.65	29.77935	417.96

Photographs of the tensile test failure specimens, both with and without SiO_2 nanoparticles, are shown in Figure 5-3. The figure shows the failure of the specimens, consisting of multizone of matrix fractures and pulled-out fibers and fractures in glass and carbon fibers.

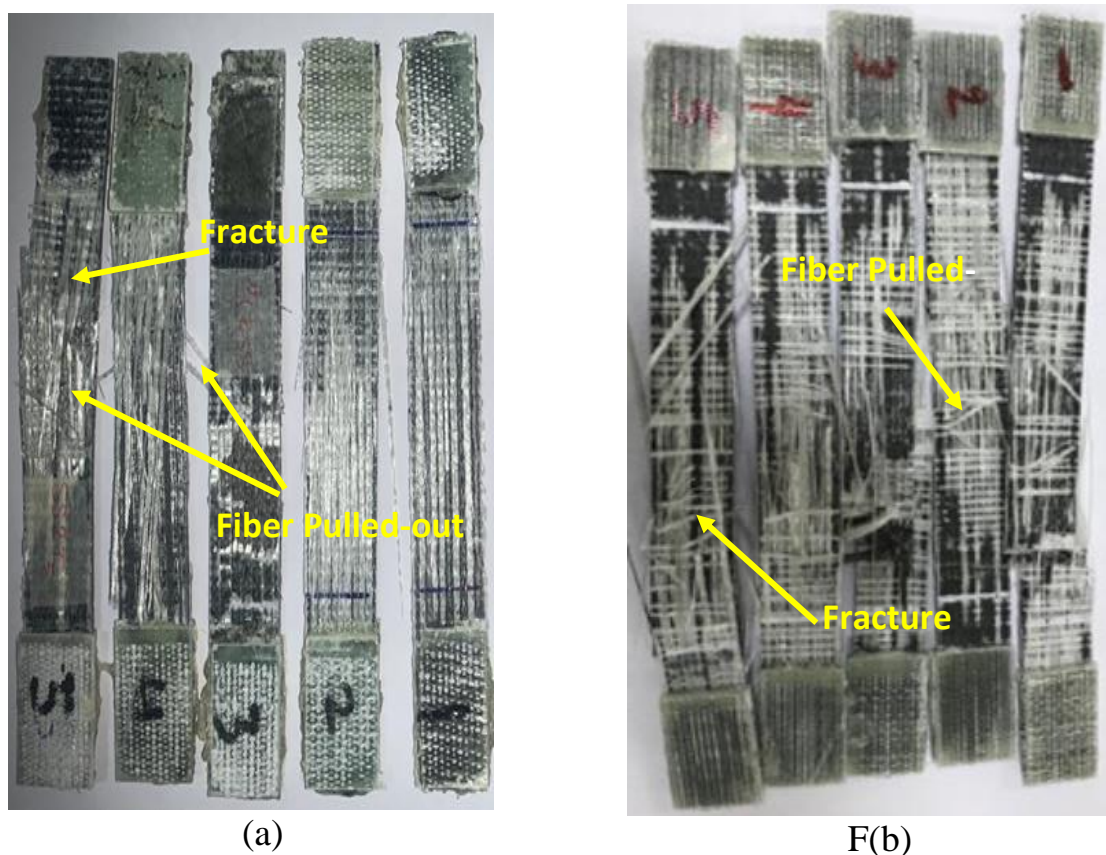


Figure 5-3 Tensile specimens after failure: (a) QS1 (without SiO_2 nanoparticles), (b) QS1N (with SiO_2 Nanoparticles)

Another finding that stands out from the results reported earlier is that the mechanical properties (modulus of elasticity and maximum stress) of glass/carbon hybrid composites were better when SiO₂ nanoparticles were added (See Figure 5-4). The addition of SiO₂ nanoparticles to QS1N resulted in an increase of 7.5% and 8.29% in the modulus of elasticity and ultimate tensile stress, respectively, when compared to QS1. To a similar extent, for the laminate consists of 10 layers with SiO₂ nanoparticles (i.e., QS2N), the increased ratios for the modulus of elasticity and ultimate tensile stress are 5.42% and 5.51%, respectively, compared to QS2. One interesting finding is that the highest increasing ratio among the specimens was recorded for the laminates, which consist of 12 layers of SiO₂ nanoparticles (QS3N), where the increasing ratio was 20.97% for the modulus of elasticity and 18.65% for maximum tensile stress compared to the specimens that lack SiO₂ nanoparticles (QS3).

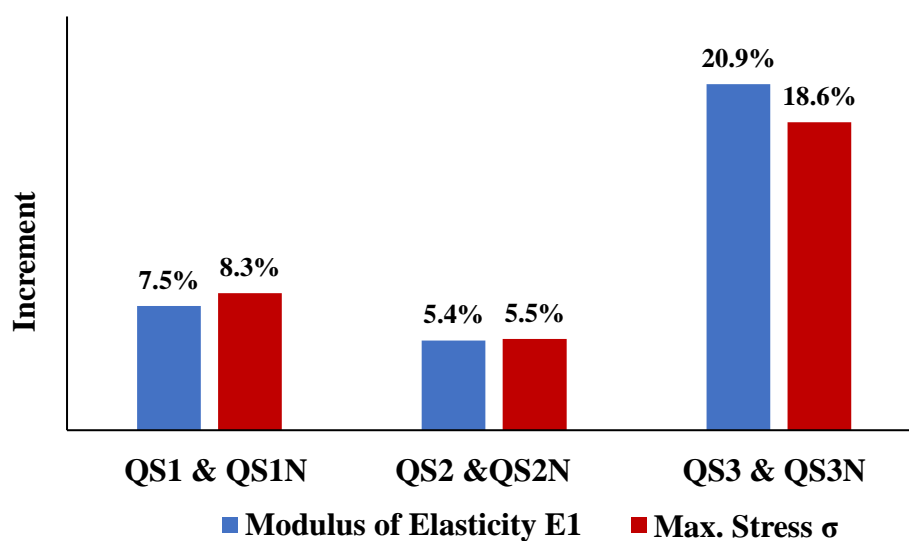
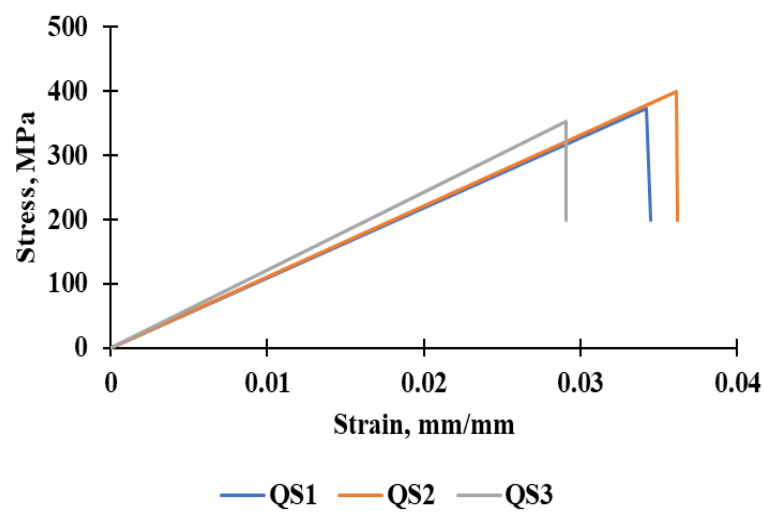


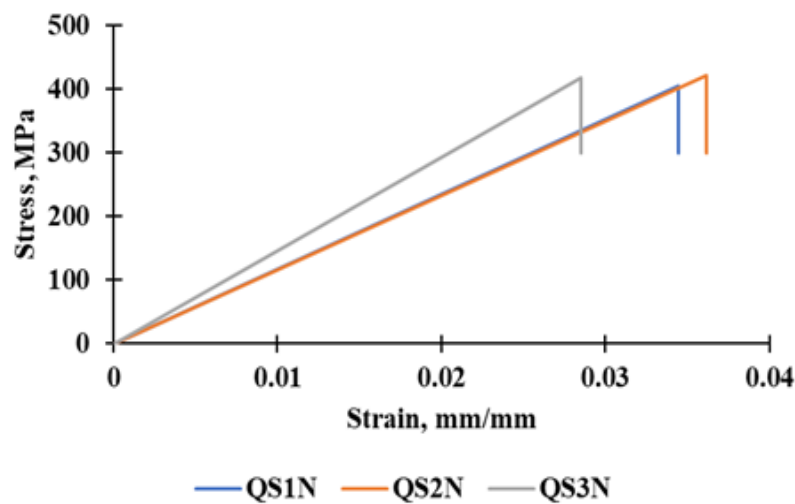
Figure 5-4 Influence of adding SiO₂ nanoparticles on modulus of elasticity and tensile stress of glass/carbon hybrid composite laminate

Due to the induction of distinct failure processes under strain, it has been shown that these three kinds of laminate thickness measuring methodologies provide remarkably varied findings (Kaddour *et al.*, 2015; Camineroa *et al.*, 2019). Placing a certain number of neighboring layers at various angles in a direction to create thick

layers is known as foil bundling (Sebaey *et al.*, 2013; Xiao-Yu *et al.*, 2018). Figure 5-5 displays the average stress-strain curves for the tensile specimens, along with the type of stacking sequence method and laminate thickness. In general, samples with the stacking sequence $(0^\circ/45^\circ/90^\circ/0^\circ/45^\circ)_s$ had superior tensile response at the laminate level when compared to samples with QS1 and QS3. That is because the angle 45 in the middle of the laminate increases the tensile strength of the QS2 with and without adding SiO_2 nanoparticles. There is a strong correlation between these results and the findings of (Caminero *et al.*, 2019).



(a)



(b)

Figure 5-5 Effect of stacking sequences on glass/carbon hybrid composite (a) without adding SiO_2 nanoparticles (b) with adding SiO_2 nanoparticles.

As mentioned in Chapter 4, in order to validate the experimental results of the tensile of quasi-isotropic laminates, a 3-D numerical model, using ANSYS workbench, was built. The results are presented in Figure 5-6. As shown in the figure, the distribution of ultimate tensile strength over each FRPC's plies.

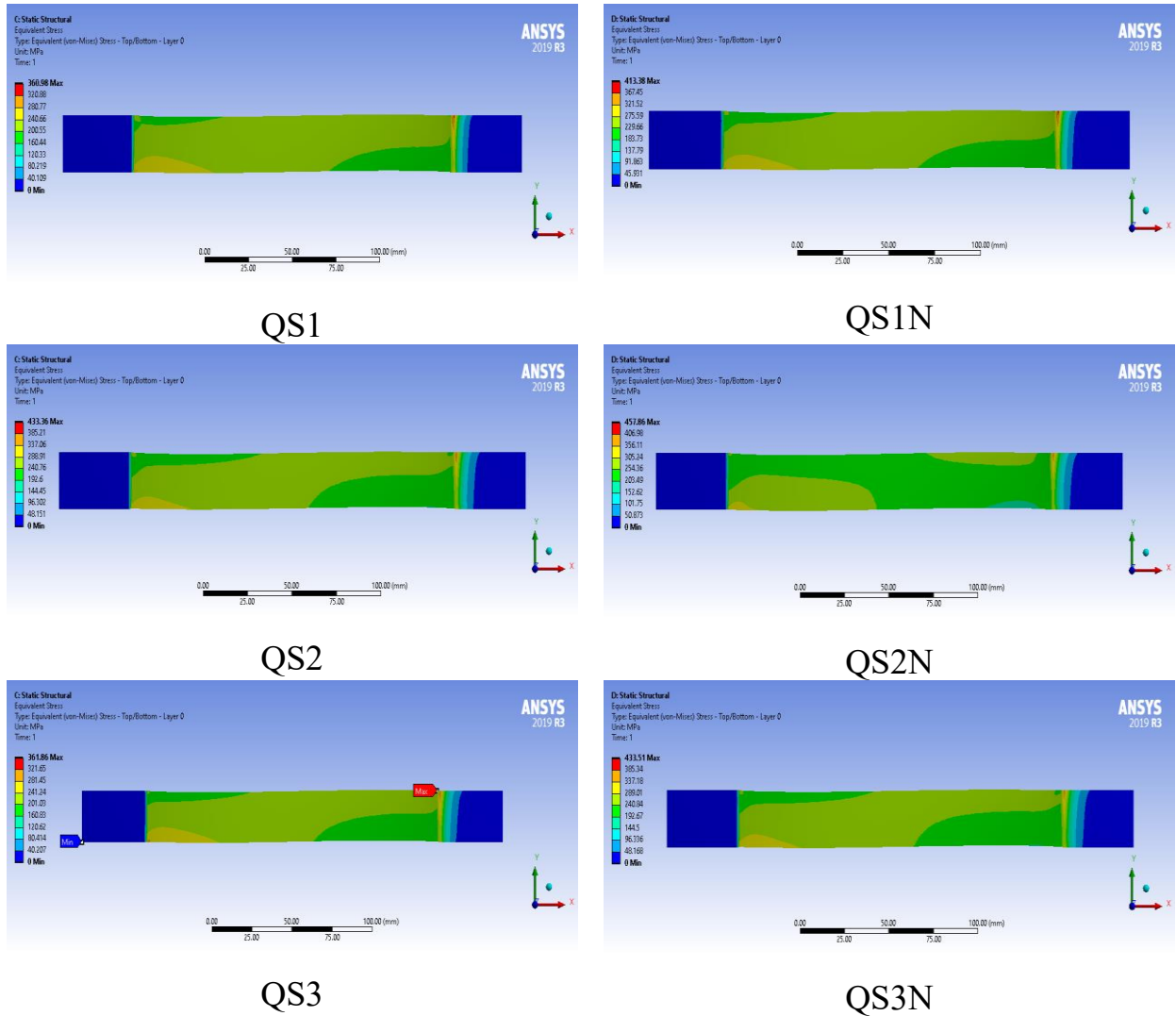


Figure 5-6 Ultimate tensile strength distribution through Quasi-isotropic hybrid laminates.

There was a significant positive correlation between the numerical and experimental tensile results. A comparison of the numerical and experimental findings of ultimate tensile stress is presented in Figure 5-7.

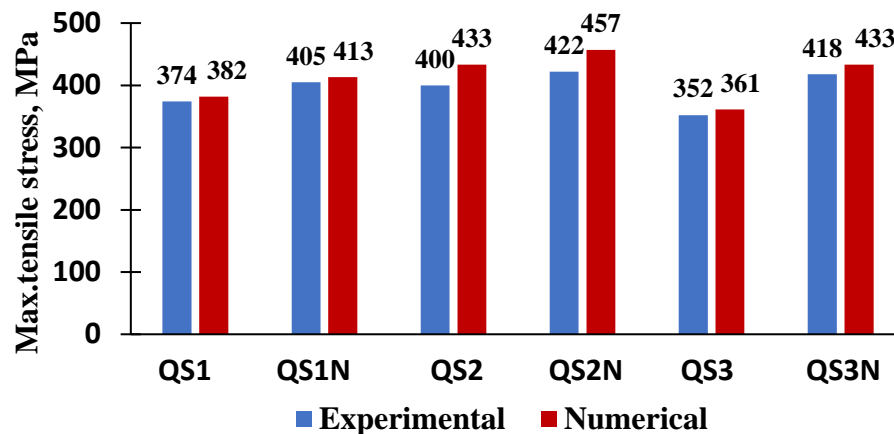


Figure 5-7 Experimental and numerical ultimate tensile strength of quasi-isotropic laminates.

5.2.2 Tensile Test of Cross-Ply Laminate

Figure 5-8 presents the cross-ply laminate tensile results of the stress-strain curve for a unidirectional glass/carbon fiber hybrid with and without 2 wt.% SiO₂ nanoparticle reinforcement. This figure reveals the effect of SiO₂ nanoparticle addition on the enhancement of the mechanical properties, which is attributable to the nanoparticles' high surface area and their ability to form robust chemical bonds with the resin and fibers. The incorporation of SiO₂ nanoparticles improves the interfacial bonding strength between fibers and resin (Karnati, Agbo and Zhang, 2020). This improved bonding delays crack propagation within the composite material, thereby increasing its tensile strength, toughness, and stiffness. Furthermore, SiO₂ nanoparticles serve as fillers, reinforcing the structure of the composite material, which enhances the load transfer between the fibers, thus increasing the strength and stiffness (Nahedh and Majeed, 2021). The uniform distribution of SiO₂ nanoparticles in the resin matrix mitigated void and defect formation, further contributing to the improvement of the mechanical properties.

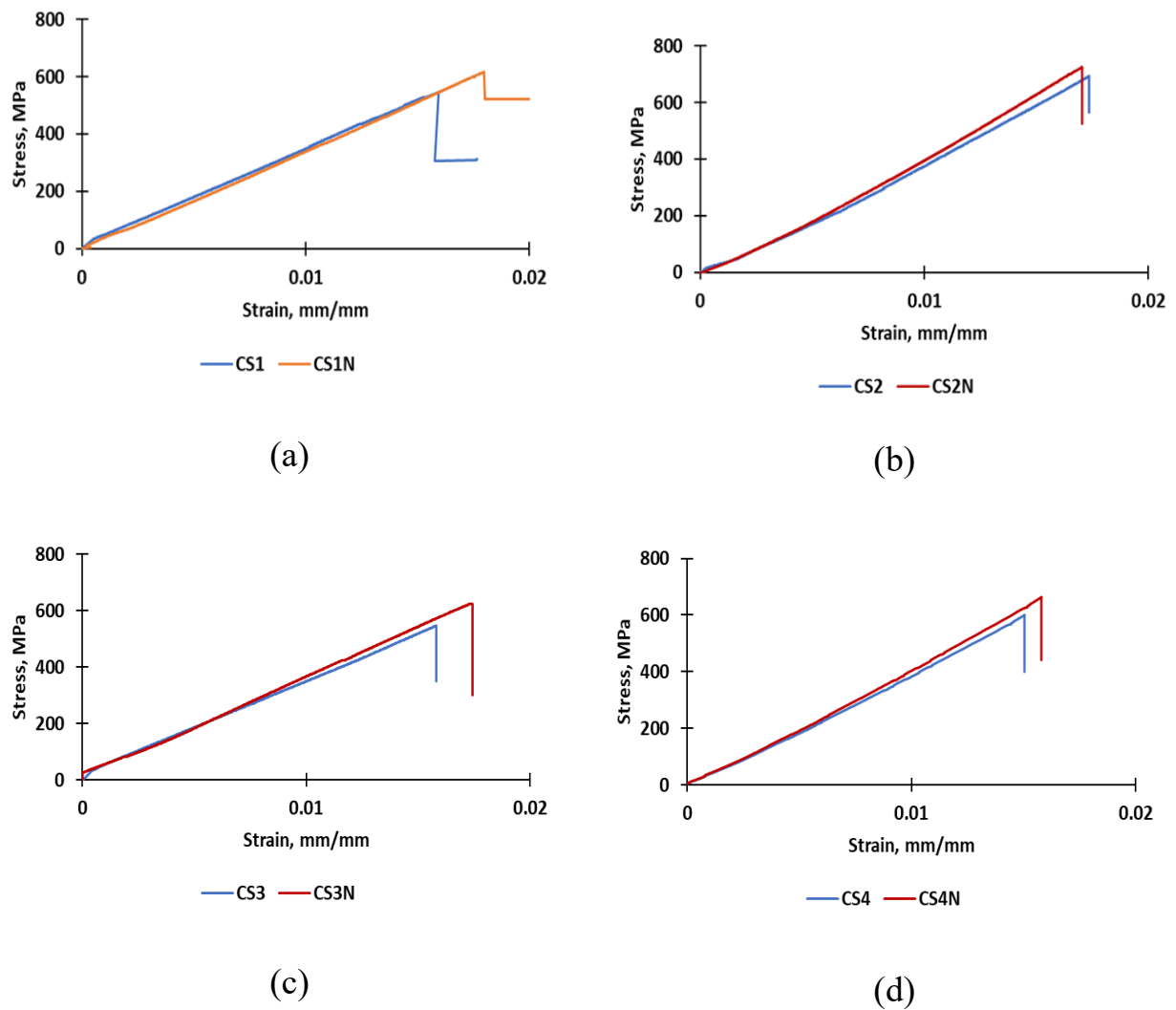


Figure 5-8 Tensile stress-strain plot of glass/carbon hybrid composites (a) 8-layer, (b) 12-layer (c) 16-layer, (d) 20-layer

Table 5-3 compares the values of the tensile test features with and without SiO_2 nanoparticles, including, maximum stress and strain, and modulus of elasticity. The table clearly shows that mechanical properties of glass/carbon hybrid composites with nanoparticles are much better than those of composites without nanoparticles (Nahedh and Majeed, 2021).

Table 5-3 Mechanical properties of glass / carbon hybrid composite at Tensile Test for Cross ply Laminates.

Sample	No. of layers	Max. stress (MPa)	Max. strain (%)	Modulus of elasticity (GPa)
CS1	8	547.16	1.593	33.6654
CS1N	8	616.64	1.797	34.49796
CS2	12	692.76	1.735	39.4364
CS2N	12	724.68	1.704	41.297
CS3	16	547.09	1.581	33.9157
CS3N	16	623.17	1.728	38.3319
CS4	20	600.63	1.5046	41.4674
CS4N	20	663.68	1.5799	43.3873

Another notable observation from the previously reported results is that the addition of SiO₂ nanoparticles improved the mechanical properties of glass/carbon hybrid composites (refer to Figure 5-9). For example, the modulus of elasticity E_1 and maximum stress σ of CS1N increased by 2.47% and 12.7%, respectively, compared to CS1, which is the same laminate without the addition of SiO₂ nanoparticles. To a similar extent, the values of E_1 and σ for CS2N are 4.72% and 4.61%, respectively, compared to CS2. Likewise, the E_1 and σ values of CS3N increased by a total of 13.02% and 13.91%, respectively, compared with CS3. Finally, there was an overall increase of 4.63% and 10.50%, respectively, in the E_1 and σ stress values for CS4N compared with CS4, as shown in Figure 5-9. There is a considerable improvement in the performance of glass/carbon hybrid composite materials when 2 wt.% SiO₂ nanoparticles are present. These findings show a high correlation with those of (Khalil *et al.*, 2017).

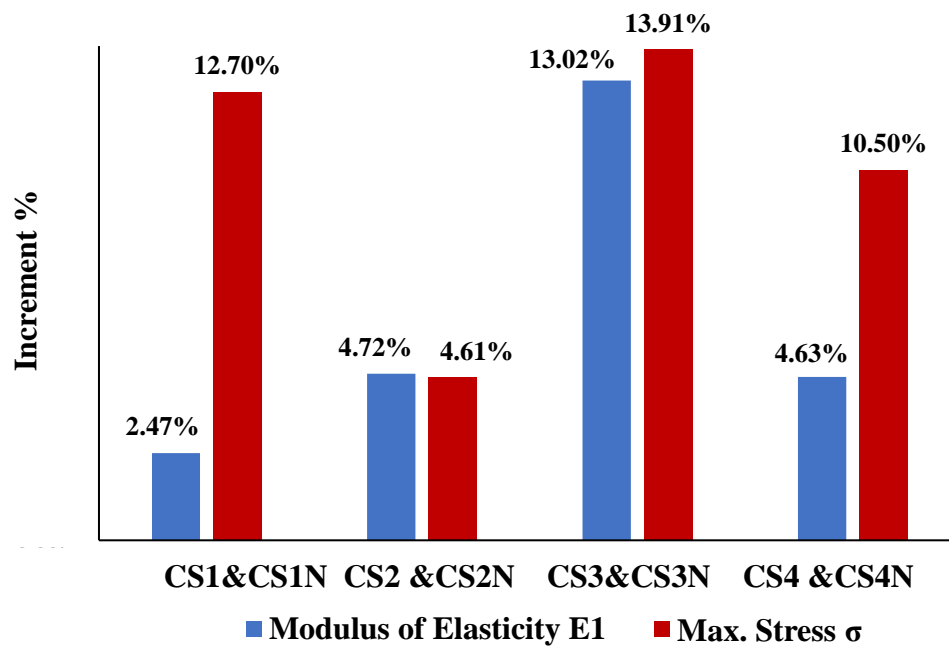
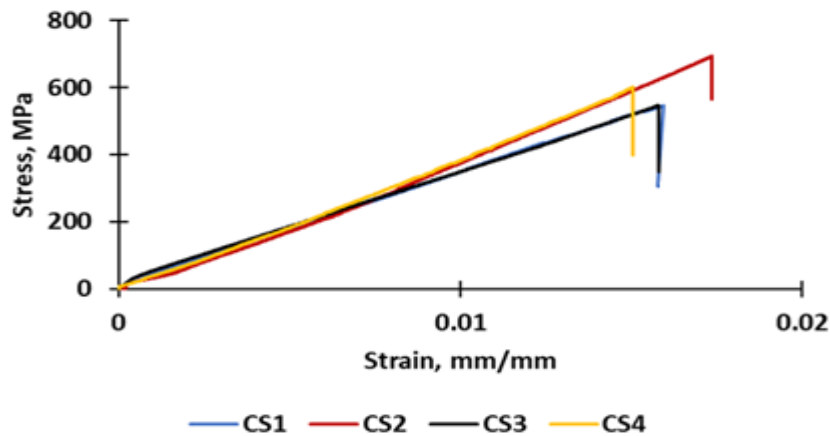


Figure 5-9 Influence of adding SiO₂ nanoparticles on modulus of elasticity and tensile stress of glass/carbon hybrid composite laminate

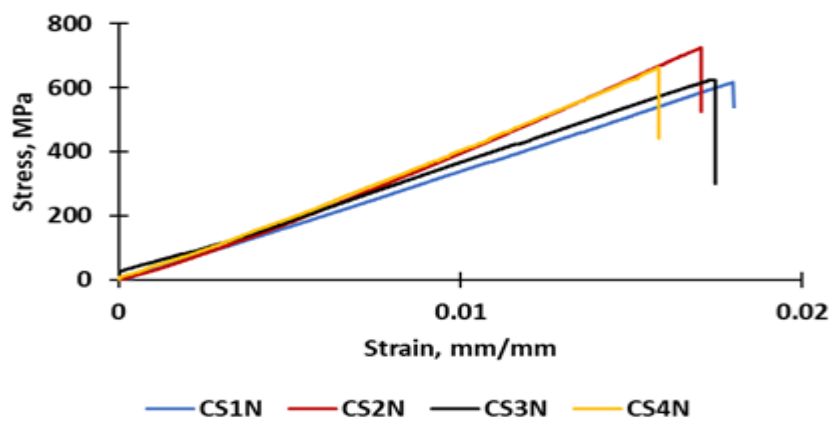
These four types of laminate thickness measurement approaches provide significantly different results due to the occurrence of different failure mechanisms under stress. Stacking sequences and thickness is the process of arranging a certain number of neighboring layers at various angles in unidirectional directions to generate thick layers.

Figure 5-10 displays the stress-strain curves of the tensile specimens for different stacking sequences and different laminate thicknesses. At the plate level, the tensile response was greater for stacked components in the CS2 order [0°/0°/90°/90°/0°/0°]s than for laminates arranged in the CS1, CS3, and CS4 orders. It was discovered that the final stress drops at the same stacking sequence angle as plate thickness increases. Specimens CS1 and CS3 exhibit consistent behavior. The consistent behavior of CS1 and CS3 may be attributed to the identical stacking sequence. The stacking sequence of CS2 and CS4 is the same and shows the same behavior. The reason for this is that the tensile strength of CS2 is increased both with and without the addition of SiO₂ nanoparticles because the middle four layers of the laminate, CS2 and CS4 for glass /carbon are in the same direction of tensile force. In the case of laminates CS1 and

CS3, the glass/carbon configuration of the middle four layers, stacked at $[0^\circ/90^\circ/90^\circ/0^\circ]$ angle, leads to a reduction in tensile strength compared with CS2 and CS4. These findings show a high correlation with those of (Mohammed, Hassan and Khdir, 2023).



(a)



(b)

Figure 5-10 Effect of stacking sequences on glass/carbon hybrid composite (a) without adding SiO_2 nanoparticles (b) with adding SiO_2 nanoparticles.

As discussed in Chapter 4, to verify the experimental results for the tensile properties of quasi-isotropic laminates, a 3-D numerical model was created using the ANSYS workbench. The outcomes are illustrated in Figure 5-11, which depicts the distribution of ultimate tensile strength across each ply of the fiber reinforced polymer composite FRPC.

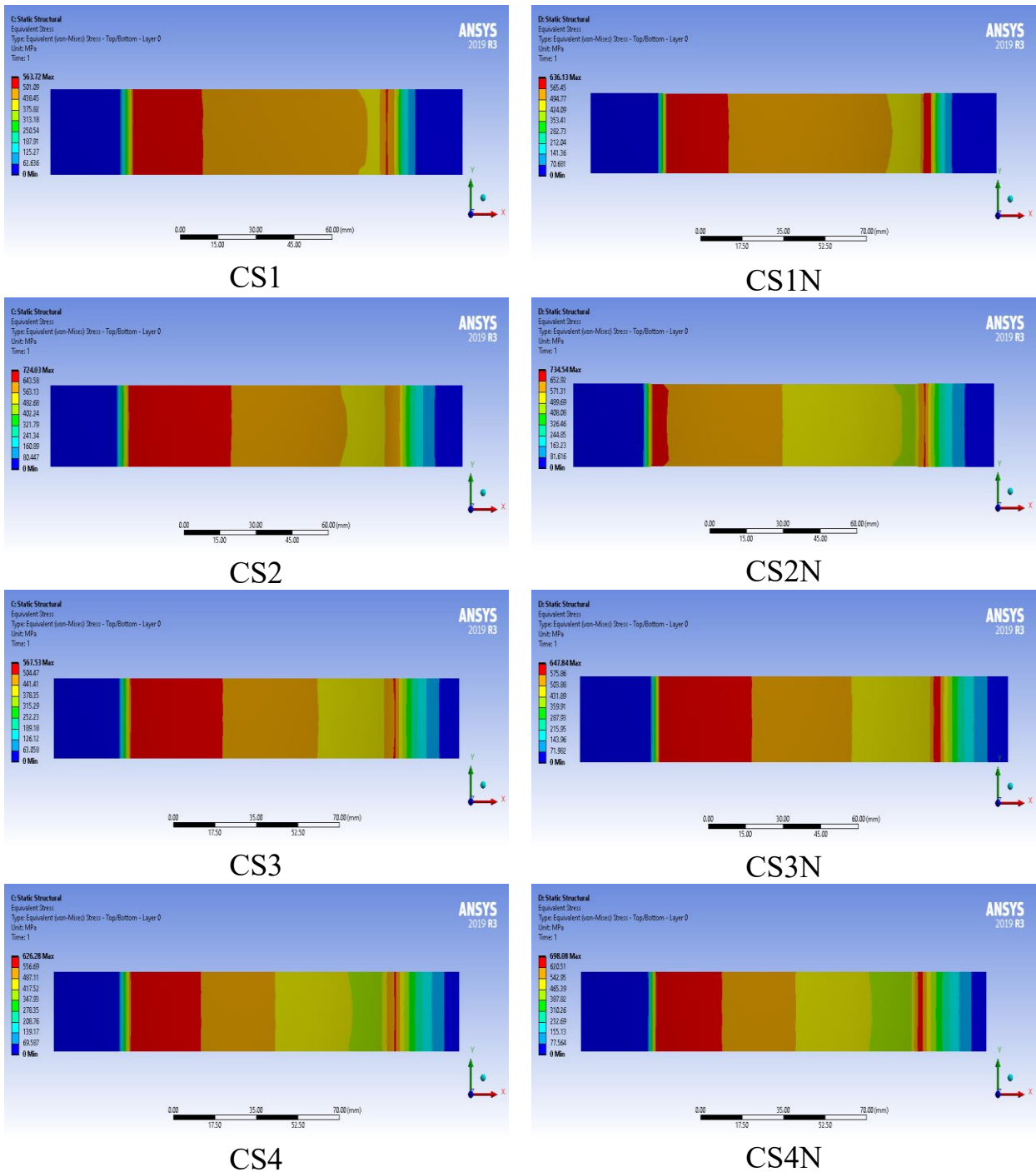


Figure 5-11 Ultimate tensile strength distribution through cross-ply laminates of FRPC plies.

There was a significant positive correlation between the numerical and experimental cross-ply laminate tensile results. A comparison of the numerical and experimental findings of ultimate tensile stress is presented in Figure 5-12.

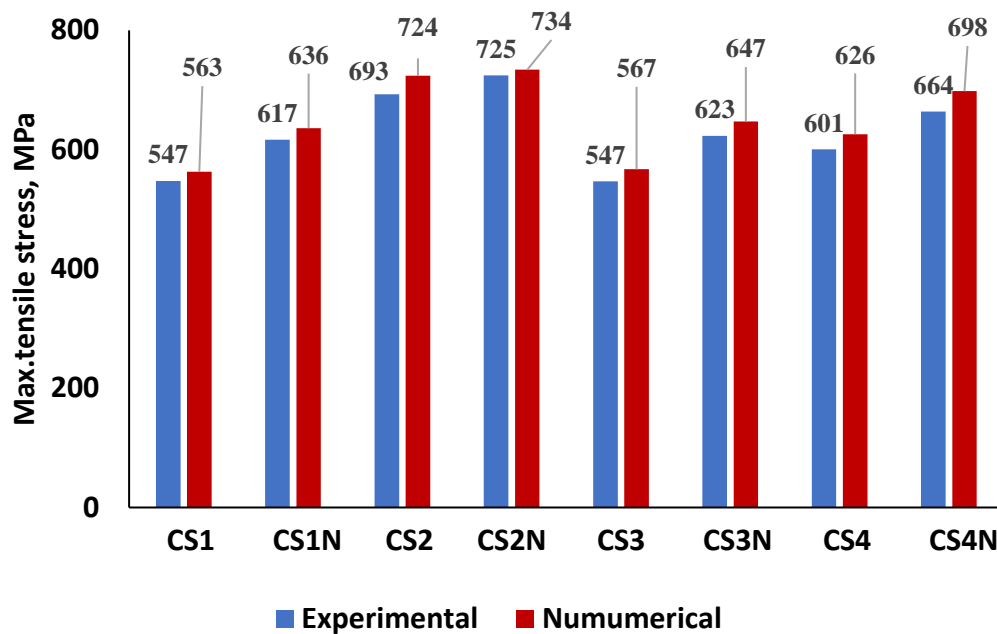


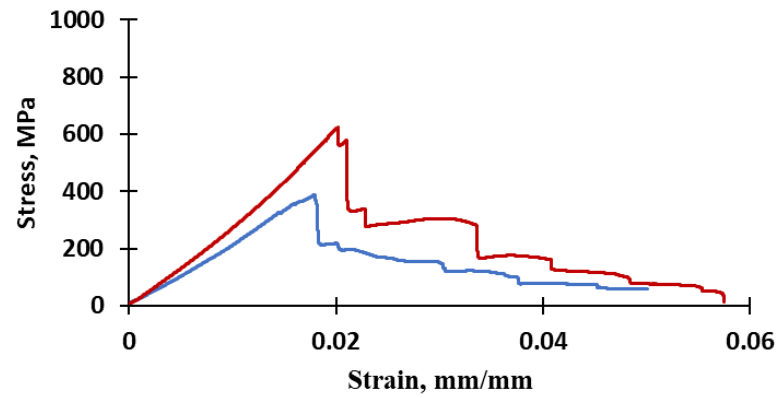
Figure 5-12 Experimental and numerical ultimate tensile strength of cross-ply laminates.

5.3 Three Points Bending Test

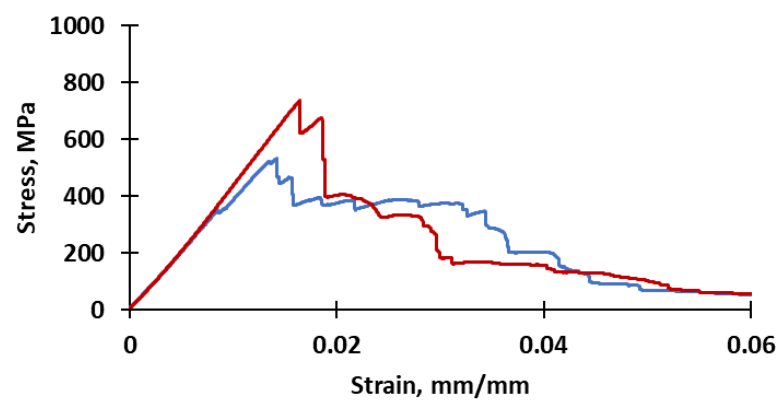
The next sections show the outcomes of the second group (quasi-isotropic laminate) and third group (cross-ply laminate) of glass/carbon hybrid composite laminates. These were made to find out how SiO₂ nanoparticles, the thickness of the laminate, and the stacking sequence affected the three-point bending properties.

5.3.1 Three Point Bending Test of Quasi-Isotropic Laminate

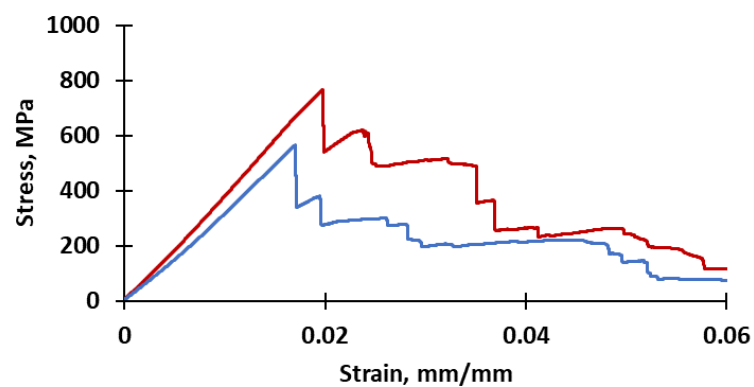
Figure 5-13 and Table 5-4 presents the three-point bending results for quasi-isotropic laminate. There is a considerable influence of silicon dioxide nanoparticles on the bending strength of hybrid composite materials, and the bending strength increases as the number of layers increases. As well, the figure shows the stress-strain curves with and without 2 wt.% SiO₂ nanoparticles, all of which exhibit comparable linear behavior until reaching the maximum stress, where the specimens begin to fracture. When silicon dioxide nanoparticles are added to epoxy, the bond strength between the epoxy and the fibers increases. It also works to reduce voids by occupying nanoparticles in their place, which improves the performance of composite materials.



(a)



(b)



(c)

Figure 5-13 Flexural stress-strain plot of Quasi isotropic-ply glass/carbon hybrid composites (a) 8-layer, (b) 10-layer (c) 12-layer.

Table 5-4 shows the experimental results of maximum flexural load P , maximum flexural stress σ_f and flexural modulus E_f . The table also shows the theoretical

flexural modulus E_f and stiffness matrix [D] as well. As stated in Chapter 3, the flexural stiffness matrix and theoretical flexural modulus were calculated for each laminate by using Equations 3.34 and 3.42 (Kaw, 2005).

Table 5-4 Experimental and theoretical results of the three points bending test for quasi-isotropic laminates

Samples	No. of layers	Experimental			Theoretical	
		Maximum Flexural load P (N)	Maximum Flexural stress σ_f (MPa)	Flexural modulus, E_f [GPa]	Flexural matrix [D] [$\text{Pa}\cdot\text{m}^3$]	Flexural modulus, E_f [GPa]
QS1	8	221.9947	391.6	21.82	$\begin{bmatrix} 19.7 & 7.65 & 06.8 \\ 7.65 & 17.3 & 6.8 \\ 6.8 & 6.8 & 9.13 \end{bmatrix}$	21.2
QS1N	8	359.8553	578.1	30.29	$\begin{bmatrix} 32.7 & 4.6 & 2.8 \\ 4.5 & 13.9 & 2.8 \\ 2.8 & 2.8 & 5.61 \end{bmatrix}$	34.3
QS2	10	480.9062	519.63	38.36	$\begin{bmatrix} 62.1 & 7.77 & 8.06 \\ 7.77 & 28.8 & 8.06 \\ 8.06 & 8.06 & 10.3 \end{bmatrix}$	40.7
QS2N	10	665.5269	737.37	44.96	$\begin{bmatrix} 60.3 & 9.09 & 5.75 \\ 9.09 & 30.6 & 5.75 \\ 5.75 & 5.75 & 11.1 \end{bmatrix}$	43
QS3	12	700.793	565.37	33.17	$\begin{bmatrix} 95.9 & 13.9 & 10.1 \\ 13.9 & 251.4 & 10.1 \\ 10.1 & 10.1 & 18.9 \end{bmatrix}$	35.8
QS3N	12	986.8887	766.1	38.83	$\begin{bmatrix} 112.4 & 16.2 & 14.6 \\ 16.2 & 51.5 & 14.6 \\ 14.6 & 14.6 & 19.2 \end{bmatrix}$	40.5

It's clear that all those parameters increase with the presence of SiO_2 nanoparticles. The data from the table illustrate that the maximum applied flexural force was increased by 62.10%, 38.39%, and 40.82 % for glass/carbon composites with (QS1 and QS1N), (QS2 and QS2N), and (QS3 and QS3N) respectively, and the maximum flexural stress was increased by 47.63%, 41.9%, and 35.5 % for glass/carbon composites with (QS1 and QS1N), (QS2 and QS2N), and (QS3 and QS3N) respectively. The flexural modulus was increased as well as by 38.83%, 17.19%, and 17.08 % for glass/carbon composites with (QS1 and QS1N), (QS2 and QS2N), and (QS3 and QS3N) respectively, as shown in the Figure 5-14.

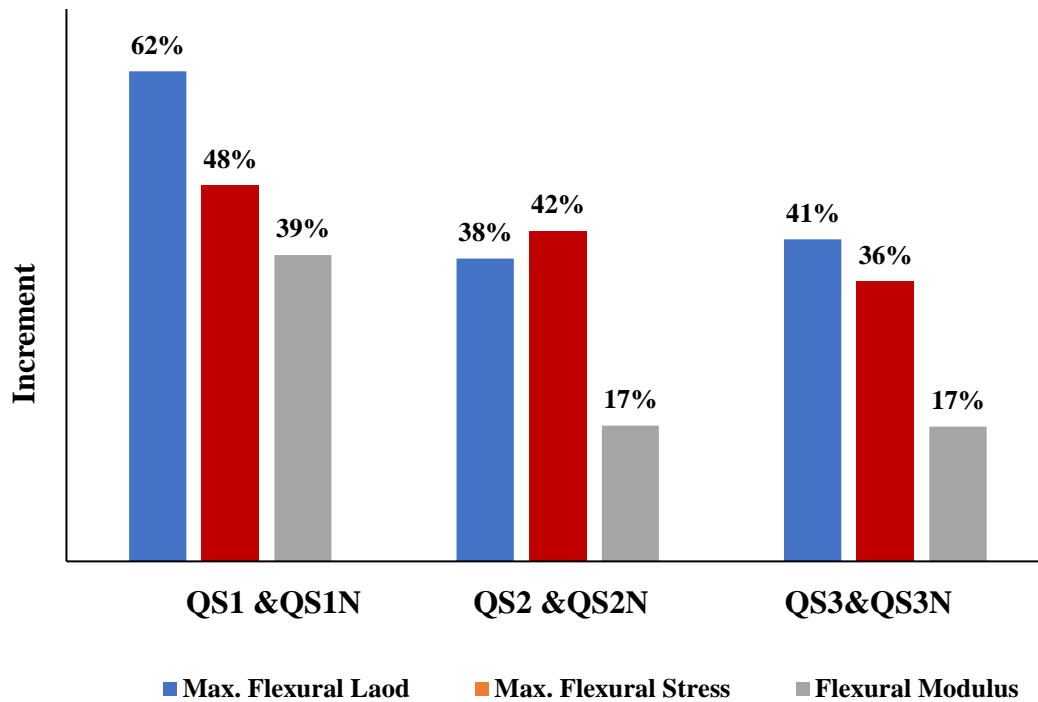


Figure 5-14 Increment of adding SiO_2 nanoparticles of Quasi-ply glass/carbon hybrid composite laminate

In most cases, flexural failure happens when fibers buckle on the compression side and break or pull out on the tension side. There isn't much internal delamination or transverse crack propagation. Figure 5-15 illustrates this, aligning with the findings of previous studies (Dong, Sudarisman and Davies, 2013; Alcludia-Zacarías *et al.*, 2020; Ghani and Mahmud, 2020).

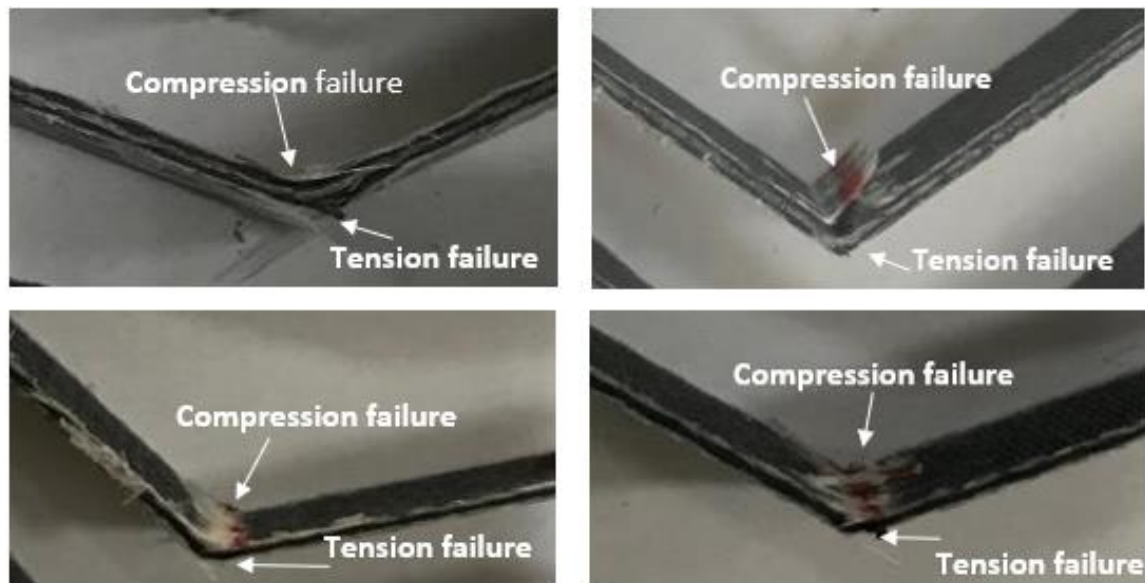
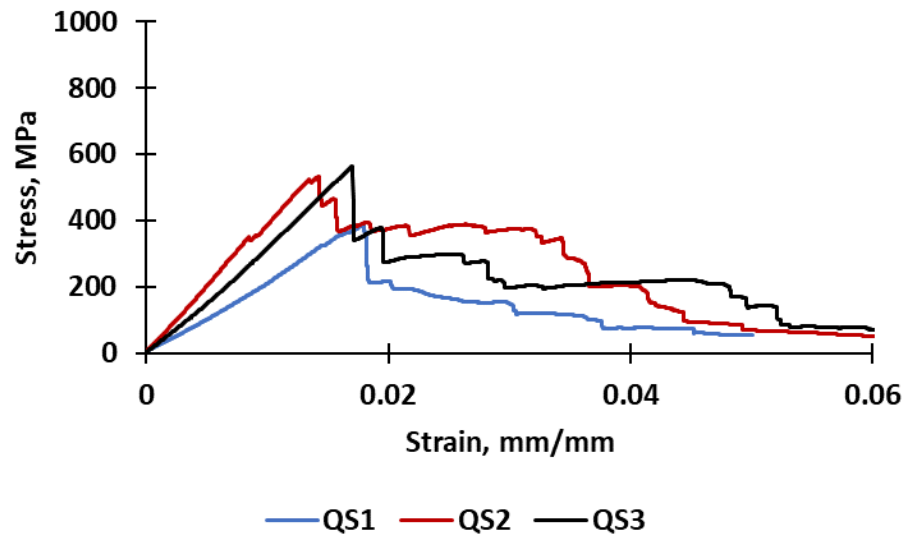
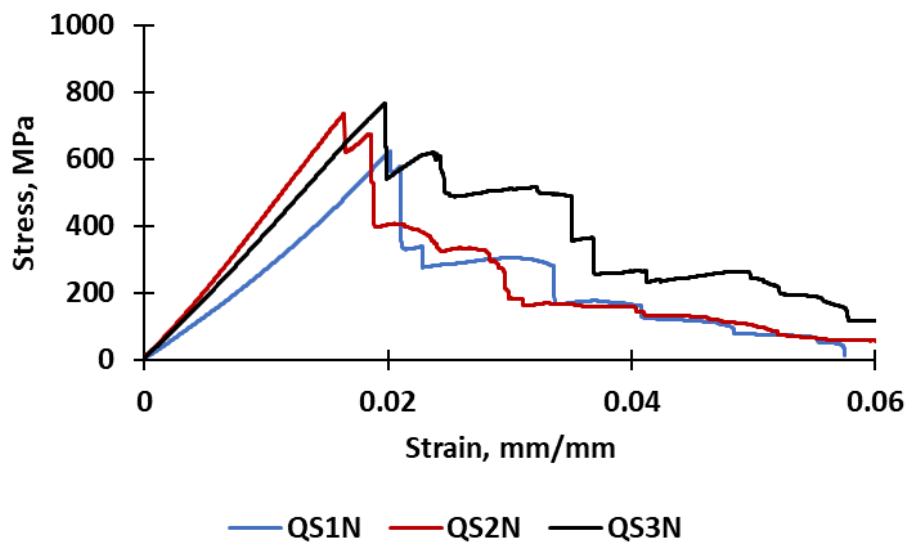


Figure 5-15 Three points bending failure specimens: (a) QS1 (without SiO₂ Nanoparticles), (b) QS1N (with SiO₂ Nanoparticles).

The induction of different failure processes under flexural stress is responsible for the remarkable diversity in results obtained from these three different types of laminate thickness measurement methods. Foil blocking, or foil stacking, refers to the process of placing a specific number of surrounding layers at varying angles in one direction to create thick layers. The stress-strain curves for the flexural specimens are shown in Figure 5-16. The type of stacking sequence and laminate thickness are also shown. In terms of flexural response at the laminate level, the specimens made with the stacking sequence of QS3 (0° /45° /90° /0° /45° /90°)_s were better than the specimens made with QS1 and QS2. It has been discovered that increasing the thickness of the plates leads to an increase in the ultimate stress. This results in increased QS3 flexural strength, with or without the addition of SiO₂ nanoparticles, due to the position of two layers of angle 90° in the middle of the plates and a minor increase in thickness of (0.5 mm) for each laminate. This small increase in laminate's thickness eliminates failure as a result of stacking the layers in the laminate. These results show a significant correlation with those presented in (Ajaj, Jubier and Majeed, 2013; Mohanty and Srivastava, 2015; Caminero *et al.*, 2019; Hashim *et al.*, 2021)



(a)



(b)

Figure 5-16 Effect of stacking sequences on Quasi-ply glass/carbon hybrid composite (a) without adding SiO_2 nanoparticles (b) with adding SiO_2 nanoparticles

As mentioned in Chapter 4, in order to validate the experimental results of the three-point bending of quasi-isotropic laminates, a 3-D numerical model, using ANSYS workbench, was built. The results are presented in Figure 5-17. As shown in the figure, the distribution of ultimate tensile strength over each FRPC's plies.

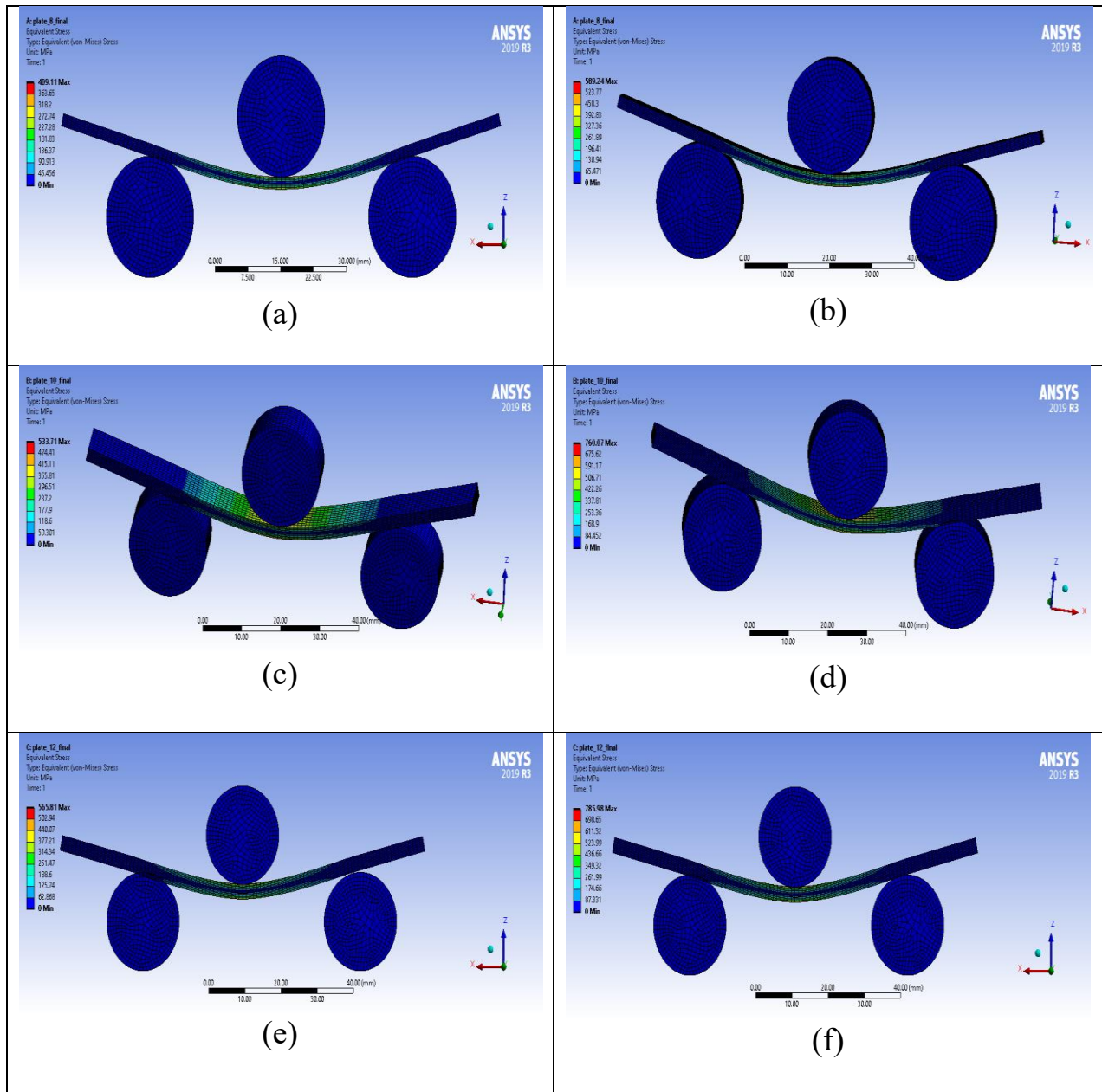


Figure 5-17 Ultimate Flexural strength distribution three points bending through quasi-isotropic laminates of FRPC plies (a) QS1, (b)QS1N, (c)QS2, (d)QS2N, (e)QS3, (f)QS3N.

Figure 5-18 illustrates a comparison of the numerical and experimental findings of ultimate tensile stress. There was a significant positive correlation between the numerical and experimental cross-ply laminate tensile results.

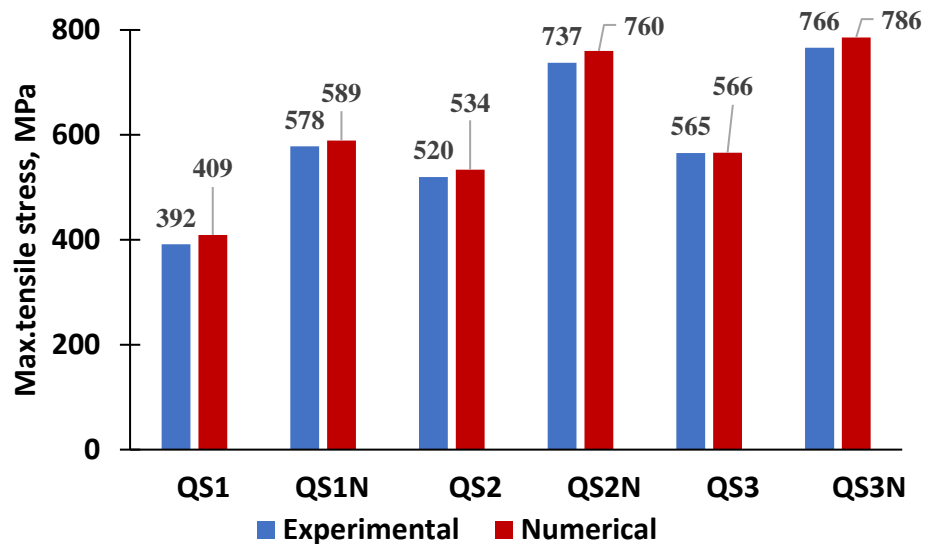
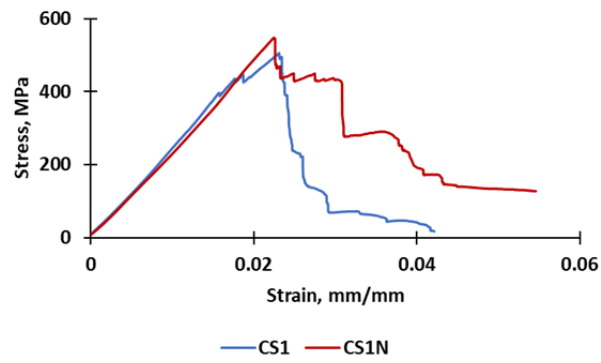


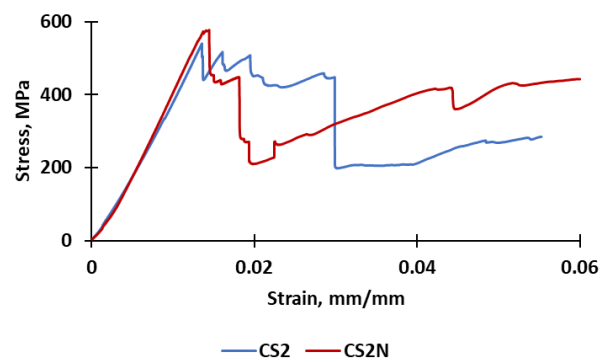
Figure 5-18 Experimental and numerical ultimate three-points bending strength of quasi-isotropic laminates.

5.3.2 Three Point Bending Test of Cross-Ply Laminate

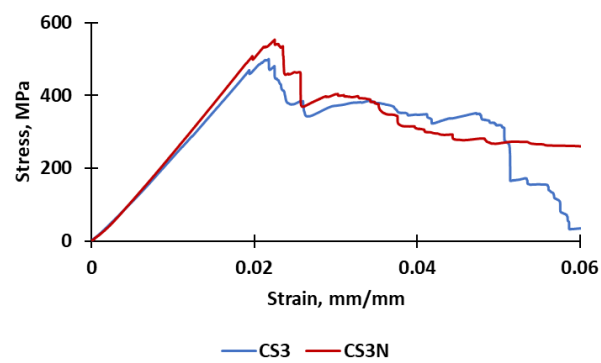
Figure 5-19 displays the results of three-point bending for a cross-ply laminate. The presence of SiO_2 nanoparticles has a positive effect on the bending strength of hybrid composite materials, with the bending strength increasing according to the number of layers. Additionally, the figure illustrates the stress-strain curves for specimens containing 2 wt.% SiO_2 nanoparticles and those without. Both sets of curves display similar linear characteristics until they reach the point of maximum stress, at which the specimens start to shatter. The addition of SiO_2 nanoparticles to epoxy enhances the adhesive strength between the epoxy and the fibers. Furthermore, it is effective at minimizing empty spaces by filling them with nanoparticles, thereby improving the performance of composite materials. (Garnich and Akula, 2009).



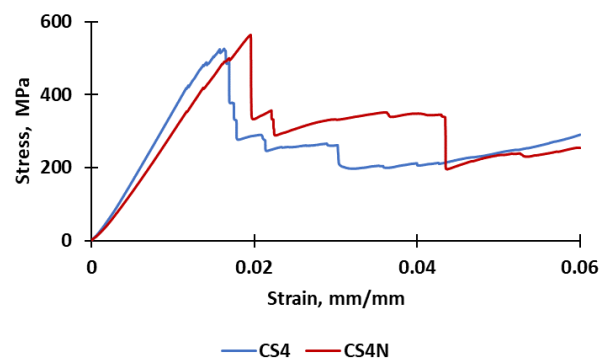
(a)



(b)



(c)



(d)

Figure 5-19 Bending stress-strain plot of glass/carbon hybrid composites (a) 8-layers, (b) 12-layers (c) 16-layers, (d) 20-layers

The fracture begins immediately after the steep slope in the curve. *Figure 5-20* illustrate that the samples with and without addition of SiO₂ nanoparticles consistently exhibited an elevated seam slope and maximum bending stress, corroborating the results of previous (Kansy, Consolati and Dauwe, 2000; Fruehmann, Dulieu-Barton and Quinn, 2010).

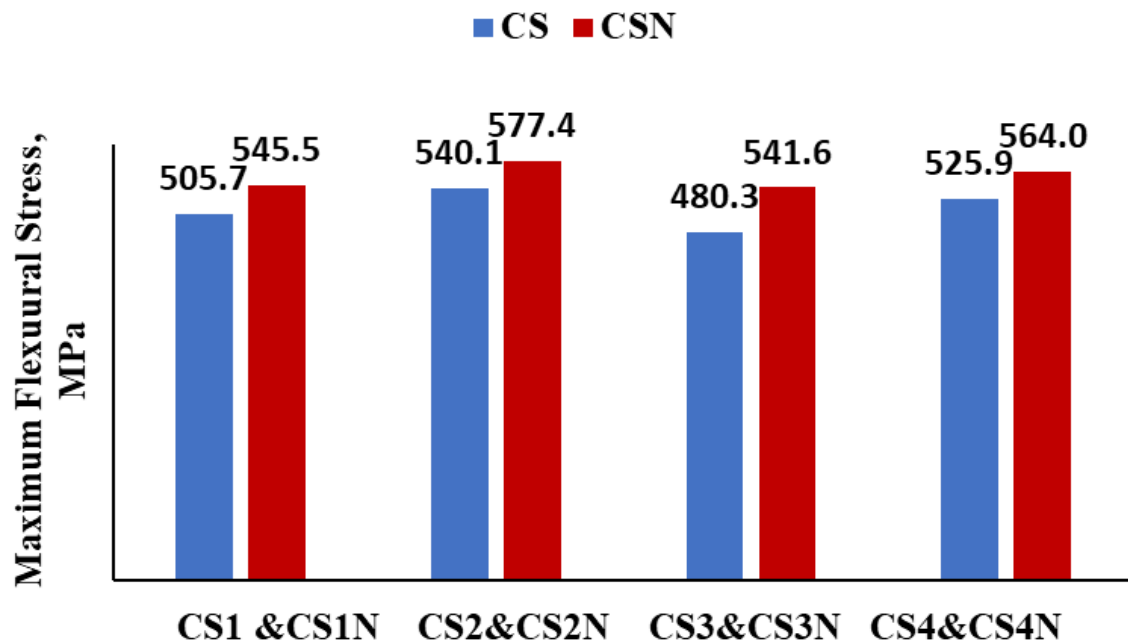


Figure 5-20 Effect of adding SiO₂ on Bending Stress of cross-ply glass/carbon hybrid composites

Table 5-5 shows the experimental results of maximum flexural load P , maximum flexural stress σ_f , and flexural modulus E_f . The theoretical flexural modulus E_f and stiffness matrix $[D]$ are also shown in the table. As mentioned in Chapter 3, the flexural stiffness matrix and theoretical flexural modulus for each laminate were calculated using Equations (3.34) and (3.42) (Kaw, 2005).

Table 5-5 Mechanical Properties of Hybrid Cross-Ply Laminates at the Three Points Bending Test

Samples	No. of layers	Experimental			Theoretical	
		Maximum Flexural load P (N)	Maximum Flexural stress σ_f (MPa)	Flexural modulus, E_f [GPa]	Flexural matrix [D] [$\text{Pa}\cdot\text{m}^3$]	Flexural modulus, E_f [GPa]
CS1	8	296.55	505.72	25.07	$\begin{bmatrix} 16.1 & 1.38 & 0 \\ 1.38 & 25.8 & 0 \\ 0 & 0 & 2.8 \end{bmatrix}$	24.05
CS1N	8	337.27	545.53	26.48	$\begin{bmatrix} 17.06 & 2.04 & 0 \\ 2.04 & 27.6 & 0 \\ 0 & 0 & 2.91 \end{bmatrix}$	25.36
CS2	12	691.33	540.10	43.71	$\begin{bmatrix} 50.7 & 4.55 & 0 \\ 4.55 & 99.84 & 0 \\ 0 & 0 & 9.4 \end{bmatrix}$	43.84
CS2N	12	739.02	577.36	45.93	$\begin{bmatrix} 53.66 & 6.67 & 0 \\ 6.67 & 105.6 & 0 \\ 0 & 0 & 9.77 \end{bmatrix}$	45.93
CS3	16	1160.03	480.33	24.62	$\begin{bmatrix} 115.8 & 10.6 & 0 \\ 10.6 & 251.4 & 0 \\ 0 & 0 & 22.2 \end{bmatrix}$	23.35
CS3N	16	1188.73	541.59	26.03	$\begin{bmatrix} 115 & 10.6 & 0 \\ 10.6 & 251 & 0 \\ 0 & 0 & 22.25 \end{bmatrix}$	25.43
CS4	20	1660.27	525.86	35.94	$\begin{bmatrix} 221 & 20.6 & 0 \\ 20.6 & 508 & 0 \\ 0 & 0 & 43.4 \end{bmatrix}$	36.5
CS4N	20	1711.98	564.03	37.71	$\begin{bmatrix} 233 & 30 & 0 \\ 30 & 535 & 0 \\ 0 & 0 & 45.1 \end{bmatrix}$	38.2

Figure 5-21 displays the maximum flexural load, maximum flexural stress, and maximum flexural modulus. It is evident that the presence of SiO_2 nanoparticles raises all those parameters. The Table 5-5 and Figure 5-21 demonstrate that the addition of 2 weight percent SiO_2 nanoparticles to the epoxy increased the maximum applied flexural load by 13.73%, 6.9%, 2.47%, and 3.11% for glass/carbon composites containing (CS1 and CS1N), (CS2 and CS2N), (CS3 and CS3N), and (CS4 and CS4N), respectively, the maximum flexural stress was increased by 7.87%, 6.9%, 12.75%, and 7.26% for glass/carbon composites with (CS1 and CS1N), (CS2 and CS2N), (CS3 and CS3N), and (CS4 and CS4N), respectively, and the flexural

modulus was also increased the efficacy by 5.6%, 5.1%, 5.73%, and 4.94% for glass/carbon composites containing (CS1 and CS1N), (CS2 and CS2N), (CS3 and CS3N), and (CS4 and CS4N), respectively.

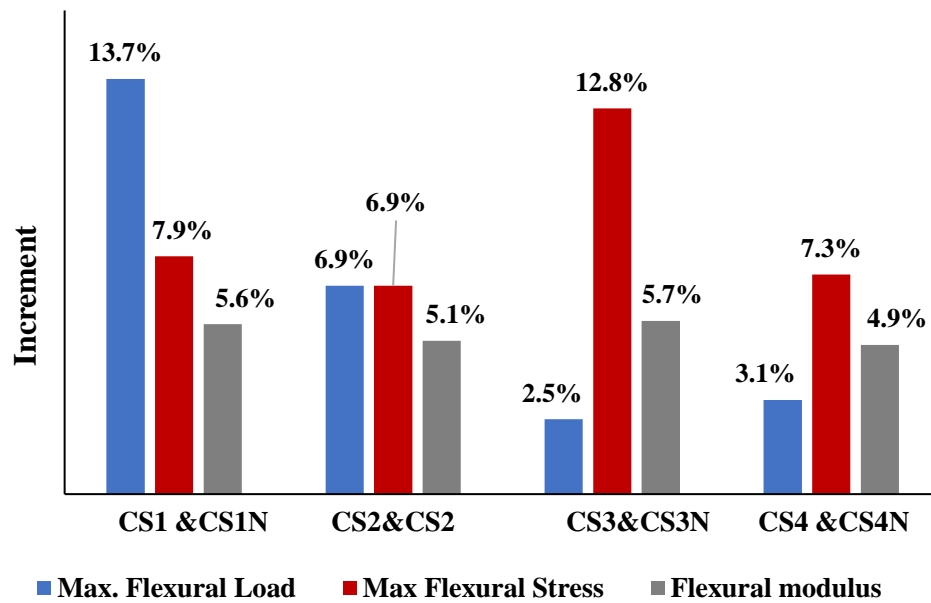


Figure 5-21 Increment of adding SiO_2 nanoparticles of cross-ply glass/carbon hybrid composite laminates

Figure 5-22 shows the three points bending failure specimens with and without adding 2 wt. % SiO_2 nanoparticles.

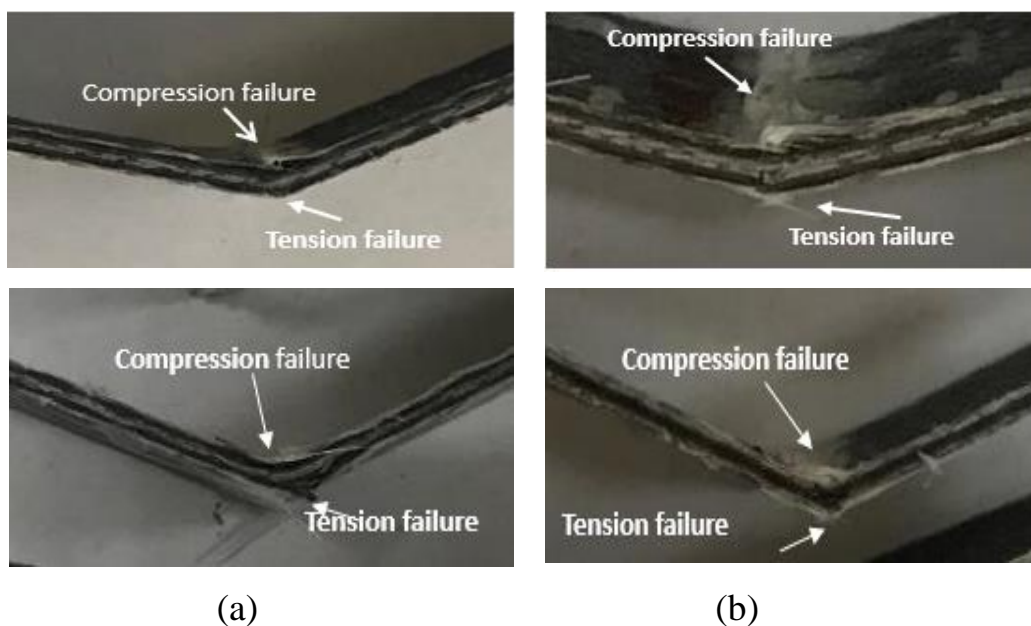


Figure 5-22 Three points bending failure specimens (a) without SiO_2 nanoparticles, (b) with SiO_2 nanoparticles

The introduction of distinct failure mechanisms under flexural stress may account for the notable variation in outcomes among these four types of laminate thickness assessment techniques. Placing a certain number of surrounding layers at (0, 90°) angles to make thick layers is known as foil blocking or foil stacking. Figure 5-23 displays the average stress-strain curves for the flexural specimens. The figure also displays the laminate thickness and the type of stacking sequence technology. The specimens made with the stacking sequence of CS2 [0°/0°/90°/90°/0°/0°]s and CS4 [0°/0°/90°/90°/0°/0°/90°/90°/0°/0°]s were superior to the specimens made with CS1 [0°/90°/90°/0°]s and CS3 [0°/90°/90°/0°/0°/90°/90°/0°]s in terms of flexural response at the laminate level. These laminates have the same behavior as the stress-strain curve, but increasing laminate thickness causes the ultimate stress to decrease, as demonstrated by laminate CS4. This is because each laminate has become thicker, and there are four layers arranged at an angle of 0 degrees in the center of the plates. This increase in thickness causes failure due to the stacking of the layers in the laminate with or without the adding of SiO₂ nanoparticles, the bending strength data in CS1 and CS3 exhibit similar behavior. There is a strong link between these findings and those in (Caminero *et al.*, 2019).

Because of this, it seems that bigger plates exhibit greater stress and stiffness in the linear response than thinner plates, which causes more significant damage to occur between the plates. These findings were consistent with earlier research findings (Wisnom, Khan and Hallett, 2008). The stress-strain curve displayed three distinct sections: a first linear response, a substantial modulus reduction, and finally, after achieving the desired stresses. Thicker slices in this instance had greater stress on failure. These specimens displayed fiber reorientation and stresses up to failure in the area, which significantly reduced the amount of stress applied to the fibers. The plates' high-pressure hardening served as evidence for this. Shear-induced splitting and fiber breakage combined to cause these laminates to fail.

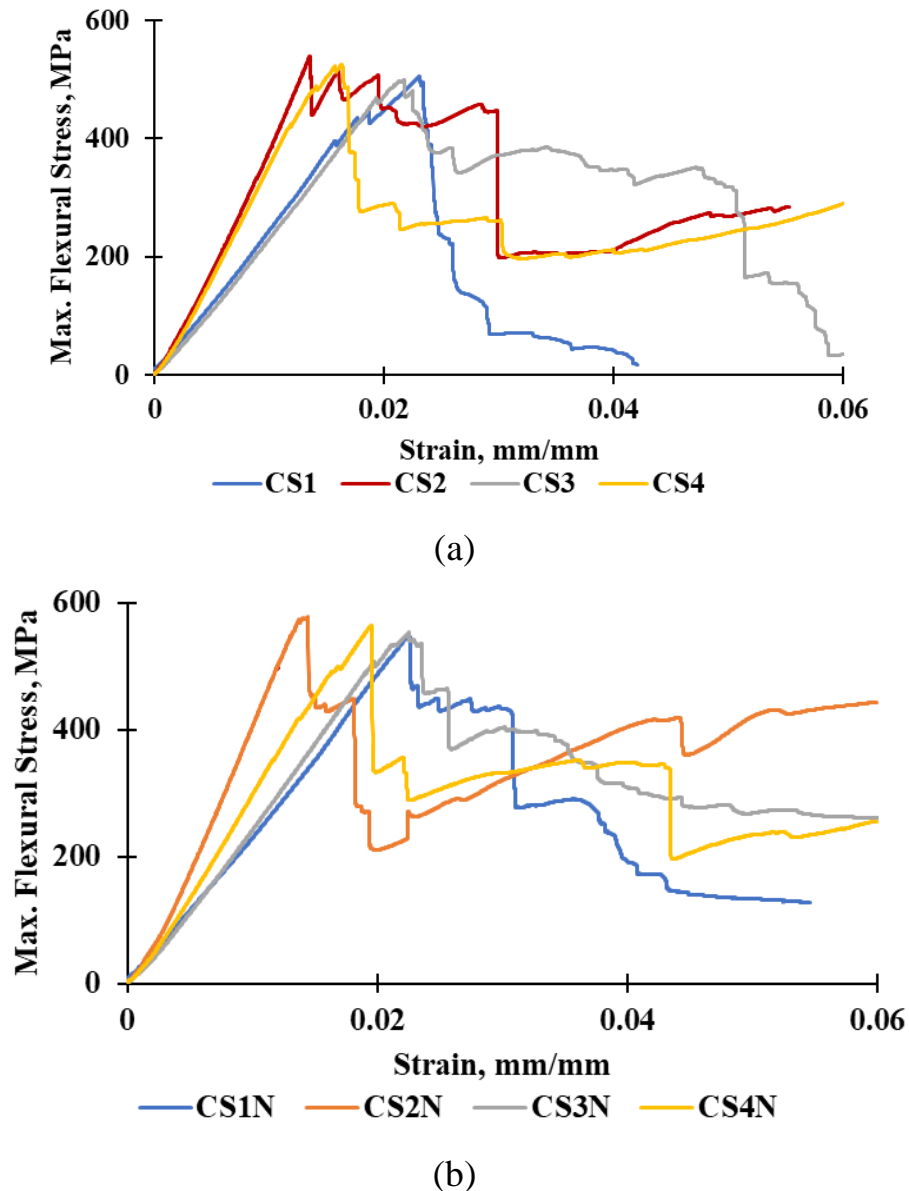
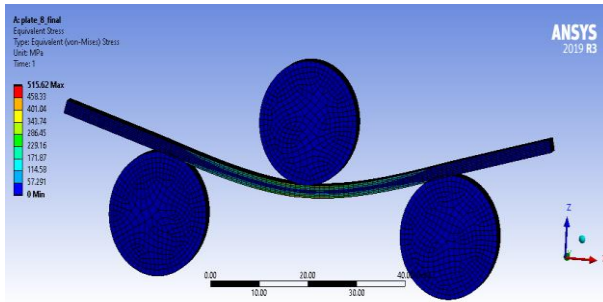
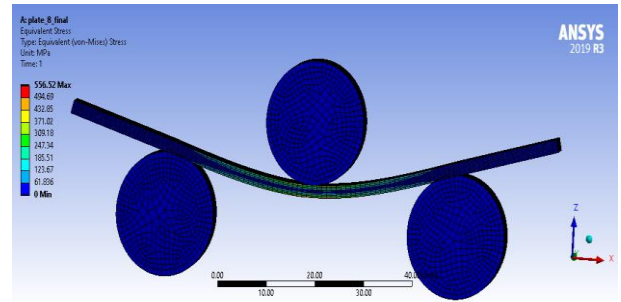


Figure 5-23 Effect of stacking sequences on three points bending test of cross-ply glass/carbon hybrid composite (a) without adding SiO_2 nanoparticles (b) with adding SiO_2 nanoparticles

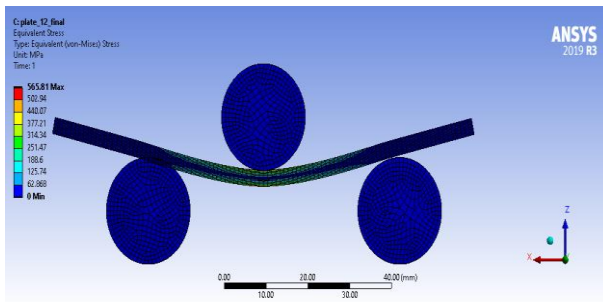
As discussed in Chapter 4, a 3-D numerical model was constructed using the ANSYS workbench to validate the experimental results of the three-point bending of cross-ply laminates. Figure 5-24 depicts the results, showing the distribution of ultimate tensile strength across each ply of the FRPC. Figure 5-25 compares the distribution of numerical analysis results with experimental data. The image clearly shows a significant relationship between the experimental data and the conclusions from ANSYS's numerical data analysis.



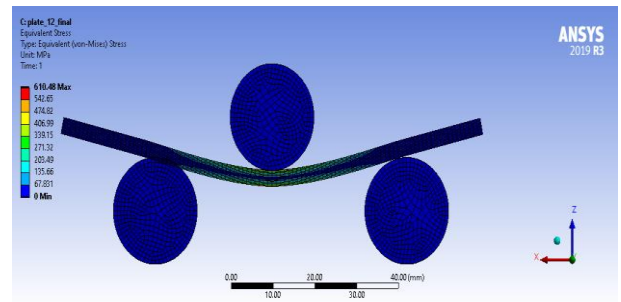
(a)



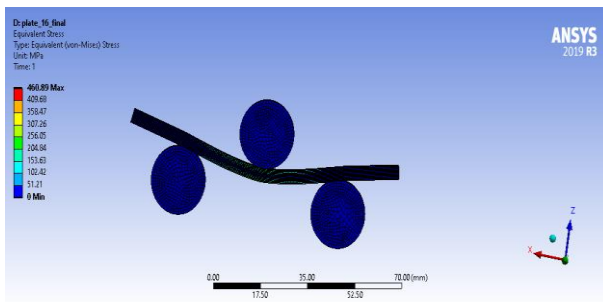
(b)



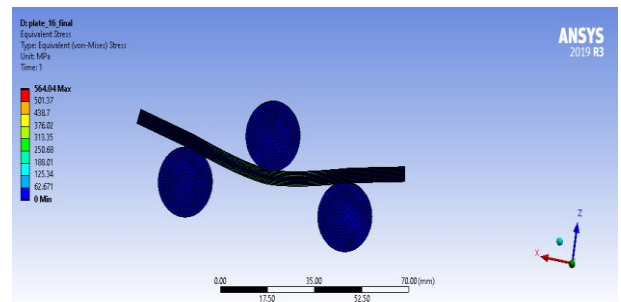
(c)



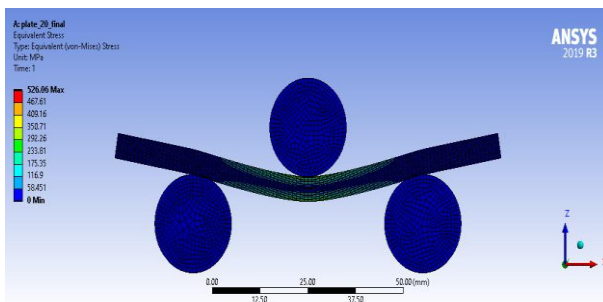
(d)



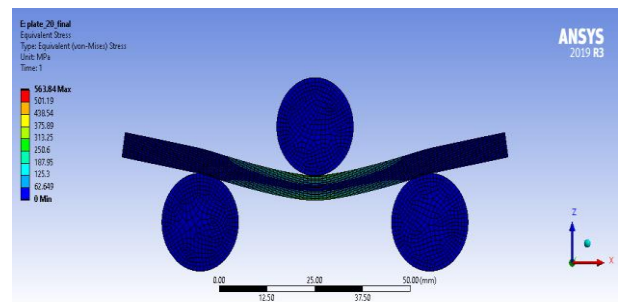
(e)



(f)



(g)



(h)

Figure 5-24 Ultimate flexural strength distribution through cross-ply laminates of FRPC plies (a) CS1, (b)CS1N, (c)CS2, (d)CS2N, (e)CS3, (f)CS3N, (g)CS4, (h)CS4N.

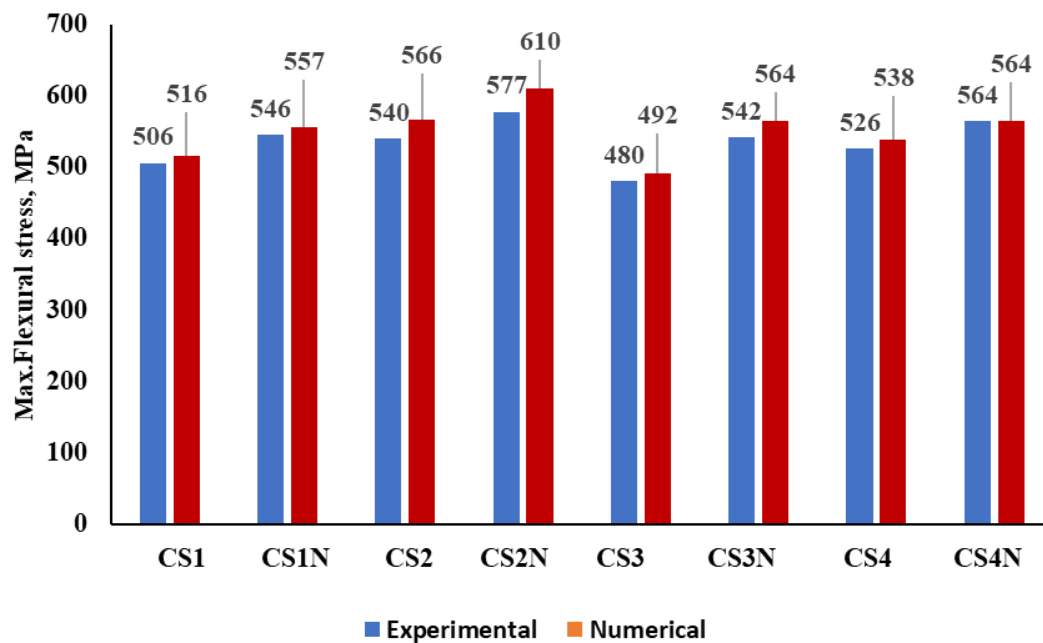


Figure 5-25 Experimental and Numerical (ANSYS) ultimate flexural strength comparison of cross-ply laminates.

5.4 Fatigue Test

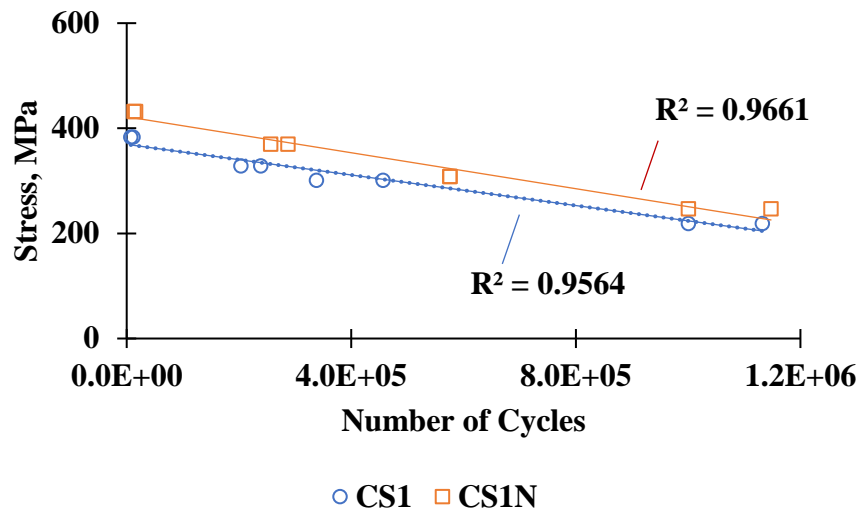
Two distinct types of fatigue tests were performed. The Shimadzu servo-hydraulic dynamic testing equipment was used for the tension-tension fatigue test. The tension-tension specimens' dimensions are primarily based on ASTM D3039 and are comparable to those of the static tensile specimens. The second type involves testing for flexural fatigue using a mechanical testing machine. This equipment was produced locally, which is discussed in Chapter 4 (Section 4.4.3.1). The flexural fatigue specimens' dimensions are largely based on ASTM D790 and are comparable to static flexural specimens.

5.4.1 Axial Fatigue Test for Cross-Ply Laminate

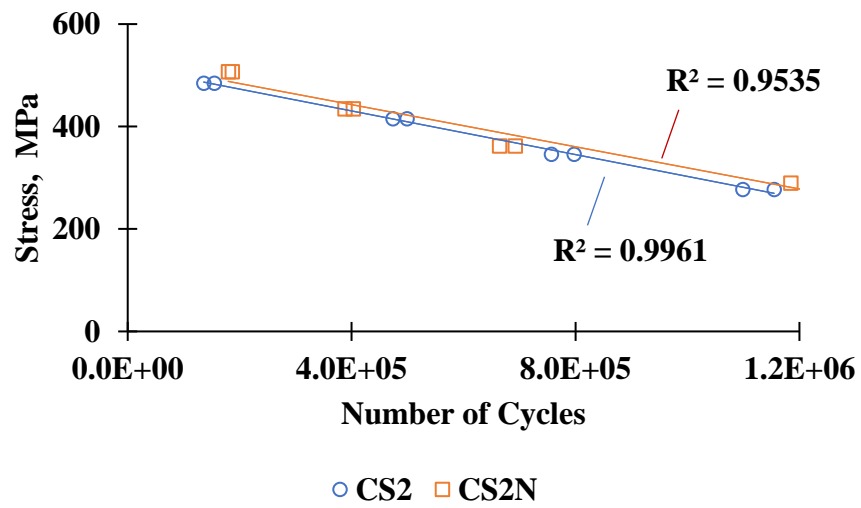
As described in Chapter 4, fatigue tests were performed by utilizing a Shimadzu brand Servo-Hydraulic Fatigue Tester machine with a 100 kN load cell. To determine the fatigue limits of the samples, the experiments were performed by applying $R = 0.1$ stress ratio, 8 Hz frequency, and sine wave load. Fatigue properties of the

glass/carbon hybrid composites reinforced with 2 wt.% of SiO₂ nanoparticles were compared to those of neat epoxy glass/carbon hybrid composites, which selected as a reference.

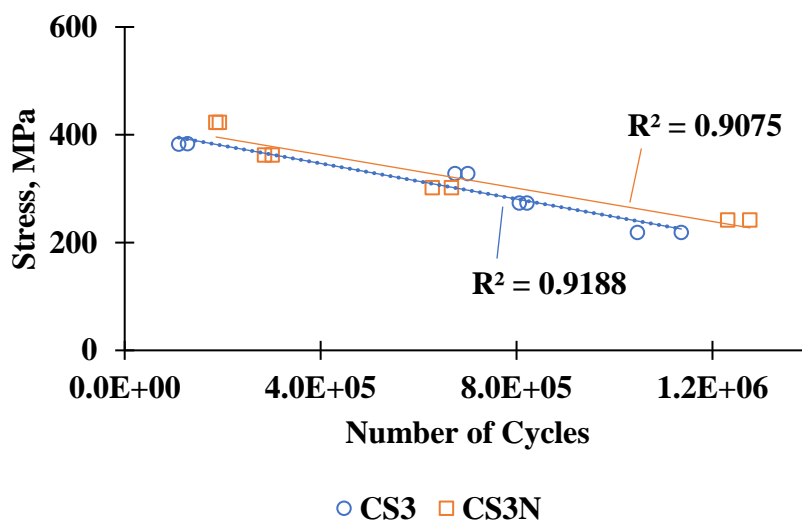
As mentioned in Section 4.4.2, in order to determine the cycle numbers of the hybrid composites, fatigue tests were conducted on a minimum of three specimens per lamination of neat epoxy hybrid composites and SiO₂ nanoparticle enhanced hybrid composites at four distinct load levels (40%, 50%, 60%, and 70%) determined by the average failure loads. The fatigue test endurance limit for the hybrid composites was established at 10⁶ cycles at a load level of 40%. Figure 5-26 displays the stress level (N/mm²) and number of cycles (N) curves of the hybrid composites reinforced with 2 wt.% of nanoparticles SiO₂ in comparison to the neat-epoxy hybrid composites. Note that (R²=0,9) in the figures means a strong positive association between variables.



(a)



(b)



(c)

Figure 5-26 S-N curves for hybrid composite (a) CS1 and CS1N (b) CS2 and CS2N (c) CS3 and CS3N

It can be seen clearly from the figure that the neat-epoxy hybrid composites showed lower cycle numbers than the nanoparticle-reinforced hybrid composites under the same fatigue loading circumstances during high-load fatigue testing. Adding 2 weight percent of SiO₂ nanoparticles to the epoxy during fatigue testing increased the cycle numbers of the hybrid composites for (CS1 and CS1N), (CS2 and CS2N), and (CS3 and CS3N) by about 55%, 27%, and 58%, respectively, at a 70% load level. The efficient transmission of fatigue stresses by the hybrid composites containing silicon dioxide nanoparticles may have led to an increase in cycle number at a high load level of 70%. The tensile strengths of the neat epoxy hybrid composites did not align with the fatigue behaviors of hybrid composites reinforced with SiO₂ nanoparticles. The cycle number fell as the load levels rose, as shown in Figure 5-26. These fatigue results had a good correlation with (Borrego *et al.*, 2014).

Figure 5-27 depicts the general stress-related increment in unidirectional hybrid glass/carbon composites. The comparison is made between specimens without the addition of silica nanoparticles (referred to as CS1, CS2, and CS3) and those with the addition of silica nanoparticles (denoted as CS1N, CS2N, and CS3N). Notably, the stress increase with respect to fatigue limit between CS1 and CS1N is measured at 10.1%, while the corresponding increase between CS2 and CS2N is found to be 4.6%. Similar percentage increments with (CS1 and CS1N) are observed for the remaining sample pair, specifically CS3 and CS3N (10.6% increase). These enhancements in stress performance can be attributed to the beneficial impact of incorporating silica nanoparticles into the composites as well as the stacking sequences of the cross-ply laminates.

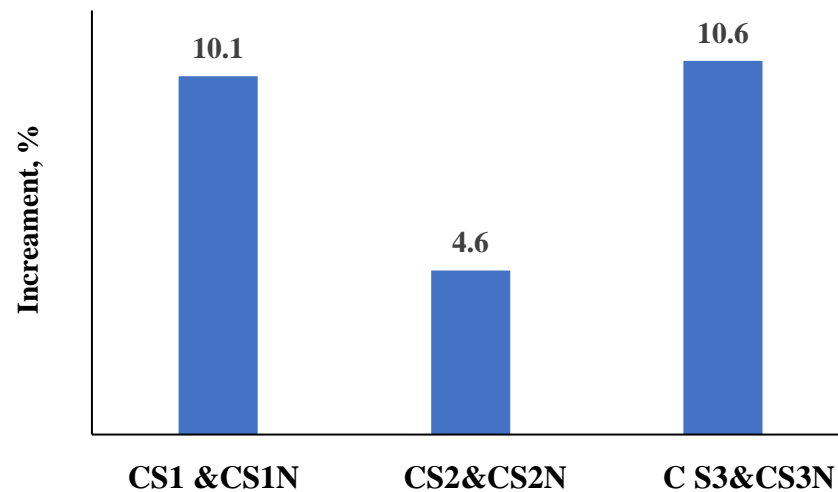
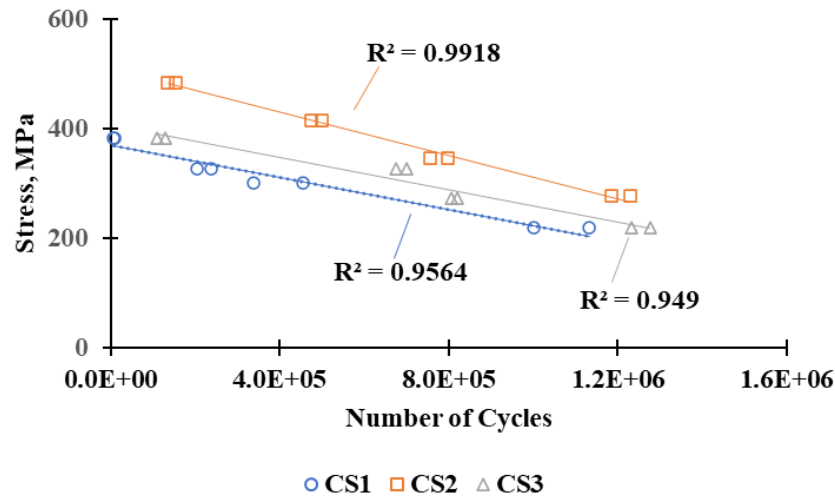
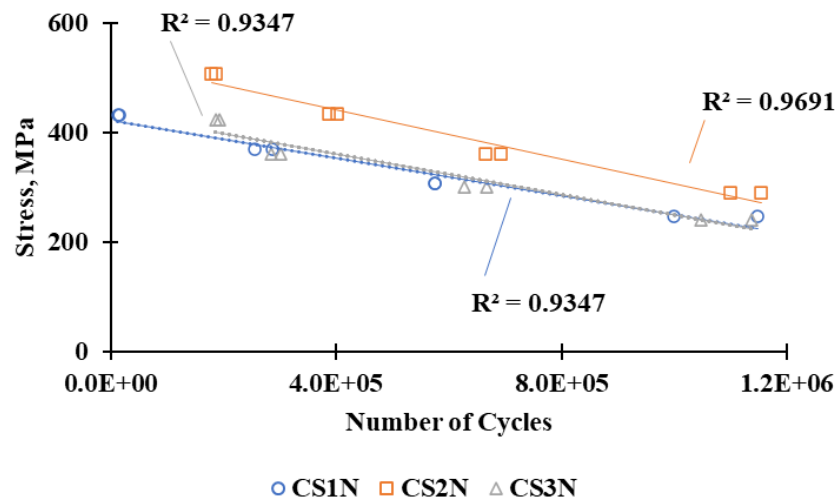


Figure 5-27 General increment percentage in axial fatigue limit of cross ply laminate.

The impact of the stacking sequence on the S-N curves with and without SiO₂ nanoparticles is seen in Figure 5-28. In every instance, it is evident that the fatigue life and fatigue limit of nano-reinforced hybrid composite materials have increased. SiO₂ nanoparticles, which plug any possible gaps in the epoxy or at the interface where the fibers and epoxy meet, are responsible for this improvement. This significantly lowers the concentration of stress and prevents fractures from forming. Furthermore, the epoxy's integration of nanoparticles facilitates the load transmission from matrix to fiber. When these components are present together, the fatigue life of the composite materials clearly increases, and these findings are consistent with (Ergün and Hamit-Adin, 2022).



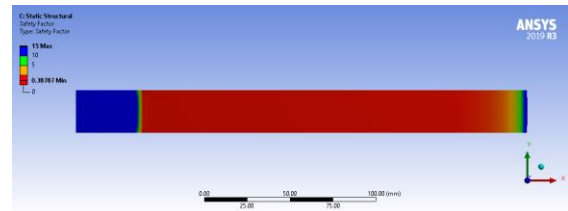
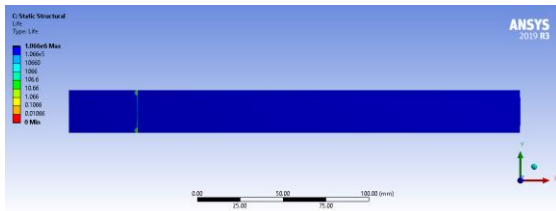
(a)



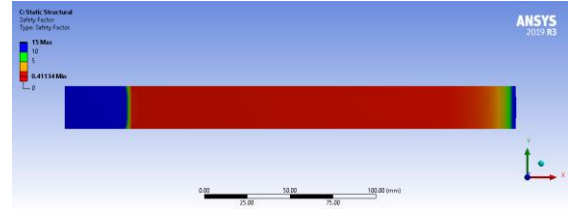
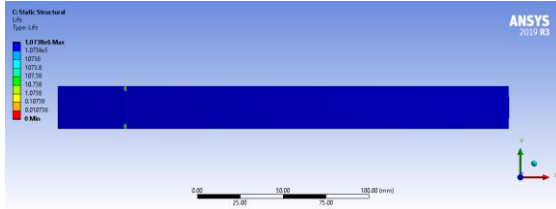
(b)

Figure 5-28 S-N curves for hybrid composite (a) without adding SiO_2 nanoparticles, (b) with adding SiO_2 nanoparticles

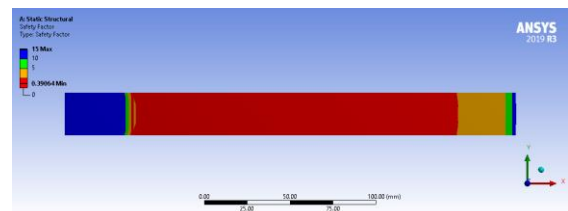
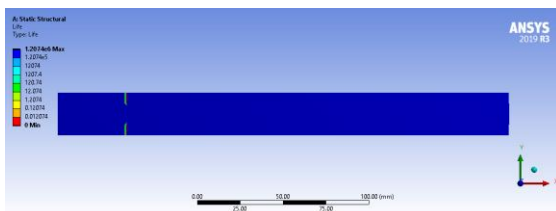
As mentioned in Chapter 4, in order to validate the experimental results of the axial fatigue of cross-ply laminates, a 3-D numerical model, using ANSYS workbench, was built that applies a repeating load and generates a specific moment. The goal is to determine the amount of alternating stress present in the specimen. Alternating stress is the stress that forecasts the fatigue S-N curve, taking into account various elements like loading type and stress ratio. Figure 5-29 contour map illustrates the remaining lifespan for the fatigue analysis on pure epoxy. This diagram illustrates the number of cycles at which fatigue from constant-amplitude stress causes the component to fail.



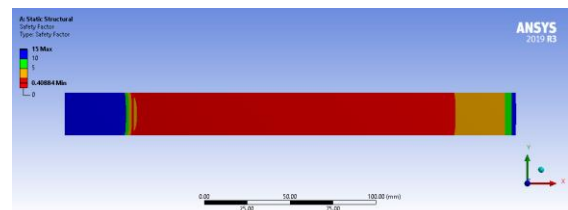
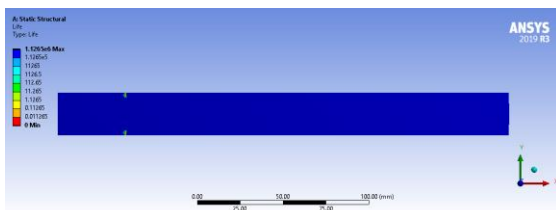
CS1



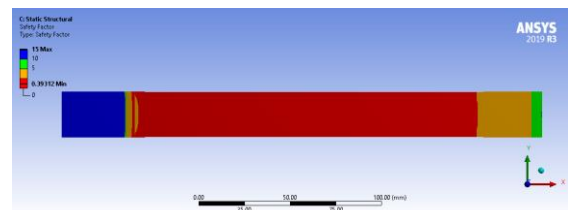
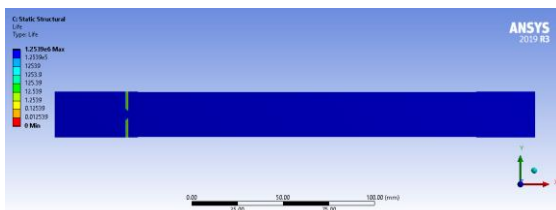
CS1N



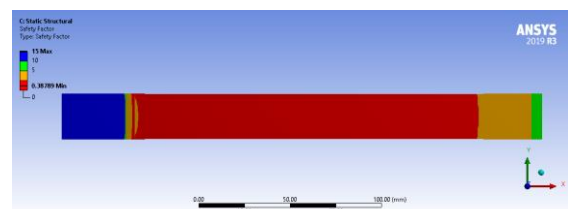
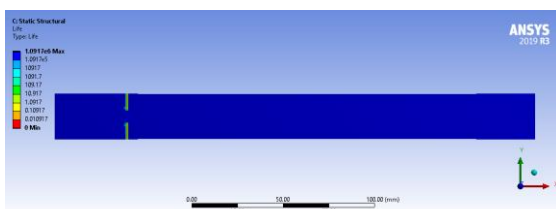
CS2



CS2N



CS3



CS3N

Figure 5-29 Fatigue life and safety factor analysis of cross ply for both neat epoxy laminates and epoxy laminates containing SiO₂ nanoparticles

Table 5-6 provides a concise overview of the fatigue testing results for the experimental and simulated component. The table presents numerical values that correspond to various thicknesses and hybrid composite materials. Additionally, it evaluates the outcomes of the fatigue life trials by comparing them with the S-N curve and the designed simulation. Table 5-6 and Figure 5-28 show the fatigue degradation model for the specified applied stress ratios. Based on these results, the fatigue degradation model demonstrates a greater level of agreement with the experimental data compared to the simulation program.

Table 5-6 Summarizes the numerical and experimental findings for cross ply laminates.

Laminates	No. of layers	Experimental	Numerical	
		Endurance limit	Endurance limit	Min. Safety factor
CS1	8	1.13E+06	1.06E+06	0.3878
CS1N	8	1.14E+06	1.07E+06	0.4113
CS2	12	1.23E+06	1.20E+06	0.3906
CS2N	12	1.15E+06	1.12E+06	0.4088
CS3	16	1.27E+06	1.25E+06	0.3931
CS3N	16	1.13E+06	1.09E+06	0.3878

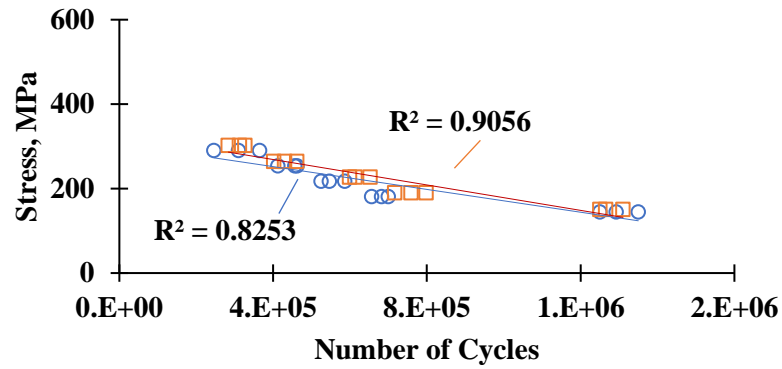
5.4.2 Flexural Fatigue

Fatigue tests were conducted at $R = -1$ (fully reversed) stress ratio, frequency of 10 Hz, and sinusoidal load to ascertain the fatigue limits of the specimens. A comparative analysis was performed between neat epoxy unidirectional hybrid composites and unidirectional hybrid composites reinforced with 2.0 wt% SiO₂ nanoparticles. Reference specimens comprising unidirectional hybrid composites without nanoparticle reinforcements were employed.

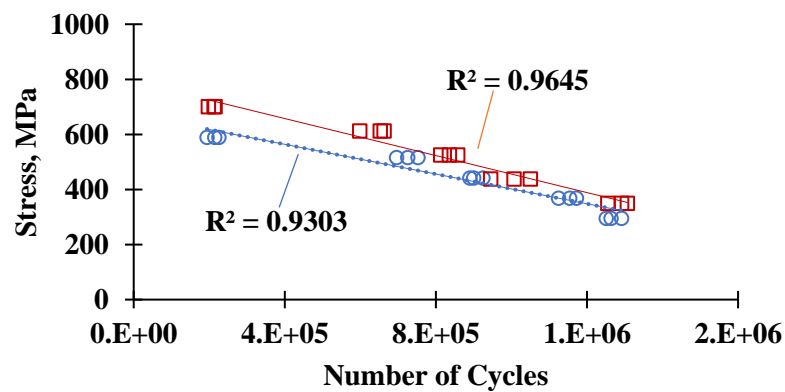
Unidirectional hybrid composites were tested under loads of 40%, 50%, 60%, 70%, and 80% of the maximum bending stress. A minimum of three samples were required for both the unidirectional hybrid composites with neat epoxy and those enhanced with nanoparticles for each load value. To plot the S-N curves, every type of unidirectional composite was subjected to five distinct stress levels based on typical failure loads. Due to the lack of clarity with regards to the endurance limit in composite materials, an endurance limit of 1.25×10^6 number of cycles was embraced as a reference point for the purpose of comparison with different cases.

5.4.2.1 Flexural fatigue Quasi Isotropic-Ply Laminate

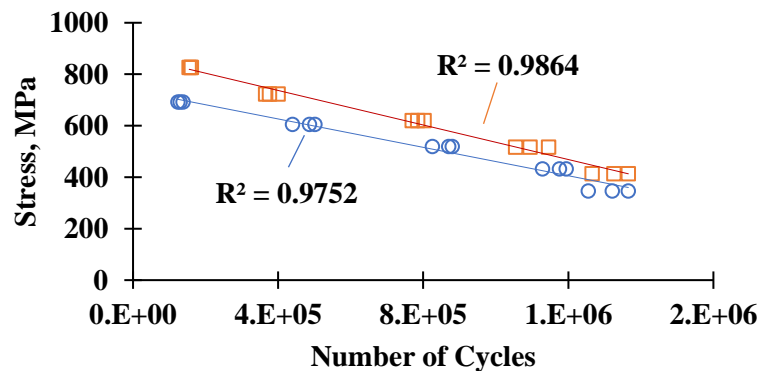
The S-N curves for the unidirectional glass-carbon hybrid composites with and without SiO_2 nanoparticles can be seen in Figure 5-30. When the applied load decreases, all S-N curves indicate an increase in the fatigue life cycle. All sets of hybrid composites had average regression coefficients (R^2) of about 0.95 for S-N curves, showing good model-data point fit. Also, Figure 5-30 shows that the neat epoxy unidirectional hybrid composites had fewer cycles than the nanoparticle-reinforced unidirectional hybrid composites under the same fatigue loading conditions. This was true for all load levels.



(a)



(b)



(c)

Figure 5-30 *S-N* curves for Quasi Isotropic - ply hybrid composite laminates (a) QS1 and QS1N (b) QS2 and QS2N (c) QS3 and QS3N

Figure 5-31 illustrates the typical stress-related escalation in unidirectional hybrid glass/carbon composites. The specimens (designated QS1, QS2, and QS3) are

compared with the specimens (designated QS1N, QS2N, and QS3N) that have silica dioxide nanoparticles added to them. Notably, there is a 4.8% stress rise with respect to fatigue life between QS1 and QS1N, but there is a 4.5% increase between QS2 and QS2N. Comparable percentage gains are observed for the remaining sample pairings, QS3 and QS3N, showing a 5.6% increase. These favorable effects of adding SiO₂ nanoparticles to the composites and the quasi-isotropic ply laminate stacking sequences are responsible for these improvements in stress performance.

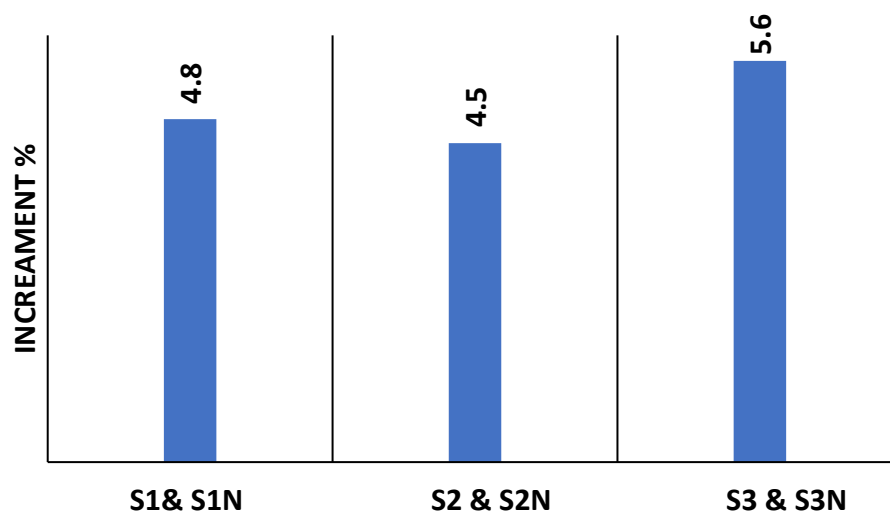


Figure 5-31 General increment percentage in fatigue life for Quasi Isotropic-ply hybrid composite laminates

Figure 5-32 shows how the S-N relationship changes for laminated samples made of hybrid glass/carbon materials as the number of layers increases. It compares these samples to QS1 and QS1N samples, which each had eight layers. The data shows that increasing the number of layers (thickness) increases the stress by approximately two to three times, in comparison to QS1 and QS1N. The significant enhancement can be attributed to the increase in the sample's thickness, which leads to a substantial increase in stress for an equivalent number of cycles. This is because more layers distribute the load over a wider area, reducing the stress on the fibers. By mixing glass and carbon fibers in a hybrid composite, the material is able to utilize the complementary characteristics of each kind of fiber. Additional layers of these fibers improve the material's strength and ability to withstand impacts, resulting in greater

overall strength. Therefore, laminates that are thicker and have more layers enhance their ability to withstand fatigue by distributing the load and deflecting cracks. This is critical for applications that are subject to cyclic loading.

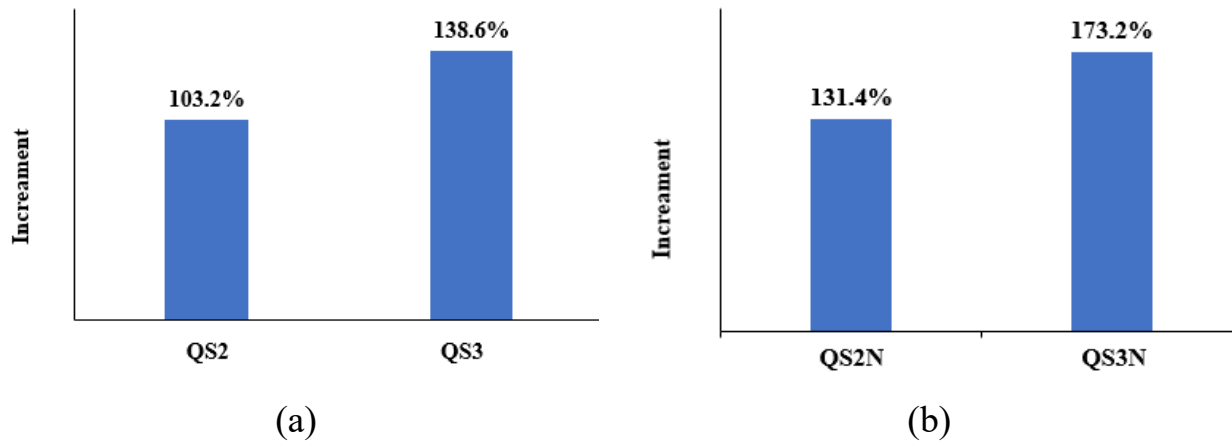
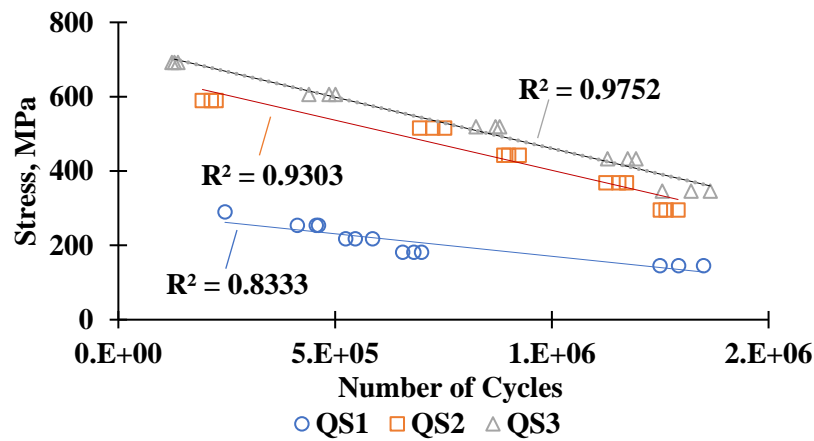
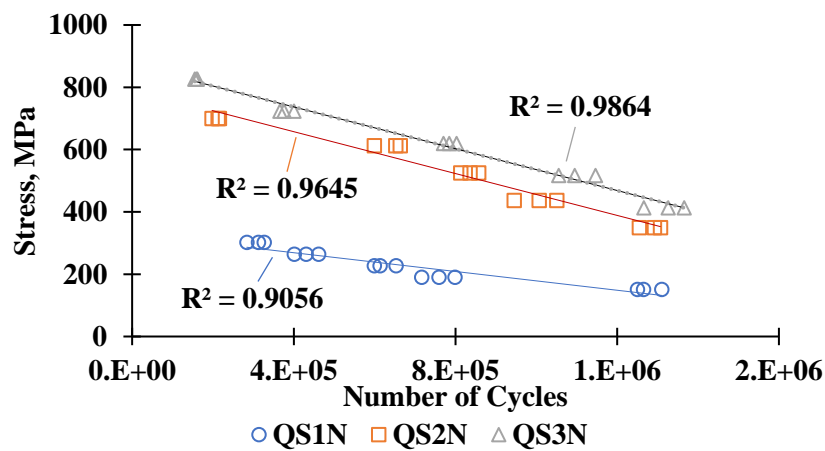


Figure 5-32 General increment percentage in stress for increasing number of layers (a) without SiO₂ nanoparticles comparing with QS1 (b) with SiO₂ nanoparticles comparing with QS1N.

Figure 5-33 demonstrates that nano-reinforced hybrid composite materials have a consistent improvement in fatigue life across all scenarios. SiO₂ nanoparticles, which occupy potential empty spaces inside the epoxy or at the boundary between the fibers and the epoxy, are responsible for the enhancement. Incorporating nanoparticles into the epoxy helps to transmit loads from the matrix to the fiber. The combined presence of these elements significantly improves the fatigue life of the composite materials, and these findings are consistent with the results reported in reference (Nagaraja *et al.*, 2020).



(a)



(b)

Figure 5-33 S-N curves for quasi-isotropic hybrid composite (a) without adding SiO_2 nano-particles, (b) with adding SiO_2 nano-particles.

Using the ANSYS software to construct a numerical representation that exerts a specific moment as a repetitive load, aiming to determine the magnitude of the corresponding alternating stress that arises in the specimen. The stress used to predict the fatigue S-N curve, taking into account several factors such as loading type and R-ratio, is referred to as alternating stress.

The contour plot in Figure 5-34 displays the available life for the given fatigue study of neat epoxy. This figure shows the cycle count at which the component succumbs to fatigue from continuous amplitude stress.

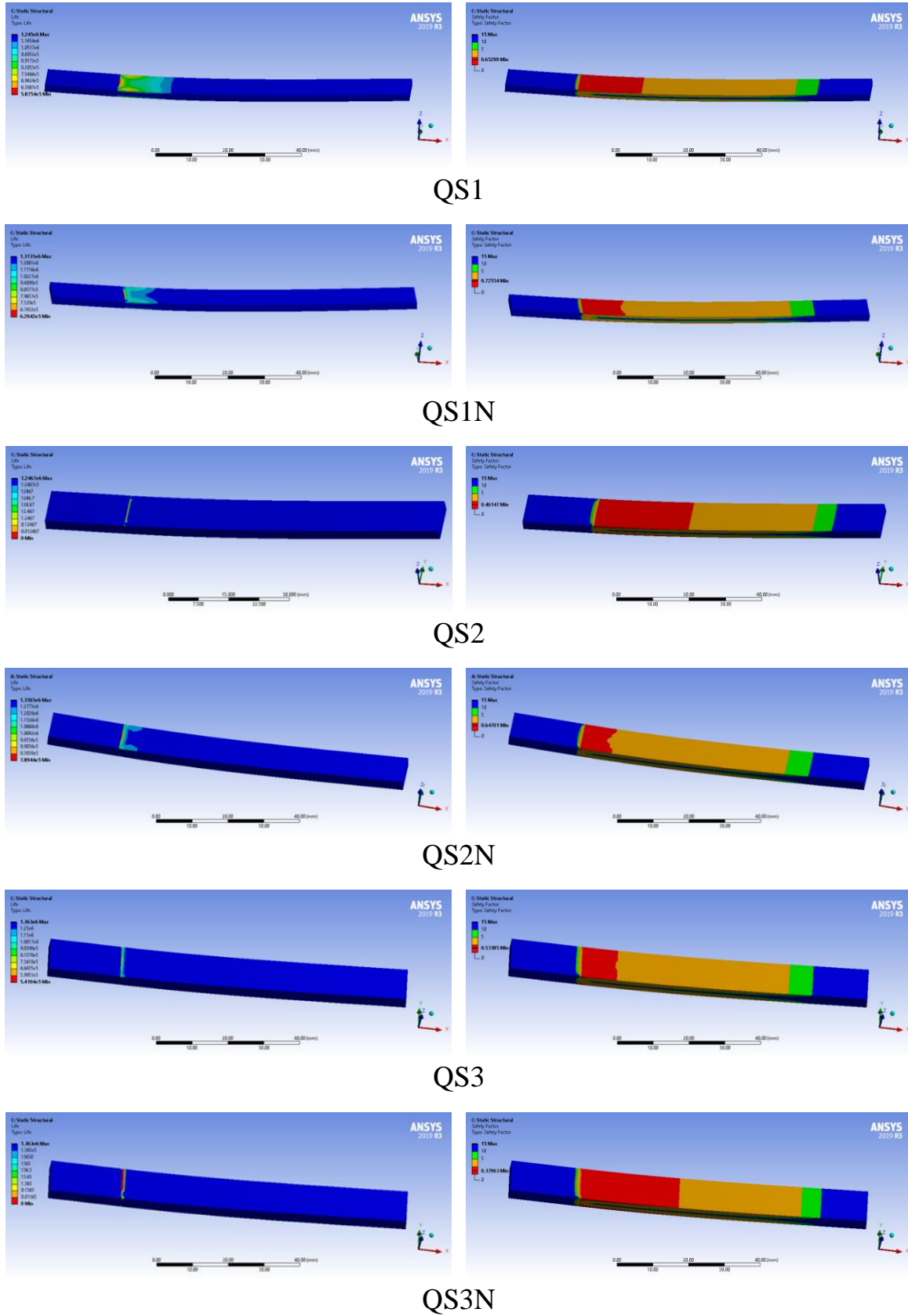


Figure 5-34 Fatigue life and safety factor analysis of quasi-isotropic ply for both QS and QSN.

Table 5-7 presents a summary of the fatigue testing findings for the simulated component. The information in table shows these numbers for different thicknesses and hybrid composite materials. It also compares the results of the fatigue life experiments using the S-N curve and the simulation programmed. Figure 5-33 and

Table 5-7 present the fatigue degradation model for the applied stress ratios mentioned in the previous sentence. According to these findings, the fatigue degradation model exhibits a higher degree of congruence with the experimental data in comparison to the simulation programmed. The correctness of the fatigue degradation model was verified using the S-N curve technique and the ANSYS simulation software.

Table 5-7 Summary of the numerical and experimental results of quasi-isotropic laminates.

Laminates	No. of layers	Experimental	Numerical	
		Endurance limit	Endurance limit	Min. Safety factor
QS1	8	1.25E+06	1.245E+06	0.65299
QS1N	8	1.31E+06	1.3131E+06	0.7255
QS2	10	1.25E+06	1.246E+06	0.46147
QS2N	10	1.306E+06	1.356E+06	0.64701
QS3	12	1.1254E+06	1.363E+06	0.53385
QS3N	12	1.325E+06	1.363E+06	0.37963

5.4.2.2 Flexural fatigue Cross-Ply Laminate

The S-N curves for the unidirectional glass/carbon hybrid composites of cross-ply with and without SiO₂ nanoparticles are shown in Figure 5-35. All S-N curves show an increase in the fatigue life cycle when the applied stress decreases. The regression coefficient (R^2) of S-N curves for all groups of hybrid composites is about 0.95 as an average, indicating that the models fit well with the data points. And as Figure 5-35 illustrates, under equivalent fatigue loading conditions, the number of cycles for the

nanoparticle-reinforced unidirectional hybrid composites was greater than that for the neat epoxy unidirectional hybrid composites at all load level.

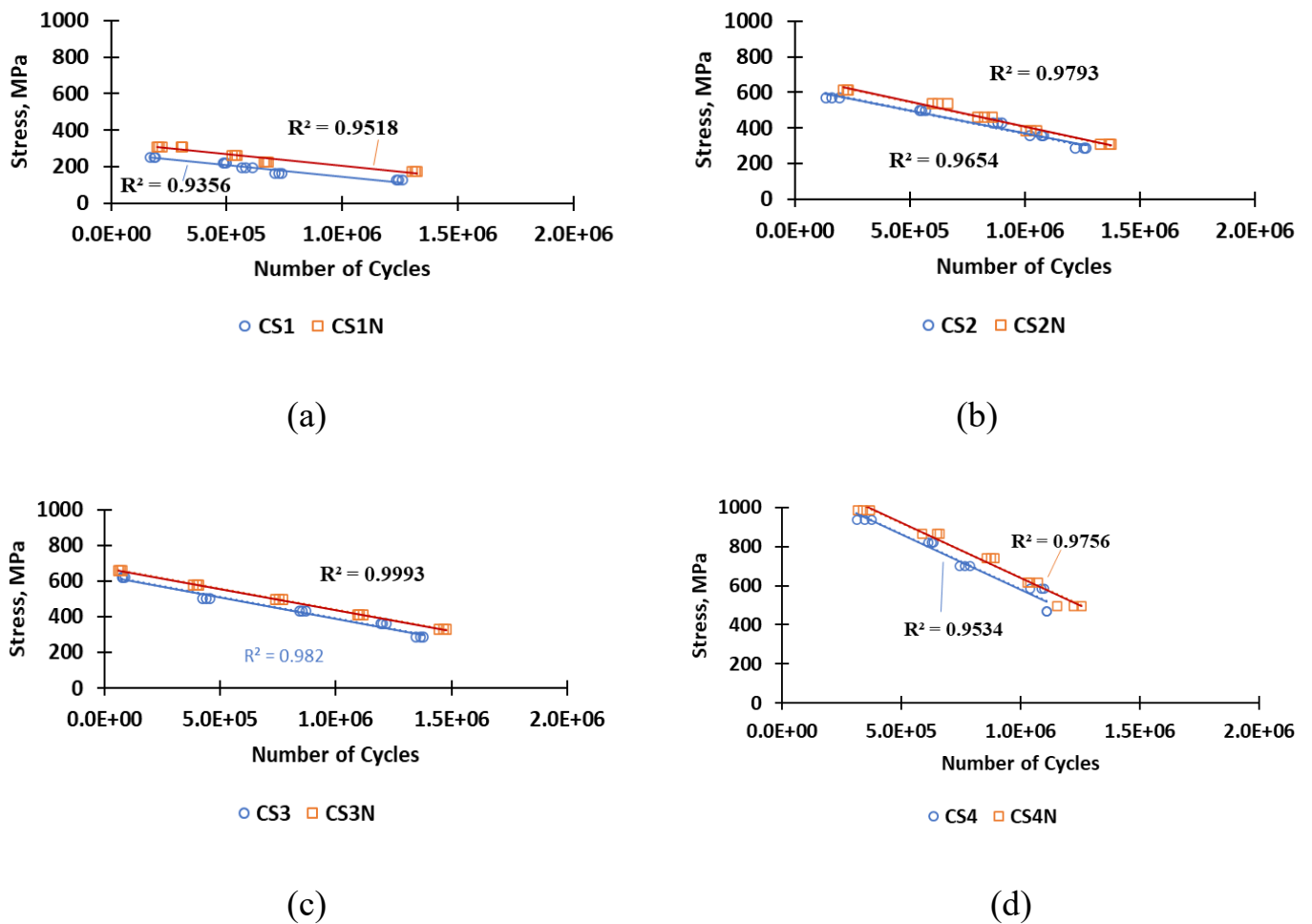


Figure 5-35 *S-N* curves for cross-ply hybrid composite (a) CS1 and CS1N (b) CS2 and CS2N (c) CS3 and CS3N (d) CS4 and CS4N

As shown in Figure 5-36, the [CSN] hybrid composite exhibited higher fatigue strength compared to the [CS] hybrid composite. The higher strength is due to the higher bending strength of the [CSN] hybrid composite compared to the [CS] hybrid composite. Material with a high bending strength would result in excellent fatigue strength.

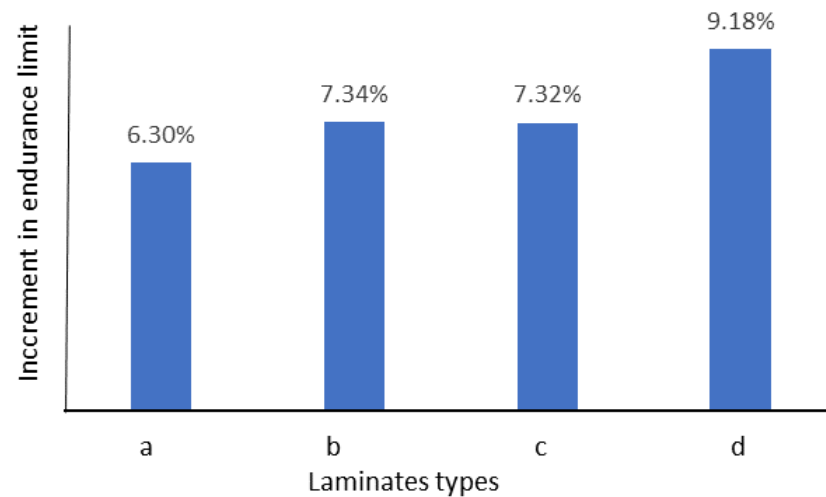


Figure 5-36 Increment percentage in endurance limit (a) CS1 and CS1N (b) CS2 and CS2N (c) CS3 and CS3N (d) CS4 and CS4N

Figure 5-37 depicts the general stress-related increment in unidirectional hybrid glass/carbon composites. The comparison is made between specimens without the addition of silica nanoparticles (referred to as CS1, CS2, CS3, and CS4) and those with the addition of silica nanoparticles (denoted as CS1N, CS2N, CS3N, and CS4N). Notably, the stress increase with respect to fatigue life between CS1 and CS1N is measured at 17.4%, while the corresponding increase between CS2 and CS2N is found to be 13.11%. Similar percentage increments are observed for the remaining sample pairs, specifically CS3 and CS3N (17.1% increase) and CS4 and CS4N (13.61% increase). These enhancements in stress performance can be attributed to the beneficial impact of incorporating silica nanoparticles into the composites as well as the stacking sequences of the cross-ply laminates.

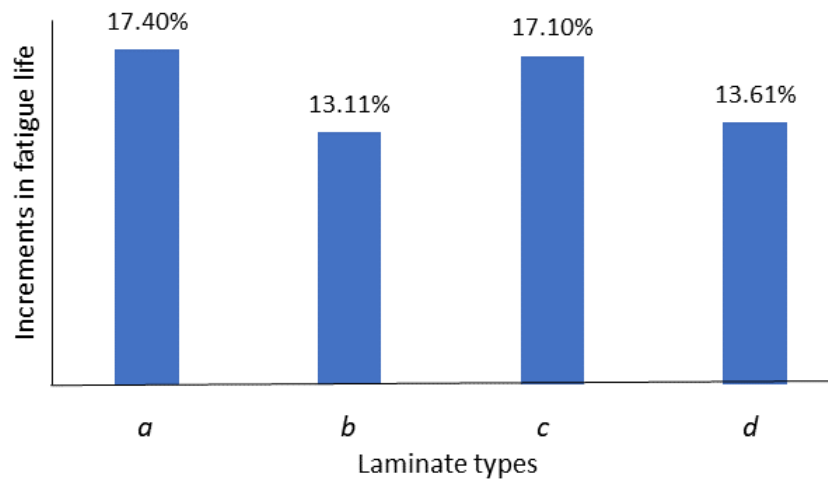
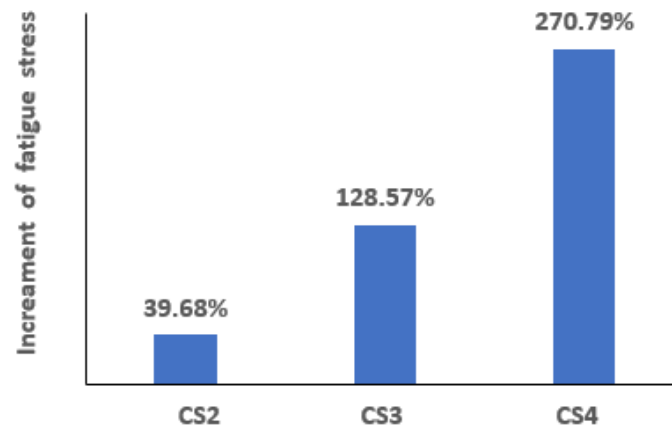
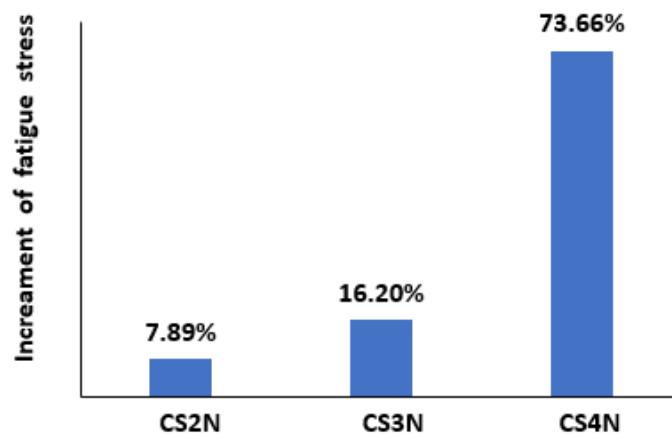


Figure 5-37 General increment percentage in fatigue life (a) CS1 and CS1N (b) CS2 and CS2N (c) CS3 and CS3N (d) CS4 and CS4N

Figure 5-38 shows how the S-N relationship of laminated samples made of hybrid glass/carbon materials changes as the number of layers increases compared to CS1 and CS1N samples with eight layers. The figure shows that the stress strength at the same number of cycles increases with increasing the number of layers (thickness) about two to three times higher with respect to CS1 and CS1N, respectively. The significant improvement is explicable by the fact that increasing the sample thickness causes a significant increase in stress for the same number of cycles. That is because more layer's transfer load across a broader region, minimizing fiber stress, and combining glass and carbon fibers in a hybrid composite lets it use their complementing qualities. More layers of these fibers increase strength and impact resistance, making the material stronger. Thus, thicker laminates with additional layers improve fatigue resistance owing to load dispersion and crack deflection. This is crucial for cyclic-loaded applications.



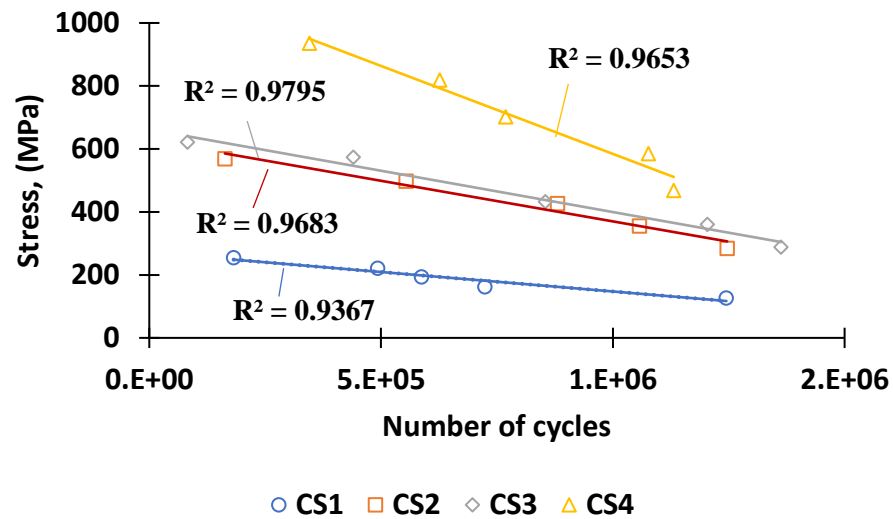
(a)



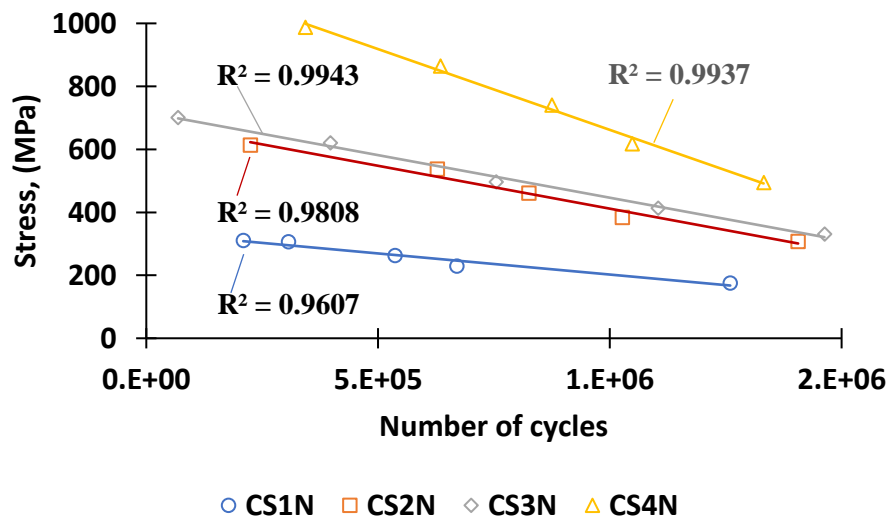
(b)

Figure 5-38 General increment percentage of fatigue stress in increasing number of layers (a) without SiO_2 nanoparticles comparing with CS1 (b) with SiO_2 nanoparticles comparing with CS1N.

Through the observation of Figure 5-39, it is apparent that there is an increase in the fatigue life of nano-reinforced hybrid composite materials in all cases. This improvement can be attributed to the presence of SiO_2 nanoparticles, which fill potential voids within the epoxy or in the interface between the fibers and the epoxy. By doing so, stress concentration is greatly reduced and the emergence of cracks is prevented. Furthermore, the stress intensity factor is significantly reduced, thereby inhibiting the growth of any cracks. Additionally, the incorporation of nanoparticles within the epoxy facilitates the transfer of loads from matrix to fiber. The collective presence of these factors leads to a clear enhancement in the fatigue life of the composite materials, these results are in good agreement with (Ding and Cheng, 2021).



(a)



(b)

Figure 5-39 S-N curves for hybrid composites at different thicknesses (a) without adding SiO₂ nanoparticles, (b) with adding SiO₂ nanoparticles.

ANSYS software is used to create a numerical model in which a given moment is applied as a cyclic load to determine the amount of equivalent alternating stress that results in the specimen. The stress that is utilized to forecast the fatigue S-N curve in relation to several variables, including loading type and R-ratio, is equivalent to alternating stress.

The contour plot of the available life for the specified fatigue analysis for neat epoxy is shown in Figure 5-40. This chart shows the number of cycles before constant amplitude stress causes the component to fail owing to fatigue.

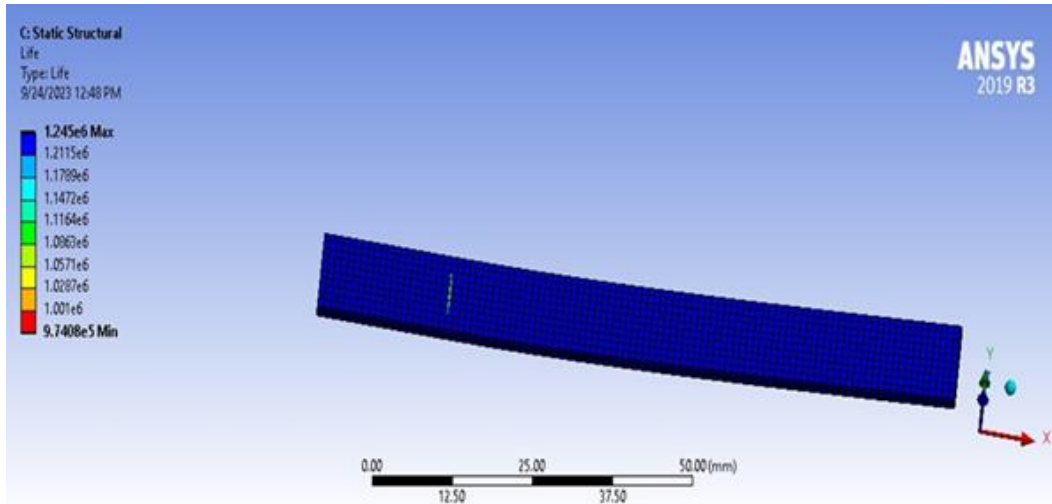
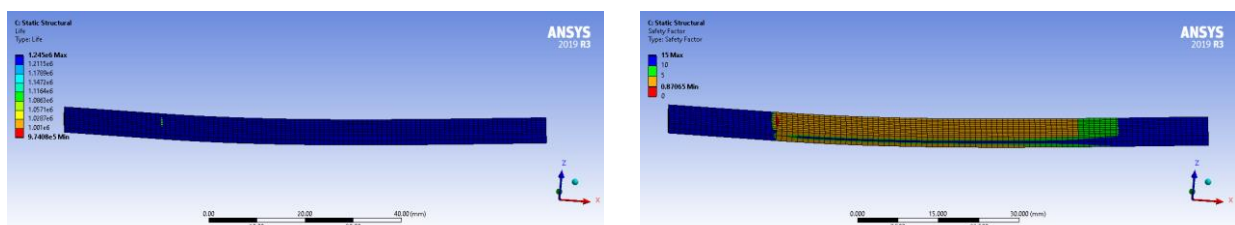
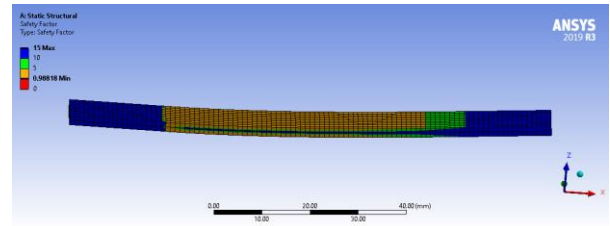
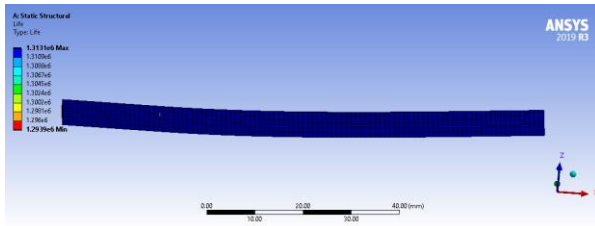


Figure 5-40 Fatigue life analysis neat epoxy of eight ply (CS1).

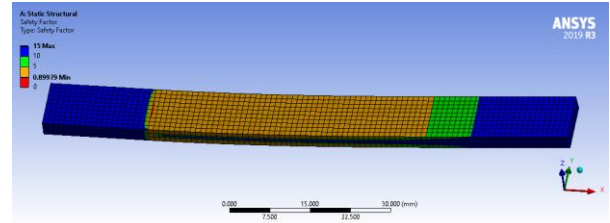
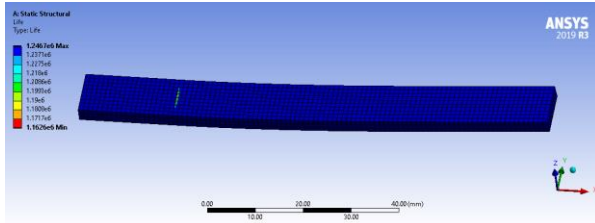
The number of cycles before constant amplitude stress causes the component to fail owing to fatigue, as well as the maximum safety factor of 15, which indicates fatigue failure over the designated design life, is shown in Figure 5-41. The same as with life and harm, this outcome is visible. Failure before the end of the design life is indicated by a fatigue safety factor less than one. The plate with 2% nanosilica particles has the best minimum safety factor. Furthermore, because the safety values of the plates containing nanosilica are higher than those of the plates without, it is evident that the materials investigated with the addition of nanosilica are safe.



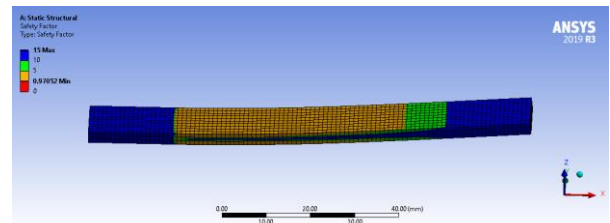
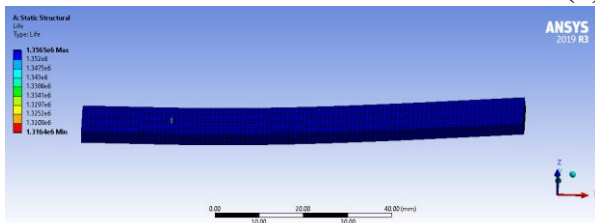
(a) CS1



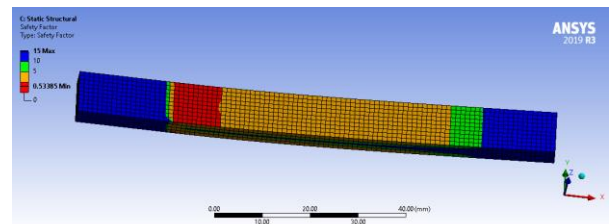
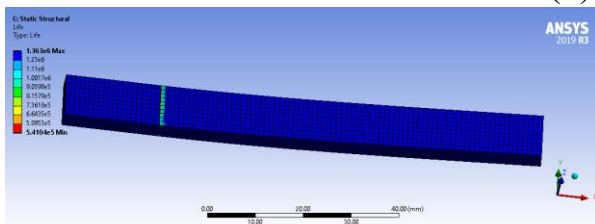
(b) CS1N



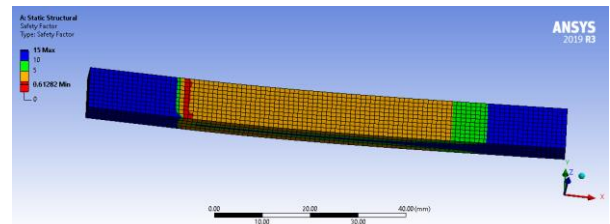
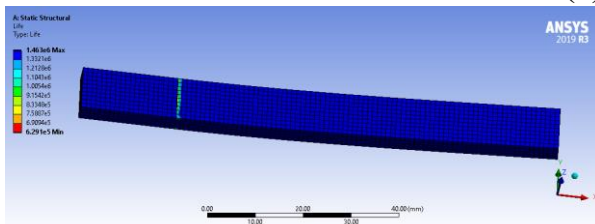
(c) CS2



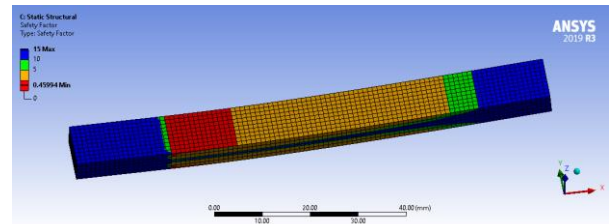
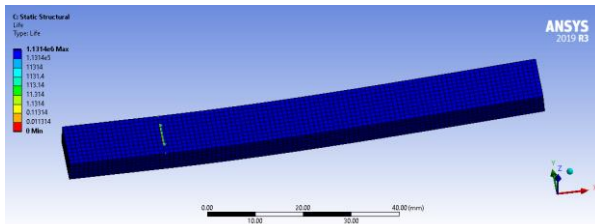
(d) CS2N



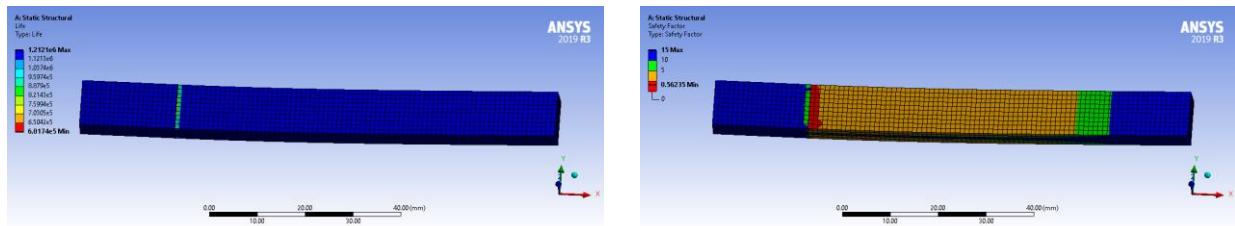
(e) CS3



(f) CS3N



(g) CS4



(h) CS4N

Figure 5-41 Fatigue life and safety factor analysis of cross ply for both neat epoxy laminates and epoxy laminates containing SiO_2 nanoparticles.

Table 5-8 presents a summary of the fatigue testing results for the simulated component for the different thicknesses and hybrid composite materials, and compares fatigue life results obtained through the experimental data of the S-N curve and the simulation program. The fatigue degradation model for the applied stress ratios is shown in Figure 5-39 and Table 5-8

These results show that the fatigue degradation model shows a closer agreement with the experimental data compared to the simulation program. The S-N curve approach and the ANSYS simulation software followed the accuracy of the fatigue degradation model.

Table 5-8 Summary of the numerical and experimental results of of cross-ply laminates

Laminates	No. of layers	Experimental	Numerical	
		Endurance limit	Endurance limit	Min. Safety factor
CS1	8	1.24E+06	1.25E+06	0.87065
CS1N	8	1.30E+06	1.31E+06	0.98818
CS2	12	1.24E+06	1.24E+06	0.89979
CS2N	12	1.35E+06	1.35E+06	0.97052
CS3	16	1.36E+06	1.36E+06	0.53385
S3N	16	1.46E+06	1.46E+06	0.6128
CS4	20	1.11E+06	1.13E+06	0.45994
CS4N	20	1.21E+06	1.21E+06	0.56235

5.5 Failure analysis

After coating with conductive elements, unidirectional hybrid composites comprising glass/carbon fibers and nano-silica particles were examined using scanning electron microscopy (SEM) (ZEISS (1000X) field-emission SEM). The hybrid composites reinforced with nano silica particles are shown in Figure 5-42. Evidently, the glass/carbon fibers were pulled out of the epoxy. Eventually, fractured surfaces appeared as a consequence of horizontal fractures propagating from one fiber to another and in the directions of other glass/carbon fibers. Resin remnants were visible when the fractures occurred. Some fibers pulled out from the fiber bundles as a result of these transverse cracks, creating gaps between them. In addition, spaces were observed between the fibers, indicating that the layers were delaminated. The epoxy resin was immersed in the glass/carbon fibers in 2 wt. % SiO₂ nanoparticles reinforced with unidirectional hybrid composites, as seen by SEM fractional imaging. The 2 wt.% increase in tensile strength of SiO₂ nanoparticles reinforced with one-way hybrid composites compared to pure epoxy unidirectional hybrid composites, as shown in Figure 5-43, was expected to strengthen the interfacial bonding between the fibers and SiO₂ nanoparticle-reinforced unidirectional hybrid composites. According to these predictions, SiO₂ nanoparticles might lessen transverse fractures, and as a result, the crack development resistance would increase. Transverse fractures may be observed in the area of the microstructure when SiO₂ nanoparticles reinforced with 2 wt. % unidirectional hybrid composites are analyzed using a scanning electron microscopy (SEM). Stress concentration may lead to interfacial bond separation and matrix cracking under fatigue loads as transverse fractures spread across the unidirectional hybrid composites. In the areas where the bonding strength was the highest, the fiber bundles were not broken apart. While traces of glass and carbon fibers were found in the wide fracture area, the majority of glass and carbon fibers were found there. Because SiO₂ nanoparticles were effective fillers, it was thought

that by improving the stress transmission, they increased the adhesive bond strength of the fiber bundles.

The fracture mode and mechanism of failure in the specimen during the fatigue test can be succinctly summarized as follows: the initiation of transverse cracks at the first lamina marks the onset of failure, which is subsequently followed by a delamination at the first layer culminating in the free end. This process is then replicated successively in the second and third layers until complete failure is attained.

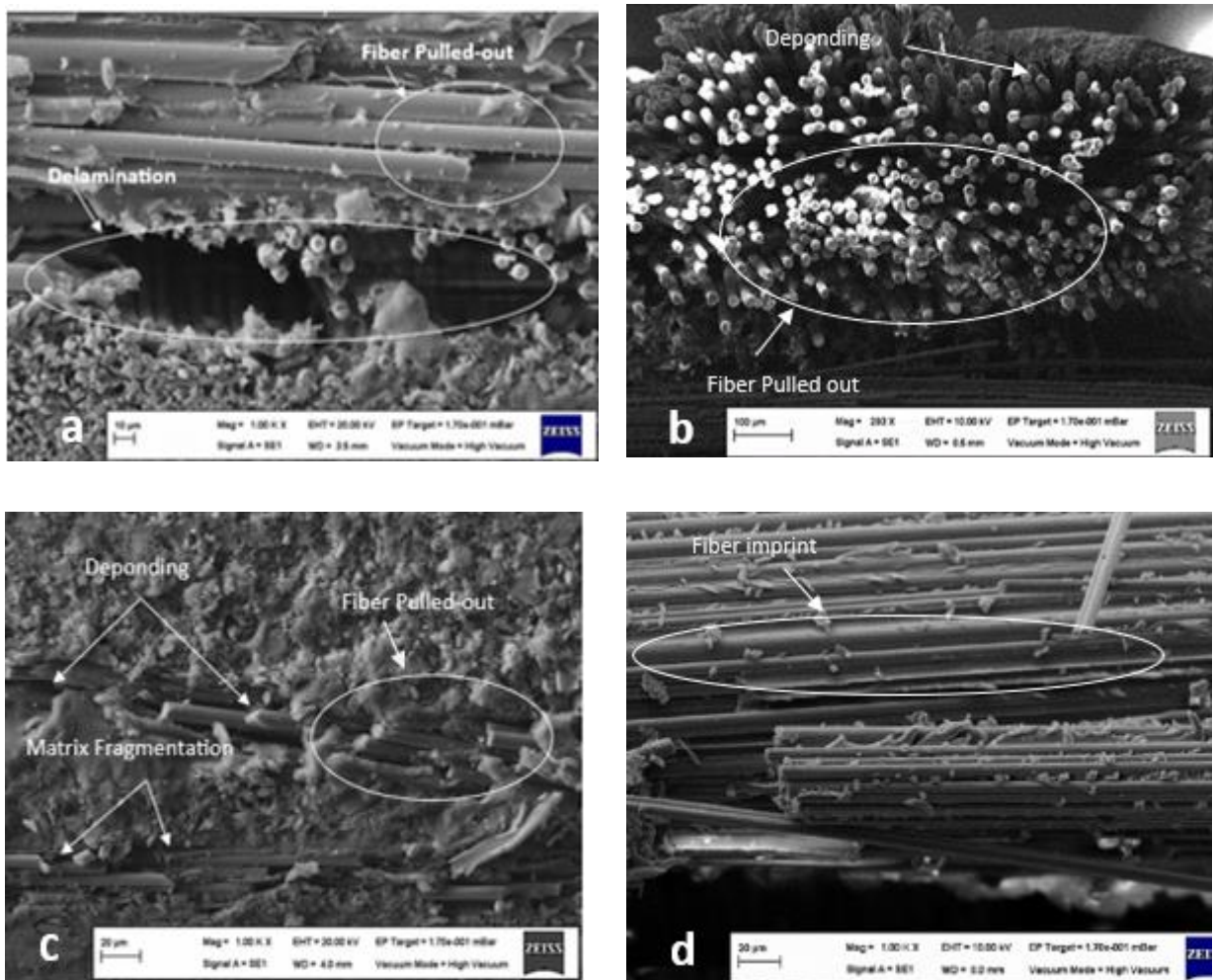


Figure 5-42 Scanning electron microscopy fractography unidirectional composite without SiO₂ Nano particles subjected to fatigue (a) Delamination, (b) Fiber pull-out, (c) Debonding and matrix fragmentation, (d) Fiber imprint.

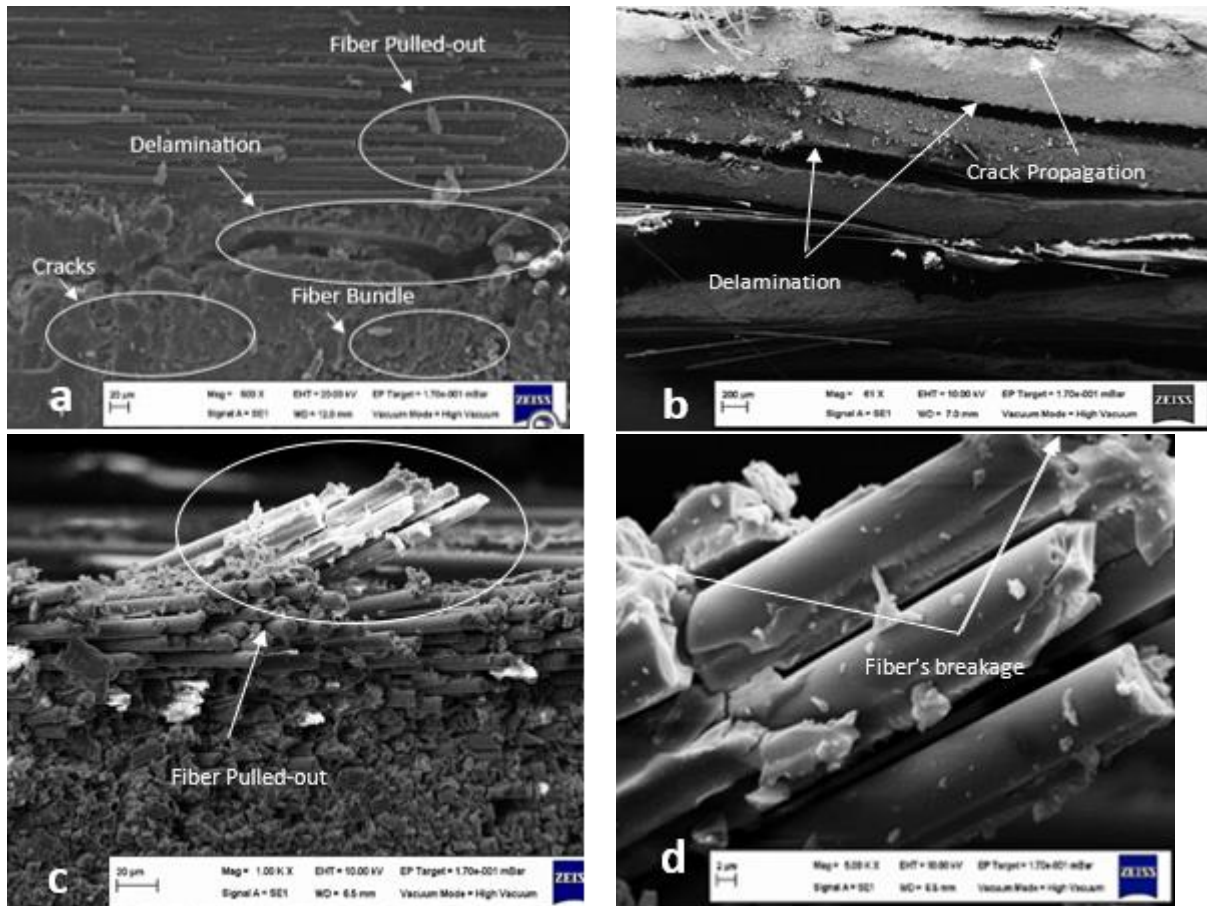


Figure 5-43 Scanning electron microscopy fractography unidirectional composite with SiO₂ Nano particles subjected to fatigue (a) Delamination and Fiber Bundle, (b) Crack propagation, (c) Fiber pull-out, (d) Fiber breakage.

CHAPTER SIX

CONCLUSIONS AND RECOMMENDATIONS

6.1 Conclusions

This study was designed to experimentally and numerically determine the effect of SiO₂ nanoparticles, stacking sequences, and laminate thickness on the tensile strength, bending strength, and fatigue life of hybrid epoxy composites. The most obvious finding is:

1. Cross-ply laminated fiber reinforced polymer composite has higher tensile and flexural properties than quasi-isotropic laminated fiber reinforced polymer composites.
2. The stacking sequence in hybrid composite materials has a significant influence on the mechanical properties of laminates.
3. The impact of SiO₂ nanoparticle incorporation on the mechanical properties was assessed. This means the glass laminate with SiO₂ nanoparticles has higher strengths, strains, and moduli than the glass laminate without nanoparticles. Similarly, the carbon laminate with SiO₂ nanoparticles experienced increases in strength, strain, and Young's modulus when compared to the carbon laminate without nanoparticles.
4. Adding SiO₂ nanoparticles to the epoxy resulted in an increase in the bending strength of glass/carbon hybrid composites.
5. These experiments confirmed that the endurance limit of composites increased with the addition of SiO₂ nanoparticles.

6. The study of fatigue life showed that adding SiO₂ nanoparticles to the epoxy extended the lifespan at all levels of out-of-maximum axial and bending stress.
7. Composite materials' complex structure presents challenges in measuring crack lengths and propagation speeds. Traditional methods like visual inspection and surface crack monitoring are insufficient for capturing comprehensive damage states. Composite materials distribute damage across their volume, making crack behavior assessment in composites require advanced techniques for internal examination and real-time monitoring.

From the above, it can be concluded that the glass and carbon fiber epoxy composites reinforced with silica nanoparticles may be useful in construction, automotive, marine, and aerospace sector. These materials can be used to build and optimize sophisticated hybrid composites for engineering applications. Additionally, designers may customize hybrid composite materials by choosing fibers and matrix components. The addition of silica dioxide nanoparticles to a toughened resin matrix enhanced the material's characteristics by incorporating various fibers.

6.2 Recommendation of Future Work

1. Investigate the environmental resistance and long-term durability of hybrid epoxy composites enhanced with SiO₂ nanoparticles under various operating conditions.
2. Explore the effects of different weight percentages of SiO₂ nanoparticles on the mechanical properties of hybrid composites to determine the optimal concentration for various applications.
3. Conduct detailed studies on the influence of SiO₂ nanoparticles on hybrid epoxy composites' thermal properties and thermal stability.
4. Develop advanced evaluation techniques for real-time monitoring and internal examination of crack propagation and damage states in composite materials.
5. Investigate the potential for different types of nanoparticles or hybrid nanoparticle combinations to improve the mechanical properties of epoxy composites.
6. Investigate the synergistic effects of SiO₂ nanoparticles with other reinforcing materials, such as carbon nanotubes, titanium nanoparticles, or aluminum oxide nanoparticles, to develop innovative composites with superior properties.
7. Examine the scalability and manufacturing procedures for SiO₂ nanoparticle-reinforced hybrid composites to assure low-cost, high-quality production for industrial applications.
8. Examine the environmental impact and recyclability of SiO₂ nanoparticle-reinforced hybrid epoxy composites to enhance sustainable and eco-friendly material development.
9. Collaborate with industry partners to undertake real-world testing and validation of SiO₂ nanoparticle-reinforced hybrid epoxy composites in specific technical applications, such as automotive, marine, and aerospace.

REFERENCES

A. Ajaj, E., J. Jubier, N. and J. Majeed, K. (2013) 'Fatigue Behavior of Epoxy/SiO₂ Nanocomposites Reinforced with E- glass Fiber', *International Journal of Application or Innovation in Engineering & Management (IJAEM)*, 2(9), pp. 62–69. Available at: www.ijaiem.org.

Ab Ghani, A. F. *et al.* (2021) 'Hybrid Carbon/Glass Fiber Reinforced Polymer; A Frontier Material for Aerospace Industry : A Review on Mechanical Properties Enhancement', *Current Science and Technology*, 1(2), pp. 41–51. doi: 10.15282/cst.v1i2.6919.

Abed, K. N., Faris, S. T. and Naemah, I. M. (2023) 'Effects of Fiber Orientations on Mechanical Properties of a Carbon Fiber Reinforced Composite Material used in Aircraft Applications', *Al-Nahrain Journal for Engineering Sciences*, 26(1), pp. 1–6. doi: 10.29194/NJES.26010001.

Abrate, S. (2011) 'Introduction to the mechanics of composite materials', *CISM International Centre for Mechanical Sciences, Courses and Lectures*, pp. 1–48. doi: 10.1007/978-3-7091-0523-8_1.

Agrawal, P. *et al.* (2022) 'A Review Paper of Composite Materials: Advantages and Applications', *International Journal of Advances in Engineering and Management (IJAEM)*, 4(11), p. 369. doi: 10.35629/5252-0411369370.

Ajaj, E. . A., Jubier, N. J. and Majeed, K. . J. (2013) 'Fatigue Behavior of Epoxy/ SiO₂ Nanocomposites Reinforced with E- glass Fiber', *International Journal of Application or Innovation in Engineering & Management (IJAEM)*, pp. 62–69.

Alcudia-Zacarias, E. *et al.* (2020) 'Experimental Assessment of Residual Integrity and Balanced Mechanical Properties of GFRP/CFRP Hybrid Laminates under Tensile and Flexural Conditions', *Applied Composite Materials*, 27(6), pp. 895–914. doi: 10.1007/s10443-020-09839-x.

Alexandre Trudel, Mario Turgeon, I. L. (2017) 'Recent trends in the design of hydropower components subjected to cycling and fatigue; towards improved technical design specifications', in *Hydrovision International 2017*, pp. 1–33. Available at: <https://www.researchgate.net/publication/320310804> .

Arora, A. *et al.* (2023) 'Fatigue Response of Glass-Filled Epoxy Composites A Crack Initiation and Propagation Study', *International Journal of Fatigue*, 170, pp. 1–12. doi: 10.1016/j.ijfatigue.2023.107542.

ASTM International (2020a) ‘Standard Test Method for Tensile Properties of Polymer Matrix Composite Materials’, *Designation: D3039/D3039M – 17 Standard*.

ASTM International (2020b) ‘Standard Test Methods for Flexural Properties of Unreinforced and Reinforced Plastics and Electrical Insulating Materials’, *Designation: D790-17*, pp. 1–12.

Awang Ngah, S. and Taylor, A. C. (2018) ‘Fracture Behaviour of Rubber- and Silica Nanoparticle-Toughened Glass Fibre Composites under Static and Fatigue Loading’, *Composites Part A: Applied Science and Manufacturing*, 109, pp. 239–256. doi: 10.1016/j.compositesa.2018.02.028.

Badie, M. A., Mahdi, E. and Hamouda, A. M. S. (2011) ‘An investigation into hybrid carbon/glass fiber reinforced epoxy composite automotive drive shaft’, *Materials and Design*, 32(3), pp. 1485–1500. doi: 10.1016/j.matdes.2010.08.042.

Balandin, A. A. (2011) ‘Thermal properties of graphene and nanostructured carbon materials’, *Nature Materials*, 10(8), pp. 569–581. doi: 10.1038/nmat3064.

Beg, M. D. H. (2007) *The Improvement of Interfacial Bonding, Weathering and Recycling of Wood Fibre Reinforced Polypropylene Composites*, *Materials and Process Engineering*.

Bieniaś, J. and Dadej, K. (2020) ‘Fatigue Delamination Growth of Carbon and Glass Reinforced Fiber Metal Laminate in Fracture Mode II’, *International Journal of Fatigue journal*, 130, pp. 1–11. doi: 10.1016/j.ijfatigue.2019.105267.

Blackman, B. R. K. *et al.* (2007) ‘The Fracture and Fatigue Behaviour of Nano-Modified Epoxy Polymers’, *Journal of Materials Science*, pp. 7049–7051. doi: 10.1007/s10853-007-1768-6.

Borrego, L. P. *et al.* (2014) ‘Fatigue Behaviour of Glass Fibre Reinforced Epoxy Composites Enhanced with Nanoparticles’, *Composites Part B: Engineering*, pp. 65–72. doi: 10.1016/j.compositesb.2014.02.016.

Brinker, C. J. and Scherer, G. W. (2013) ‘Sol-Gel Science: The Physics and Chemistry of Sol-Gel Processing’, *Sol-Gel Science: The Physics and Chemistry of Sol-Gel Processing*, pp. 1–908. doi: 10.1016/C2009-0-22386-5.

Camargo, P. H. C., Satyanarayana, K. G. and Wypych, F. (2009) ‘Nanocomposites: Synthesis, Structure, Properties and New Application Opportunities’, *Materials Research*, 12(1), pp. 1–39. doi: 10.1590/S1516-14392009000100002.

- Camirero, M. A. *et al.* (2019) 'Tensile and Flexural Damage Response of Symmetric Angle-Ply Carbon Fiber-Reinforced Epoxy Laminates: Non-Linear Response and Effects of Thickness and Ply-Stacking Sequence', *Polymer Composites*, pp. 3678–3690. doi: 10.1002/pc.25230.
- Camirero, M. A. *et al.* (2019) 'Internal Damage Evaluation of Composite Structures Using Phased Array Ultrasonic Technique: Impact Damage Assessment in CFRP and 3D Printed Reinforced Composites', *Composites Part B: Engineering*, 165, pp. 131–142. doi: 10.1016/j.compositesb.2018.11.091.
- Chandel, R., Sharma, N. and Bansal, S. A. (2021) 'A Review on Recent Developments of Aluminum-Based Hybrid Composites For Automotive Applications', *Emergent Materials*, 4(5), pp. 1243–1257. doi: 10.1007/s42247-021-00186-6.
- Chen, J. *et al.* (2021) 'Micromechanical analysis of UD CFRP composite lamina under multiaxial loading with different loading paths', *Composite Structures*, 269(October 2020), p. 114024. doi: 10.1016/j.compstruct.2021.114024.
- Cho, J., Joshi, M. S. and Sun, C. T. (2006) 'Effect of Inclusion Size on Mechanical Properties of Polymeric Composites with Micro and Nano Particles', *Composites Science and Technology*, 66(13), pp. 1941–1952. doi: 10.1016/j.compscitech.2005.12.028.
- D. Booker, J., Raines, M. and Swift, K. G. (2001) *Designing Capable and Reliable Products, Designing Capable and Reliable Products*. doi: 10.1016/b978-0-7506-5076-2.x5000-4.
- Dani, M. S. H. and Venkateshwaran, N. (2021) 'Role of Surface Functionalized Crystalline Nano-silica on Mechanical, Fatigue and Drop Load Impact Damage Behaviour of Effective Stacking Sequenced E-glass Fibre-reinforced Epoxy Resin Composite', *Silicon*, pp. 757–766. doi: 10.1007/s12633-020-00486-2.
- Ding, J. and Cheng, L. (2021) 'Ultra-High Three-Point Bending Fatigue Performance of Nano-Silica-Reinforced CFRP', *International Journal of Fatigue*, 145, p. 106085. doi: 10.1016/j.ijfatigue.2020.106085.
- Dixit, S. and Padhee, S. S. (2019) 'Finite Element Analysis of Fiber Reinforced Hybrid Composites', *Materials Today: Proceedings*, 18, pp. 3340–3347. doi: 10.1016/j.matpr.2019.07.255.
- Dong, C. and Davies, I. J. (2012) 'Optimal design for the flexural behaviour of glass and carbon fibre reinforced polymer hybrid composites', *Materials and Design*, 37, pp. 450–457. doi: 10.1016/j.matdes.2012.01.021.

- Dong, C., Sudarisman and Davies, I. J. (2013) 'Flexural Properties of E Glass and TR50S Carbon Fiber Reinforced Epoxy Hybrid Composites', *Journal of Materials Engineering and Performance*, 22(1), pp. 41–49. doi: 10.1007/s11665-012-0247-7.
- El-Assal, A. M. and Khashaba, U. A. (2007) 'Fatigue Analysis of Unidirectional GFRP Composites Under Combined Bending and Torsional Loads', *Composite Structures*, pp. 599–605. doi: 10.1016/j.compstruct.2006.02.026.
- EL-Wazery, M. S., EL-Elamy, M. I. and Zoalfakar, S. H. (2017) 'Mechanical properties of glass fiber reinforced polyester composites', *International Journal of Applied Science and Engineering*, 14(3), pp. 121–131. doi: 10.6703/IJASE.2017.14(3).121.
- Erdogan, F. (2000) 'Fracture Mechanics', *International Journal of Solid and Structure*, 37(1–2), pp. 171–183. doi: 10.1088/0305-4624/13/4/405.
- Farahmand, B. (2001) *Fracture Mechanics of Metals, Composites, Welds, and Bolted Joints Application of LEFM, EPFM, and FMDM Theory*. Kluwer Academic Publishers 101 Philip Drive.
- Favela-Gallegos, C. A. and Soutis, C. (2012) 'Damage Evolution Under Bending Fatigue in Cross-Ply Composite Laminates', *ECCM 2012 - Composites at Venice, Proceedings of the 15th European Conference on Composite Materials*, (June), pp. 24–28.
- Friedrich, K. (1989) *Application of Fracture Mechanics to Composite Materials*.
- Fruehmann, R. K., Dulieu-Barton, J. M. and Quinn, S. (2010) 'Assessment of Fatigue Damage Evolution in Woven Composite Materials Using Infra-Red Techniques', *Composites Science and Technology*, pp. 937–946. doi: 10.1016/j.compscitech.2010.02.009.
- Fu, S. Y. *et al.* (2008) 'Effects of particle size, particle/matrix interface adhesion and particle loading on mechanical properties of particulate-polymer composites', *Composites Part B: Engineering*, 39(6), pp. 933–961. doi: 10.1016/j.compositesb.2008.01.002.
- Garnich, M. R. and Akula, V. M. K. (2009) 'Review of Degradation Models for Progressive Failure Analysis of Fiber Reinforced Polymer Composites', *Applied Mechanics Reviews*, 62(1), pp. 1–33. doi: 10.1115/1.3013822.
- Ghafaar, M. A., Mazen, A. A. and El-Mahallawy, N. A. (2006) 'Behavior of Woven Fabric Reinforced Epoxy Composites Under Bending and Compressive Loads', *JES. Journal of Engineering Sciences*, 34(2), pp. 453–469. doi:

10.21608/jesaun.2006.110472.

Ghani, A. F. A. and Mahmud, J. (2020) ‘Characterisation of Hybrid Carbon Glass Fibre Reinforced Polymer (C/GFRP) of Balanced Cross Ply and Quasi Isotropic under Tensile and Flexural Loading’, *International Journal of Automotive and Mechanical Engineering*, 17(1), pp. 7792–7804. doi: 10.15282/IJAME.17.1.2020.25.0580.

Giurgiutiu, V. (2016) ‘Damage and Failure of Aerospace Composites’, in *Structural Health Monitoring of Aerospace Composites*, pp. 125–175. doi: 10.1016/b978-0-12-409605-9.00005-2.

Goutianos, S. and Sørensen, B. F. (2021) ‘Fatigue Crack Growth Rate at Material and Geometry Transitions in Glass-Epoxy Composites’, *Composite Structures journal*, 275, pp. 1–13. doi: 10.1016/j.compstruct.2021.114445.

Haider, M. F. and Majumdar, P. K. (2016) *Anisotropic Electrical Response of Carbon Fiber Reinforced Composite Materials*.

Haller, C. L. (2020) *Study of Fatigue Failure of Composite Materials, Naval Postgraduate School*.

Harris, B. (2004) *Fatigue in Composites, Fatigue in composites*. doi: 10.1533/9781855738577.

Hashim, M. K. R. *et al.* (2021) ‘The Effect of Stacking Sequence and Ply Orientation on the Mechanical Properties of Pineapple Leaf Fibre (PALF)/Carbon Hybrid Laminate Composites.’, *Polymer*, 13, pp. 1–24. doi: <https://doi.org/10.3390/polym13030455>.

He, K., Hoa, S. V. and Ganesan, R. (2000) ‘The study of tapered laminated composite structures: A review’, *Composites Science and Technology*, pp. 2643–2657. doi: 10.1016/S0266-3538(00)00138-X.

Hofer, K. E., Stander, M. and Bennett, L. C. (1978) ‘Degradation and Enhancement of the Fatigue Behavior of Glass/Graphite/Epoxy Hybrid Composites After Accelerated Aging’, *Polymer Engineering & Science*, 18(2), pp. 120–127. doi: 10.1002/pen.760180210.

Hussain, C. M. (2020) ‘Handbook of Functionalized Nanomaterials for Industrial Applications’, in *Elsevier*, p. 1038.

Irina, M. M. W. *et al.* (2015) ‘Evaluation of Mechanical Properties of Hybrid Fiber Reinforced Polymer Composites and their Architecture’, in *Procedia Manufacturing*. Elsevier B.V., pp. 236–240. doi: 10.1016/j.promfg.2015.07.041.

- Jagannatha, T. D. and Harish, G. (2015) 'Mechanical Properties of Carbon/Glass Fiber Reinforced Epoxy Hybrid Polymer Composites', *International Journal of Medical Engineering and Robotics Research*, 4(2), pp. 131–137.
- Jangam, S., Reddy, K. H. and Raja, S. (2018) 'Fabrication & Characterization of Hybrid fibers and Hybrid Fiber reinforced composites - A Novel Approach', *Materials Today: Proceedings*, pp. 2795–2802. doi: 10.1016/j.matpr.2018.01.067.
- Jesthi, D. K., Mandal, P., *et al.* (2018) 'Effect of Carbon/Glass Fiber Symmetric Inter-Ply Sequence on Mechanical Properties of Polymer Matrix Composite', *ScienceDirect*, 20, pp. 530–535. doi: 10.1016/j.promfg.2018.02.079.
- Jesthi, D. K., Nayak, A., *et al.* (2018) 'Evaluation of mechanical properties of hybrid composite laminates reinforced with glass/carbon woven fabrics', *IOP Conference Series: Materials Science and Engineering*, 377(1). doi: 10.1088/1757-899X/377/1/012157.
- Jesthi, D. K., Mohanty, S. S., *et al.* (2018) 'Improvement of mechanical properties of carbon/glass fiber reinforced polymer composites through inter-ply arrangement', *IOP Conference Series: Materials Science and Engineering*, 377(1). doi: 10.1088/1757-899X/377/1/012182.
- Jesthi, D. K. and Nayak, R. K. (2019) 'Improvement of mechanical properties of hybrid composites through interply rearrangement of glass and carbon woven fabrics for marine application', *Composites Part B: Engineering*, 168, pp. 467–475. doi: 10.1016/j.compositesb.2019.03.042.
- John, A., Alex, S. and M, B. (2014) 'A Review on the Composite Materials used for Automotive Bumper in Passenger Vehicles', *International Journal of Engineering and Management Research*, pp. 98–101.
- Jones, R. M. (1999) *Mechanics of Composite Materials*. doi: 10.1201/9781498711067.
- K. Nahedh, G. and H. Majeed, A. (2021) 'Effect of Silicon Dioxide Nanoparticles on Mechanical Properties of Carbon Fiber/Unsaturated Polyester Composite', *Journal of Engineering and Sustainable Development*, 25(Special), pp. 2-91-2-98. doi: 10.31272/jeasd.conf.2.2.13.
- Kaddour, A. *et al.* (2015) 'Mechanical Properties and Details of Composite Laminates for the Test Cases Used in the Third World-Wide Failure Exercise', *JOURNAL OF COMPOSITE MATERIALS*, 47(1), pp. 2427–2442. doi: 10.1177/0021998313499477.

- Kamal, A. A., Hassan, G. I. and Khdir, Y. K. (2024) *Investigation Of Mechanical Behavior Of Laminated Composite At Several Conditions*. Erbil Polytechnic University.
- Kaminski, M. *et al.* (2015) 'Fatigue Damage Modeling of Composite Structures : the ONERA Viewpoint', *Journal aerospace lab*, (9), pp. 1–12. doi: 10.12762/2015.AL09-06.
- KAN, Y. R. and ITO, Y. M. (1972) 'Shear Deformation in Heterogeneous Anisotropic Plates', *J.Composite Materials*, 6(4), pp. 316–319.
- Kango, S. *et al.* (2013) 'Surface Modification of Inorganic Nanoparticles for Development of Organic-Inorganic Nanocomposites - A review', *Progress in Polymer Science*, 38(8), pp. 1232–1261. doi: 10.1016/j.progpolymsci.2013.02.003.
- Kansy, J., Consolati, G. and Dauwe, C. (2000) 'Positronium Trapping in Free Volume of Polymers', *Radiation Physics and Chemistry*, 58(5–6), pp. 427–431. doi: 10.1016/S0969-806X(00)00195-X.
- Karnati, S. R., Agbo, P. and Zhang, L. (2020) 'Applications of Silica Nanoparticles in Glass/Carbon Fiber-Reinforced Epoxy Nanocomposite', *Composites Communications*, 17, pp. 32–41. doi: 10.1016/j.coco.2019.11.003.
- Kaw, A. K. (2005) *Mechanics of composite materials*. CRC press.
- Kaw, A. K. (2006) *Mechanics of Composite Materials*. CRC Press Taylor & Francis Group.
- Kennedy, R. C., Brádaigh, C. M. Ó. and Leen, S. B. (2013) 'A Multiaxial Fatigue Damage Model for Fibre Reinforced Polymer Composites', *Composite Structures*, 106, pp. 201–210. doi: 10.1016/j.compstruct. 2013.05.024.
- Khalil, A. S. *et al.* (2017) 'Effect of SiO₂ Nanoparticles on Some Mechanical Properties of Epoxy/MWCNT Composites', *Asian Journal of Chemistry*, 29(3), pp. 675–678. doi: 10.14233/ajchem.2017.20305.
- Kim, J.-S. and Chung, S.-K. (2007) 'A Study on the Low-Velocity Impact Response of Laminates for Composite Railway Bodyshells', *Composite Structures*, 77, pp. 484–492. doi: 10.1016/j.compstruct.2005.08.020.
- Kinloch, I. A. *et al.* (2018) 'Composites with carbon nanotubes and graphene: An outlook', *Science*, 362(6414), pp. 547–553. doi: 10.1126/science.aat7439.
- Kumar, S. K. *et al.* (2017) '50th Anniversary Perspective: Are Polymer Nanocomposites Practical for Applications?', *Macromolecules*, 50(3), pp. 714–

731. doi: 10.1021/acs.macromol.6b02330.

Li, Y. *et al.* (2019) ‘A review of the electrical and mechanical properties of carbon nanofiller-reinforced polymer composites’, *Journal of Materials Science*, 54(2), pp. 1036–1076. doi: 10.1007/s10853-018-3006-9.

Liu, X. and Wang, G. (2007) ‘Progressive failure analysis of bonded composite repairs’, *Composite Structures*, pp. 331–340. doi: 10.1016/j.compstruct.2006.08.024.

Lu, Y., Weng, L. and Cao, X. (2006) ‘Morphological, Thermal and Mechanical Properties of Ramie Crystallites—Reinforced Plasticized Starch Biocomposites’, *Carbohydrate Polymers*, pp. 198–204. doi: 10.1016/j.carbpol.2005.08.027.

Luca Motoc, D., Ferrandiz Bou, S. and Balart Gimeno, R. (2015) ‘Effects of Fiber Orientation and Content on the Mechanical, Dynamic Mechanical and Thermal Expansion Properties of Multi-Layered Glass/Carbon Fiber-Reinforced Polymer Composites’, *Journal of Composite Materials*, 49(10), pp. 1211–1221. doi: 10.1177/0021998314532151.

Luthada, P. (2016) *Tension-Tension Fatigue Testing of Pultruded Carbon Fibre Composite Profiles*. Aalto University. doi: 10.13140/RG.2.1.1739.4805.

Lvov, Y. *et al.* (2016) ‘Halloysite Clay Nanotubes for Loading and Sustained Release of Functional Compounds’, *Advanced Materials*, 28(6), pp. 1227–1250. doi: 10.1002/adma.201502341.

M., S. K., S., G. G. K. and Rajanna, S. (2014) ‘Study on Effect of Thickness and Fibre Orientation on a Tensile and Flexural Properties of a Hybrid Composite’, *Journal of Engineering Research and Applications www.ijera.com*, 4(8), pp. 56–66. Available at: www.ijera.com.

Ma, P. C. *et al.* (2013) ‘Development of functional glass fibres with nanocomposite coating: A comparative study’, *Composites Part A: Applied Science and Manufacturing*, 44(1), pp. 16–22. doi: 10.1016/j.compositesa.2012.08.027.

Ma, Y. *et al.* (2017) ‘A Comparative Study of the Mechanical Properties and Failure Behavior of Carbon Fiber/Epoxy and Carbon Fiber/Polyamide 6 Unidirectional Composites’, *Composite Structures*, pp. 89–99. doi: 10.1016/j.compstruct.2016.10.037.

Madhavi, P. *et al.* (2021) ‘Flexural and Inter- Laminar Shear Strength of Glass/Carbon Fabric Reinforced Composite’, *IOP Conference Series: Materials*

- Science and Engineering*, 1057(1), p. 012016. doi: 10.1088/1757-899x/1057/1/012016.
- Mallakpour, S. and Mani, L. (2014) 'Improvement of the Interactions between Modified ZrO₂ and Poly(amide-imide) Matrix by Using Unique Biosafe Diacid as a Monomer and Coupling Agent', *Polymer - Plastics Technology and Engineering*, 53(15), pp. 1574–1582. doi: 10.1080/03602559.2014.919639.
- Matykiewicz, D. (2020) 'Hybrid epoxy composites with both powder and fiber filler: A review of mechanical and thermomechanical properties', *Materials*, 13(8). doi: 10.3390/MA13081802.
- Megahed, M., Megahed, A. and Agwa, M. (2019) 'The Influence of Incorporation of Silica and Carbon Nanoparticles on the Mechanical Properties of Hybrid Glass Fiber Reinforced Epoxy', *Journal of Industrial Textiles*, 49(2), pp. 181–199. doi: 10.1177/1528083718775978.
- Meyers, M. and Chawla, K. (2009) *Mechanical Behavior of Materials*, Cambridge University Press. doi: www.cambridge.org/9780521866750.
- Mittal, G. *et al.* (2015) 'A review on carbon nanotubes and graphene as fillers in reinforced polymer nanocomposites', *Journal of Industrial and Engineering Chemistry*, 21, pp. 11–25. doi: 10.1016/j.jiec.2014.03.022.
- Mohammed, A. A. K., Hassan, G. I. and Khdir, Y. K. (2023) 'Mechanical Behavior of Hybrid Laminated Nano Composite Containing Equal Numbers of Glass and Carbon Fiber Plies', *INTERNATIONAL JOURNAL OF AUTOMOTIVE AND MECHANICAL ENGINEERING*, 20(2), pp. 10335 – 10350. doi: 10.15282/ijame.20.2.2023.01.0799.
- Mohanty, A. and Srivastava, V. K. (2015) 'Effect of Alumina Nanoparticles on the Enhancement of Impact and Flexural Properties of the Short Glass/Carbon Fiber Reinforced Epoxy Based Composites', *Fibers and Polymers*, 16(1), pp. 188–195. doi: 10.1007/s12221-015-0188-5.
- Morampudi, P. *et al.* (2021) 'Review on Glass Fiber Reinforced Polymer Composites', *Materials Today: Proceedings*, pp. 314–319. doi: 10.1016/j.matpr.2020.11.669.
- Mouritz, A. P. (2012) *Introduction to Aerospace Materials, Introduction to Aerospace Materials*. doi: 10.2514/4.869198.
- N, G. M. and HariRao, A. N. (2013) 'Hybrid Effects on Tensile Properties of Carbon/Glass Angle Ply Composites', *Advances in Materials*, 2(3), pp. 36–41. doi: 10.11648/j.am.20130203.13.

- Nagaraja, K. C. *et al.* (2019) 'The Role of Stacking Order on Mechanical Properties of Glass/Carbon Reinforced Epoxy Hybrid Composites Prepared by Resin Infusion Technique', *Materials Today: Proceedings*, 22, pp. 2446–2451. doi: 10.1016/j.matpr.2020.03.371.
- Nagaraja, K. C. *et al.* (2020) 'Studying the effect of different carbon and glass fabric stacking sequence on mechanical properties of epoxy hybrid composite laminates', *Composites Communications*, 21, p. 100425. doi: 10.1016/j.coco.2020.100425.
- Naito, K. and Oguma, H. (2017) 'Tensile properties of novel carbon/glass hybrid thermoplastic composite rods', *Composite Structures*, 161, pp. 23–31. doi: 10.1016/j.compstruct.2016.11.042.
- Nestor, P. (2017) 'Linear Elastic Fracture Mechanics', in *Fracture mechanics*, pp. 39–130.
- Ngo, T.-D. (2020) 'Composite and Nanocomposite Materials - From Knowledge to Industrial Applications', *Composite and Nanocomposite Materials - From Knowledge to Industrial Applications*. doi: 10.5772/intechopen.80186.
- nickel (2016) 'Laminating resin MGS ® L 285 Characteristics Content'. doi: <https://m.aircraftspruce.com/catalog/pdf/mgs285tech.pdf>(accessed on 23 September 2020).
- O'Regan, D. F., Akay, M. and Meenan, B. (1999) 'A Comparison of Young's Modulus Predictions in Fibre-Reinforced- Polyamide Injection Mouldings', *Composites Science and Technology*, 59, pp. 419–427.
- Ortega, A. *et al.* (2017) 'Translaminar Fracture Toughness of Interply Hybrid Laminates Under Tensile and Compressive Loads', *Composites Science and Technology*, 143, pp. 1–12.
- Oskouei, A. V. and Taleie, S. M. (2010) 'Experimental investigation of relaxation of fiber-reinforced polymer composites', *Journal of Reinforced Plastics and Composites*, 29(17), pp. 2705–2718. doi: 10.1177/0731684409357256.
- Park, S. J. (2018) 'Matrices for carbon fiber composites', *Springer Series in Materials Science*, pp. 69–103. doi: 10.1007/978-981-13-0538-2_3.
- Patel, K. K. and Purohit, R. (2018) 'Dispersion of SiO₂ Nano Particles on Epoxy Based Polymer Nano Composites and its Characterization', *Oriental Journal of Chemistry*, 34(6), pp. 2998–3003. doi: 10.13005/ojc/340641.

- Pellicer, E. (2021) *Smart Composite Materials: An Introduction, Encyclopedia of Materials: Composites*. doi: 10.1016/B978-0-12-819724-0.00092-6.
- Pettarin, V. (2016) *Injected polymer-matrix nanocomposites : Morphology-performance relationship*.
- Rabbi, M. S. *et al.* (2023) ‘Effect of Nano-filler on the Manufacturing and Properties of Natural Fiber-based Composites: A Review’, *Journal of Engineering Advancements*, 04(04), pp. 101–115. doi: 10.38032/jea.2023.04.001.
- Rajak, D. K. *et al.* (2019) ‘Recent progress of reinforcement materials: A comprehensive overview of composite materials’, *Journal of Materials Research and Technology*, 8(6), pp. 6354–6374. doi: 10.1016/j.jmrt.2019.09.068.
- Raşit Koray Ergün and Hamit Adin (2022) ‘Investigation of The Effects of Nanoparticle Reinforcement on The Mechanical Properties of Woven Composites’, *Polymer Composites*, pp. 1–9. doi: 10.1002/pc.27182.
- Reddy, J. N. (2004) ‘An Introduction to Nonlinear Finite Element Analysis Compress’, pp. 1–459.
- Ribeiro, F., Sena-Cruz, J. and Vassilopoulos, A. P. (2021a) ‘Tension-tension fatigue behavior of hybrid glass/carbon and carbon/carbon composites’, *International Journal of Fatigue*, 146, p. 106143. doi: 10.1016/j.ijfatigue.2021.106143.
- Ribeiro, F., Sena-Cruz, J. and Vassilopoulos, A. P. (2021b) ‘Tension-Tension Fatigue Behavior of Hybrid Glass/Carbon and Carbon/Carbon Composites’, *International Journal of Fatigue*, 146. doi: 10.1016/j.ijfatigue.2021.106143.
- Ritchie, R. O. (2011) ‘The Conflicts Between Strength and Toughness’, *Nature Materials*, 10(11), pp. 817–822. doi: 10.1038/nmat3115.
- Rizzo, F. (2020) *Impact on Hybrid Composite Materials*. University of Bath. Available at: https://researchportal.bath.ac.uk/files/210522981/PhD_Thesis_Francesco_Rizzo.pdf.
- Robertson, I. D. *et al.* (2018) ‘Rapid energy-efficient manufacturing of polymers and composites via frontal polymerization’, *Nature*, 557(7704), pp. 223–227. doi: 10.1038/s41586-018-0054-x.
- Safri, S. N. A. *et al.* (2018) ‘Impact Behaviour of Hybrid Composites For

- Structural Applications: A Review', *Composites Part B: Engineering*, 133, pp. 112–121. doi: 10.1016/j.compositesb.2017.09.008.
- Sasaki, Y. *et al.* (2023) 'Nanoparticle-Based Tough Polymers with Crack-Propagation Resistance', *Langmuir*, 39(26), pp. 9262–9272. doi: 10.1021/acs.langmuir.3c01226.
- Sathishkumar, T. P., Satheeshkumar, S. and Naveen, J. (2014) 'Glass fiber-reinforced polymer composites - A review', *Journal of Reinforced Plastics and Composites*, 33(13), pp. 1258–1275. doi: 10.1177/0731684414530790.
- Schijve, J. (2009) *Fatigue of Structures and Materials, Fatigue of Structures and Materials*. doi: 10.1007/978-1-4020-6808-9.
- Schlüter, A., Kuhn, C. and Müller, R. (2014) *Phase Field Approximation of Dynamic Brittle Fracture, Pamm*. doi: 10.1002/pamm.201410059.
- Sebaey, T. A. *et al.* (2013) 'Damage Resistance and Damage Tolerance of Dispersed CFRP Laminates: Design and Optimization', *Composite Structures*, 95, pp. 569–576. doi: 10.1016/j.compstruct.2012.07.005.
- Shah, O. R. and Tarfaoui, M. (2014) 'Investigation of Self Heating and Damage Progression in a Polyester Fiberglass Composite Under Tension-Tension Cyclic Loading', *16th European Conference on Composite Materials, ECCM 2014*, (June), pp. 22–26.
- Shah, S. Z. H. *et al.* (2019) 'Impact Resistance and Damage Tolerance of Fiber Reinforced Composites: A review', *Composite Structures*, 217, pp. 100–121. doi: 10.1016/j.compstruct.2019.03.021.
- Sivakandhan, C. and Prabhu, P. S. (2015) 'Investigation of Hybrid Composite Drive Shaft under Tensile, Bending and Torsion Testing', *International Journal of Vehicle Structures and Systems*, pp. 110–114. doi: 10.4273/ijvss.6.4.05.
- Song, J. H. and Lim, J. K. (2007) 'Fatigue Crack Growth Behavior and Fiber Orientation of Glass Fiber Reinforced Polycarbonate Polymer Composites', *Metals and Materials International*, pp. 371–377. doi: 10.1007/BF03027870.
- Sudarisman, R., de San Miguel, B. and Davies, I. (2009) 'The effect of partial substitution of E-glass fibre for carbon fibre on the mechanical properties of CFRP composites.', *Proceedings of the International Conference on Materials and Metallurgical Technology, ICONNET 2009*, (June 2009), pp. 125–128.
- SURESH, S. (2013) 'Fatigue of Materials', in *Encyclopedia of Tribology*, pp. 132–162. doi: 10.1007/978-0-387-92897-5_100470.

- Talreja, R. (2008) 'Damage and Fatigue in Composites - A personal account', *Composites Science and Technology*, 68(13), pp. 2585–2591. doi: 10.1016/j.compscitech.2008.04.042.
- Tavares, R. P. (2015) 'Mechanics of hybrid polymer composites', p. 186.
- Vasiliev, V. V and Morozov, E. V. (2013) *Advanced Mechanics of Composite Materials and Structural Elements*.
- Vassilopoulos, A. P. (2020) 'The History of Fiber-Reinforced Polymer Composite Laminate Fatigue Anastasios', *International Journal of Fatigue*, 134, pp. 1–20. doi: 10.1016/j.ijfatigue.2020.105512.
- Wetzel, B., Hauptert, F. and Zhang, M. Q. (2003) 'Epoxy Nano-Composites with High Mechanical and Tribological Performance', *Composites Science and Technology*, 63(14), pp. 2055–2067. doi: 10.1016/S0266-3538(03)00115-5.
- William F. Hosford (2011) *Mechanical Behaviour of Materials*, CAMBRIDGE UNIVERSITY PRESS. doi: www.cambridge.org/9780521195690.
- Wisnom, M. R. (2009) 'The Role of Delamination in Notched and Unnotched Tensile Strength', in *International Conferences on Composite Materials*.
- Wisnom, M. R., Khan, B. and Hallett, S. R. (2008) 'Size Effects in Unnotched Tensile Strength of Unidirectional and Quasi-Isotropic Carbon/Epoxy Composites', *Composite Structures*, 84(1), pp. 21–28. doi: 10.1016/j.compstruct.2007.06.002.
- Xiao-Yu, S. *et al.* (2018) 'A Study on the Failure Mechanisms of Composite Laminates Simultaneously Impacted by Two Projectiles', *Advanced Composites Letters*, 27(3), pp. 96–107. doi: 10.1177/096369351802700302.
- Yeh, H.-Y. and Kim, C. H. (1994) 'The Yeh-Stratton Criterion for Composite Materials', *Journal of Composite Materials*, 28(10), pp. 926–939. doi: 10.1177/002199839402801003.
- Zakaria, M. R. *et al.* (2019) 'Hybrid carbon fiber-carbon nanotubes reinforced polymer composites: A review', *Composites Part B: Engineering*, 176(August), p. 107313. doi: 10.1016/j.compositesb.2019.107313.
- Zhang, Jin *et al.* (2012) 'Hybrid Composite Laminates Reinforced with Glass/Carbon Woven Fabrics for Lightweight Load Bearing Structures', *Materials and Design*, 36, pp. 75–80. doi: org/10.1016/j.matdes.2011.11.006.
- Zhang, J *et al.* (2012) 'Sustainable Automotive Technologies 2012', *Sustainable Automotive Technologies 2012*, (September). doi: 10.1007/978-3-642-24145-1.

Zhang, Z. *et al.* (2002) 'A Dynamic Model of Ceramic-Fibre-Reinforced Plastic Hybrid Composites under Projectile Striking', 216(G6), pp. 325–331.

Zheng, Yaping, Ning, R. and Zheng, Ying (2005) 'Study of SiO₂ nanoparticles on the improved performance of epoxy and fiber composites', *Journal of Reinforced Plastics and Composites*, 24(3), pp. 223–233. doi: 10.1177/0731684405043552.

LIST OF PUBLICATIONS

International journals (Published)

1. Dawood, T. S., Fadhil, B. M. and Ramadan, D. O. (2023) 'Effects of Silica Nanoparticles on Glass and Carbon Fiber Epoxy Composites', *Nexo Revista Cientifica*, 36(05), pp. 75–86. doi: <https://doi.org/10.5377/nexo.v36i05.17286>.
2. Dawood, T. S., Fadhil, B. M. and Ramadan, D. O. (2024) 'Experimental Characterization of Glass /Carbon Hybrid Composite Reinforced by SiO₂ Nanoparticles', *Tikrit Journal of Engineering Sciences*.
3. Dawood, T. S., Fadhil, B. M. and Ramadan, D. O. (2022) 'Effect of Adding SiO₂ Nanoparticles on Tensile and Bending Tests of Glass/Carbon Hybrid Composite Materials', *Jilin Daxue Xuebao (Gongxueban)/Journal of Jilin University (Engineering and Technology Edition)*, 41, pp. 55–68. doi: 10.17605/OSF.IO/VCX68.

Local journals (Published)

1. Dawood, T. S., M. Fadhil, B. And Ramadan, D. O. (2023) 'Improving the Mechanical Properties of Carbon-Epoxy and Glass-Epoxy Composites by Incorporating Silica Nanoparticles', *Journal of University of Duhok*, 26(2), Pp. 682–692. Doi: 10.26682/Csjuod.2023.26.2.61.

كورتەيەك بەزماني كوردى

تايپەتمەندىيە ميكانيكىەكانى پىكھاتەى ھايپىرىد بە بەكارھىنانى ماترىكىسى ھايپىرىد تۇفنىد

ئەم تىزە لىكۆلنەھەى لە رىكخستنى گونجاوى چىنەكان كورد لە پىكھاتەكانى شووشە و كاربۆن، كە تىايدا سەرنجى خستە سەر كارىگەرىيەكانى ئاراستەى رىشالى درىژخايەن، ئەستوورى و زيادكردنى نانۆگەردىلەكانى SiO_2 . سى كۆمەلە پانئالى پىكھاتەى بەرھەم ھىنران. گروپى يەكەم پىكدىت لە پەرى رىشالى شووشەى كە بە رىككەوتى كۆكردنەھەى 0° ($[G/G/G/G]_s$) رىكخراون بە زيادكردنى 2% و بەى زيادكردنى 2% نانۆگەردىلەكانى سىلىكا، و پەرى رىشالى كاربۆن كە بە شىوھى a رىككەوتى كۆكردنەھەى 0° ($[C/C/C/C]_s$) لەگەل زيادكردنى 2% و بەى زيادكردنى 2% نانۆگەردىلەكانى دووم ئوكسىدى سىلىكا. ئەم پەرانە بە تايپەتى بۆ ھەلسەنگاندنى تايپەتمەندىيە ميكانيكىەكان دارىژراون، ئەوانىش مۇدىولى لاسىكى لە ئاراستە درىژخايەن و تەرادەيىيەكاندا (E_2, E_1)، مۇدىولى برىن (G_{12})، و رىژھى پۇيسون (ν_{12}) پىكھاتەكانى شووشە/ئىپۆكىسى و كاربۆن/ئىپۆكىسى.

گروپى دووم كە بە زنجىرەى جىاوازى كۆكردنەھەى ھاوسەنگى نىمچە ئەنتروپى تايپەتمەندە، لە سى ئاراستەى بنەرتى رىشالى يەك ئاراستەى پىكدىت: 0° ، 45° ، و 90° . ئەم زنجىرەيانە لە ئەستوورىدا جىاوازان، پىكھاتوون لە ھەشت چىن (2 مەلم)، دە چىن (2.5 مەلم) و دوانزە چىن (3 مەلم). سەرەرى ئەوھش، نانۆگەردىلەكانى SiO_2 وەكو مادەى بەھىزكەر لەناو ماترىكىسى ئىپۆكىسىدا بەكارھىنران.

گروپى سىيەم پىكھاتووه لە پىكھاتەى چىنە براوھەكان، كە زنجىرە جىاوازەكانى كۆكردنەھە دەپشكنن. ئەم زنجىرەيانە دوو ئاراستەى بنەرتى رىشالى يەك ئاراستەى لەخۆگرتبوو: 0° و 90° ، و ئەستوورى جىاوازيان نىشان دا. بە تايپەتى كۆمەلەكە ھەشت چىن (2 مەلم)، دوانزە چىن (3 مەلم)، شانزە چىن (4 مەلم) و بىست چىن (5 مەلم) لەخۆگرتبوو. جگە لەوھش، نانۆگەردىلەكانى SiO_2 وەكو مادەى بەھىزكەر لەناو ماترىكىسى ئىپۆكىسىدا بەكارھىنران.

تايپەتمەندىيە ميكانيكىە نىمچە ئىستاناتىكىيەكان (تاقىكردنەھەى سى خالىى كىشكردن و چەمانەھەى) و ھەلسوكەوتى داينامىكى (تاقىكردنەھەى ماندوتى ئەكسىالى و چەمانەھەى) مادەكە بە شىكارى ئەزموونى لىكۆلنەھەيان لەسەر كرا و بە بەكارھىنانى ھاوشىوھەكردنى ژمارەى لە رىگەى شىوازى توخمە سنووردارەكانەھە (ANSYS Workbench) پىشتراستكرانەھە. پروسەى ئىنفىوژنى رزىن بە يارمەتى بۆشايى بەكارھات بۆ دوستكردنى چوار دە زنجىرەى ئىپۆكىسى بەھىزكراوى رىشال لەوانەش بە

زیادکردنی و بهی زیادکردنی 2% نانویکتهاتهکانی دووهم ئوکسیدی سیلیکا، که به Q1، Q1N، Q2، Q2N، Q3، Q3N، C1، C1N، C2، C2N، C3، C3N، C4، C4N و C4N دهستنیشانکراون .

مؤدیولی لاستیکی (E1) و زورترین فشاری S3 و S3N به ریژهی 20.97% و 18.65% زیادی کردوه. به بهراورد لهگهل CS1 که نانوگهردیلهکانی SiO_2 ی نییه، CS1N زیادبوونی E_1 و زورترین فشاری به ریژهی 2.5% و 12.7% نیشان دا. تیکهلهکردنی نانوگهردیلهکانی SiO_2 به شیوهیهکی بهرچاو کارایی ماده پیکهاتهیهکانی شوشه/کاربوئی تیکهلهباشتر دهکات. تاقیکردنهوکانی ماندویتی نهکسیالی دهریانخست که ژمارهی خولی ئوتومبیله تیکهلهکان (CS1 و CS1N)، (CS2 و CS2N)، و (CS3 و CS3N) به ریژهی نزیکهی 55%، 27%، و 58% زیادی کردوه، به ریککهوت، له ناستی بارگاویکردندا 70%. له تاقیکردنهوئی فشاری چرچبووندا، زیادبوونی فشاری 17.4% له نیوان CS1 و CS1N دا ههبوو، و زیادبوونی هاوشیوهی 13.11% له نیوان CS2 و CS2N دا ههبوو. جووته نمونهیهکانی CS3 و CS3N بهرزبوونهوئی بهراوردکارییان به ریژهی 17.1% نیشان دا، له کاتیکدا CS4 و CS4N زیادبوونی 13.61% یان نیشان دا.



MECHANICAL PROPERTIES OF HYBRID COMPOSITE USING HYBRID TOUGHENED MATRIX

تیزیکه

پیشکەشی ئەنجومەنی کۆلیژی تەکنیکی ئەندازیاری هەولێر گراوه له زانکۆی
پۆلیتەکنیکی هەولێر وەکو بەشێک له پێداوێستیهکانی بەدەست هێنانی پلهی
دکتۆرای فەلسەفه له زانستی ئەندازیاری میکانیکی و وزه

له لایهن

ذاکر صالح داود

به کالۆریۆس له ئەندازیاری میکانیک

ماستەر له ئەندازیاری میکانیک

به سه ره پهرشتیاری

پ.د. باسم محمد فاضل

پ.ی.د. دلیر عبید رمضان

عێراق - کوردستان - هەولێر

2024